

AD-752 558

V/STOL AIRCRAFT AERODYNAMIC PREDICTION
METHODS INVESTIGATION. VOLUME II. APPLI-
CATION OF PREDICTION METHODS

Peter T. Wooler, et al

Northrop Corporation

Prepared for:

Air Force Flight Dynamics Laboratory

January 1972

DISTRIBUTED BY:

NTIS

National Technical Information Service
U. S. DEPARTMENT OF COMMERCE
5285 Port Royal Road, Springfield Va. 22151

AD 752558

V/STOL AIRCRAFT AERODYNAMIC PREDICTION METHODS INVESTIGATION

Volume II. Application of Prediction Methods

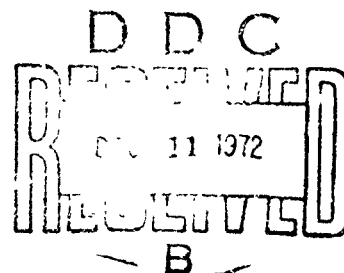
P.T. Wooler
H.C. Kao
M.F. Schwendemann
H.R. Wasson
H. Ziegler

Northrop Corporation
Aircraft Division

TECHNICAL REPORT AFFDL-TR-72-26, Volume II
January 1972

Approved for public release, distribution unlimited.

Reproduced by
NATIONAL TECHNICAL
INFORMATION SERVICE
15 Reynolds Road
Springfield, MA 01104



AIR FORCE FLIGHT DYNAMICS LABORATORY
AIR FORCE SYSTEMS COMMAND
WRIGHT-PATTERSON AIR FORCE BASE, OHIO 45433

NOTICE

When Government drawings, specifications, or other data are used for any purpose other than in connection with a definitely related Government procurement operation, the United States Government thereby incurs no responsibility nor any obligation whatsoever; and the fact that the Government may have formulated, furnished, or in any way supplied the said drawings, specifications, or other data, is not to be regarded by implication or otherwise as in any manner licensing the holder or any other person or corporation, or conveying any rights or permission to manufacture, use, or sell any patented invention that may in any way be related thereto.

ACCESSION NO.		
NTIS	Write Section	<input checked="" type="checkbox"/>
DDC	Dist. Section	<input type="checkbox"/>
UNAL. DIVISION		<input type="checkbox"/>
JUSTIFICATION		
BY		
DISTRIBUTION/AVAILABILITY CODES		
Dist.	AVAIL. and/or SPECIAL	
A		

Copies of this report should not be returned unless return is required by security considerations, contractual obligations, or notice on a specific document.

Unclassified

Security Classification

DOCUMENT CONTROL DATA - R & D

(Security classification of title, body of abstract and indexing annotation must be entered when the overall report is classified)

1. ORIGINATING ACTIVITY (Corporate author) Northrop Corporation Aircraft Division Hawthorne, California		2a. REPORT SECURITY CLASSIFICATION Unclassified	
		2b. GROUP	
3. REPORT TITLE V/STOL AIRCRAFT AERODYNAMIC PREDICTION METHODS INVESTIGATION - Volume II			
4. DESCRIPTIVE NOTES (Type of report and inclusive dates) Final Report - 1 May 1969 to 31 January 1972			
5. AUTHOR(S) (First name, middle initial, last name) Peter T. Wooler Hsiao C. Kao Myles F. Schwendemann Howard R. Wasson Henry Ziegler			
6. REPORT DATE January 1972	7a. TOTAL NO. OF PAGES 228 248	7b. NO. OF REFS 11	
8a. CONTRACT OR GRANT NO. F33615-69-C-1602	8b. ORIGINATOR'S REPORT NUMBER(S) NOR 72-9, Volume II		
8c. PROJECT NO. 698 BT c. Task No. 698 BT 01	8d. OTHER REPORT NO(S) (Any other numbers that may be assigned this report) AFFDL-TR-72-26, Volume II		
10. DISTRIBUTION STATEMENT Approved for public release; distribution unlimited.			
11. SUPPLEMENTARY NOTES		12. SPONSORING MILITARY ACTIVITY Air Force Flight Dynamics Laboratory Wright-Patterson Air Force Base Ohio 45433	
13. ABSTRACT Analytical engineering methods are developed for use in predicting the static and dynamic stability and control derivatives and force and moment coefficients of lift-jet, lift-far, and vectored thrust V/STOL aircraft in the hover and transition flight regimes. The methods take into account the strong power effects, large variations in angle of attack and sideslip, and changes in aircraft geometry that are associated with high disk loaded V/STOL aircraft operating in the aforementioned flight regimes. The aircraft configurations studied have a conventional wing, fuselage and empennage. The prediction methods are suitable for use by design personnel during the preliminary design and evaluation of V/STOL aircraft of the type previously mentioned. This report consists of four volumes. The prediction methods are applied to a number of V/STOL configurations in this volume. The theoretical development of the prediction methods may be found in Volume I. Details of the computer programs associated with the prediction methods are given in Volume III. The results of a literature survey are presented in Volume IV. Details of illustrations in this document may be better studied on microfiche			

DD FORM 1 NOV 65 1473

Unclassified

Security Classification

Unclassified

Security Classification

14	KEY WORDS	LINK A		LINK B		LINK C	
		ROLE	WT	ROLE	WT	ROLE	WT
	V/STOL Aircraft						
	XV-5A						
	V/STOL Stability and Control						
	Aerodynamic Characteristics (Subsonic)						
	Forces (Normal Force, Lift, Side Force)						
	Moments (Pitching, Rolling, Yawing)						
	Rotary Derivatives						
	V/STOL Aerodynamics						
	Nonlinear Aerodynamics						
	Wing Stall						
	Separated Flows						
	V/STOL Transitional Flight						
	Engine Wake Effects						
	Jet Exhaust Fields						
	Jet Interference Effects						
	Jet in Cross Flow						
	Jet Path						
	Multiple Jets						
	Jet Interaction						
	Power Effects						
	Engine Inlet Effects						
	Vortices						
	Computer Programs						

Unclassified

Security Classification

**V/STOL AIRCRAFT AERODYNAMIC
PREDICTION METHODS INVESTIGATION**

**Volume II
Application of Prediction Methods**

**P.T. Wooler
H.C. Kao
M.F. Schwendemann
H.R. Wasson
H. Ziegler**

Approved for public release, distribution unlimited.

ic

FOREWORD

This report summarizes the work accomplished by the Aircraft Division of Northrop Corporation, Hawthorne, California for the Air Force Flight Dynamics Laboratory, AFSC, Wright Patterson Air Force Base, Ohio, and USAF Contract No. F33615-69-C-1602 (Project 698 BT). This document constitutes the Final Report under the contract.

This work was accomplished during the period 1 May 1969 to 31 January 1972, and this report was released by the authors in January 1972. The Air Force Project Engineers were Mr. Robert Nicholson and Mr. Henry W. Woolard of the Control Criteria Branch, Flight Control Division, AFFDL. Their assistance in monitoring the work and providing data is greatly appreciated.

The authors gratefully acknowledge the assistance and cooperation of NASA Langley Research Center personnel during the wind tunnel model testing in the NASA Langley V/STOL tunnel.

Special recognition is due Mr. Richard J. Margason of NASA Langley Research Center who, besides being actively involved in the testing at Langley, has made valuable contributions to other areas of the investigation.

Various people at Northrop's Aircraft Division contributed to the investigation, particularly the following persons in the areas designated:


Lynn B. Fricke	Developed empirical methods for the wing. Was Test Engineer for the wind tunnel testing of the component model.
Hsiao C. Kao	Developed the transformation method for estimating power effects on wings and fuselages. Developed the empirical method for the body.
Myles F. Schwendemann	Developed the method for estimating engine inlet effects. Provided prediction method wind tunnel testing interface for the configuration model. Participated in the hover analysis.

Martin F. Silady	Assembled the V/STOL bibliography and was responsible for the literature survey.
Howard R. Wasson	Developed the method for mapping general sections. Developed the nonlinear body prediction method. Assisted with the development of the perturbation method.
Peter T. Wooler	Directed the technical effort and developed the nonlinear wing prediction method.
Henry Ziegler	Developed the jet flow field prediction method. Performed the analysis of wing power effects employing lifting surface theory.

Contributions have also been made by U. A. G. Brynjestad to this study in a number of areas, particularly the literature search and perturbation method development; by M. S. Cahn in the development of the method for mapping general sections and perturbation method development; by members of the Northrop Aerosciences Laboratories in respect to model design, fabrication, testing and data reduction — especially T. Comerinsky, F. W. Peitzman, E. G. Kontos and W. S. Ramos.

This report contains no classified information.

This technical report has been reviewed and is approved.


 C. B. Westbrook
 Chief, Control Criteria Branch
 Flight Control Division
 Air Force Flight Dynamics Laboratory

ABSTRACT

Analytical engineering methods are developed for use in predicting the static and dynamic stability and control derivatives and force and moment coefficients of lift-jet, lift-fan, and vectored thrust V/STOL aircraft in the hover and transition flight regimes. The methods take into account the strong power effects, large variations in angle of attack and sideslip, and changes in aircraft geometry that are associated with high disk loaded V/STOL aircraft operating in the aforementioned flight regimes. The aircraft configurations studied have a conventional wing, fuselage and empennage. The prediction methods are suitable for use by design personnel during the preliminary design and evaluation of V/STOL aircraft of the type previously mentioned.

This report consists of four volumes. The prediction methods are applied to a number of V/STOL configurations in this volume. The theoretical development of the prediction methods may be found in Volume I. Details of the computer programs associated with the prediction methods are given in Volume III. The results of a literature survey are presented in Volume IV.

Preceding page blank

TABLE OF CONTENTS

Section	Page
I INTRODUCTION	1
1. PURPOSE	1
2. SCOPE	1
3. TECHNICAL APPROACH	2
4. ORGANIZATION OF VOLUME II.....	2
II POWER EFFECTS ON THE WING	4
1. SAMPLE PROBLEM	5
2. APPLICATION OF MAPPING METHOD TO THE WING.....	7
3. APPLICATION OF JET FLOW FIELD THEORY TO WING	19
a. Transformation Method.....	19
(1) Sample Problem Computation.....	19
(a) Input for Sample Problem.....	20
(b) Output for Sample Problem	22
(2) Applicability and Limitations	30
b. Lifting Surface Theory	31
(1) Sample Problem Computation.....	32
(a) Input for Sample Problem	32
(b) Output for Sample Problem	34
(2) Applicability and Limitations	36
4. APPLICATION OF TRANSFORMATION METHOD TO WING.....	36
a. Inputs to Transformation Method for Sample Problem.....	36
b. Outputs from Transformation Method for Sample Problem ..	38
c. Method Applicability and Limitations	52
5. APPLICATION OF LIFTING SURFACE THEORY TO WING	58
a. Sample Problem Computation.....	58
(1) Input for Sample Problem	59
(2) Output for Sample Problem	64
b. Applicability and Limitations	64
c. Additional Calculations and Comparison with Test Data.....	67

Preceding page blank

TABLE OF CONTENTS (Continued)

Section	Page
III POWER EFFECTS ON THE FUSELAGE	76
1. SAMPLE PROBLEM.....	76
2. APPLICATION OF THE MAPPING METHOD.....	77
3. APPLICATION OF JET FLOW FIELD THEORY TO FUSELAGE ..	87
a. Sample Problem Computation.....	87
(1) Input for Sample Problem	88
(2) Output for Sample Problem.....	90
b. Applicability and Limitations.....	93
4. APPLICATION OF TRANSFORMATION METHOD TO FUSELAGE	98
a. Inputs to Transformation Method for Sample Problem.....	98
b. Outputs from Transformation Method for Sample Problem..	98
c. Method Applicability and Limitations.....	123
IV POWER EFFECTS ON CONTROL SURFACES	124
1. SAMPLE PROBLEM.....	124
2. APPLICATION OF JET FLOW FIELD PROGRAM TO CONTROL SURFACES	125
3. CALCULATION OF POWER INDUCED FORCES AND MOMENTS ON CONTROL SURFACES.....	125
V APPLICATION OF INLET METHOD.....	128
1. SELECTION OF PARAMETERS	130
a. Inlet Method	130
b. Fan Flow Model	131
2. EXAMPLES OF APPLICATION	131
a. Fan Flow Calculations	132
b. Fan-in-Nacelle.....	132
c. Fan-in-Fuselage	133
d. Fan-in-Wing	134
VI NONLINEAR BODY AERODYNAMICS	145
1. SAMPLE PROBLEM	145
a. Description of Body Coordinate System	145
b. Body Description for Nonlinear Force and Moment Program	147
c. Modification of Mapping Function for Body Aerodynamics Program	148

TABLE OF CONTENTS (Continued)

Section	Page
d. Simplified Handbook Method for Obtaining Coefficients	150
e. Viscous Cross Flow Input	150
2. SAMPLE COMPUTATIONS FOR TEST BODY	152
a. Sample Inputs for Force and Moment Program.....	152
b. Sample Outputs from Force and Moment Program.....	159
3. COMPARISON WITH TEST DATA	161
VII NONLINEAR WING AERODYNAMICS	166
1. SAMPLE PROBLEM	166
a. Determination of Section Parameters.....	167
b. Inputs to Nonlinear Wing Aerodynamics Program for Sample Problem.....	167
c. Outputs to Nonlinear Wing Aerodynamics Program for Sample Problem.....	170
d. Method Applicability and Limitations	170
2. COMPARISON WITH TEST DATA	171
APPENDIX I - WIND TUNNEL TESTING OF V/STOL CONFIGURATION MODEL	175
1. MODEL AND APPARATUS	175
2. TEST PROCEDURE.....	176
a. Balance Calibration and Corrections	176
b. Calibration of Engine Simulators	177
c. Wall Corrections.....	178
d. Test Parameters.....	178
e. Test Program.....	179
3. RESULTS	180
a. Presentation of Results	180
b. Selection of Unpowered Baseline Data	180
APPENDIX II - BALANCE CORRECTIONS AND CALIBRATION.....	220
APPENDIX III - EFFECT OF FORWARD SPEED ON EJECTOR JET ENGINE SIMULATORS	222
APPENDIX IV - NORMAL FORCE AND PITCHING MOMENT IN THE LIFT JET WAKE	225
REFERENCES	228

LIST OF ILLUSTRATIONS

Figure		Page
1	Mapping Program Input Data for Sample Problem (Wing).	8
2	Mapping Program Output Data for Sample Problem (Wing).	10
3	Comparison of Original and Mapped Airfoil.	15
4	Coordinate System for Typical Wing.	19
5	Jet Flow Field Program Input Data for Sample Problem (Wing; Transformation Method)	21
6a	Input Parameters for Sample Problem	23
6b	Jet Centerline for Sample Problem	23
6c	Induced Velocity Components at Station $Y = 0$	24
6d	Induced Velocity Components at Station $Y = 20.125$	25
7	Jet Flow Field Program Punched Output for Sample Problem (Wing; Transformation Method)	26
8	Control Points on Wing for Sample Problem	32
9	Jet Flow Field Program Input Data for Sample Problem (Wing; Lifting Surface Theory)	33
10	Induced Velocity Components at Control Points.	35
11	Jet Flow Field Program Punched Output for Sample Problem (Wing; Lifting Surface Theory)	35
12	Transformation Method Program Input Data for Sample Problem (Wing)	37
13	Partial List of Input Data for Sample Wing	40
14	Correspondence Between Angular Increments of Mapping Circles and Cartesian Coordinates of Wing Sections.	41
15	Power-Effect Pressure Coefficients on Sample Wing After Application of Segment Method.	43
16	Power-Effect Pressure Coefficients on Sample Wing After Residual Source and Sink Modification.	44
17	Power-Effect Pressure Coefficients on Sample Wing After One Iteration	45
18	Power-Effect Pressure Coefficients on Sample Wing After Residual Source and Sink Modification (Second Time).	46
19	Power-Effect Pressure Coefficients on Sample Wing After Two Iterations	47

LIST OF ILLUSTRATIONS (Cont'd)

Figure		Page
20	Forces and Moments on Sample Wing by Transformation Method	48
21a	Power-Effect Pressure Coefficients on Sample Wing at Station $Y = 5.04$, $U_{\infty}/U_j = 0.2$, $\alpha = \beta = 0^\circ$, Lift Jet	49
21b	Power-Effect Pressure Coefficients on Sample Wing at Station $Y = 7.7925$, $U_{\infty}/U_j = 0.2$, $\alpha = \beta = 0^\circ$, Lift Jet	50
21c	Power-Effect Pressure Coefficients on Sample Wing at Stations $Y = 10.545$ and $Y = 16.05$, $U_{\infty}/U_j = 0.2$, $\alpha = \beta = 0^\circ$, Lift Jet	51
22	Power-Effect Lift for Wing with Lift Jet	53
23	Configurations Tested at Northrop	54
24	Power-Effect Pressure Coefficients on Northrop Wing at Station $Y = 2.0$, $U_{\infty}/U_j = 0.1$, $\alpha = \beta = 0^\circ$, Two Midspan Jets at $X/C = 0.5$ and 0.8	55
25	Power-Effect Pressure Coefficients on Northrop Wing at Station $Y = 2.0$, $U_{\infty}/U_j = 0.1$, $\alpha = \beta = 0^\circ$, Two Midspan Jets at $X/C = 0.2$ and 0.5	56
26	Downwash Control Points on Wing.	59
27	Lifting Surface Theory Program Input Data for Sample Problem	60
28	Lifting Surface Theory Program Printed Output for Sample Problem	65
29a	Interference Lift for Vectored Thrust, Forward Position, 90° Deflection Angle	69
29b	Interference Lift for Vectored Thrust, Forward Position, 45° Deflection Angle	70
29c	Lift for Vectored Thrust, Forward Position, 90° Deflection Angle	71
29d	Interference Lift for Vectored Thrust, Aft Position, 90° Deflection Angle	72
29e	Interference Lift for Vectored Thrust, Aft Position, 45° Deflection Angle	73
29f	Induced Lift Versus Angle of Attack, Lift Jet ($U_{\infty}/U_{j0} = .20$)	74
29g	Induced Lift Versus Angle of Attack, Vectored Thrust, Forward Position, 90° Deflection Angle ($U_{\infty}/U_{j0} = .20$)	75
30	Station 264.25 of Test Model Fuselage	78

LIST OF ILLUSTRATIONS (Cont'd)

Figure		Page
31	Inputs to Mapping Program for Section at Station 264.25	79
32	Output of Mapping Function Program at Test Fuselage Station 264.25	81
33	Mapping of Fuselage at Station 264.25.	85
34	Jet Flow Field Program Input Data for Sample Problem (Fuselage)	89
35a	Input Parameters for Sample Problem	91
35b	Jet Centerline for Sample Problem	91
35c	Induced Velocity Components at Stations 23.7 and 497	92
36	Jet Flow Field Program Punched Output for Sample Problem (Fuselage)	94
37	Transformation Method Program Input Data for Sample Problem (Fuselage)	99
38	Partial List of Input Data for Sample Fuselage	101
39	Correspondence Between Angular Increments of Mapping Circles and Cartesian Coordinates of Fuselage Sections	102
40	Power-Effect Pressure Coefficients on Sample Fuselage After Application of Segment Method	106
41	Power-Effect Pressure Coefficients on Sample Fuselage After One Iteration.	109
42	Forces and Moments on Sample Fuselage by Transformation Method	112
43a	Power-Effect Pressure Coefficients on Sample Fuselage at Stations $X = 73.0$ and $X = 118.0$, $U_{\infty}/U_j = 0.2$, $\alpha = \beta = 0^\circ$, Lift Jet	113
43b	Power-Effect Pressure Coefficients on Sample Fuselage at Station $X = 185.5$, $U_{\infty}/U_j = 0.2$, $\alpha = \beta = 0^\circ$, Lift Jet	114
43c	Power-Effect Pressure Coefficients on Sample Fuselage at Station $X = 264.25$, $U_{\infty}/U_j = 0.2$, $\alpha = \beta = 0^\circ$, Lift Jet	115
43d	Power-Effect Pressure Coefficients on Sample Fuselage at Station $X = 343.0$, $U_{\infty}/U_j = 0.2$, $\alpha = \beta = 0^\circ$, Lift Jet	116
44a	Power-Effect Pressure Coefficients on Fuselage at Stations $X = 73.0$ and $X = 118.0$, $U_{\infty}/U_j = 0.2$, $\alpha = 0^\circ$, $\beta = 10^\circ$, Lift Jet	117

LIST OF ILLUSTRATIONS (Cont'd)

Figure		Page
44b	Power-Effect Pressure Coefficient on Fuselage at Station $X = 185.5$, $U_{\infty}/U_j = 0.2$, $\alpha = 0^\circ$, $\beta = 10^\circ$, Lift Jet	118
44c	Power-Effect Pressure Coefficients on Fuselage at Stations $X = 264.25$ and $X = 343.0$, $U_{\infty}/U_j = 0.2$, $\alpha = 0^\circ$, $\beta = 10^\circ$, Lift Jet	119
45	Power-Effect Lift for Fuselage Alone with Lift Jet	120
46a	Power-Effect Pressure Coefficients on Northrop Body at Stations $X = 8.1$ and $X = 8.9$, $U_{\infty}/U_j = 0.1$, $\alpha = \beta = 0^\circ$, Center Jet at $X = 10.0$	121
46b	Power-Effect Pressure Coefficients on Northrop Body at Stations $X = 11.1$ and $X = 11.9$, $U_{\infty}/U_j = 0.1$, $\alpha = \beta = 0^\circ$, Center Jet at $X = 10.0$	122
47	Lift Jet Power Induced Downwash at Rake Location	126
48	Lift Jet Power Induced Sidewash at Rake Location	127
49	Fan-in-Nacelle Configuration	133
50	Fan Flow Parameters	137
51	Fan-in-Nacelle, Inlet Leading	138
52	Fan-in-Nacelle, Inlet Trailing	139
53	Fan-in-Fuselage, Propulsion Parameters	140
54	Fan-in-Fuselage	141
55	1/6-Scale XV-5A, Fan-in-Wing, Lift Force	142
56	1/6-Scale XV-5A, Fan-in-Wing, Drag Force	143
57	1/6-Scale XV-5A, Fan-in-Wing, Pitching Moment	144
58	Sign Convention for Body Aerodynamic Coefficients	146
59	Change of Mapping Function for Body Aerodynamics Program	149
60	Nonlinear Body Aerodynamics Program Input Data for Sample Body	154
61	Nonlinear Body Aerodynamics Program Output for Sample Problem	160
62	Theory and Test Conditions of C_N and C_m for Wind Tunnel Test Model Fuselage	162
63	Theory and Test Comparison of C_y and C_n for Wind Tunnel Test Model Fuselage	163

LIST OF ILLUSTRATIONS (Cont'd)

Figure		Page
64	Computed C_{N_q} and C_{m_q} for Wind Tunnel Test Model Fuselage	164
65	Computed C_{y_r} and C_{n_r} for Wind Tunnel Test Model Fuselage	165
66	Wing Planform with Lifting Lines and Downwash Control Line Shown	166
67	Nonlinear Wing Aerodynamics Program Input Data for Sample Problem	169
68	Sample Outputs for Nonlinear Wing Aerodynamics Program	172
69	Wing Calculations for an Aspect Ratio 6 Wing	173

APPENDIX ILLUSTRATIONS

I-1	Model General Arrangement	192
I-2	Wing-Body-Nacelle with Tail Flow Angularity Rake, Powered by Small Forward Nozzles	193
I-3	Wing-Body-Nacelle-Tail with Flap, Powered by Aft Small Nozzles	194
I-4	Wing-Body-Tail, Powered by Lift Jet	195
I-5 a	Ejector Operating Characteristics Forward Small Nozzles.	196
I-5 b	Ejector Operating Characteristics Aft Small Nozzles.	197
I-5 c	Ejector Operating Characteristics Aft Large Nozzles	198
I-6	Typical Exit Profiles Along Longitudinal Nozzle Centerline	199
I-7	Circumferential Fuselage Pressure Ports	200
I-8	Nacelle Centerline Pressure Ports	202
I-9	Air Supply Sting - Balance Assembly	203
I-10	Effect of Model Height, $\alpha = 6^\circ$	204
I-11	Effect of Free Flow Through Inlet on Model Aerodynamic Loads	205
I-12	Inlet Weight Flow for Unpowered Ejector	206
I-13	Thrust Due to Free Flow Inlet.	207
I-14	Effect of Open Inlet on Power Model Loads	208

APPENDIX ILLUSTRATIONS (Cont'd)

Figure		Page
I-15	Unpowered Aerodynamic Coefficients	209
I-16	Effect of Free Flow Through Inlet on Wing Pressure Loading	210
I-17	Effect of Free Flow Through Inlet on Section Pressure Loading	211
I-18	Effect of Free Flow Through Inlet on Fuselage Pressures	212
I-19	Effect of Free Flow Through Inlet on Nacelle Centerline Pressures	215
I-20	Free Flow Inlet Effect on Lower Fuselage Centerline Pressures	216
I-21	Effect of Free Flow Through Inlet on Downwash at the Tail Flow Angularity Rake	217
I-22	Free Flow Inlet Effect on Lower Fuselage Centerline Pressures	218
I-23	Effect of Open Inlet on Lower Fuselage Centerline Pressures with Forward and Aft Nozzles	219
III-1	Effect of Forward Speed on Inlet Flow from Bellmouth Measurements	224
IV-1	Jet Wake Contributions to Fuselage Lift	226
IV-2	Jet Wake Contributions to Fuselage Pitching Moment	227

LIST OF SYMBOLS

SECTION V

A_f	fan flow area
\bar{c}	mean aerodynamic chord
C_{D_0}	drag coefficient at $\alpha = 0$ deg, D/QS
$C_{D_0}^s$	slipstream drag coefficient at $\alpha = 0$ deg, $D/q^s A_f$
$C_{D_{SCB}}$	fan centerbody drag area
C_F	fan thrust coefficient, T_f/QS
C_{L_0}	lift coefficient at $\alpha = 0$ deg, L/QS
$C_{L_0}^s$	slipstream lift coefficient at $\alpha = 0$ deg, $L/q^s A_f$
C_{m_0}	pitching moment coefficient at $\alpha = 0$ deg, $M/QS \bar{c}$
$C_{m_0}^s$	slipstream pitching moment coefficient at $\alpha = 0$ deg, $M/q^s A_f D_f$
C_t	fan pressure rise coefficient, $\Delta P / \frac{1}{2} \rho U_t^2$
D	drag force
D_f	effective fan diameter, $\sqrt{4A_f/\pi}$
D_L	inlet lip lift force
K	ratio of freestream component of velocity at fan entrance to freestream velocity
L	lift force
L_L	inlet lip lift force
L_s	inlet surface lift force
M	pitching moment
$M_{/L}$	inlet lip rolling moment

M_{l_s}	inlet surface rolling moment
M_{M_L}	inlet lip pitching moment
M_{M_S}	inlet surface pitching moment
q^s	slipstream dynamic pressure, $Q + T_o/A_f$
Q	freestream dynamic pressure
r	radius
R_l	inlet "lip" radius
S	wing area or reference area
T_f	thrust of fan rotor
T_o	total static lift
U_f	fan flow velocity corresponding to A_f
U_{jt}	static fan flow velocity
U_t	fan tip speed
U	freestream velocity
α	angle of attack
β	angle of sideslip
η	inlet dynamic head recovery factor
ρ	density
Θ	reference angle in plane of inlet surface

APPENDIX I

A_j	total area of operating nozzles
b	wing span
c	local chord
\bar{c}	wing mean aerodynamic chord
C_D	drag coefficient, D/QS
C_L	lift coefficient, L/QS
C_M	moment coefficient, $M/QS\bar{c}$
C_p	pressure coefficient, $(P - P_\infty)/Q$

C_T	thrust coefficient, T/Q_S
D	drag force, jet diameter
D_e	effective jet diameter, $\sqrt{4A_j/\pi}$
FS	fuselage station
h	height above tunnel floor. measured to center of lift jet exit
L	lift force
L_f	fuselage reference length, 50 inches
M_y	pitching moment
P	pressure
P_{ep}	ejector primary nozzle plenum pressure
P_o	ambient pressure
P_T	total pressure
Q	freestream dynamic pressure, $\frac{1}{2}\rho_\infty U_\infty^2$
r	radius
R_j	jet radius
S	wing area
T	total thrust
T'	thrust of one nozzle
U	velocity
V/V_j	effective velocity ratio, $\sqrt{2A_j Q/T}$
\dot{w}_p	ejector primary nozzle weight flow
\dot{w}_s	ejector secondary (inlet) weight flow
WL	waterline
WS	wing station (butt line)
x	distance aft of wing leading edge
X	distance aft of longitudinal reference
Y	lateral distance
Z	vertical distance
α	angle of attack
δ	deflection, ratio of pressure to standard pressure
ϵ	downwash angle
λ	ratio of specific heats
Θ	ratio of temperature to standard temperature
ρ	density

Subscripts:

j	jet
F	flap
H	horizontal
V	vertical
∞	freestream condition

APPENDIX II

A	axial force
\tilde{F}_{BAL}	matrix of loads measured by balance
\tilde{F}_C	matrix of corrected loads exerted on model
\tilde{K}	matrix of balance-coupling correction coefficients
M_x	rolling moment
M_y	pitching moment
M_z	yawing moment
N	normal force
Y	side force

APPENDIX III

A_j	jet exit area
Q	freestream dynamic pressure
T	thrust
T_o	thrust under static conditions
U_j	jet exit velocity
U_{j_o}	jet exit velocity under static conditions
V/V_j	effective velocity ratio
\dot{w}_s	ejector secondary (inlet) weight flow
δ_j	jet deflection angle
ρ	density

SECTION I

INTRODUCTION

This volume is the second of three volumes treating V/STOL Aerodynamic prediction methods. This volume is directed toward presenting applications of the methods developed during the study program. These applications represent the complete prediction techniques developed except for empirical methods for treating power effects on wings and bodies which are presented in Volume I.

1. PURPOSE

The purpose of this volume is to demonstrate the use of the prediction methods in computing the aerodynamic coefficients and derivatives of V/STOL aircraft. To accomplish this purpose example problems are worked out using the prediction techniques. The accuracy of the methods can be assessed by comparing the predicted aerodynamic coefficients against test results. Limitations of the methods are described and the necessary assumptions and simplifications which must be made are pointed out. It should be possible for the user to evaluate the described methods and to assess their limitations for use in his problems by examining the included sample problems.

2. SCOPE

The methods which are applied in this volume represent the theoretical prediction techniques which have been developed during the study contract. The one theoretical technique which is not presented is the vortex tracking method which is not applied to a given example problem since the method was not operable. Also not included in this volume are the empirical methods for treating wing or body. These methods are treated completely in Volume I.

In presenting samples of the use of the method the specific nature of the chosen problem often does not demonstrate the full capability of the methods being employed. To further demonstrate the method capabilities it is frequently pointed out where the methods are more general and where different problems can be treated by the same methods.

3. TECHNICAL APPROACH

The method of demonstrating the application of the individual methods which was adopted for this volume was to select a sample problem and to apply the methods to this problem where applicable. The details involved in using each method are explained by presenting a complete treatment of the sample problem. Where computer programs are involved complete inputs, outputs and comparison of results with experiments are presented. Where computer programs are not involved the equations used are presented and comparison with experiment is presented.

Sample problems have been chosen where test data is available for comparison with theoretical results. This permits the accuracy of the prediction techniques to be evaluated and permits a better understanding of the difficulties to be encountered in predicting the aerodynamics of V/STOL aircraft.

4. ORGANIZATION OF VOLUME II

The main body of Volume II is devoted to sample problems treating V/STOL aircraft configurations. The treatment is divided into sections considering the power induced effects and the power off effects.

Section II presents two methods of treating power effects on the wing of a V/STOL configuration. Each of these methods has certain advantages for the user and both will be useful in treating power induced effects on wings.

Section III presents the method of predicting power induced effects on the fuselage and illustrates the accuracy which can be obtained.

Section IV demonstrates the use of the prediction methods in obtaining downwash and sidewash effects at the empennage location and illustrates how these results can be used to estimate power effects on the tail surfaces.

Section V presents the method applicable to predicting the power effects of the inlets. Comparisons are made with test data to illustrate the accuracy of the method.

Sections VI and VII present the methods for treating the unpowered effects of nonlinear body and wing aerodynamics. Section VI presents the nonlinear body method and shows comparisons with test data. Section VII presents similar comparisons for wing aerodynamics.

Four appendices are added to this volume to complete the documentation of work performed under the contract. The first three appendices describe the wind tunnel test program undertaken during the study. This description is presented in this volume to permit the details of the test program and model description to be available to the user. This is desirable since much of the test data used for comparison with the prediction method came from the test program. A method for estimating normal force and pitching moment in the lift jet wake region is presented in Appendix IV.

SECTION II

POWER EFFECTS ON THE WING

There are two alternative procedures for computing the power induced effects on the wing. The first of these combines the mapping method, the jet flow field program and the transformation method. In this method the mapping program is used to describe the wing, the jet program calculates velocities induced by the jet at the wing surface and the transformation method calculates pressures, forces and moments induced by the jet on the wing.

In the second procedure the jet program is used in conjunction with the lifting surface theory to predict power induced wing effects. The jet program computes a downwash field at the wing plane which gives an effective camber distribution for the wing. The lifting surface theory then utilizes this camber distribution to compute lift and pitching moment on the wing. This method does not give the pressure distribution about the wing but is simpler and easier to use than the first method.

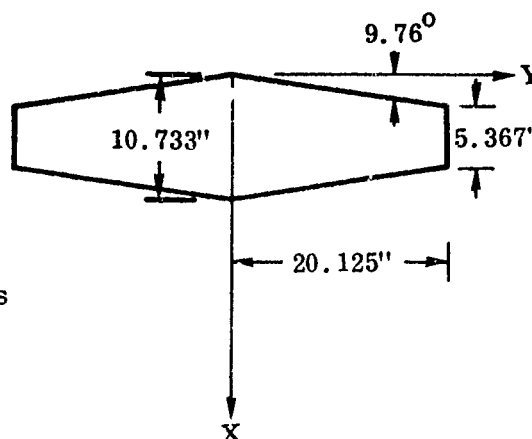
The following subsections will describe the use of both of these methods as applied to a given wing. The use of the methods will be described in detail so that a complete understanding of the methods can be obtained.

1. SAMPLE PROBLEM

To demonstrate the method of predicting the power induced aerodynamic effects on a wing, a sample problem is given. This problem is for a single jet in the presence of an isolated wing. The wing of the sample problem is the one tested in the configuration wind tunnel test program discussed in Appendix I.

Wing Description:

Root chord: 10.733 inches
 Tip chord: 5.367 inches
 Semispan: 20.125 inches
 Leading Edge sweep: 9.76 degrees
 Section: NACA 63A010 at all wing stations



Section coordinates:

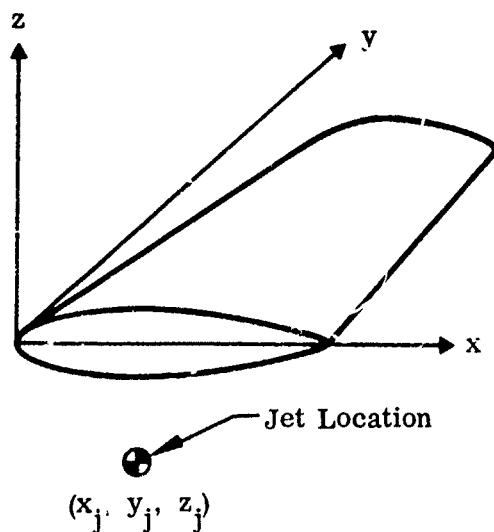
x (Percent c)	z (Percent c)
0	0
0.25	0.555
0.5	0.816
0.75	0.983
1.25	1.250
2.5	1.737
5.0	2.412
7.5	2.917
10	3.324
15	3.950
20	4.400
25	4.714
30	4.913
35	4.995

x (Percent c)	z (Percent c)
40	4.968
45	4.837
50	4.613
55	4.311
60	3.943
65	3.517
70	3.044
75	2.545
80	2.040
85	1.535
90	1.030
95	0.525
100	0.021

Leading Edge radius 0.742 percent c

Jet location and description:

A sketch of the coordinate system defining the jet location relative to the wing is shown below.



For the sample problem:

$$x_j = .6 \text{ inches}$$

$$y_j = 0$$

$$z_j = -6.635 \text{ inches (positive upward)}$$

$$\text{Jet diameter } d_j = 2.25 \text{ inches}$$

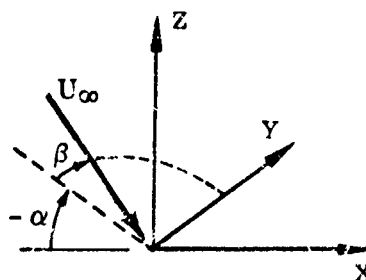
The jet exhausts into the mainstream along the negative z -direction, that is perpendicular to the wing planform.

$$\text{Velocity ratio } \frac{U_\infty}{U_{j_0}} = .2$$

Wing attitude:

$$\text{Angle of attack } \alpha = 0 \text{ degrees}$$

$$\text{Sideslip angle } \beta = 0 \text{ degrees}$$



2. APPLICATION OF MAPPING METHOD TO THE WING

In the sample problem all the wing sections are geometrically similar so that it is only necessary to map a single section and then to scale the coefficients to provide a mapping for different spanwise stations. Figure 1 shows the inputs to the mapping program used to obtain the initial mapping.

The first card lists in order the number of coordinates being input, the number of corners (and pseudo-corners) being input, the number of terms to be taken in the expansion for the potential and the mapping, and a zero to indicate that the section being mapped is symmetrical about the x-axis.

Cards 2 through 5 give the x-coordinates selected as input points starting at the section trailing edge and proceeding around to the nose. Cards 6 through 9 are the z-coordinates of the airfoil at the same points. Since the section is symmetrical only the upper half plane coordinates are input.

Card number 10 specifies that the airfoil is to be shifted .5 units in the negative x-direction. This is necessary since to obtain the mapping it is necessary that the airfoil be centered with respect to the origin to some degree. It is not necessary to center the section exactly but it should be centered somewhere near the centroid of area.

Card 11 specifies which input points are corner points. This card indicates that the first input point (the trailing edge) is a corner point. The second number, the zero, indicates that the second corner is a pseudo-corner; that is, is not a true corner but merely indicates a region of large curvature. This second number refers to the nose of the airfoil.

Card 12 specifies the x and z coordinates of the first corner and the angle turned through at the corner in radians.

Card 13 similarly describes the second corner specifying the location of the center of the leading edge radius and specifying that a corner of π radians is turned. This angle turned is only an approximation; it is not necessary to specify the angle exactly.

Card 14 specifies parameters needed to tell the program how to write out the mapped section with the corners included. The first two numbers are the x- and z-coordinates of the initial point to be mapped, in this case the leading edge point. The third and fourth numbers specify the first and last points to be mapped specified as angular distances around the mapping circle. In the sample section the mapping is to start at the nose (180 degrees) and proceed around the lower surface until just

ahead of the trailing edge (355 degrees). The last number specifies that mapped points are to be obtained at increments about 5 degrees apart. In this example, it was necessary to choose these parameters to avoid specifying the trailing edge as one of the end points. This is because the trailing edge is a corner and a corner point cannot be specified as one of the end points.

Card 15 specifies the necessary parameters needed to map out points on the section with the corners removed. This card specifies that 37 points are to be printed out with a spacing increment of 5 degrees about the mapping circle and that the mapping is to start at $\theta = 0$ degrees on the mapping circle.

The outputs of the mapping functions for the inputs of Figure 1 are shown in Figure 2. The first page of outputs, Figure 2(a), relates to the computations made in calculating the potential and the point-to-point correspondence between points on the section and points on the mapping circle.

The first two columns represent x- and y-coordinates of the input points with the x-coordinate shifted by the incremental value of ΔX input (in this case, -.5). The third column represents the distance, R, from the new origin to the point on the section. The fourth column gives the computed perimeter, S, of the section from the positive real axis to the point in question. The fifth column gives the velocity, V, calculated due to the unit vortex about the body. The velocities written out for corner points are meaningless. ALPHA is the angle of the section slope at each point as calculated in the program. OMEGA specifies the angular distance in degrees around the section measured about the new origin. THETA is the predicted angular distance of the points around the mapping circle in degrees.

The second page of printouts, Figure 2(b), represents the results obtained by computing the derivative of the mapping function with the corners contained explicitly and integrating the resulting expression numerically. The location of the first point was specified as explained above (this point is not printed out). The three columns give the x-coordinate, the y-coordinate and the angle around the mapping circle θ for a series of points as specified by the parameters specified in the input cards. The degree to which these points agree with the original section represents the degree of accuracy obtained by using the mapping method.

The third page of outputs, Figure 2(c), represents the results of multiplying out factors representing any corner singularities and integrating the resulting expression analytically.

COMPUTATIONS FOR S AND ALPHA VERSUS THETA.

X	Y	R	S	V	ALPHA	UMEGA	THETA
0.5000E 00	0.0	0.5000E 00	0.0	0.0	0.17424E 03	0.0	0.0
0.4500E 00	0.5250CE-02	0.45003E 00	0.50275E-01	0.44006E 01	0.17395E 03	0.66842E 00	0.24190E 02
0.4000E 00	0.10300E-01	0.40013E 00	0.10053E 00	0.32384E 01	0.17438E 03	0.14750E 01	0.34865E 02
0.3500E 00	0.15350E-01	0.35034E 00	0.15078E 00	0.27429E 01	0.17416E 03	0.25112E 01	0.43375E 02
0.3000E 00	0.20400E-01	0.30069E 00	0.20104E 00	0.24635E 01	0.17427E 03	0.38901E 01	0.50816E 02
0.2500E 00	0.25450E-01	0.25129E 00	0.25129E 00	0.22869E 01	0.17423E 03	0.58127E 01	0.57618E 02
0.2000E 00	0.30440E-01	0.20230E 00	0.30154E 00	0.21695E 01	0.17441E 03	0.86540E 01	0.64003E 02
0.1500E 00	0.35170E-01	0.15407E 00	0.35176E 00	0.20901E 01	0.17482E 03	0.13196E 02	0.70106E 02
0.1000E 00	0.39430E-01	0.10749E 00	0.40195E 00	0.20395E 01	0.17545E 03	0.21519E 02	0.76019E 02
0.5000E-01	0.43110E-01	0.6019F-01	0.45208E 00	0.20643E 01	0.17615E 03	0.40768E 02	0.81864E 02
0.0	0.45130E-01	0.46130E-01	0.50217E 00	0.20645E 01	0.17696E 03	0.90000E 02	0.87752E 02
-0.5000E-01	0.48370E-01	0.69568E-01	0.55222E 00	0.20728E 01	0.17794E 03	0.13595E 03	0.93679E 02
-0.1000E 00	0.49680E-01	0.11166E 00	0.60224E 00	0.21647E 01	0.17908E 03	0.15358E 03	0.99759E 02
-0.1500E 00	0.49950E-01	0.15810E 00	0.65224E 00	0.22038E 01	0.18031E 03	0.16158E 03	0.10600E 03
-0.2000E 00	0.49130E-01	0.20595E 00	0.70225E 00	0.22752E 01	0.18159E 03	0.16620E 03	0.11238E 03
-0.2500E 00	0.47140E-01	0.25441E 00	0.75229E 00	0.23949E 01	0.18294E 03	0.16932E 03	0.11905E 03
-0.3000E 00	0.44000E-01	0.30321E 00	0.80239E 00	0.25832E 01	0.18430E 03	0.17165E 03	0.12615E 03
-0.3500E 00	0.39500E-01	0.35222E 00	0.85259E 00	0.28873E 01	0.18606E 03	0.17356E 03	0.13396E 03
-0.4000E 00	0.33240E-01	0.40130E 00	0.90299E 00	0.34334E 01	0.18843E 03	0.17525E 03	0.14297E 03
-0.42500E 00	0.29170E-01	0.42600E 00	0.92832E 00	0.39114E 01	0.19020E 03	0.17607E 03	0.14826E 03
-0.45000E 00	0.24120E-01	0.45065F 00	0.95383E 00	0.47294E 01	0.19295F 03	0.17693E 03	0.15450E 03
-0.47500E 00	0.17370E-01	0.47532E 00	0.97973E 00	0.65641E 01	0.19855E 03	0.17790E 03	0.16264E 03
-0.48750E 00	0.12500E-01	0.48766E 00	0.99316E 00	0.88241F 01	0.20550E 03	0.17853E 03	0.16843E 03
-0.49250E 00	0.9830CE-02	0.49260E 00	0.99883E 00	0.10311E 02	0.21143E 03	0.17885E 03	0.17153E 03
-0.49500E 00	0.8160CE-02	0.49507E 00	0.10018E 01	0.11066E 02	0.21771E 03	0.17905E 03	0.17336E 03
-0.49750E 00	0.55500F-02	0.49753E 00	0.10055E 01	0.11839E 02	0.23446E 03	0.17936E 03	0.17574E 03
-0.5000E 00	0.0	0.50000E 00	0.10118E 01	0.11821E 02	0.27739E 03	0.18000E 03	0.18000E 03

(a) COMPUTATIONS FOR S AND ALPHA VERSUS THETA

FIGURE 2. MAPPING PROGRAM OUTPUT DATA FOR SAMPLE PROBLEM (Wing)

SECTION MAPPING BY NUMERICAL INTEGRATION.

X	Y	THETA
C.16133E-02	-C.52736E-02	0.32289E 01
C.65728E-02	-C.10205E-01	C.33161E 01
C.15147E-01	-C.14651E-01	C.34034E 01
C.27545E-01	-C.18730E-01	C.34907E 01
C.43736E-01	-C.22711E-01	0.35779E 01
C.63415E-01	-C.26798E-01	C.36652E 01
C.86139E-01	-C.30974E-01	0.37525E 01
C.11154E 00	-C.35001E-01	0.38397E 01
C.13545E 00	-C.38570E-01	0.39270E 01
C.16536E 00	-C.41525E-01	0.40143E 01
C.20279E 00	-C.43853E-01	0.41015E 01
C.23805E 00	-C.45818E-01	0.41888E 01
C.27523E 00	-C.47569E-01	0.42760E 01
C.31378E 00	-C.49069E-01	0.43633E 01
C.35323E 00	-C.50050E-01	0.44506E 01
C.39337E 00	-C.50156E-01	0.45378E 01
C.43420E 00	-C.49166E-01	0.46251E 01
C.47584E 00	-C.47144E-01	0.47124E 01
C.51824E 00	-C.44415E-01	0.47796E 01
C.56108E 00	-C.41385E-01	0.48865E 01
C.60331E 00	-C.38323E-01	0.49742E 01
C.64563E 00	-C.35278E-01	0.50614E 01
C.68684E 00	-C.32083E-01	0.51487E 01
C.72614E 00	-C.28596E-01	0.52360E 01
C.76409E 00	-C.24835E-01	0.53232E 01
C.80041E 00	-C.21035E-01	0.54105E 01
C.83477E 00	-C.17491E-01	0.54978E 01
C.86667E 00	-C.14414E-01	0.55850E 01
C.89557E 00	-C.11795E-01	0.56723E 01
C.92105E 00	-C.94623E-02	0.57596E 01
C.94305E 00	-C.72019E-02	0.58468E 01
C.96148E 00	-C.49643E-02	0.59341E 01
C.97637E 00	-C.29018E-02	0.60214E 01
C.98757E 00	-C.12800E-02	0.61086E 01
C.99472E 00	-C.30513E-03	0.61959E 01

(b) SECTION MAPPING BY NUMERICAL INTEGRATION

FIGURE 2. (Continued)

RADIUS OF MAPPING CIRCLE = 0.26916E 00

REAL PARTS OF COEFFICIENTS.

C.6C815E-C1	0.75779E-03	0.69368E-04	C.12786F-06	-0.23231E-06	0.15404E-C6	0.11822E-07
-0.46527E-10	-0.44495CF-C9					

IMAGINARY PARTS OF COEFFICIENTS.

0.0	0.0	0.0	0.0	0.0	0.0	0.0
0.0	0.0	0.0				

(c) COEFFICIENTS OF MAPPING FUNCTION

FIGURE 2. (Continued)

MAPPING OF SECTION WITH CORNERS REMOVED.

X	Y
C.50544	C.C
C.50723	C.C0C87
C.50065	C.C0146
C.48975	O.00310
C.47484	O.00455
C.45603	O.C0667
C.43363	C.C0905
C.40792	C.C1178
C.37920	O.C1479
C.34770	O.01799
C.31370	C.C2131
C.27743	C.C2470
C.23915	O.02815
C.19013	C.C3164
C.15821	O.03516
C.11627	C.03861
C.07389	C.C4187
C.03142	O.C4476
-C.01084	C.C4711
-C.05268	C.C4878
-C.09391	C.C4970
-O.13436	C.C4984
-C.17382	C.C4526
-C.21207	O.04802
-C.24885	C.C4622
-C.24392	C.C4392
-C.31657	C.C4115
-O.34775	O.03810
-C.37601	O.C3471
-C.40151	O.C3107
-C.42400	C.C2721
-O.44325	C.C2315
-C.45921	C.C1889
-C.47165	O.C1441
-C.48055	C.C0575
-O.49588	O.00492
-C.44766	C.C0C00

(d) MAPPING OF SECTION WITH CORNERS REMOVED

FIGURE 2. (Concluded)

First, the radius of the mapping circle is printed out as computed. Next, the coefficients of the mapping function are written out - first the real parts a_n - then the imaginary parts b_n . The mapping function is written in the form

$$Z = \zeta + \frac{a_1 + ib_1}{\zeta} + \frac{a_2 + ib_2}{\zeta^2} + \dots + \frac{a_n + ib_n}{\zeta^n}$$

The coefficients are written out in order $a_1, a_2, a_3, \dots, a_n$ and for this particular case, all the imaginary parts of the coefficients are zero since the section is symmetrical.

Page four, Figure 2(d), prints out the x- and y-coordinates obtained with the analytically integrated mapping function. It is not possible to obtain the location of the body directly by this method of computation; i.e., the constant term in the above mapping is missing. This prevents the location of the section being mapped from being specified. This is readily remedied by plotting the original section and the mapped section and the displacement required to obtain a good fit between the two sections represents the constant term of the mapping.

Figure 3 shows a comparison between the mapped output and the original input section, the lower surface also being shown since the section is symmetrical and the mapping retains the property of symmetry.

To obtain coefficients for the wing of the sample problem it is necessary to change the coefficients to account for the size of the actual wing. The coefficients of Figure 2 are based on a unit chord and the mapping for this section can be written:

$$\frac{Z}{c} = \zeta_1 + a'_0 + \frac{a'_1}{\zeta_1} + \dots + \frac{a'_n}{\zeta_1^n} \quad (1)$$

where

$$a'_1 = .60815 \times 10^{-1}$$

$$a'_2 = .75779 \times 10^{-3}$$

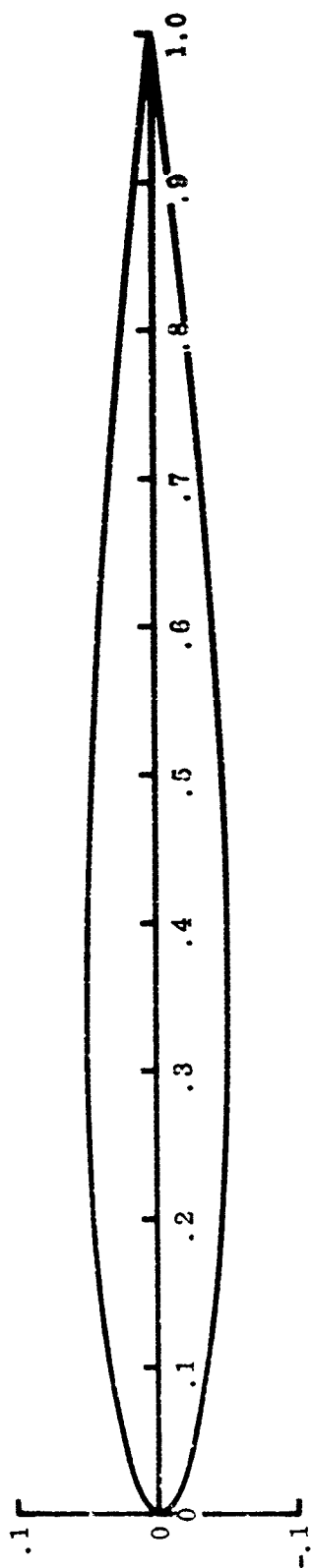
$$a'_3 = .69368 \times 10^{-4}$$

$$a'_4 = .12786 \times 10^{-6}$$

$$a'_5 = -.23231 \times 10^{-6}$$

$$a'_6 = 15.404 \times 10^{-6}$$

Original Airfoil



Mapped Airfoil

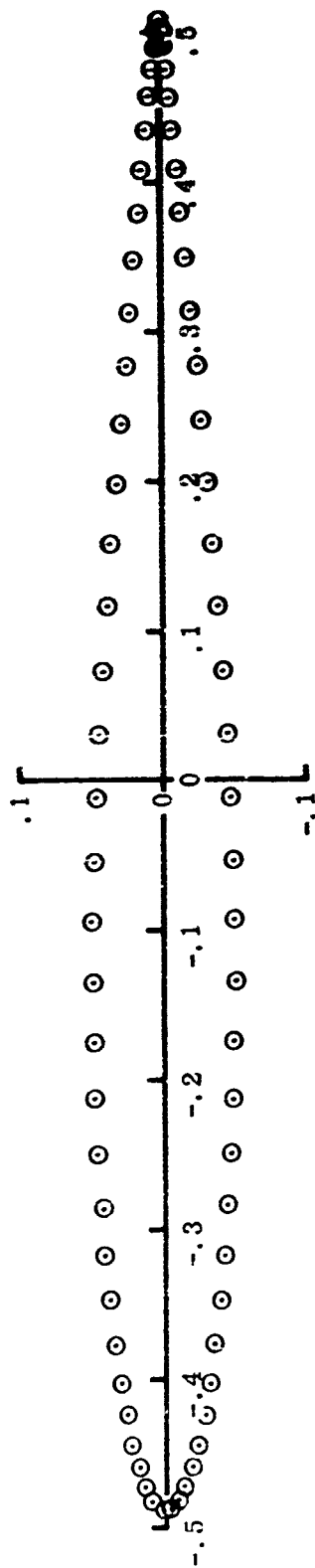


FIGURE 3. COMPARISON OF ORIGINAL AND MAPPED AIRFOIL

$$a'_7 = .11822 \times 10^{-7}$$

$$a'_8 = -.46527 \times 10^{-10}$$

$$a'_9 = -.44950 \times 10^{-9}$$

and

$$\zeta_1 = r'_c e^{i\theta} \quad r'_c = .26976$$

a'_0 has not been determined and it is best to leave this coefficient undefined until the coefficients have been ratioed up to true size.

It is desired to reexpress Equation (1) in the form:

$$Z = \zeta + a_0 + \frac{a_1}{\zeta} + \dots + \frac{a_9}{\zeta^9} \quad (2)$$

where the coefficients $a_0, a_1, a_2, \dots, a_9$ reflect the true wing dimensions at given stations along the wing. Rewriting Equation (1) in the form

$$Z = \zeta + a_0 + \frac{a_1}{\zeta} + \dots + \frac{a_9}{\zeta^9}$$

and equating $c_1 \zeta_1$ to ζ we obtain

$$Z = \zeta + c a'_0 + \frac{c^2 a'_1}{\zeta} + \frac{c^3 a'_2}{\zeta^2} + \dots + \frac{c^{10} a'_9}{\zeta^9}$$

so that it can be shown that

$$a_n = c^{n+1} a'_n \quad n = 1, 2, \dots, 9$$

The radius of the new mapping circle defined by $\zeta = r_c e^{i\theta}$ is now $r_c = c r'_c$

To obtain the coefficient a_0 it is sufficient to note that from the first and last numbers of the last page of Figure 2, the mapping without the constant coefficient maps the section about a chordwise point of .4891, so that for the origin of the wing located at the

nose of the root chord and a leading edge sweep of 9.76 degrees, the coefficient a_0 can be found as

$$a_0 = .4891c + y \cdot \tan 9.76 \text{ degrees,}$$

$$\text{where } c = c_r - (c_r - c_t) y / b/2$$

For use in the transformation method, it is also necessary to define $\frac{dr_c}{dy}$ for the wing.

This can be done by noting that

$$r_c = .26916 c$$

$$\frac{dr_c}{dy} = .26916 \frac{dc}{dy}$$

It is now possible to compute all of the numbers needed for the transformation method.

These numbers are tabulated in Table 1.

TABLE I. COEFFICIENTS FOR WING OF SAMPLE PROBLEM

WING STA	r_c	dr_c/dy	a_0	a_1	a_2	a_3	a_4	a_5	a_6	a_7	a_8	a_9
0	2.8839	0.0	5.2495	7.0057	.93694	.92054	.018211	-.35514	2.5274	2.0819	-.087942	-9.1189
2.5	2.7094	-.071767	5.3533	6.1820	.77289	.71218	.013214	-.24166	1.6130	1.2461	-.049365	-4.8006
5.04	2.5272	-.071767	5.4592	5.3613	.62724	.53911	.0093299	-.15916	.99091	.71404	-.026385	-2.3934
7.7925	2.3296	-.071767	5.5735	4.5556	.49130	.38925	.0062097	-.097650	.56041	.37224	-.012680	-1.0602
10.545	2.1320	-.071767	5.6880	3.8157	.37661	.27307	.0039869	-.057378	.39137	.18320	-.0057112	-.43705
13.00	1.9559	-.071767	5.7903	3.2114	.29079	.19343	.0025909	-.034208	.16483	.091926	-.0026290	-.18457
16.050	1.7372	-.071767	5.9174	2.5332	.20372	.12036	.0014318	-.016790	.071852	.035590	-.00090399	-.056366
20.125	1.4446	-.071767	6.0867	1.7518	.11715	.057555	.00056937	-.0055521	.019759	.0081385	-.00017191	-.0089134

3. APPLICATION OF JET FLOW FIELD THEORY TO WING

a. Transformation Method

The purpose of the Jet Flow Field theory, when used in conjunction with the Transformation Method, is to predict jet-induced velocity components at those control points on the wing at which the Transformation Method requires them to evaluate power effects. This is accomplished by executing the Jet Flow Field computer program to generate the required data for the Transformation Method in the form of punched data cards. To insure compatibility with the Transformation Method, the control points on the wing are specified by utilizing the mapping coefficients for the wing cross sections obtained by the procedure described in Section II.2. The punched output is generated in a manner to provide a continuous block of input data to the Transformation Method computer program. Both of the above features will be described in greater detail in the discussion below.

(1) Sample Problem Computation

For the sample problem being considered, the Jet Flow Field program is now used to compute the jet-induced velocities at the eight spanwise stations on the wing described in Section II.2. Figure 4(a) shows a sketch of the wing and the location of the jet with respect to the input/output coordinate system. Figure 4(b) defines the jet exhaust angles ϕ and ψ . It should be noted that the input/output coordinate system shown below differs from the general coordinate system utilized in Section II, Volume I.

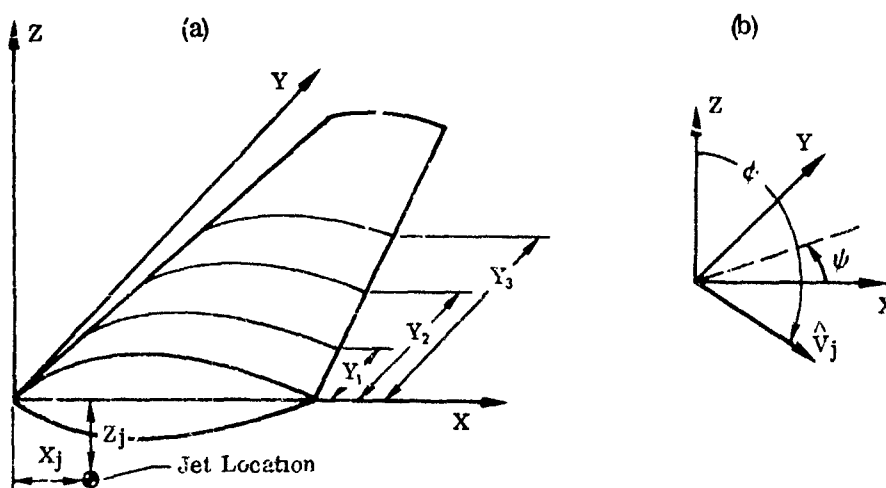


FIGURE 4. COORDINATE SYSTEM FOR TYPICAL WING

(a) Input for Sample Problem

The input cards required for the sample problem are tabulated in Figure 5.

Card 1 lists three control indices. The first one, $MULT = 1$, indicates that a single jet configuration is being treated. The second one, $IGEQM = 1$, specifies that control points on wing cross sections will be generated, utilizing the mapping coefficients obtained in Section II. 2. The third control index, $IPUNCH = 1$, generates the punched output for the Transformation Method program.

Card 2 specifies angle of attack $\alpha = 0$, and angle of sideslip $\beta = 0$.

Card 3 controls the number of steps and the step size in the numerical integration of the equations of motion for the jet path. For the sample problem, 90 steps with a step size of 0.4 jet exit diameters are chosen.

Cards 4 and 5 contain information about the jet. The jet location in the coordinate system of Figure 4 is $X = 0.6$, $Y = 0.$, $Z = -6.63$. The jet exhaust angles ϕ and ψ , defined in Figure 4(b) are 180 and 0 degrees respectively. The jet exit diameter, $d_0 = 2.25$ and the velocity ratio $U_\infty/U_{j0} = 0.2$.

Card 6 may be left blank for computations involving a single jet. For a multiple-jet configuration it would be used to control the geometry of the jet resulting from the intersection of two other jets.

The remaining input cards provide data to generate the control points at which jet-induced velocities are to be evaluated. These control points are generated by utilizing the mapping coefficients and mapping radii obtained in Section II. 2 for the eight wing stations of the sample problem. The number of control points generated at each spanwise station is governed by the input variable $NTHT$, which is the number of increments $\Delta\theta$ into which the mapping circle is to be divided in the Transformation Method computer program.

Card 7 specifies that $NTHT$, the number of control points at each spanwise station or the number of $\Delta\theta$ increments around the mapping circle is 36, and that the number of spanwise stations $NS = 8$. It also defines the number of terms used in the mapping expansion of Section II. 2, $NCOEf = 11$, and through the control index $IRECT = 1$ indicates that the wing is nonrectangular.

Cards 8 - 12 provide the data from which the wing cross section at the first spanwise station can be generated by the computer program. Card 8 specifies the location of the station, $Y = 0.$, the mapping circle radius $R = 2.8889$ and the rate of

change of R with Y , $DRDY = 0$. Cards 9 — 12 list the real and imaginary parts of the coefficients to be used in the mapping expansion. Cards 13 — 47 are similar data blocks for the spanwise stations $Y = 2.5, 5.04, 7.7925, 10.545, 13., 16.05$ and 20.125 . The data in cards 8 — 47 are taken from the Table I in Section II.2.

Note: The rate of change of the mapping circle radius with spanwise distance, $DRDY$, is not required for any of the computations performed by the Jet Flow Field program. It will, however, be required by the Transformation Method program and is read as part of the input that it may be punched out in the proper sequence in the data package to be provided to the Transformation Method program.

(b) Output for Sample Problem

For the problem being considered both printed and punched outputs are obtained.

- Printed Output:

Figure 6(a) shows the first page of printed output. The jet configuration being treated is identified both by appropriate heading and by other pertinent input information. Input controlling the numerical integration procedure is also displayed. Figure 6(b) shows the location of the computed jet centerline. The nondimensionalized jet speed U_j/U_{j0} and the nondimensionalized major diameter of the ellipse representing the cross section of the jet, d/d_0 are also printed out. These properties are printed out at each integration interval. Output shown in Figure 6(b) shows only the initial portion of the printed output generated for this example. The centerline was computed to $Z = 87.63$, which represents integration of the jet equations over the range $Z = 90 \times 0.4 \times 2.25 = 81$. The variables $XCOORD$ and DIA show a monotonic increase over this region, while $UJ = U_j/U_{j0} \approx .2$ as the mean jet speed approaches the freestream speed U_∞ . Figure 6(c) shows the printout for the jet-induced velocity components at the first spanwise station specified, $Y = 0$. The coordinates of the 36 control points at the station are identified. The induced velocity components U, V, W all nondimensionalized by U_∞ are printed out for each control point. Figure 6(d) shows the output for the last station considered in the sample problem, $Y = 20.125$. Similar printouts are obtained for the other intermediate stations specified as part of the input.

*** SINGLE JET CONFIGURATION ***

XJET	VJET	ZJET	PHI	PSI	U/UJC
0.6000	0.0	-6.6300	180.0000	0.0	0.2000

ANGLE OF ATTACK = 0.0
 ANGLE OF SIDESLIP = 0.0

NUMBER OF STEPS IN INTEGRATION = 90
 INTEGRATION INTERVAL = 0.40 JET EXIT DIAMETERS

FIGURE 6(a). INPUT PARAMETERS FOR SAMPLE PROBLEM

** SINGLE JET CENTERLINE **

XCOORD	YCOORD	ZCOORD	UJ	DIA
0.60	0.0	-6.63	1.000	1.00
0.61	0.0	-7.53	0.948	1.18
0.64	0.0	-8.43	0.893	1.45
0.71	0.0	-9.33	0.833	1.90
0.83	0.0	-10.23	0.760	2.64
1.01	0.0	-11.13	0.688	2.93
1.27	0.0	-12.03	0.626	3.23
1.62	0.0	-12.93	0.573	3.55
2.06	0.0	-13.83	0.528	3.88
2.61	0.0	-14.73	0.489	4.23
3.28	0.0	-15.63	0.456	4.60
4.09	0.0	-16.53	0.427	4.98
5.06	0.0	-17.43	0.402	5.37
6.21	0.0	-18.33	0.381	5.77
7.56	0.0	-19.23	0.363	6.18
9.15	0.0	-20.13	0.347	6.60
11.02	0.0	-21.03	0.333	7.03
13.21	0.0	-21.93	0.321	7.47
15.78	0.0	-22.83	0.311	7.92
18.78	0.0	-23.73	0.301	8.38
22.29	0.0	-24.63	0.293	8.86
26.39	0.0	-25.53	0.285	9.34
31.18	0.0	-26.43	0.278	9.85
36.78	0.0	-27.33	0.272	10.37
43.34	0.0	-28.23	0.266	10.91
51.00	0.0	-29.13	0.261	11.47

FIGURE 6(b). JET CENTERLINE FOR SAMPLE PROBLEM

*** INDUCED VELOCITIES ON WING ***

X	Y	Z	U	V	W
10.717	0.0	0.0	0.11367E-01	0.0	-0.47648E-01
10.623	0.0	0.020	0.11582E-01	0.0	-0.47592E-01
10.346	0.0	0.050	0.12220E-01	0.0	-0.47586E-01
9.904	0.0	0.097	0.13282E-01	0.0	-0.47535E-01
9.319	0.0	0.159	0.14771E-01	0.0	-0.47360E-01
8.616	0.0	0.229	0.16691E-01	0.0	-0.46985E-01
7.817	0.0	0.302	0.19044E-01	0.0	-0.46294E-01
6.948	0.0	0.377	0.21786E-01	0.0	-0.45121E-01
6.043	0.0	0.449	0.24799E-01	0.0	-0.43336E-01
5.133	0.0	0.506	0.27913E-01	0.0	-0.40918E-01
4.242	0.0	0.533	0.30975E-01	0.0	-0.37918E-01
3.394	0.0	0.529	0.33823E-01	0.0	-0.34394E-01
2.578	0.0	0.496	0.36272E-01	0.0	-0.30461E-01
1.847	0.0	0.442	0.38173E-01	0.0	-0.26360E-01
1.214	0.0	0.373	0.39493E-01	0.0	-0.22435E-01
0.699	0.0	0.292	0.40340E-01	0.0	-0.19039E-01
0.321	0.0	0.203	0.40931E-01	0.0	-0.16461E-01
0.092	0.0	0.105	0.41508E-01	0.0	-0.14885E-01
0.015	0.0	-0.000	0.42236E-01	0.0	-0.14410E-01
0.092	0.0	-0.105	0.43145E-01	0.0	-0.15127E-01
0.321	0.0	-0.203	0.44135E-01	0.0	-0.17164E-01
0.699	0.0	-0.292	0.44971E-01	0.0	-0.20619E-01
1.214	0.0	-0.373	0.45273E-01	0.0	-0.25421E-01
1.847	0.0	-0.442	0.44584E-01	0.0	-0.31202E-01
2.578	0.0	-0.496	0.42576E-01	0.0	-0.37266E-01
3.394	0.0	-0.529	0.39280E-01	0.0	-0.42753E-01
4.242	0.0	-0.533	0.35097E-01	0.0	-0.46970E-01
5.133	0.0	-0.506	0.30601E-01	0.0	-0.49642E-01
6.043	0.0	-0.449	0.26276E-01	0.0	-0.50929E-01
6.948	0.0	-0.377	0.22435E-01	0.0	-0.51223E-01
7.817	0.0	-0.302	0.19220E-01	0.0	-0.50918E-01
8.616	0.0	-0.229	0.16644E-01	0.0	-0.50293E-01
9.319	0.0	-0.159	0.14654E-01	0.0	-0.49538E-01
9.904	0.0	-0.097	0.13177E-01	0.0	-0.48809E-01
10.346	0.0	-0.050	0.12154E-01	0.0	-0.48223E-01
10.623	0.0	-0.020	0.11553E-01	0.0	-0.47839E-01

FIGURE 6(c). INDUCED VELOCITY COMPONENTS AT STATION Y = 0.

*** INDUCED VELOCITIES ON WING ***

X	Y	Z	U	V	W
8.821	20.125	0.0	0.11150E-01	-0.13150E-01	-0.43097E-02
8.774	20.125	0.010	0.11103E-01	-0.13115E-01	-0.42903E-02
8.635	20.125	0.025	0.11206E-01	-0.13024E-01	-0.42270E-02
8.414	20.125	0.049	0.11273E-01	-0.12878E-01	-0.41249E-02
8.122	20.125	0.079	0.11357E-01	-0.12682E-01	-0.39885E-02
7.770	20.125	0.114	0.11454E-01	-0.12443E-01	-0.38213E-02
7.370	20.125	0.151	0.11554E-01	-0.12167E-01	-0.36273E-02
6.936	20.125	0.189	0.11661E-01	-0.11862E-01	-0.34126E-02
6.483	20.125	0.225	0.11758E-01	-0.11538E-01	-0.31849E-02
6.029	20.125	0.253	0.11847E-01	-0.11211E-01	-0.29503E-02
5.583	20.125	0.267	0.11929E-01	-0.10892E-01	-0.27121E-02
5.154	20.125	0.264	0.12004E-01	-0.10588E-01	-0.24743E-02
4.751	20.125	0.249	0.12070E-01	-0.10303E-01	-0.22434E-02
4.385	20.125	0.221	0.12127E-01	-0.10046E-01	-0.20272E-02
4.069	20.125	0.186	0.12174E-01	-0.98250E-02	-0.18339E-02
3.811	20.125	0.146	0.12214E-01	-0.96477E-02	-0.16705E-02
3.622	20.125	0.101	0.12249E-01	-0.95225E-02	-0.15429E-02
3.508	20.125	0.052	0.12280E-01	-0.94554E-02	-0.14541E-02
3.469	20.125	-0.000	0.12311E-01	-0.94487E-02	-0.14057E-02
3.508	20.125	-0.057	0.12339E-01	-0.95020E-02	-0.13995E-02
3.622	20.125	-0.101	0.12362E-01	-0.96145E-02	-0.14375E-02
3.811	20.125	-0.146	0.12377E-01	-0.97845E-02	-0.15195E-02
4.069	20.125	-0.186	0.12383E-01	-0.10007E-01	-0.16427E-02
4.385	20.125	-0.221	0.12374E-01	-0.10273E-01	-0.18025E-02
4.751	20.125	-0.248	0.12347E-01	-0.10571E-01	-0.19943E-02
5.154	20.125	-0.264	0.12299E-01	-0.10489E-01	-0.22176E-02
5.583	20.125	-0.267	0.12225E-01	-0.11212E-01	-0.24522E-02
6.029	20.125	-0.253	0.12126E-01	-0.11531E-01	-0.27081E-02
6.483	20.125	-0.225	0.12004E-01	-0.11836E-01	-0.29737E-02
6.936	20.125	-0.189	0.11965E-01	-0.12123E-01	-0.32386E-02
7.370	20.125	-0.151	0.11719E-01	-0.12385E-01	-0.34906E-02
7.770	20.125	-0.114	0.11574E-01	-0.12614E-01	-0.37198E-02
8.122	20.125	-0.079	0.11440E-01	-0.12804E-01	-0.39191E-02
8.414	20.125	-0.049	0.11322E-01	-0.12954E-01	-0.40830E-02
8.635	20.125	-0.025	0.11231E-01	-0.13064E-01	-0.42056E-02
8.774	20.125	-0.010	0.11173E-01	-0.13131E-01	-0.42818E-02

FIGURE 6(d). INDUCED VELOCITY COMPONENTS AT STATION Y = 20.125

Punched Output for Station Y = 0.

0.0	2.888900	0.0				1
0.10000E 01 0.0		0.52495E 01 0.0		0.70057E 01 0.0		1 1
0.93694E 00 0.0		0.92054E 00 0.0		0.18211E-01 0.0		1 2
-0.35514E 00 0.0		0.25274E 01 0.0		0.20819E 01 0.0		1 3
-0.87942E-01 0.0		-0.91189E 01 0.0				1 4
0.11362E-01 0.11582E-01	0.12220E-01 0.13202E-01	0.14771E-01 0.16691E-01	U			1 1
0.19044E-01 0.21786E-01	0.24798E-01 0.27913E-01	0.30975E-01 0.33823E-01	U			1 2
0.36272E-01 0.38173E-01	0.39493E-01 0.40340E-01	0.40931E-01 0.41508E-01	U			1 3
0.42236E-01 0.43145E-01	0.44135E-01 0.44971E-01	0.45273E-01 0.44584E-01	U			1 4
0.42576E-01 0.39280E-01	0.35099E-01 0.30601E-01	0.26276E-01 0.22435E-01	U			1 5
0.19220E-01 0.16644E-01	0.14654E-01 0.13177E-01	0.12154E-01 0.11553E-01	U			1 6
0.0	0.0	0.0	0.0	0.0	0.0	V 1 1
0.0	0.0	0.0	0.0	0.0	0.0	V 1 2
0.0	0.0	0.0	0.0	0.0	0.0	V 1 3
0.0	0.0	0.0	0.0	0.0	0.0	V 1 4
0.0	0.0	0.0	0.0	0.0	0.0	V 1 5
0.0	0.0	0.0	0.0	0.0	0.0	V 1 6
-0.47648E-01-0.47592E-01-0.47586E-01-0.47535E-01-0.47360E-01-0.46985E-01	W					1 1
-0.46294E-01-0.45121E-01-0.43336E-01-0.40918E-01-0.37918E-01-0.34394E-01	W					1 2
-0.30461E-01-0.26360E-01-0.22435E-01-0.19039E-01-0.16461E-01-0.14885E-01	W					1 3
-0.14410E-01-0.15127E-01-0.17164E-01-0.20619E-01-0.25421E-01-0.31202E-01	W					1 4
-0.37266E-01-0.42753E-01-0.46970E-01-0.49642E-01-0.50929E-01-0.51223E-01	W					1 5
-0.50918E-01-0.50293E-01-0.49538E-01-0.48809E-01-0.48223E-01-0.47839E-01	W					1 6
2.500000	2.709399	-0.071767				2
0.10000E 01 0.0		0.53533E 01 0.0		0.61620E 01 0.0		2 1
0.77289E 00 0.0		0.71218E 00 0.0		0.13214E-01 0.0		2 2
-0.24166E 00 0.0		0.16130E 01 0.0		0.12461E 01 0.0		2 3
-0.49365E-01 0.0		-0.48006E 01 0.0				2 4
0.12325E-01 0.12530E-01	0.13133E-01 0.14131E-01	0.15516E-01 0.17283E-01	U			2 1
0.19419E-01 0.21872E-01	0.24526E-01 0.27241E-01	0.29896E-01 0.32376E-01	U			2 2
0.34548E-01 0.36300E-01	0.37600E-01 0.38516E-01	0.39194E-01 0.39805E-01	U			2 3
0.40465E-01 0.41184E-01	0.41866E-01 0.42329E-01	0.42304E-01 0.41493E-01	U			2 4
0.39697E-01 0.36945E-01	0.33499E-01 0.29741E-01	0.26035E-01 0.22652E-01	U			2 5
0.19746E-01 0.17366E-01	0.15494E-01 0.14084E-01	0.13098E-01 0.12514E-01	U			2 6
-0.95974E-02-0.95911E-02-0.96194E-02-0.96592E-02-0.96937E-02-0.97102E-02	V					2 1
-0.96874E-02-0.95914E-02-0.93949E-02-0.90961E-02-0.87079E-02-0.82380E-02	V					2 2
-0.76951E-02-0.71089E-02-0.65313E-02-0.60244E-02-0.56478E-02-0.54480E-02	V					2 3
-0.54534E-02-0.56833E-02-0.61559E-02-0.68779E-02-0.78195E-02-0.88918E-02	V					2 4
-0.99505E-02-0.10833E-01-0.11412E-01-0.11648E-01-0.11591E-01-0.11345E-01	V					2 5
-0.11011E-01-0.10654E-01-0.10314E-01-0.10021E-01-0.98005E-02-0.96614E-02	V					2 6
-0.45398E-01-0.45330E-01-0.45268E-01-0.45131E-01-0.44851E-01-0.44363E-01	W					2 1
-0.43370E-01-0.42383E-01-0.40639E-01-0.38415E-01-0.35756E-01-0.32725E-01	W					2 2
-0.29415E-01-0.26011E-01-0.22772E-01-0.19971E-01-0.17849E-01-0.16573E-01	W					2 3
-0.16235E-01-0.16907E-01-0.18663E-01-0.21537E-01-0.25428E-01-0.30030E-01	W					2 4
-0.34843E-01-0.39282E-01-0.42857E-01-0.45330E-01-0.46750E-01-0.47357E-01	W					2 5
-0.47420E-01-0.47150E-01-0.46704E-01-0.46225E-01-0.45819E-01-0.45545E-01	W					2 6

FIGURE 7. JET FLOW FIELD PROGRAM PUNCHED OUTPUT
FOR SAMPLE PROBLEM
(Wing; Transformation Method)

5.040000	2.527200	-0.071767					3
0.10000E 01 0.0		0.54592E 01 0.0		0.53613E 01 0.0			3 1
0.62724E 00 0.0		0.53911E 00 0.0		0.93239E 02 0.0			3 2
-0.15916E 00 0.0		0.99091E 00 0.0		0.71404E 00 0.0			3 3
-0.26385E-01 0.0		-0.23934E 01 0.0					3 4
0.13806E-01 0.13983E-01	0.14512E-01 0.15378E-01	0.16561E-01 0.18039E-01	U				3 5
0.19781E-01 0.21724E-01	0.23762E-01 0.25790E-01	0.27730E-01 0.29518E-01	U				3 6
0.31078E-01 0.32354E-01	0.33332E-01 0.34055E-01	0.34603E-01 0.35093E-01	U				3 7
0.35573E-01 0.36045E-01	0.36446E-01 0.36669E-01	0.36568E-01 0.35985E-01	U				3 8
0.34803E-01 0.33009E-01	0.30704E-01 0.28074E-01	0.25341E-01 0.22713E-01	U				3 9
0.20349E-01 0.18335E-01	0.16697E-01 0.15430E-01	0.14528E-01 0.13987E-01	U				3 10
-0.16935E-01-0.16911E-01	-0.16913E-01-0.16905E-01	-0.16861E-01-0.16764E-01	V				3 11
-0.16585E-01-0.16284E-01	-0.15837E-01-0.15259E-01	-0.14582E-01-0.13829E-01	V				3 12
-0.13017E-01-0.12186E-01	-0.11397E-01-0.10721E-01	-0.10232E-01-0.99864E-02	V				3 13
-0.10018E-01-0.10343E-01	-0.10975E-01-0.11908E-01	-0.13102E-01-0.14458E-01	V				3 14
-0.15833E-01-0.17060E-01	-0.17994E-01-0.18556E-01	-0.18758E-01-0.18690E-01	V				3 15
-0.18454E-01-0.18131E-01	-0.17777E-01-0.17448E-01	-0.17188E-01-0.17019E-01	V				3 16
-0.39000E-01-0.38916E-01	-0.38763E-01-0.38484E-01	-0.38033E-01-0.37366E-01	W				3 17
-0.36426E-01-0.35144E-01	-0.33494E-01-0.31519E-01	-0.29291E-01-0.26873E-01	W				3 18
-0.24344E-01-0.21829E-01	-0.19490E-01-0.17495E-01	-0.15995E-01-0.15095E-01	W				3 19
-0.14854E-01-0.15309E-01	-0.16493E-01-0.18408E-01	-0.20981E-01-0.24037E-01	W				3 20
-0.27316E-01-0.30509E-01	-0.33327E-01-0.35578E-01	-0.37210E-01-0.38288E-01	W				3 21
-0.38923E-01-0.39224E-01	-0.39296E-01-0.39242E-01	-0.39149E-01-0.39067E-01	W				3 22
7.792500	2.329599	-0.071767					4
0.10000E 01 0.0		0.55735E 01 0.0		0.45556E 01 0.0			4 1
0.49130E 00 0.0		0.38925E 00 0.0		0.62097E 02 0.0			4 2
-0.97650E-01 0.0		0.56041E 00 0.0		0.37224E 00 0.0			4 3
-0.12680E-01 0.0		-0.10602E 01 0.0					4 4
0.15026E-01 0.15160E-01	0.15570E-01 0.16231E-01	0.17116E-01 0.18193E-01	U				4 5
0.19426E-01 0.20754E-01	0.22100E-01 0.23398E-01	0.24612E-01 0.25712E-01	U				4 6
0.26666E-01 0.27450E-01	0.28062E-01 0.28529E-01	0.28896E-01 0.29214E-01	U				4 7
0.29516E-01 0.29796E-01	0.30020E-01 0.30133E-01	0.30069E-01 0.29748E-01	U				4 8
0.29105E-01 0.28116E-01	0.26800E-01 0.25227E-01	0.23500E-01 0.21748E-01	U				4 9
0.20089E-01 0.18610E-01	0.17357E-01 0.16356E-01	0.15626E-01 0.15181E-01	U				4 10
-0.20817E-01-0.20771E-01	-0.20705E-01-0.20587E-01	-0.20395E-01-0.20116E-01	V				4 11
-0.19733E-01-0.19219E-01	-0.18571E-01-0.17821E-01	-0.17014E-01-0.16175E-01	V				4 12
-0.15324E-01-0.14497E-01	-0.13741E-01-0.13113E-01	-0.12668E-01-0.12449E-01	V				4 13
-0.12482E-01-0.12775E-01	-0.13331E-01-0.14141E-01	-0.15174E-01-0.16361E-01	V				4 14
-0.17603E-01-0.18787E-01	-0.19803E-01-0.20572E-01	-0.21073E-01-0.21340E-01	V				4 15
-0.21430E-01-0.21390E-01	-0.21268E-01-0.21114E-01	-0.20976E-01-0.20877E-01	V				4 16
-0.29937E-01-0.29848E-01	-0.29637E-01-0.29274E-01	-0.28138E-01-0.28013E-01	W				4 17
-0.27073E-01-0.25901E-01	-0.24508E-01-0.22944E-01	-0.21267E-01-0.19524E-01	W				4 18
-0.17769E-01-0.16078E-01	-0.14541E-01-0.13247E-01	-0.12276E-01-0.11685E-01	W				4 19
-0.11500E-01-0.11740E-01	-0.12418E-01-0.13532E-01	-0.15040E-01-0.16861E-01	W				4 20
-0.18875E-01-0.20941E-01	-0.22915E-01-0.24681E-01	-0.26174E-01-0.27374E-01	W				4 21
-0.28291E-01-0.28951E-01	-0.29394E-01-0.29676E-01	-0.29845E-01-0.29931E-01	W				4 22

FIGURE 7. (Continued)

10.544999	2.132000	-0.071767					5
0.10000E 01 0.0	0.56880E 01 0.0	0.38157E 01 0.0					5 1
0.37661E 00 0.0	0.27307E 00 0.0	0.39869E 02 0.0					5 2
-0.57378E 01 0.0	0.30137E 00 0.0	0.18320E 00 0.0					5 3
-0.57112E 02 0.0	-0.43705E 00 0.0						5 4
0.15256E 01 0.15346E 01	0.15627E 01 0.16077E 01	0.16667E 01 0.17370E 01	U				5 1
0.18154E 01 0.18975E 01	0.19784E 01 0.20547E 01	0.21249E 01 0.21879E 01	U				5 2
0.22425E 01 0.22875E 01	0.23232E 01 0.23510E 01	0.23733E 01 0.23928E 01	U				5 3
0.24110E 01 0.24276E 01	0.24405E 01 0.24474E 01	0.24447E 01 0.24288E 01	U				5 4
0.23960E 01 0.23443E 01	0.22735E 01 0.21855E 01	0.20850E 01 0.19786E 01	U				5 5
0.18738E 01 0.17767E 01	0.16916E 01 0.16216E 01	0.15695E 01 0.15371E 01	U				5 6
-0.21136E 01 0.21077E 01	-0.20959E 01 0.20759E 01	-0.20467E 01 0.20082E 01	V				5 1
-0.19596E 01 0.19002E 01	-0.18313E 01 0.17565E 01	-0.16796E 01 0.16029E 01	V				5 2
-0.15281E 01 0.14578E 01	-0.13953E 01 0.13443E 01	-0.13085E 01 0.12908E 01	V				5 3
-0.12927E 01 0.13146E 01	-0.13564E 01 0.14174E 01	-0.14954E 01 0.15861E 01	V				5 4
-0.16834E 01 0.17805E 01	-0.18700E 01 0.19463E 01	-0.20067E 01 0.20518E 01	V				5 5
-0.20832E 01 0.21028E 01	-0.21128E 01 0.21163E 01	-0.21168E 01 0.21160E 01	V				5 6
-0.21226E 01 0.21149E 01	-0.20942E 01 0.20597E 01	-0.20111E 01 0.19481E 01	W				5 1
-0.18705E 01 0.17786E 01	-0.16748E 01 0.15630E 01	-0.14468E 01 0.13290E 01	W				5 2
-0.12132E 01 0.11037E 01	-0.10055E 01 0.92333E 02	-0.86148E 02 0.82271E 02	W				5 3
-0.80838E 02 0.81932E 02	-0.85626E 02 0.91900E 02	-0.10054E 01 0.11115E 01	W				5 4
-0.12319E 01 0.13599E 01	-0.14889E 01 0.16126E 01	-0.17268E 01 0.18278E 01	W				5 5
-0.19136E 01 0.19829E 01	-0.20363E 01 0.20756E 01	-0.21026E 01 0.21182E 01	W				5 6
13.000000	1.955899	-0.071767					6
0.10000E 01 0.0	0.57903E 01 0.0	0.32114E 01 0.0					6 1
0.29079E 00 0.0	0.19343E 00 0.0	0.25909E 02 0.0					6 2
-0.34208E 01 0.0	0.16483E 00 0.0	0.91926E 01 0.0					6 3
-0.26290E 02 0.0	-0.18457E 00 0.0						6 4
0.14669E 01 0.14728E 01	0.14914E 01 0.15209E 01	0.15591E 01 0.16039E 01	U				6 1
0.16531E 01 0.17036E 01	0.17525E 01 0.17980E 01	0.18394E 01 0.18767E 01	U				6 2
0.19089E 01 0.19357E 01	0.19572E 01 0.19743E 01	0.19883E 01 0.20006E 01	U				6 3
0.20121E 01 0.20225E 01	0.20307E 01 0.20353E 01	0.20346E 01 0.20265E 01	U				6 4
0.20089E 01 0.19804E 01	0.19404E 01 0.18894E 01	0.18296E 01 0.17645E 01	U				6 5
0.16987E 01 0.16363E 01	0.15802E 01 0.15331E 01	0.14975E 01 0.14751E 01	U				6 6
-0.19649E 01 0.19590E 01	-0.19455E 01 0.19232E 01	-0.18920E 01 0.18523E 01	V				6 1
-0.18041E 01 0.17479E 01	-0.16853E 01 0.16195E 01	-0.15535E 01 0.14890E 01	V				6 2
-0.14275E 01 0.13706E 01	-0.13208E 01 0.12806E 01	-0.12524E 01 0.12382E 01	V				6 3
-0.12390E 01 0.12548E 01	-0.12854E 01 0.13305E 01	-0.13885E 01 0.14565E 01	V				6 4
-0.15307E 01 0.16067E 01	-0.16796E 01 0.17457E 01	-0.18028E 01 0.18504E 01	V				6 5
-0.18887E 01 0.19177E 01	-0.19381E 01 0.19517E 01	-0.19603E 01 0.19649E 01	V				6 6
-0.14866E 01 0.14806E 01	-0.14635E 01 0.14354E 01	-0.13966E 01 0.13476E 01	W				6 1
-0.12889E 01 0.12213E 01	-0.11472E 01 0.10690E 01	-0.98897E 02 0.90887E 02	W				6 2
-0.83089E 02 0.75782E 02	-0.69265E 02 0.63822E 02	-0.59693E 02 0.57032E 02	W				6 3
-0.55912E 02 0.56383E 02	-0.53493E 02 0.62230E 02	-0.67473E 02 0.74004E 02	W				6 4
-0.81541E 02 0.87752E 02	-0.98287E 02 0.10682E 01	-0.11508E 01 0.12277E 01	W				6 5
-0.12963E 01 0.13548E 01	-0.14024E 01 0.14393E 01	-0.14657E 01 0.14815E 01	W				6 6

FIGURE 7. (Continued)

16.049908	1.737200	-0.071767				7
0.10000E 01 0.0	0.59174E 01 0.0	0.25332E 01 0.0				7 1
0.20372E 00 0.0	0.12034E 00 0.0	0.14310E-02 0.0				7 2
-0.16790E-01 0.0	0.71852E-01 0.0	0.35590E-01 0.0				7 3
-0.90399E-03 0.0	-0.56366E-01 0.0					7 4
0.13312E-01 0.13343E-01	0.13447E-01 0.13609E-01	0.13817E-01 0.14058E-01	U			7 1
0.14318E-01 0.14581E-01	0.14831E-01 0.15062E-01	0.15272E-01 0.15461E-01	U			7 2
0.15426E-01 0.15765E-01	0.15878E-01 0.15970E-01	0.16047E-01 0.16116E-01	U			7 3
0.16181E-01 0.16240E-01	0.16287E-01 0.16317E-01	0.16320E-01 0.16287E-01	U			7 4
0.16287E-01 0.16072E-01	0.15878E-01 0.15623E-01	0.15316E-01 0.14975E-01	U			7 5
0.14622E-01 0.14280E-01	0.13966E-01 0.13698E-01	0.13491E-01 0.13361E-01	U			7 6
-0.16887E-01-0.16836E-01	-0.16711E-01-0.16508E-01	-0.16231E-01-0.15886E-01	V			7 1
-0.15481E-01-0.15023E-01	-0.14527E-01-0.14017E-01	-0.13515E-01-0.13032E-01	V			7 2
-0.12578E-01-0.12163E-01	-0.11804E-01-0.11515E-01	-0.11313E-01-0.11208E-01	V			7 3
-0.11206E-01-0.11307E-01	-0.11509E-01-0.11810E-01	-0.12199E-01-0.12660E-01	V			7 4
-0.13171E-01-0.13705E-01	-0.14235E-01-0.14737E-01	-0.15199E-01-0.15612E-01	V			7 5
-0.15971E-01-0.16268E-01	-0.16502E-01-0.16677E-01	-0.16800E-01-0.16872E-01	V			7 6
-0.90788E-02-0.90399E-02	-0.89215E-02-0.87288E-02	-0.84680E-02-0.81444E-02	W			7 1
-0.77638E-02-0.73361E-02	-0.68762E-02-0.63986E-02	-0.59139E-02-0.54313E-02	W			7 2
-0.49637E-02-0.45272E-02	-0.41384E-02-0.38128E-02	-0.35628E-02-0.33961E-02	W			7 3
-0.33163E-02-0.33265E-02	-0.34297E-02-0.36256E-02	-0.39076E-02-0.42651E-02	W			7 4
-0.46852E-02-0.51529E-02	-0.56529E-02-0.61707E-02	-0.66910E-02-0.71948E-02	W			7 5
-0.76613E-02-0.80740E-02	-0.84233E-02-0.87035E-02	-0.89092E-02-0.90352E-02	W			7 6
20.125000	1.444599	-0.071767				8
0.10000E 01 0.0	0.60867E 01 0.0	0.17518E 01 0.0				8 1
0.11715E 00 0.0	0.57555E-01 0.0	0.56937E-03 0.0				8 2
-0.55521E-02 0.0	0.19759E-01 0.0	0.81385E-02 0.0				8 3
-0.17191E-03 0.0	-0.89134E-02 0.0					8 4
0.11150E-01 0.11163E-01	0.11206E-01 0.11273E-01	0.11357E-01 0.11454E-01	U			8 1
0.11538E-01 0.11661E-01	0.11758E-01 0.11847E-01	0.11929E-01 0.12044E-01	U			8 2
0.12070E-01 0.12127E-01	0.12174E-01 0.12214E-01	0.12249E-01 0.12280E-01	U			8 3
0.12311E-01 0.12339E-01	0.12362E-01 0.12377E-01	0.12383E-01 0.12374E-01	U			8 4
0.12347E-01 0.12299E-01	0.12225E-01 0.12126E-01	0.12004E-01 0.11865E-01	U			8 5
0.11719E-01 0.11574E-01	0.11440E-01 0.11322E-01	0.11231E-01 0.11173E-01	U			8 6
-0.13150E-01-0.13115E-01	-0.13024E-01-0.12878E-01	-0.12682E-01-0.12443E-01	V			8 1
-0.12167E-01-0.11862E-01	-0.11538E-01-0.11211E-01	-0.10892E-01-0.10588E-01	V			8 2
-0.10303E-01-0.10046E-01	-0.98250E-02-0.96477E-02	-0.95225E-02-0.94554E-02	V			8 3
-0.9487E-02-0.95020E-02	-0.96145E-02-0.97845E-02	-0.10007E-01-0.10273E-01	V			8 4
-0.10571E-01-0.10889E-01	-0.11212E-01-0.11531E-01	-0.11836E-01-0.12123E-01	V			8 5
-0.12385E-01-0.12614E-01	-0.12804E-01-0.12954E-01	-0.13064E-01-0.13131E-01	V			8 6
-0.43037E-02-0.42903E-02	-0.42270E-02-0.41249E-02	-0.39885E-02-0.38213E-02	W			8 1
-0.36273E-02-0.34126E-02	-0.31849E-02-0.29503E-02	-0.27121E-02-0.24743E-02	W			8 2
-0.22434E-02-0.20272E-02	-0.18339E-02-0.16705E-02	-0.15429E-02-0.14541E-02	W			8 3
-0.14057E-02-0.13995E-02	-0.14375E-02-0.15195E-02	-0.16427E-02-0.18025E-02	W			8 4
-0.19943E-02-0.22126E-02	-0.24522E-02-0.27081E-02	-0.29737E-02-0.32386E-02	W			8 5
-0.34906E-02-0.37198E-02	-0.39191E-02-0.40830E-02	-0.42056E-02-0.42818E-02	W			8 6

FIGURE 7. (Concluded)

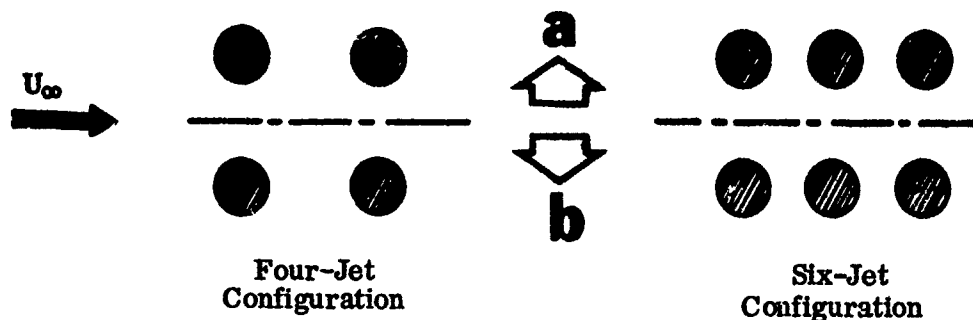
- **Punched Output:**

The punched card output for the sample problem is shown in tabulated form in Figure 7. The output data block for the first spanwise station is identified. The first card lists the spanwise station $Y = 0.$, the mapping radius $R = 2.8889$ and the rate of change of R with Y , $DRDY = 0$. The next four cards list the real and imaginary parts of the coefficients used in the mapping expansion. Cards 6 — 11 list the induced velocity components in the X direction for each of the 36 control points at $Y = 0$. The induced velocity components in the Y -direction are listed on cards 12 — 17 and cards 18 — 23 specify induced velocity components in the Z -direction. Data blocks of this type, each consisting of 23 cards, follow for each of the other 7 spanwise stations specified as part of the input. The punched output is identified in columns 73 — 80. The spanwise station number is shown in columns 75 — 77. Sequence numbers for each station appear in columns 78 — 80. The letters U , V , W in column 74 identify the velocity components listed on the data cards.

Note: From the tabulations of Figure 7 it is apparent that the first five cards of the data generated for each spanwise station represent an exact duplication of input cards described previously. They are generated as part of the punched output so that a more complete data package for the Transformation Method program may be obtained and additional card handling circumvented.

(2) Applicability and Limitations

The Jet Flow Field program may be utilized to evaluate the induced flow field at given control points due to one, two or three exhausting jets. For a single jet the initial jet exhaust direction, specified by ϕ and ψ , and the freestream direction, specified by α and β are arbitrary. For a two-jet configuration the jet exits must both lie in the same XY plane and the jet exhaust planes, defined by the freestream vector and the initial jet exhaust vectors, must be parallel. The same restrictions apply to a three-jet configuration. Additionally, three-jet configurations must be colinear and negative angle-of-attack cases cannot be treated. More complex configurations, as shown below, may be treated by reduction to two- or three-jet type configurations, as indicated, and adding the induced velocities at each control point due to configurations (a) and (b).



Extensive comparisons between computations and experimental data have been made for velocity ratios $0.10 < U_{\infty}/U_{jo} < 0.30$ and the Jet Flow Field program may be considered most applicable in this range of velocity ratios.

The choice of the variables governing the numerical integration for the jet path is related to the velocity ratio of the problem being considered. For $U_{\infty}/U_{jo} < 0.125$ integration in the direction normal to the freestream over an extent of at least 30 jet exit diameters has been found desirable. As U_{∞}/U_{jo} increases this may be decreased, as the jet penetrates less at the higher velocity ratios. For the above range of velocity ratios an integration step size of ≤ 0.5 jet exit diameters has been found satisfactory.

Control points at which jet-induced velocity components are to be evaluated may not lie within the jet itself, as the Jet Flow Field theory is not valid in this region. Generally, control points positioned less than 2 jet exit diameters from the center of the jet exit should be avoided, to avoid distortion in the computed velocity distributions.

b. Lifting Surface Theory

The purpose of the Jet Flow Field theory, when used in conjunction with the Lifting Surface theory, is to predict jet-induced downwash distributions on the wing to be utilized by the Lifting Surface theory in evaluating power effects. This is accomplished by executing the Jet Flow Field computer program to generate required input data for the Lifting Surface program in the form of punched data cards. These data cards will then constitute the downwash matrix $[W]$, which forms part of the input for the Lifting Surface program described in Section II.5.

It should be noted that the manner in which the Jet Flow Field program is utilized to provide data for the Lifting Surface program is almost identical to its application in

conjunction with the Transformation Method described in Section II.3. a. The discussion below will treat in detail only those areas of input and output which differ from Section II.3.a

(1) Sample Problem Computation

For the sample problem being considered, the Jet Flow Field program is now used to compute jet-induced downwash distributions at 10 spanwise stations on the wing. Figure 8 shows details of the planform of the wing and indicates the network of control points to be utilized in the computations.

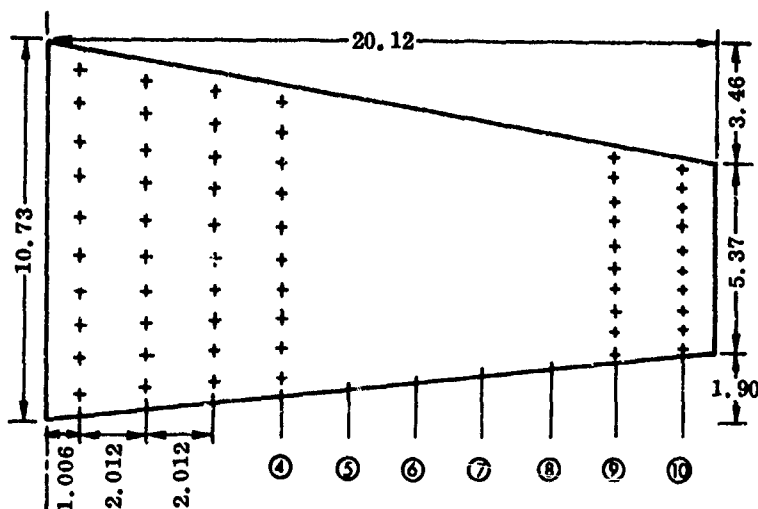


FIGURE 8. CONTROL POINTS ON WING FOR SAMPLE PROBLEM

The wing is treated as a planar surface, $Z = 0$. Each spanwise station has 10 control points spaced evenly between 0.05 and 0.95 of the local chord. The spanwise stations are distributed evenly between 0.05 and 0.95 of the semi-span.

(a) Input for Sample Problem

The input cards required for the sample problem are tabulated in Figure 9.

Card 1 again lists the three control indices. $IGEO\bar{M} = 3$ indicates that the coordinates of all control points will be provided directly as part of the input. The other two indices remain unchanged from Section II.3. a. The punched output generated will, of course, now be suitable for use with the Lifting Surface program.

Card 2 remains unchanged from Section II.3. a.

Card 3 controls the number of steps and the step size in the numerical integration of the equations of motion for the jet path. For this case, the number of steps has been cut down to 50, as computations in Section II.3. a showed that after a penetration of 20 jet exit diameters into the crossflow, the nondimensionalized jet speed $U_j/U_{j0} = 0.202$, i.e., the jet has virtually slowed to the speed of the crossflow and further contributions to the jet-induced velocities will be negligible.

Cards 4 — 6 see Section II.3. a.

Card 7 lists the number of spanwise control stations, $NS = 10$ and specifies that the number of control points at each station $NC = 10$.

Cards 8 — 57 list the coordinates for the control points of the grid shown schematically in Figure 8. The coordinates for each control point appear in the order X, Y, Z. Control points are listed from leading edge to trailing edge for each spanwise station, with the spanwise stations appearing in a root-to-tip sequence. The total number of control points is $NC \times NS$. The listing is continuous, i.e., no new record is required for the first control point at each spanwise station.

(b) Output for Sample Problem

Both printed and punched outputs are obtained.

- Printed Output :

The initial part of the printout dealing with configuration identification and jet centerline printout will be identical to that shown in Figures 6(a) and 6(b) of Section II.3. The centerline computations are now carried out to $Z = 51.63$ consistent with the 50 integration steps specified. Figure 10 shows a portion of the printout for the jet-induced velocity components at the control points specified as part of the input. The control points are listed in the order in which they were read in. All three velocity components are printed out, although only the downwash component W needed in conjunction with the Lifting Surface theory.

- Punched Output :

The punched output for the sample problem is shown in tabulated form in Figure 11. The data block for the first spanwise station is identified. The cards list the downwash component $-W$, nondimensionalized by U_∞ , for each control point at the first spanwise station in a leading to trailing edge

*** INDUCED VELOCITIES AT CONTROL POINTS ***					
X	Y	Z	U	V	W
0.696	1.006	0.0	0.42185E-01	-0.25052E-02	-0.19470E-01
1.742	1.006	0.0	0.41069E-01	-0.31934E-02	-0.27364E-01
2.788	1.006	0.0	0.38306E-01	-0.37568E-02	-0.34289E-01
3.835	1.006	0.0	0.34488E-01	-0.41490E-02	-0.39742E-01
4.881	1.006	0.0	0.30233E-01	-0.43711E-02	-0.43625E-01
5.927	1.006	0.0	0.26004E-01	-0.44536E-02	-0.46118E-01
6.973	1.006	0.0	0.22069E-01	-0.44349E-02	-0.47507E-01
8.019	1.006	0.0	0.18547E-01	-0.43495E-02	-0.48074E-01
9.066	1.006	0.0	0.15463E-01	-0.42236E-02	-0.48055E-01
10.112	1.006	0.0	0.12797E-01	-0.40755E-02	-0.47630E-01
1.015	3.018	0.0	0.39548E-01	-0.73734E-02	-0.19404E-01
2.008	3.018	0.0	0.38348E-01	-0.89783E-02	-0.25778E-01
3.000	3.018	0.0	0.35964E-01	-0.10302E-01	-0.31410E-01
3.993	3.018	0.0	0.32795E-01	-0.11266E-01	-0.35995E-01
4.986	3.018	0.0	0.29248E-01	-0.11869E-01	-0.39455E-01
5.978	3.018	0.0	0.25651E-01	-0.12161E-01	-0.41875E-01
6.971	3.018	0.0	0.22215E-01	-0.12211E-01	-0.43418E-01
7.963	3.018	0.0	0.19056E-01	-0.12087E-01	-0.44267E-01
8.956	3.018	0.0	0.16219E-01	-0.11845E-01	-0.44586E-01
9.949	3.018	0.0	0.13710E-01	-0.11529E-01	-0.44514E-01

FIGURE 10. INDUCED VELOCITY COMPONENTS AT CONTROL POINTS

Station
1.006

0.1946997E-01	0.2736357E-01	0.3428907E-01	0.3974187E-01	0.4362537E-01
0.4611834E-01	0.4750663E-01	0.4807373E-01	0.4805501E-01	0.4763048E-01
0.1940424E-01	0.2577788E-01	0.3140971E-01	0.3599505E-01	0.3945525E-01
0.4187481E-01	0.4341806E-01	0.4426672E-01	0.4458629E-01	0.4451389E-01
0.1722910E-01	0.2192676E-01	0.2618271E-01	0.2982682E-01	0.3278734E-01
0.3507354E-01	0.3674650E-01	0.3789202E-01	0.3860138E-01	0.3896004E-01
0.1413587E-01	0.1745114E-01	0.2054700E-01	0.2331698E-01	0.2571272E-01
0.2771608E-01	0.2933651E-01	0.3060186E-01	0.3153021E-01	0.3222350E-01
0.1101770E-01	0.1332559E-01	0.1552317E-01	0.1756243E-01	0.1940951E-01
0.2104460E-01	0.2246060E-01	0.2366059E-01	0.2465511E-01	0.2545955E-01
0.8287247E-02	0.9881828E-02	0.1142634E-01	0.1289609E-01	0.1427143E-01
0.1553807E-01	0.1668714E-01	0.1771446E-01	0.1862001E-01	0.1940690E-01
0.6058868E-02	0.7158797E-02	0.8237526E-02	0.9282477E-02	0.1028281E-01
0.1122979E-01	0.1211669E-01	0.1293890E-01	0.1369373E-01	0.1438010E-01
0.4310101E-02	0.5068891E-02	0.5819704E-02	0.6556150E-02	0.7272489E-02
0.7963751E-02	0.8625664E-02	0.9254884E-02	0.9848863E-02	0.1040578E-01
0.2969740E-02	0.3493453E-02	0.4014853E-02	0.4530825E-02	0.5038351E-02
0.5534708E-02	0.6017454E-02	0.6484497E-02	0.6934032E-02	0.7364653E-02
0.1957927E-02	0.2319387E-02	0.2680826E-02	0.3040665E-02	0.3397372E-02
0.3749519E-02	0.4095748E-02	0.4434913E-02	0.4765924E-02	0.5087804E-02

FIGURE 11. JET FLOW FIELD PROGRAM PUNCHED OUTPUT
FOR SAMPLE PROBLEM
(Wing; Lifting Surface Theory)

sequence. The sign of W is changed to provide compatibility with the Lifting Surface theory where downwash is conventionally considered to be positive. Similar data blocks are generated for the other 9 spanwise stations. Each spanwise station starts on a new record.

(2) Applicability and Limitations

See discussion in Section II.3.a.

Additionally, since the punched output variable $-W$ serves as an approximation to the tangent of the downwash angle when it is utilized as input to the Lifting Surface program, the application of the Jet Flow Field program must be restricted to small angles of attack.

4. APPLICATION OF TRANSFORMATION METHOD TO WING

The transformation method uses the jet-induced velocity components at a number of stations on the wing to determine wing power effects in the form of surface pressure distributions and integrated force and moment. The transformation method requires that the mapping function for each of the wing sections is known. The jet induced velocity components are determined using the jet flow field program described in Volume I. The mapping function is determined using the techniques developed in Section III of Volume I.

The generation of the coefficients of the mapping function for the sample problem has been described in Section II.2. A description of the application of the jet flow field program to the sample problem has been given in Section II.3. The punched card output of the jet flow field program is compatible with the transformation method and includes the mapping coefficients and jet induced velocity components for each of the wing sections. To complete the input to the transformation method program various flow indices must also be specified. Most of these indices have already been defined in the preceding section.

a. Inputs to Transformation Method for Sample Problem

Shown in Figure 12 are the input data for this sample problem in which the punched outputs from the jet flow field program constitute the major portion. However, to activate the computation two cards must precede this basic input block. There may be none, two or three cards following this block, depending on the specified options.

Card 1 lists in order the classification index (1 specifies a wing), the modification index (1 denotes the option of three-dimensional modification being exercised), the number of iterations, the number of layers for distributing residual sources and sinks, the power index (0 indicates the power effect), the configuration index (1 refers to a nonrectangular wing), and the force index (1 indicates forces and moments to be computed).

Card 2 lists in order the number of stations, the number of pairs of the mapping coefficients, the number of coefficients in the Fourier series expansion, the computation index, the number of angular increments on the mapping circle, the free-stream to the jet velocity ratio, the angle of attack in degrees, and the sideslip angle in degrees.

Cards 3 through 186 contain the punched output data provided by the jet flow field program, which include the y coordinate, the mapping coefficients, and the induced velocity components for stations No. 1 through No. 8. There are 23 cards for each station.

Card 187 lists in order the option index (0 denotes no average value used for the station next to the exhausting jet) and the station number where the jet is located.

Card 188 lists the number of stations on which the downwash modification is to be applied.

Card 189 lists in order the number of jets, the jet exit diameter, X coordinate of the moment center, Z coordinate of the moment center, and the reference length for making the computed moments dimensionless.

b. Outputs from Transformation Method for Sample Problem

Figure 13 lists directly or indirectly a portion of the input data on Card 1 through Card 186.

Figure 14 establishes the correspondence between the angular increments of the mapping circle and their corresponding locations on the wing section at every station. The first column states the angular increments in degrees.

Figure 15 gives the pressure distributions in coefficient form $(p - p_{\infty})/q_{\infty}$, at every station after completion of the segment method. These coefficients are tabulated against the angular increments. To obtain the actual location, reference must be made to the previous figure. The second and the third lines in this table list the radius of the mapping circle (RB) and the gradient of this radius in y-direction (DRDY).

Figure 16 lists the pressure distributions at various sections after imposing the residual sources and sinks in the network. Columns 7, 8, 9 in this table remain the same as those in Figure 15, since the flow properties near the wingtip are not modified.

Figure 17 lists the pressure distributions after completion of a three-dimensional modification of one iteration.

Figures 18 and 19 show printout of the pressure coefficients after imposing the residual sources and sinks for the second time and the completion of a three-dimensional modification of two iterations.

Figure 20 lists the parameters used in the three-dimensional modification and in the force and moment computations, originally read in as input data on Cards 187, 188, and 189. Also tabulated are the computed forces (normalized to the thrust) and moments (normalized by the thrust and reference length) on this wing after two iterations.

Figures 21(a) through 21(c) show the comparison between the computed pressure coefficients and wind tunnel test data at stations $y = 5.04''$, $7.2925''$, $10.545''$, and $16.0''$.

WING COMPUTATION

OPTIONS SPECIFIED FOR THIS RUN ARE

1. THREE DIMENSIONAL MODIFICATION OF 2 ITERATION
2. POWER EFFECT ONLY

INPUT DATA

YSTA= 8 N= 11 NFUN= 20 NSYM= 1 MTHET= 16 IRECT= 1 IFORCE= 1
UJ= 0.200 ALPHA= 0.0 BETA= 0.0

STATION= 0.0 RADIUS= 2.888900 DERIV= 0.0

GEOMETRY COEFFICIENTS *A*,*B* FOR STATION 1

0.100000E 01	0.0	0.524950E 01	0.0	0.700570E 01	0.0
0.316940E 00	0.0	0.920540E 00	0.0	0.182110E-01	0.0
-0.355140E 00	0.0	0.252740E 01	0.0	0.208190E 01	0.0
-0.579419E-01	0.0	-0.911890E 01	0.0		

VELOCITY COMPONENT *U* AT STATION 1

0.11362E-01	0.11582E-01	0.12220E-01	0.13287E-01	0.14771E-01	0.16691E-01
0.19044E-01	0.21796E-01	0.24798E-01	0.27913E-01	0.31075E-01	0.33823E-01
0.36272E-01	0.39173E-01	0.39493E-01	0.40340E-01	0.40931E-01	0.41508E-01
0.42236E-01	0.43145E-01	0.44135E-01	0.44971E-01	0.45271E-01	0.44584E-01
0.42576E-01	0.39240E-01	0.35099E-01	0.30601E-01	0.26276E-01	0.22435E-01
0.19220E-01	0.16644E-01	0.14654E-01	0.13177E-01	0.12154E-01	0.11553E-01

VELOCITY COMPONENT *V* AT STATION 1

0.0	0.0	0.0	0.0	0.0	0.0
0.0	0.0	0.0	0.0	0.0	0.0
0.0	0.0	0.0	0.0	0.0	0.0
0.0	0.0	0.0	0.0	0.0	0.0
0.0	0.0	0.0	0.0	0.0	0.0
0.0	0.0	0.0	0.0	0.0	0.0

VELOCITY COMPONENT *W* AT STATION 1

-0.47548E-01	-0.47592E-01	-0.47586E-01	-0.47535E-01	-0.47360E-01	-0.46985E-01
-0.46294E-01	-0.45121E-01	-0.43336E-01	-0.40918E-01	-0.37418E-01	-0.34394E-01
-0.30461E-01	-0.26360E-01	-0.22435E-01	-0.19039E-01	-0.16461E-01	-0.14885E-01
-0.14410E-01	-0.15127E-01	-0.17164E-01	-0.20619E-01	-0.25421E-01	-0.31202E-01
-0.37266E-01	-0.42753E-01	-0.46970E-01	-0.49642E-01	-0.50929E-01	-0.51223E-01
-0.50919E-01	-0.50293E-01	-0.49538E-01	-0.48809E-01	-0.48223E-01	-0.47839E-01

FIGURE 13. PARTIAL LIST OF INPUT DATA FOR SAMPLE WING

TABLE FOR WING GEOMETRY

THETA	Y= 0.0	Z(1)	X(1)	Y= 2.50	Z(1)	X(1)	Y= 5.04	Z(1)	X(1)	Y= 7.79	Z(1)
0.0	0.10717E 02	0.0	0.10431E 02	0.0	0.10242E 02	0.0	0.10242E 02	0.0	0.99827E 01	0.0	0.0
10.00	0.10623E 02	0.51993E -01	0.10393E 02	0.18753E -01	0.10160E 02	0.14777E -01	0.10160E 02	0.14777E -01	0.99066E 01	0.16118E -01	0.0
20.00	0.10346E 02	0.50346E -01	0.10133E 02	0.47240E -01	0.99176E 01	0.44034E -01	0.99176E 01	0.44034E -01	0.96832E 01	0.40603E -01	0.0
30.00	0.99036E 01	0.97133E -01	0.97182E 01	0.91130E -01	0.95308E 01	0.38961E -01	0.95308E 01	0.38961E -01	0.93266E 01	0.78333E -01	0.0
40.00	0.93194E 01	0.15882E 00	0.91703E 01	0.14894E 00	0.90196E 01	0.13892E 00	0.90196E 01	0.13892E 00	0.88534E 01	0.12808E 00	0.0
50.00	0.96164E 01	0.22876E 00	0.85110E 01	0.21459E 00	0.84046E 01	0.20010E 00	0.84046E 01	0.20010E 00	0.82886E 01	0.19448E 00	0.0
60.00	0.78168E 01	0.30213E 00	0.77610E 01	0.28341E 00	0.77050E 01	0.26428E 00	0.77050E 01	0.26428E 00	0.76437E 01	0.24345E 00	0.0
70.00	0.69476E 01	0.37739E 00	0.69459E 01	0.35800E 00	0.69447E 01	0.33012E 00	0.69447E 01	0.33012E 00	0.69428E 01	0.30434E 00	0.0
80.00	0.60425E 01	0.44942E 00	0.60970E 01	0.42155E 00	0.61529E 01	0.39313E 00	0.61529E 01	0.39313E 00	0.62130E 01	0.36243E 00	0.0
90.00	0.51331E 01	0.50570E 00	0.52442E 01	0.47633E 00	0.53576E 01	0.44236E 00	0.53576E 01	0.44236E 00	0.54797E 01	0.40780E 00	0.0
100.00	0.42415E 01	0.53345E 00	0.44080E 01	0.50035E 00	0.45774E 01	0.46664E 00	0.45774E 01	0.46664E 00	0.47607E 01	0.43018E 00	0.0
110.00	0.33839E 01	0.52875E 00	0.36036E 01	0.49594E 00	0.38271E 01	0.46253E 00	0.38271E 01	0.46253E 00	0.40691E 01	0.42639E 00	0.0
120.00	0.25794E 01	0.49609E 00	0.28492E 01	0.46531E 00	0.31225E 01	0.43396E 00	0.31225E 01	0.43396E 00	0.34196E 01	0.40004E 00	0.0
130.00	0.18474E 01	0.44215E 00	0.21626E 01	0.41471E 00	0.24831E 01	0.38677E 00	0.24831E 01	0.38677E 00	0.28301E 01	0.33655E 00	0.0
140.00	0.12137E 01	0.37261E 00	0.15683E 01	0.34949E 00	0.19287E 01	0.33594E 00	0.19287E 01	0.33594E 00	0.23191E 01	0.30048E 00	0.0
150.00	0.69870E 00	0.29207E 00	0.10853E 01	0.27395E 00	0.14782E 01	0.25549E 00	0.14782E 01	0.25549E 00	0.19038E 01	0.23551E 00	0.0
160.00	0.32082E 00	0.20270E 00	0.73091E 00	0.19013E 00	0.11476E 01	0.17732E 00	0.11476E 01	0.17732E 00	0.15990E 01	0.16344E 00	0.0
170.00	0.91803E -01	0.10461E 00	0.51613E 00	0.98113E -01	0.94724E 00	0.91507E -01	0.94724E 00	0.91507E -01	0.14144E 01	0.84357E -01	0.0
180.00	0.15412E -01	0.33107E -06	0.44448E 00	0.35742E -06	0.89047E 00	0.31334E -06	0.89047E 00	0.31334E -06	0.13528E 01	0.30730E -06	0.0
190.00	0.91802E -01	-0.10461E 00	0.51613E 00	-0.98117E -01	0.94724E 00	-0.91507E -01	0.94724E 00	-0.91507E -01	0.14144E 01	-0.84357E -01	0.0
200.00	0.32082E 00	-0.20270E 00	0.73091E 00	-0.19013E 00	0.11476E 01	-0.17732E 00	0.11476E 01	-0.17732E 00	0.15990E 01	-0.16344E 00	0.0
210.00	0.69870E 00	-0.29207E 00	0.10853E 01	-0.27395E 00	0.14782E 01	-0.25549E 00	0.14782E 01	-0.25549E 00	0.19038E 01	-0.23551E 00	0.0
220.00	0.12137E 01	-0.37261E 00	0.15683E 01	-0.34949E 00	0.19287E 01	-0.33594E 00	0.19287E 01	-0.33594E 00	0.23191E 01	-0.30048E 00	0.0
230.00	0.13474E 01	-0.44215E 00	0.21626E 01	-0.41471E 00	0.24831E 01	-0.38677E 00	0.24831E 01	-0.38677E 00	0.28301E 01	-0.33655E 00	0.0
240.00	0.25784E 01	-0.49609E 00	0.28492E 01	-0.46531E 00	0.31225E 01	-0.43396E 00	0.31225E 01	-0.43396E 00	0.34196E 01	-0.40004E 00	0.0
250.00	0.33933E 01	-0.52875E 00	0.36036E 01	-0.49594E 00	0.38271E 01	-0.46253E 00	0.38271E 01	-0.46253E 00	0.40691E 01	-0.42639E 00	0.0
260.00	0.42415E 01	-0.53345E 00	0.44080E 01	-0.50035E 00	0.45774E 01	-0.46664E 00	0.45774E 01	-0.46664E 00	0.47607E 01	-0.43018E 00	0.0
270.00	0.51331E 01	-0.50570E 00	0.52442E 01	-0.47633E 00	0.53576E 01	-0.44236E 00	0.53576E 01	-0.44236E 00	0.54797E 01	-0.40780E 00	0.0
280.00	0.60425E 01	-0.44942E 00	0.60970E 01	-0.42155E 00	0.61529E 01	-0.39313E 00	0.61529E 01	-0.39313E 00	0.62130E 01	-0.36243E 00	0.0
290.00	0.69476E 01	-0.37739E 00	0.69459E 01	-0.35800E 00	0.69447E 01	-0.33012E 00	0.69447E 01	-0.33012E 00	0.69428E 01	-0.30434E 00	0.0
300.00	0.78168E 01	-0.30213E 00	0.77610E 01	-0.28341E 00	0.77050E 01	-0.26428E 00	0.77050E 01	-0.26428E 00	0.76437E 01	-0.24345E 00	0.0
310.00	0.86164E 01	-0.22876E 00	0.85110E 01	-0.21459E 00	0.84046E 01	-0.20010E 00	0.84046E 01	-0.20010E 00	0.82886E 01	-0.19448E 00	0.0
320.00	0.93194E 01	-0.15882E 00	0.91703E 01	-0.14894E 00	0.90196E 01	-0.13892E 00	0.90196E 01	-0.13892E 00	0.88534E 01	-0.12808E 00	0.0
330.00	0.97133E 01	-0.97133E -01	0.97182E 01	-0.91130E -01	0.95308E 01	-0.38961E -01	0.95308E 01	-0.38961E -01	0.93266E 01	-0.78333E -01	0.0
340.00	0.99036E 01	-0.99036E -01	0.99036E 01	-0.99036E -01	0.99036E 01	-0.99036E -01	0.99036E 01	-0.99036E -01	0.99036E 01	-0.99036E -01	0.0
350.00	0.10623E 02	-0.51993E -01	0.10393E 02	-0.18753E -01	0.10160E 02	-0.14777E -01	0.10160E 02	-0.14777E -01	0.99827E 01	-0.16118E -01	0.0

FIGURE 14. CORRESPONDENCE BETWEEN ANGULAR INCREMENTS OF MAPPING CIRCLES AND CARTESIAN COORDINATES OF WING SECTIONS

TABLE FOR WING GEOMETRY

THETA	Y = 10.54				Y = 13.00				16.05				Y = 20.13			
	X(1)	Z(1)	X(1)	Z(1)	X(1)	Z(1)	X(1)	Z(1)	X(1)	Z(1)	X(1)	Z(1)	X(1)	Z(1)	X(1)	Z(1)
0.0	0.97233E 01	0.0	0.94293E 01	0.0	0.92053E 01	0.0	0.92053E 01	0.0	0.92053E 01	0.0	0.88209E 01	0.0	0.88209E 01	0.0	0.99917E -02	0.0
10.00	0.94536E 01	0.14736E -01	0.94284E 01	0.13517E -01	0.91486E 01	0.13020E 01	0.91486E 01	0.12029E -01	0.89220E 01	0.10729E -01	0.86332E 01	0.10729E -01	0.86332E 01	0.25176E -01	0.25176E -01	0.48569E -01
20.00	0.94492E 01	0.37133E -01	0.92409E 01	0.34062E -01	0.87160E 01	0.34062E -01	0.87160E 01	0.34062E -01	0.84140E 01	0.34062E -01	0.84140E 01	0.34062E -01	0.84140E 01	0.79413E -01	0.79413E -01	0.11439E 00
30.00	0.91228E 01	0.71653E -01	0.86414E 01	0.65729E -01	0.85458E 01	0.65729E -01	0.85458E 01	0.65729E -01	0.83647E 01	0.65729E -01	0.83647E 01	0.65729E -01	0.83647E 01	0.11439E 00	0.11439E 00	0.18871E 00
40.00	0.86916E 01	0.11717E 00	0.80699E 01	0.10748E 00	0.79420E 01	0.10748E 00	0.79420E 01	0.10748E 00	0.7612E 01	0.10748E 00	0.7612E 01	0.10748E 00	0.7612E 01	0.11439E 00	0.11439E 00	0.22473E 00
50.00	0.81728E 01	0.16879E 00	0.75285E 01	0.20450E 00	0.74200E 01	0.20450E 00	0.74200E 01	0.20450E 00	0.69385E 01	0.20450E 00	0.69385E 01	0.20450E 00	0.69385E 01	0.11439E 00	0.11439E 00	0.22473E 00
60.00	0.75827E 01	0.22292E 00	0.69400E 01	0.25545E 00	0.64400E 01	0.25545E 00	0.64400E 01	0.25545E 00	0.63433E 01	0.25545E 00	0.63433E 01	0.25545E 00	0.63433E 01	0.11439E 00	0.11439E 00	0.22473E 00
70.00	0.69412E 01	0.27946E 00	0.63272E 01	0.30422E 00	0.57115E 01	0.30422E 00	0.57115E 01	0.30422E 00	0.53113E 01	0.30422E 00	0.53113E 01	0.30422E 00	0.53113E 01	0.11439E 00	0.11439E 00	0.22473E 00
80.00	0.62733E 01	0.33162E 00	0.51079E 01	0.34232E 00	0.45272E 01	0.34232E 00	0.45272E 01	0.34232E 00	0.43112E 01	0.34232E 00	0.43112E 01	0.34232E 00	0.43112E 01	0.11439E 00	0.11439E 00	0.22473E 00
90.00	0.56021E 01	0.37315E 00	0.39363E 00	0.36111E 00	0.35793E 00	0.36111E 00	0.35793E 00	0.36111E 00	0.34906E 01	0.36111E 00	0.34906E 01	0.36111E 00	0.34906E 01	0.11439E 00	0.11439E 00	0.22473E 00
100.00	0.49441E 01	0.39363E 00	0.31079E 01	0.35793E 00	0.29931E 00	0.35793E 00	0.29931E 00	0.35793E 00	0.28159E 01	0.35793E 00	0.28159E 01	0.35793E 00	0.28159E 01	0.11439E 00	0.11439E 00	0.22473E 00
110.00	0.43111E 01	0.36607E 00	0.30818E 01	0.33583E 00	0.27092E 01	0.33583E 00	0.27092E 01	0.33583E 00	0.25797E -01	0.33583E 00	0.25797E -01	0.33583E 00	0.25797E -01	0.11439E 00	0.11439E 00	0.22473E 00
120.00	0.37167E 01	0.32626E 00	0.30818E 01	0.33583E 00	0.25797E -01	0.33583E 00	0.25797E -01	0.33583E 00	0.24159E 01	0.33583E 00	0.24159E 01	0.33583E 00	0.24159E 01	0.11439E 00	0.11439E 00	0.22473E 00
130.00	0.31772E 01	0.27499E 00	0.30818E 01	0.33583E 00	0.25797E -01	0.33583E 00	0.25797E -01	0.33583E 00	0.23159E 01	0.33583E 00	0.23159E 01	0.33583E 00	0.23159E 01	0.11439E 00	0.11439E 00	0.22473E 00
140.00	0.27096E 01	0.21552E 00	0.27092E 01	0.25224E 00	0.22466E 01	0.25224E 00	0.22466E 01	0.25224E 00	0.2159E 01	0.25224E 00	0.2159E 01	0.25224E 00	0.2159E 01	0.11439E 00	0.11439E 00	0.22473E 00
150.00	0.23595E 01	0.14958E 00	0.22466E 01	0.19771E 00	0.19771E 00	0.19771E 00	0.19771E 00	0.19771E 00	0.1809E 01	0.19771E 00	0.1809E 01	0.19771E 00	0.1809E 01	0.11439E 00	0.11439E 00	0.22473E 00
160.00	0.20506E 01	0.11495E 00	0.22466E 01	0.17081E -01	0.17081E -01	0.17081E -01	0.17081E -01	0.17081E -01	0.159E 01	0.17081E -01	0.159E 01	0.17081E -01	0.159E 01	0.11439E 00	0.11439E 00	0.22473E 00
170.00	0.18165E 01	0.077192E -01	0.22466E 01	0.15708E -01	0.15708E -01	0.15708E -01	0.15708E -01	0.15708E -01	0.14958E 00	0.15708E -01	0.14958E 00	0.15708E -01	0.14958E 00	0.11439E 00	0.11439E 00	0.22473E 00
180.00	0.15721E 01	0.028120E -06	0.22466E 01	0.14958E 00	0.14958E 00	0.14958E 00	0.14958E 00	0.14958E 00	0.13722E 00	0.14958E 00	0.13722E 00	0.14958E 00	0.13722E 00	0.11439E 00	0.11439E 00	0.22473E 00
190.00	0.13722E 01	0.00000E 00	0.22466E 01	0.13722E 00	0.13722E 00	0.13722E 00	0.13722E 00	0.13722E 00	0.12191E 00	0.13722E 00	0.12191E 00	0.13722E 00	0.12191E 00	0.11439E 00	0.11439E 00	0.22473E 00
200.00	0.12191E 01	0.00000E 00	0.22466E 01	0.12191E 00	0.12191E 00	0.12191E 00	0.12191E 00	0.12191E 00	0.11439E 00	0.12191E 00	0.11439E 00	0.12191E 00	0.11439E 00	0.11439E 00	0.11439E 00	0.22473E 00
210.00	0.11439E 01	0.00000E 00	0.22466E 01	0.11439E 00	0.11439E 00	0.11439E 00	0.11439E 00	0.11439E 00	0.10729E 00	0.11439E 00	0.10729E 00	0.11439E 00	0.10729E 00	0.11439E 00	0.11439E 00	0.22473E 00
220.00	0.10729E 01	0.00000E 00	0.22466E 01	0.10729E 00	0.10729E 00	0.10729E 00	0.10729E 00	0.10729E 00	0.10000E 00	0.10729E 00	0.10000E 00	0.10729E 00	0.10000E 00	0.11439E 00	0.11439E 00	0.22473E 00
230.00	0.10000E 01	0.00000E 00	0.22466E 01	0.10000E 00	0.10000E 00	0.10000E 00	0.10000E 00	0.10000E 00	0.09279E 00	0.10000E 00	0.09279E 00	0.10000E 00	0.09279E 00	0.11439E 00	0.11439E 00	0.22473E 00
240.00	0.09279E 01	0.00000E 00	0.22466E 01	0.09279E 00	0.09279E 00	0.09279E 00	0.09279E 00	0.09279E 00	0.08559E 00	0.09279E 00	0.08559E 00	0.09279E 00	0.08559E 00	0.11439E 00	0.11439E 00	0.22473E 00
250.00	0.08559E 01	0.00000E 00	0.22466E 01	0.08559E 00	0.08559E 00	0.08559E 00	0.08559E 00	0.08559E 00	0.07839E 00	0.08559E 00	0.07839E 00	0.08559E 00	0.07839E 00	0.11439E 00	0.11439E 00	0.22473E 00
260.00	0.07839E 01	0.00000E 00	0.22466E 01	0.07839E 00	0.07839E 00	0.07839E 00	0.07839E 00	0.07839E 00	0.07119E 00	0.07839E 00	0.07119E 00	0.07839E 00	0.07119E 00	0.11439E 00	0.11439E 00	0.22473E 00
270.00	0.07119E 01	0.00000E 00	0.22466E 01	0.07119E 00	0.07119E 00	0.07119E 00	0.07119E 00	0.07119E 00	0.06400E 00	0.07119E 00	0.06400E 00	0.07119E 00	0.06400E 00	0.11439E 00	0.11439E 00	0.22473E 00
280.00	0.06400E 01	0.00000E 00	0.22466E 01	0.06400E 00	0.06400E 00	0.06400E 00	0.06400E 00	0.06400E 00	0.05680E 00	0.06400E 00	0.05680E 00	0.06400E 00	0.05680E 00	0.11439E 00	0.11439E 00	0.22473E 00
290.00	0.05680E 01	0.00000E 00	0.22466E 01	0.05680E 00	0.05680E 00	0.05680E 00	0.05680E 00	0.05680E 00	0.04960E 00	0.05680E 00	0.04960E 00	0.05680E 00	0.04960E 00	0.11439E 00	0.11439E 00	0.22473E 00
300.00	0.04960E 01	0.00000E 00	0.22466E 01	0.04960E 00	0.04960E 00	0.04960E 00	0.04960E 00	0.04960E 00	0.04240E 00	0.04960E 00	0.04240E 00	0.04960E 00	0.04240E 00	0.11439E 00	0.11439E 00	0.22473E 00
310.00	0.04240E 01	0.00000E 00	0.22466E 01	0.04240E 00	0.04240E 00	0.04240E 00	0.04240E 00	0.04240E 00	0.03520E 00	0.04240E 00	0.03520E 00	0.04240E 00	0.03520E 00	0.11439E 00	0.11439E 00	0.22473E 00
320.00	0.03520E 01	0.00000E 00	0.22466E 01	0.03520E 00	0.03520E 00	0.03520E 00	0.03520E 00	0.03520E 00	0.02800E 00	0.03520E 00	0.02800E 00	0.03520E 00	0.02800E 00	0.11439E 00	0.11439E 00	0.22473E 00
330.00	0.02800E 01	0.00000E 00	0.22466E 01	0.02800E 00	0.02800E 00	0.02800E 00	0.02800E 00	0.02800E 00	0.02080E 00	0.02800E 00	0.02080E 00	0.02800E 00	0.02080E 00	0.11439E 00	0.11439E 00	0.22473E 00
340.00	0.02080E 01	0.00000E 00	0.22466E 01	0.02080E 00	0.02080E 00	0.02080E 00	0.02080E 00	0.02080E 00	0.01360E 00	0.02080E 00	0.01360E 00	0.02080E 00	0.01360E 00	0.11439E 00	0.11439E 00	0.22473E 00
350.00	0.01360E 01	0.00000E 00	0.22466E 01	0.01360E 00	0.01360E 00	0.01360E 00	0.01360E 00	0.01360E 00	0.00640E 00	0.01360E 00	0.00640E 00	0.01360E 00	0.00640E 00	0.11439E 00	0.11439E 00	0.22473E 00

FIGURE 14. (Concluded)

PRESSURE COEFFICIENTS AT 41NG, SEGMENT METHOD.

	Y= 2.0	Y= 2.50	Y= 5.04	Y= 7.74	Y= 10.54	Y= 13.00	Y= 16.05	Y= 20.13
	RM= 0.0	RM= 2.71	RM= 2.51	RM= 2.33	RM= 2.13	RM= 1.96	RM= 1.74	RM= 1.44
Y-4ETA DROV=	0.0	0.0	0.0	0.0	0.0	0.0	0.0	0.0
0.0	-0.27623E-02	-0.55281E-07	-0.81147E-02	-0.93307E-02	-0.93502E-02	-0.86181E-02	-0.73706E-02	-0.57606E-02
10.00	-0.18446E-01	-0.27459E-01	-0.27459E-01	-0.31566E-01	-0.32430E-01	-0.31210E-01	-0.28223E-01	-0.23469E-01
20.00	-0.17562E-02	-0.11716E-01	-0.17604E-01	-0.23047E-01	-0.26006E-01	-0.26463E-01	-0.25123E-01	-0.21027E-01
30.00	0.53716E-03	-0.35914E-02	-0.10229E-01	-0.17127E-01	-0.21621E-01	-0.23324E-01	-0.23183E-01	-0.20927E-01
40.00	0.83716E-02	0.41669E-02	0.33363E-02	-0.11691E-01	-0.17710E-01	-0.20585E-01	-0.21555E-01	-0.20242E-01
50.00	0.16160E-01	0.11803E-01	0.33445E-02	-0.64963E-02	-0.14000E-01	-0.17989E-01	-0.20001E-01	-0.19575E-01
60.00	0.24217E-01	0.19659E-01	0.10144E-01	-0.12594E-02	-0.10268E-01	-0.15371E-01	-0.18418E-01	-0.18875E-01
70.00	0.32936E-01	0.28070E-01	0.17275E-01	0.41115E-02	-0.65192E-02	-0.12787E-01	-0.16897E-01	-0.17712E-01
80.00	0.42749E-01	0.37496E-01	0.25141E-01	0.99572E-02	-0.25148E-02	-0.10094E-01	-0.15384E-01	-0.17058E-01
90.00	0.54212E-01	0.44995E-01	0.34394E-01	0.16791E-01	0.21574E-02	-0.69402E-02	-0.13599E-01	-0.16084E-01
100.00	0.66891E-01	0.60725E-01	0.47172E-01	0.24547E-01	0.75831E-02	-0.31271E-02	-0.11348E-01	-0.14648E-01
110.00	0.81560E-01	0.74961E-01	0.54859E-01	0.33825E-01	0.14213E-01	0.15376E-02	-0.44022E-02	-0.12738E-01
120.00	0.94852E-01	0.92754E-01	0.72117E-01	0.45538E-01	0.22619E-01	0.75482E-02	-0.44040E-02	-0.10191E-01
130.00	0.12450E 00	0.11631E 00	0.92854E-01	0.61496E-01	0.34039E-01	0.15697E-01	0.51383E-03	-0.65044E-02
140.00	0.16120E 00	0.15259E 00	0.12374E 00	0.85260E-01	0.51046E-01	0.27745E-01	0.80258E-02	-0.40003E-03
150.00	0.22064E 00	0.21052E 00	0.17394E 00	0.12472E 00	0.74783E-01	0.47386E-01	0.20211E-01	-0.35365E-01
160.00	0.32413E 00	0.31334E 00	0.26391E 00	0.19431E 00	0.12976E 00	0.83784E-01	0.42986E-01	-0.15696E-02
170.00	0.47190E 00	0.45774E 00	0.39641E 00	0.30866E 00	0.21805E 00	0.14985E 00	0.86448E-01	-0.33536E-01
180.00	-0.44790E 00	-0.44694E 00	-0.31236E 00	-0.17021E 00	-0.73662E-01	-0.33467E-01	-0.12162E-01	-0.15696E-02
190.00	-0.94408E 00	-0.89214E 00	-0.72164E 00	-0.51331E 00	-0.34350E 00	-0.23345E 00	-0.14165E 00	-0.70071E-01
200.00	-0.62850E 00	-0.59214E 00	-0.48607E 00	-0.35250E 00	-0.24314E 00	-0.17063E 00	-0.10830E 00	-0.58231E-01
210.00	-0.47868E 00	-0.44766E 00	-0.36618E 00	-0.26916E 00	-0.13858E 00	-0.13477E 00	-0.88056E-01	-0.49946E-01
220.00	-0.40158E 00	-0.37237E 00	-0.30429E 00	-0.22504E 00	-0.15945E 00	-0.11549E 00	-0.77086E-01	-0.54144E-01
230.00	-0.35221E 00	-0.32457E 00	-0.26576E 00	-0.19805E 00	-0.14182E 00	-0.10393E 00	-0.70590E-01	-0.42815E-01
240.00	-0.31117E 00	-0.28694E 00	-0.23682E 00	-0.17451E 00	-0.12939E 00	-0.95920E-01	-0.66175E-01	-0.41112E-01
250.00	-0.27198E 00	-0.25112E 00	-0.21104E 00	-0.16198E 00	-0.11417E 00	-0.89470E-01	-0.62693E-01	-0.39798E-01
260.00	-0.23111E 00	-0.21641E 00	-0.18556E 00	-0.14565E 00	-0.10929E 00	-0.83258E-01	-0.59305E-01	-0.38432E-01
270.00	-0.14995E 00	-0.18075E 00	-0.15926E 00	-0.12460E 00	-0.94727E-01	-0.76489E-01	-0.55463E-01	-0.36700E-01
280.00	-0.15192E 00	-0.14720E 00	-0.13364E 00	-0.11133E 00	-0.87716E-01	-0.69241E-01	-0.51237E-01	-0.34657E-01
290.00	-0.12028E 00	-0.11674E 00	-0.11105E 00	-0.95648E-01	-0.77548E-01	-0.62523E-01	-0.47238E-01	-0.32646E-01
300.00	-0.94413E-01	-0.95537E-01	-0.92119E-01	-0.82131E-01	-0.68625E-01	-0.56591E-01	-0.43754E-01	-0.31035E-01
310.00	-0.74424E-01	-0.76438E-01	-0.75946E-01	-0.70183E-01	-0.60526E-01	-0.51127E-01	-0.40518E-01	-0.29494E-01
320.00	-0.57163E-01	-0.60134E-01	-0.61855E-01	-0.59327E-01	-0.52429E-01	-0.45373E-01	-0.37325E-01	-0.27924E-01
330.00	-0.42422E-01	-0.46025E-01	-0.49325E-01	-0.49405E-01	-0.45768E-01	-0.40400E-01	-0.34161E-01	-0.26311E-01
340.00	-0.29842E-01	-0.33944E-01	-0.38554E-01	-0.40769E-01	-0.39470E-01	-0.36317E-01	-0.31367E-01	-0.24923E-01
350.00	-0.16212E-01	-0.21309E-01	-0.27624E-01	-0.32304E-01	-0.33491E-01	-0.32204E-01	-0.28962E-01	-0.23898E-01

FIGURE 15. POWER-EFFECT PRESSURE COEFFICIENTS ON SAMPLE WING
AFTER APPLICATION OF SEGMENT METHOD

PRESSURE COEFFICIENTS AT WING AFTER RESIDUAL SOURCE/SINK MODIFICATION.

THETA	Y= 0.0 RB= 2.89 DRDY= 0.0	Y= 2.50 RB= 2.71 DRDY= -0.07	Y= 5.04 RB= 2.53 DRDY= -0.07	Y= 7.79 RB= 2.33 DRDY= -0.07	Y= 12.54 RB= 2.13 DRDY= -0.07	Y= 13.00 RB= 1.96 DRDY= -0.07	Y= 16.05 RB= 1.74 DRDY= -0.07	Y= 20.13 RB= 1.44 DRDY= -0.07
0.0	-0.1044E-02	-0.5734E-02	-0.8385E-02	-0.9526E-02	-0.9367E-02	-0.8618E-02	-0.7370E-02	-0.5740E-02
10.00	-0.7137E-01	-0.2271E-01	-0.1707E-01	-0.3101E-01	-0.3276E-01	-0.3121E-01	-0.2822E-01	-0.2346E-01
20.00	-0.1165E-01	-0.1270E-01	-0.1738E-01	-0.2251E-01	-0.2276E-01	-0.2646E-01	-0.2512E-01	-0.2142E-01
30.00	-0.4471E-02	-0.4506E-02	-0.1049E-01	-0.1654E-01	-0.2090E-01	-0.2332E-01	-0.2183E-01	-0.2092E-01
40.00	0.2043E-02	0.1161E-02	-0.4091E-02	-0.1105E-01	-0.1675E-01	-0.2058E-01	-0.2155E-01	-0.2024E-01
50.00	0.4035E-02	0.7444E-02	0.2028E-02	-0.5749E-02	-0.1267E-01	-0.1798E-01	-0.2001E-01	-0.1957E-01
60.00	0.1384E-01	0.1365E-01	0.8230E-02	-0.3504E-03	-0.4487E-02	-0.1537E-01	-0.1841E-01	-0.1487E-01
70.00	0.1974E-01	0.2006E-01	0.1462E-01	0.5724E-02	-0.4172E-02	-0.1278E-01	-0.1689E-01	-0.1624E-01
80.00	0.7624E-01	0.2710E-01	0.2166E-01	0.1133E-01	0.5139E-03	-0.1009E-01	-0.1534E-01	-0.1771E-01
90.00	0.3376E-01	0.3523E-01	0.2986E-01	0.1845E-01	0.5481E-02	-0.6940E-02	-0.1359E-01	-0.1709E-01
100.00	0.4215E-01	0.4452E-01	0.3907E-01	0.2651E-01	0.1226E-01	-0.3172E-02	-0.1134E-01	-0.1408E-01
110.00	0.5274E-01	0.5551E-01	0.5001E-01	0.3613E-01	0.1940E-01	0.1537E-02	-0.8402E-02	-0.1464E-01
120.00	0.6536E-01	0.6962E-01	0.6387E-01	0.4819E-01	0.2927E-01	0.7542E-02	-0.4604E-02	-0.1273E-01
130.00	0.8347E-01	0.8415E-01	0.8284E-01	0.6456E-01	0.4190E-01	0.1569E-01	0.5138E-03	-0.1019E-01
140.00	0.1117E-00	0.1183E-00	0.1114E-00	0.6440E-01	0.6002E-01	0.2774E-01	0.8025E-02	-0.6504E-02
150.00	0.1583E-00	0.1773E-00	0.1582E-00	0.1245E-00	0.9092E-01	0.4738E-01	0.2021E-01	-0.4000E-03
160.00	0.2437E-00	0.2567E-00	0.2428E-00	0.2705E-00	0.1464E-00	0.8378E-01	0.4298E-01	0.1057E-01
170.00	0.3777E-00	0.3928E-00	0.3137E-00	0.3165E-00	0.2407E-00	0.1498E-00	0.8644E-01	0.3353E-01
180.00	0.2552E-00	0.3108E-00	-0.2695E-00	-0.1798E-00	-0.9718E-01	-0.3667E-01	-0.1216E-01	-0.1549E-02
190.00	0.7076E-00	-0.7355E-00	-0.6854E-00	-0.5282E-00	-0.3781E-00	-0.2336E-00	-0.1416E-00	-0.7007E-01
200.00	0.4038E-00	-0.5038E-00	-0.4540E-00	-0.3613E-00	-0.2463E-00	-0.1706E-00	-0.1083E-00	-0.5821E-01
210.00	0.3832E-00	-0.3887E-00	-0.3462E-00	-0.2725E-00	-0.2029E-00	-0.1347E-00	-0.8806E-01	-0.4494E-01
220.00	0.3372E-00	-0.3283E-00	-0.2994E-00	-0.2297E-00	-0.1704E-00	-0.1154E-00	-0.7086E-01	-0.4541E-01
230.00	0.2917E-00	-0.2896E-00	-0.2540E-00	-0.2018E-00	-0.1506E-00	-0.1039E-00	-0.7090E-01	-0.4281E-01
240.00	0.2671E-00	-0.2583E-00	0.2272E-00	-0.1817E-00	-0.1357E-00	-0.9920E-01	-0.6617E-01	-0.4112E-01
250.00	0.2349E-00	-0.2281E-00	-0.2031E-00	-0.1645E-00	-0.1229E-00	-0.8947E-01	-0.6269E-01	-0.3974E-01
260.00	0.2006E-00	-0.1972E-00	-0.1703E-00	-0.1479E-00	-0.1134E-00	-0.8325E-01	-0.5930E-01	-0.3843E-01
270.00	-0.1655E-00	-0.1655E-00	-0.1543E-00	-0.1303E-00	-0.1027E-00	-0.7648E-01	-0.5543E-01	-0.3670E-01
280.00	-0.1329E-00	-0.1355E-00	-0.1295E-00	-0.1126E-00	-0.9086E-01	-0.6928E-01	-0.5123E-01	-0.3465E-01
290.00	-0.1058E-00	-0.1100E-00	-0.1079E-00	-0.9657E-01	-0.7987E-01	-0.6723E-01	-0.4723E-01	-0.3269E-01
300.00	-0.8427E-01	-0.8431E-01	-0.8978E-01	-0.8274E-01	-0.7031E-01	-0.5659E-01	-0.4375E-01	-0.3103E-01
310.00	-0.6679E-01	-0.7218E-01	-0.7426E-01	-0.7054E-01	-0.6170E-01	-0.5112E-01	-0.4051E-01	-0.2944E-01
320.00	-0.5243E-01	-0.5744E-01	-0.6064E-01	-0.5748E-01	-0.5369E-01	-0.4587E-01	-0.3725E-01	-0.2702E-01
330.00	-0.4013E-01	-0.4474E-01	-0.4941E-01	-0.4938E-01	-0.4619E-01	-0.4080E-01	-0.3416E-01	-0.2611E-01
340.00	-0.3000E-01	-0.3345E-01	-0.3784E-01	-0.4053E-01	-0.3759E-01	-0.3631E-01	-0.3136E-01	-0.2492E-01
350.00	-0.1948E-01	-0.2146E-01	-0.2715E-01	-0.3177E-01	-0.3324E-01	-0.3220E-01	-0.2896E-01	-0.2384E-01

FIGURE 16. POWER-EFFECT PRESSURE COEFFICIENTS ON SAMPLE WING AFTER RESIDUAL SOURCE AND SINK MODIFICATION

PRESSURE COEFFICIENTS AT WING, END OF THREE DIMENSIONAL MODIFICATION OF 1 ITERATION.

THETA	Y= 0.0 RB= 0.0 DRDY= 0.0	Y= 2.50 RB= 2.71 DRDY= -0.07	Y= 5.04 RB= 2.53 DRDY= -0.07	Y= 7.74 RB= 2.33 DRDY= -0.07	Y= 10.54 RB= 2.13 DRDY= -0.07	Y= 13.00 RB= 1.96 DRDY= -0.07	Y= 16.05 RB= 1.74 DRDY= -0.07	Y= 20.13 RB= 1.44 DRDY= -0.07
0.0	-0.74190E-03	-0.50720E-02	-0.79456E-02	-0.93214E-02	-0.93742E-02	-0.86181E-02	-0.73706E-02	-0.57606E-02
10.00	-0.21177E-01	-0.22572E-01	-0.26978E-01	-0.30967E-01	-0.32277E-01	-0.31210E-01	-0.28222E-01	-0.23469E-01
20.00	-0.14372E-01	-0.15119E-01	-0.19024E-01	-0.23335E-01	-0.25515E-01	-0.26463E-01	-0.25123E-01	-0.21827E-01
30.00	-0.95504E-02	-0.10043E-01	-0.13584E-01	-0.18102E-01	-0.20960E-01	-0.23324E-01	-0.23183E-01	-0.20927E-01
40.00	-0.54948E-02	-0.55752E-02	-0.86683E-02	-0.13361E-01	-0.16621E-01	-0.20585E-01	-0.21555E-01	-0.20242E-01
50.00	-0.20791E-02	-0.15934E-02	-0.40871E-02	-0.81411E-02	-0.12498E-01	-0.17989E-01	-0.20001E-01	-0.19575E-01
60.00	0.92636E-03	0.21144E-02	0.39450E-03	-0.43024E-02	-0.82590E-02	-0.15371E-01	-0.18418E-01	-0.18875E-01
70.00	0.37043E-02	0.57077E-02	0.48743E-02	0.30566E-03	-0.38866E-02	-0.12787E-01	-0.16897E-01	-0.18247E-01
80.00	0.63697E-02	0.36777E-02	0.96188E-02	0.32598E-02	0.86567E-03	-0.10094E-01	-0.15384E-01	-0.17172E-01
90.00	0.93879E-02	0.13577E-01	0.15099E-01	0.11009E-01	0.64127E-02	-0.69402E-02	-0.13599E-01	-0.17058E-01
100.00	0.12646E-01	0.18214E-01	0.21221E-01	0.17519E-01	0.12741E-01	-0.31721E-02	-0.11348E-01	-0.16084E-01
110.00	0.22894E-01	0.31803E-01	0.38233E-01	0.35238E-01	0.20429E-01	0.15376E-02	-0.84022E-02	-0.14648E-01
120.00	0.31911E-01	0.43102E-01	0.51676E-01	0.48739E-01	0.42825E-01	0.15697E-01	0.51303E-03	-0.10191E-01
130.00	0.47036E-01	0.61310E-01	0.72471E-01	0.69175E-01	0.61750E-01	0.27745E-01	0.80258E-02	-0.65044E-02
140.00	0.73748E-01	0.92752E-01	0.10742E 00	0.10279E 00	0.92489E-01	0.47386E-01	0.40211E-01	-0.60003E-03
150.00	0.12700E 00	0.15340E 00	0.17316E 00	0.16489E 00	0.14857E 00	0.83784E-01	0.42986 01	0.10574E-01
160.00	0.22570E 00	0.26241E 00	0.28521E 00	0.26995E 00	0.24361E 00	0.15985E 00	0.86448E-01	0.35536E-01
170.00	-0.10155E 00	-0.14442E 00	-0.15198E 00	-0.12882E 00	-0.99592E-01	-0.36667E-01	-0.12162E-01	-0.15496E-02
180.00	-0.43301E 00	-0.64878E 00	-0.50219E 00	-0.44781E 00	-0.38254E 00	-0.23365E 00	-0.14165E 00	-0.70071E-01
190.00	-0.33615E 00	-0.46194E 00	-0.35873E 00	-0.31472E 00	-0.26664E 00	-0.17063E 00	-0.10830E 00	-0.58231E-01
200.00	-0.28358E 00	-0.29495E 00	-0.28324E 00	-0.24328E 00	-0.20464E 00	-0.13477E 00	-0.88056E-01	-0.49946E-01
210.00	-0.25670E 00	-0.25958E 00	-0.24330E 00	-0.20597E 00	-0.17163E 00	-0.11549E 00	-0.77086E-01	-0.45414E-01
220.00	-0.23785E 00	-0.21594E 00	-0.21896E 00	-0.18409E 00	-0.15163E 00	-0.10393E 00	-0.70590E-01	-0.42815E-01
230.00	-0.21368E 00	-0.21515E 00	-0.19825E 00	-0.16735E 00	-0.13753E 00	-0.9520E-01	-0.66175E-01	-0.41112E-01
240.00	-0.17525E 00	-0.19276E 00	-0.17934E 00	-0.1574E 00	-0.12596E 00	-0.8470E-01	-0.62693E-01	-0.39798E-01
250.00	-0.16810E 00	-0.16913E 00	-0.15948E 00	-0.13809E 00	-0.11490E 00	-0.83258E-01	-0.59305E-01	-0.38432E-01
260.00	-0.13908E 00	-0.14186E 00	-0.13810E 00	-0.12235E 00	-0.10323E 00	-0.76488E-01	-0.5463E-01	-0.35700E-01
270.00	-0.11168E 00	-0.11652E 00	-0.11669E 00	-0.10619E 00	-0.91230E-01	-0.69281E-01	-0.51237E-01	-0.34657E-01
280.00	-0.88495E-01	-0.94878E-01	-0.97660E-01	-0.91422E-01	-0.80182E-01	-0.62523E-01	-0.47238E-01	-0.32696E-01
290.00	-0.70318E-01	-0.77252E-01	-0.81599E-01	-0.78637E-01	-0.70554E-01	-0.56591E-01	-0.43754E-01	-0.31035E-01
300.00	-0.56526E-01	-0.62926E-01	-0.67915E-01	-0.67356E-01	-0.61845E-01	-0.51127E-01	-0.40518E-01	-0.29494E-01
310.00	-0.44748E-01	-0.50537E-01	-0.55908E-01	-0.57124E-01	-0.53825E-01	-0.45873E-01	-0.3725E-01	-0.27924E-01
320.00	-0.34483E-01	-0.39927E-01	-0.45276E-01	-0.47406E-01	-0.46288E-01	-0.40800E-01	-0.34161E-01	-0.26311E-01
330.00	-0.27281E-01	-0.31020E-01	-0.36191E-01	-0.39705E-01	-0.39644E-01	-0.36317E-01	-0.31367E-01	-0.26923E-01
340.00	-0.19577E-01	-0.27100E-01	-0.27246E-01	-0.31925E-01	-0.33222E-01	-0.32204E-01	-0.28962E-01	-0.23898E-01
350.00								

FIGURE 17. POWER-EFFECT PRESSURE COEFFICIENTS ON SAMPLE WING AFTER ONE ITERATION

PRESSURE COEFFICIENTS AT WING AFTER RESIDUAL SOURCE/SINK MODIFICATION.

THETA	Y= 0.0 RB= 2.89 DRDY= 0.0	Y= 2.50 RB= 2.71 DRDY= -0.07	Y= 5.04 RB= 2.53 DRDY= -0.07	Y= 7.74 RB= 2.37 DRDY= -0.07	Y= 10.54 RB= 2.13 DRDY= -0.07	Y= 13.00 RB= 1.96 DRDY= -0.07	Y= 16.05 RB= 1.74 DRDY= -0.07	Y= 20.11 RB= 1.44 DRDY= -0.07
0.0	-0.17328E-02	-0.56176E-02	-0.81943E-02	-0.93440E-02	-0.92755E-02	-0.86181E-02	-0.73706E-02	-0.57674E-02
1.0	-0.26211E-01	-0.21895E-01	-0.25812E-01	-0.30256E-01	-0.32225E-01	-0.31210E-01	-0.28223E-01	-0.2369E-01
2.0	-0.15212E-01	-0.12612E-01	-0.16971E-01	-0.22047E-01	-0.23225E-01	-0.22643E-01	-0.25124E-01	-0.21827E-01
3.0	-0.70060E-02	-0.59946E-02	-0.10738E-01	-0.16310E-01	-0.21649E-01	-0.23244E-01	-0.23183E-01	-0.2027E-01
4.0	0.4210E-04	0.15572E-03	-0.49160E-02	-0.11045E-01	-0.17747E-01	-0.20585E-01	-0.21555E-01	-0.20247E-01
5.0	0.62329E-02	0.59175E-02	-0.62186E-01	-0.59452E-02	-0.13958E-01	-0.17989E-01	-0.20001E-01	-0.19375E-01
6.0	0.11985E-01	0.11565E-01	0.61345E-02	-0.91429E-03	-0.10064E-01	-0.15371E-01	-0.18418E-01	-0.18875E-01
7.0	0.17669E-01	0.17311E-01	0.11774E-01	0.42522E-02	-0.6063E-02	-0.12787E-01	-0.16897E-01	-0.18247E-01
8.0	0.23710E-01	0.23511E-01	0.17931E-01	0.38679E-02	-0.17532E-02	-0.1094E-01	-0.15384E-01	-0.17127E-01
9.0	0.30701E-01	0.30955E-01	0.25120E-01	0.16411E-01	0.32574E-02	-0.69402E-02	-0.13599E-01	-0.17058E-01
10.0	0.38544E-01	0.39214E-01	0.33233E-01	0.23848E-01	0.90794E-02	-0.31721E-02	-0.11348E-01	-0.14044E-01
11.0	0.48138E-01	0.49200E-01	0.42964E-01	0.32772E-01	0.15910E-01	0.15376E-02	-0.84022E-02	-0.14648E-01
12.0	0.60807E-01	0.62169E-01	0.55645E-01	0.45093E-01	0.24536E-01	0.75482E-02	-0.46040E-02	-0.12738E-01
13.0	0.78667E-01	0.80277E-01	0.72718E-01	0.59563E-01	0.36143E-01	0.1597E-01	0.51383E-03	-0.10191E-01
14.0	0.10618E-00	0.10778E-00	0.98909E-01	0.82717E-01	0.53319E-01	0.27745E-01	0.80258E-02	-0.65044E-02
15.0	0.15172E-00	0.15386E-00	0.14211E-00	0.12068E-00	0.81325E-01	0.47386E-01	0.20211E-01	-0.6003E-03
16.0	0.23502E-00	0.23806E-00	0.22117E-00	0.18998E-00	0.13283E-00	0.83784E-01	0.42986E-01	0.10574E-01
17.0	0.36511E-00	0.37042E-00	0.34725E-00	0.30309E-00	0.22193E-00	0.14985E-00	0.86448E-01	0.33536E-01
18.0	0.26290E-00	0.27276E-00	-0.22987E-00	-0.18431E-00	-0.92538E-01	-0.36567E-01	-0.12162E-01	-0.15496E-02
19.0	-0.67252E-00	-0.68779E-00	-0.61687E-00	-0.50517E-00	-0.34994E-00	-0.23365E-00	-0.14165E-00	-0.70071E-01
20.0	-0.47096E-00	-0.47616E-00	-0.42473E-00	-0.34308E-00	-0.24756E-00	-0.17063E-00	-0.10830E-00	-0.58231E-01
21.0	-0.37164E-00	-0.36988E-00	-0.32668E-00	-0.26632E-00	-0.19204E-00	-0.13477E-00	-0.85056E-01	-0.49966E-01
22.0	-0.32045E-00	-0.31391E-00	-0.27486E-00	-0.23033E-00	-0.16243E-00	-0.11549E-00	-0.77086E-01	-0.45414E-01
23.0	-0.27869E-00	-0.27732E-00	-0.24240E-00	-0.19653E-00	-0.14459E-00	-0.10393E-00	-0.70390E-01	-0.42815E-01
24.0	-0.25773E-00	-0.24843E-00	-0.21765E-00	-0.17734E-00	-0.13179E-00	-0.95920E-01	-0.66175E-01	-0.41112E-01
25.0	-0.22700E-00	-0.21483E-00	-0.19512E-00	-0.16095E-00	-0.12122E-00	-0.89470E-01	-0.62693E-01	-0.39798E-01
26.0	-0.19416E-00	-0.19038E-00	-0.17237E-00	-0.14469E-00	-0.11094E-00	-0.83258E-01	-0.59305E-01	-0.38432E-01
27.0	-0.16047E-00	-0.16006E-00	-0.14857E-00	-0.12796E-00	-0.99907E-01	-0.76488E-01	-0.55463E-01	-0.37000E-01
28.0	-0.12927E-00	-0.13135E-00	-0.12512E-00	-0.11078E-00	-0.88431E-01	-0.69281E-01	-0.51237E-01	-0.37657E-01
29.0	-0.10350E-00	-0.10695E-00	-0.10440E-00	-0.91646E-01	-0.77814E-01	-0.62523E-01	-0.47238E-01	-0.32696E-01
30.0	-0.83107E-01	-0.87068E-01	-0.86930E-01	-0.81668E-01	-0.68548E-01	-0.56591E-01	-0.43754E-01	-0.31035E-01
31.0	-0.66844E-01	-0.70599E-01	-0.71975E-01	-0.67726E-01	-0.60218E-01	-0.51127E-01	-0.40518E-01	-0.29494E-01
32.0	-0.53401E-01	-0.56335E-01	-0.58751E-01	-0.58847E-01	-0.52545E-01	-0.45873E-01	-0.37325E-01	-0.27924E-01
33.0	-0.42205E-01	-0.43695E-01	-0.46868E-01	-0.44843E-01	-0.45528E-01	-0.40800E-01	-0.34161E-01	-0.26311E-01
34.0	-0.33486E-01	-0.32698E-01	-0.36464E-01	-0.40099E-01	-0.39979E-01	-0.36317E-01	-0.31367E-01	-0.24923E-01
35.0	-0.24533E-01	-0.23217E-01	-0.25951E-01	-0.31236E-01	-0.32976E-01	-0.32204E-01	-0.28962E-01	-0.23898E-01

FIGURE 18. POWER-EFFECT PRESSURE COEFFICIENTS ON SAMPLE WING AFTER RESIDUAL SOURCE AND SINK MODIFICATION (Second Time)

PRESSURE COEFFICIENTS AT WING, END OF THREE DIMENSIONAL MUJIFICATION OF C ITERATION.

Y= C.O	Y= 2.50	Y= 5.04	Y= 7.74	Y= 10.54	Y= 13.00	Y= 16.05	Y= 20.14
RB= 2.59	RB= 2.71	RB= 2.53	RB= 2.33	RB= 2.13	RB= 1.96	RB= 1.74	RB= 1.44
DRDY= 0.0	DRDY= -0.07	DRDY= -0.07	DRDY= -0.07	DRDY= -0.07	DRDY= -0.07	DRDY= -0.07	DRDY= -0.07
0.0	-0.52336E-02	-0.78013E-02	-0.92046E-02	-0.93080E-02	-0.86181E-02	-0.73706E-02	-0.57606E-02
10.00	-0.21761E-01	-0.25726E-01	-0.30207E-01	-0.32231E-01	-0.31210E-01	-0.28223E-01	-0.23469E-01
20.00	-0.14833E-01	-0.13636E-01	-0.12697E-01	-0.12697E-01	-0.12697E-01	-0.12697E-01	-0.12697E-01
30.00	-0.10119E-01	-0.13546E-01	-0.17907E-01	-0.21442E-01	-0.23183E-01	-0.20427E-01	-0.16947E-01
40.00	-0.60560E-02	-0.90834E-02	-0.13405E-01	-0.17441E-01	-0.20584E-01	-0.21555E-01	-0.20242E-01
50.00	-0.24174E-02	-0.49704E-02	-0.31654E-02	-0.13546E-01	-0.17989E-01	-0.20001E-01	-0.19575E-01
60.00	-0.92234E-03	-0.10043E-02	-0.49744E-02	-0.95376E-02	-0.15371E-01	-0.18418E-01	-0.18847E-01
70.00	-0.40791E-02	0.28870E-02	-0.40301E-03	-0.54099E-02	-0.12787E-01	-0.16897E-01	-0.17712E-01
80.00	-0.72375E-02	0.69516E-02	0.35277E-02	-0.94533E-03	-0.10094E-01	-0.15384E-01	-0.17712E-01
90.00	-0.10872E-01	0.11657E-01	0.87510E-02	0.42519E-02	-0.69402E-02	-0.11359E-01	-0.17058E-01
100.00	-0.14906E-01	0.16939E-01	0.14541E-01	0.10213E-01	-0.31721E-02	-0.11348E-01	-0.16084E-01
110.00	-0.20063E-01	0.23442E-01	0.21664E-01	0.17353E-01	-0.15376E-02	-0.84022E-02	-0.14648E-01
120.00	-0.27192E-01	0.32013E-01	0.30749E-01	0.26270E-01	0.75482E-02	-0.46040E-02	-0.12738E-01
130.00	-0.37660E-01	0.4776E-01	0.43317E-01	0.34265E-01	0.15697E-01	0.51383E-03	-0.10191E-01
140.00	-0.54692E-01	0.6221E-01	0.62349E-01	0.55973E-01	0.27745E-01	0.80258E-02	-0.65044E-02
150.00	-0.84232E-01	0.95214E-01	0.94064E-01	0.84813E-01	0.47386E-01	0.20211E-01	-0.60003E-03
160.00	-0.14218E-01	0.15690E-01	0.15299E-01	0.13771E-01	0.83784E-01	0.42986E-01	0.10574E-01
170.00	-0.24702E-01	0.26406E-01	0.25424E-01	0.22864E-01	0.14985E-01	0.86448E-01	0.33536E-01
180.00	-0.12018E-01	-0.13082E-01	-0.11454E-01	-0.87604E-01	-0.36667E-01	-0.12162E-01	-0.15496E-02
190.00	-0.46241E-01	-0.46802E-01	-0.42343E-01	-0.35999E-01	-0.23305E-01	-0.14165E-01	-0.70071E-01
200.00	-0.34640E-01	-0.33800E-01	-0.30043E-01	-0.25353E-01	-0.17063E-01	-0.10830E-01	-0.58231E-01
210.00	-0.26870E-01	-0.26974E-01	-0.23464E-01	-0.19603E-01	-0.13477E-01	-0.88056E-01	-0.49946E-01
220.00	-0.25078E-01	-0.23306E-01	-0.19474E-01	-0.16538E-01	-0.11549E-01	-0.77086E-01	-0.54414E-01
230.00	-0.22741E-01	-0.20979E-01	-0.17834E-01	-0.14691E-01	-0.10393E-01	-0.70590E-01	-0.42815E-01
240.00	-0.20975E-01	-0.19134E-01	-0.16263E-01	-0.13366E-01	-0.95920E-01	-0.66175E-01	-0.41112E-01
250.00	-0.18735E-01	-0.17351E-01	-0.14844E-01	-0.12277E-01	-0.89470E-01	-0.62693E-01	-0.37998E-01
260.00	-0.16364E-01	-0.15457E-01	-0.13430E-01	-0.11221E-01	-0.83258E-01	-0.59305E-01	-0.38432E-01
270.00	-0.13830E-01	-0.13435E-01	-0.11979E-01	-0.10095E-01	-0.76488E-01	-0.55463E-01	-0.36700E-01
280.00	-0.11386E-01	-0.11343E-01	-0.10419E-01	-0.89276E-01	-0.69281E-01	-0.51237E-01	-0.34667E-01
290.00	-0.92971E-01	-0.93038E-01	-0.99876E-01	-0.78494E-01	-0.65223E-01	-0.47238E-01	-0.37696E-01
300.00	-0.75962E-01	-0.79486E-01	-0.77455E-01	-0.69090E-01	-0.56591E-01	-0.43754E-01	-0.31035E-01
310.00	-0.61932E-01	-0.66198E-01	-0.66450E-01	-0.60640E-01	-0.51127E-01	-0.40518E-01	-0.27494E-01
320.00	-0.45963E-01	-0.54480E-01	-0.56423E-01	-0.52606E-01	-0.45873E-01	-0.37325E-01	-0.27424E-01
330.00	-0.39441E-01	-0.44013E-01	-0.47227E-01	-0.45496E-01	-0.40800E-01	-0.34161E-01	-0.26311E-01
340.00	-0.30450E-01	-0.34958E-01	-0.39153E-01	-0.39037E-01	-0.36317E-01	-0.31367E-01	-0.24923E-01
350.00	-0.21450E-01	-0.26038E-01	-0.31285E-01	-0.32969E-01	-0.32204E-01	-0.28962E-01	-0.23898E-01

FIGURE 19. POWER-EFFECT PRESSURE COEFFICIENTS ON SAMPLE WING AFTER TWO ITERATIONS

PARAMETERS USED IN 3D MODIFICATION OF WING COMPUTATION IDIS= 4 N800L= 0 MEXIT= 1 MOD= 5
 PARAMETERS IN FORCE/MOMENT COMPUTATION IJET OF DIAMETER= 2.250 XCG= 10.718 ZCG= 0.0 REFERENCE LENGTH= 8.350

****FORCES AND MOMENTS****

X-FORCE Y-FORCE Z-FORCE
 -0.599E-02 0.0 -0.213E 00

PITCHING MOMENT COMPUTED ABOUT AXIS THRU C.G.= -0.176E 00

YAWING MOMENT COMPUTED ABOUT AXIS THRU C.G.= 0.0

ROLLING MOMENT COMPUTED ABOUT AXIS THRU C.G.= 0.0

*****END OF WING COMPUTATION*****

FIGURE 20. FORCES AND MOMENTS ON SAMPLE WING BY TRANSFORMATION METHOD

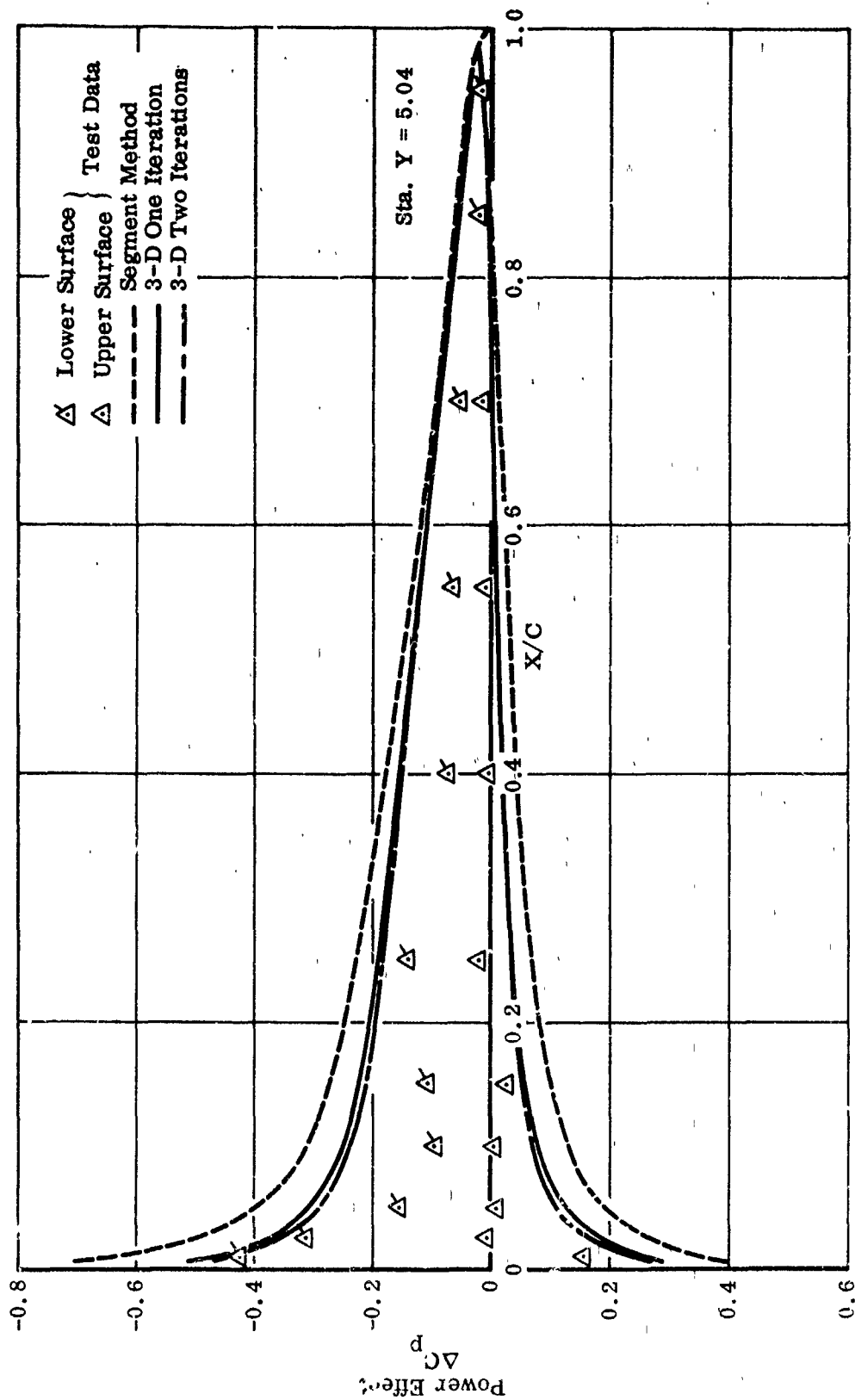


FIGURE 21a. POWER-EFFECT PRESSURE COEFFICIENTS ON SAMPLE WING AT STATION Y = 5.04

$U_\infty/U_j = 0.2$, $\alpha = \beta = 0^\circ$, Lift Jet

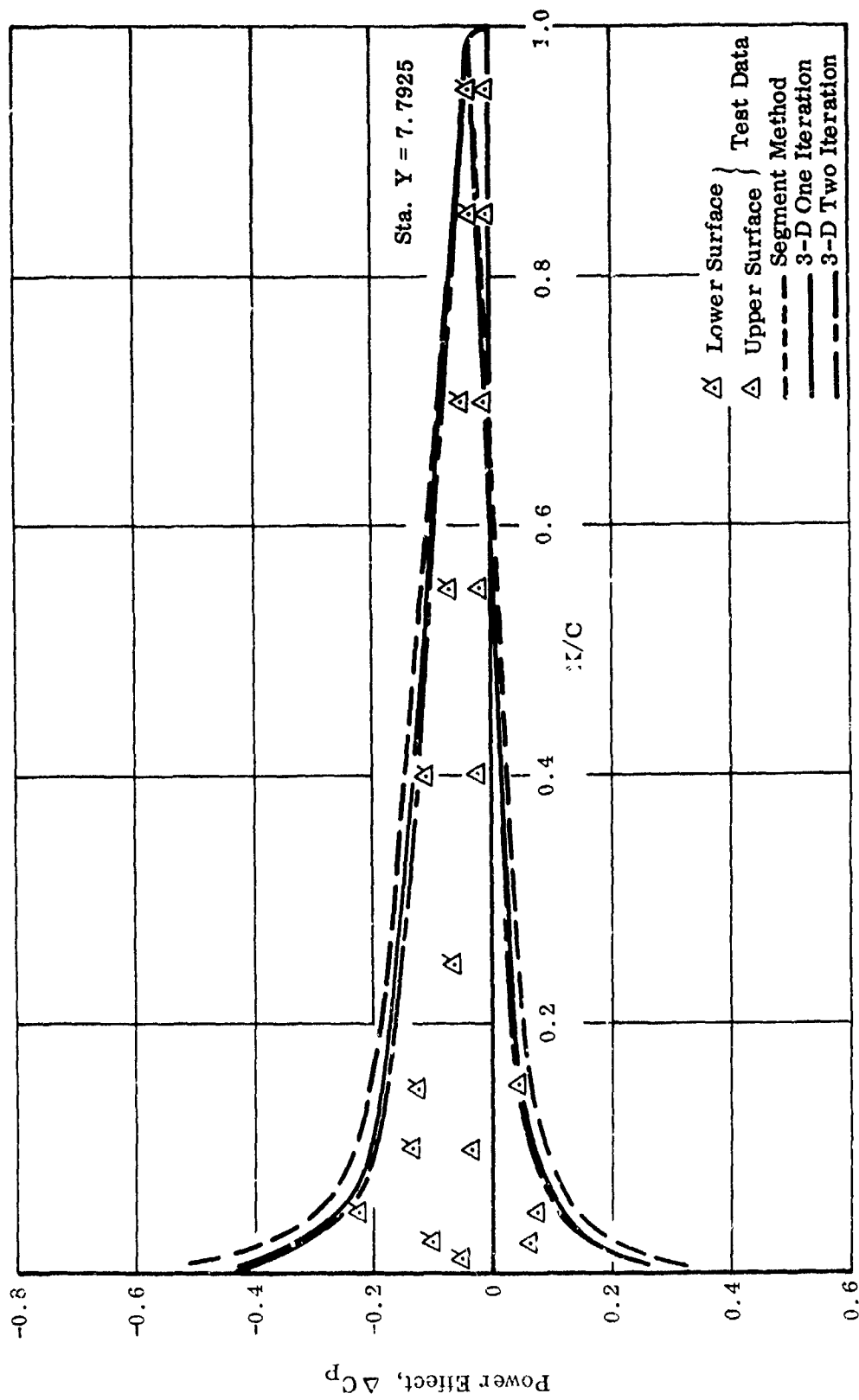


FIGURE 21b. POWER-EFFECT PRESSURE COEFFICIENTS ON SAMPLE
WING AT STATION Y = 7.7925"

$U_\infty/U_j = 0.2$, $\alpha = \beta = 0^\circ$, Lift Jet

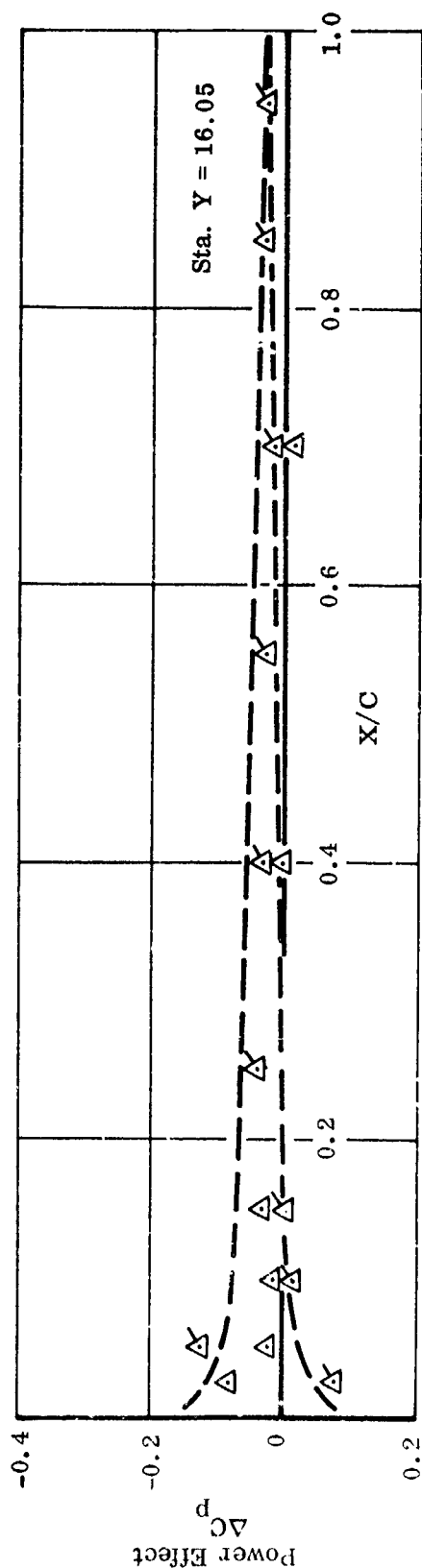
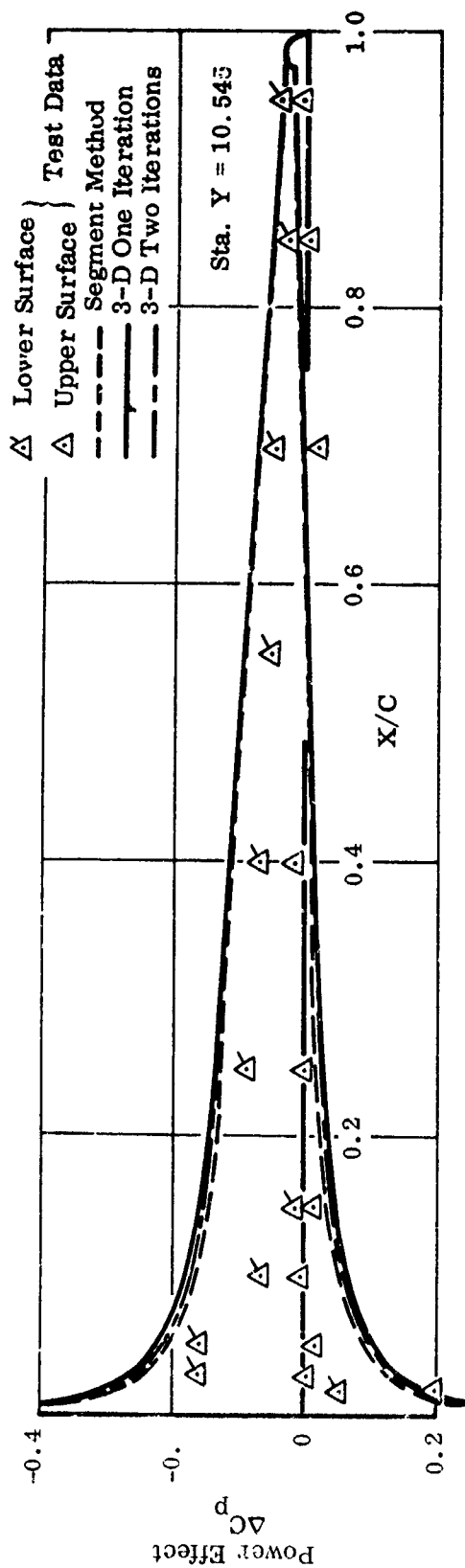


FIGURE 21c. POWER-EFFECT PRESSURE COEFFICIENTS ON SAMPLE WING AT STATIONS Y = 10.545 AND Y = 16.05

$$U_\infty/U_j = 0.2, \quad \alpha = \beta = 0^\circ, \quad \text{Lift Jet}$$

Comparison of forces for sample problem with wind tunnel test data of Appendix I is shown in Figure 22, together with further calculations and test data. The calculated power-induced lift follows the trend of the test data. The calculated values show a greater loss in lift than the test data. This is consistent with the surface pressure results shown in Figure 21. The reasons for these differences are not known at the present time.

c. Method Applicability and Limitations

This method is generally applicable to power effects on the wing. In addition to the present configuration, fairly extensive calculations on a rectangular wing of aspect ratio equal to 3 with a modified NACA 65-010 section have also been performed (Figure 23(b)). The jet (or jets) was (were) situated at the midspan of the wing and exhausted directly from the lower surface. But the chordwise location of the jet was allowed to vary (three positions: 20 percent, 50 percent and 80 percent of the chord length from the leading edge) and the number of the jets could be one or two. Most of those calculations have been compared with the wind tunnel test data which were obtained at Northrop prior to the present study. Some of these comparisons are shown in Figures 24 and 25.

When the jet exhausts directly from the wing surface, the induced velocity distribution generally shows large and abrupt changes across the jet station. If two iterations are planned these iterations should be smoothed out. Otherwise, the computed results following the second iteration may exhibit unacceptable oscillations. If the calculation is limited to one iteration no smoothing was found to be necessary. Since the lift jet did not exhaust directly from the wing surface in this sample problem, the input data was not smoothed, even though two iterations were computed.

Under the present scheme all the vertical velocity components at any given station, regardless of the chordwise position, are reduced equally to a magnitude of one third of the lifting line downwash value (see pages 101-102 of Volume I for details). Since the aforementioned procedure is somewhat arbitrary some limitations on the method presumably exist. For flow conditions radically different from the present one, the approach given here may have to be modified.

The present method, even when the three-dimensional modification is used, does not include all the three-dimensional effects. The method is, in effect, a quasi-two-dimensional one. Like the widely used quasi-one-dimensional approximation for diffusers and nozzles, its applicability is not as restricted as it may appear. In every example considered, the agreement between calculation and test data is fairly satisfactory. Because of the quasi-two-dimensional nature, however, computations beyond two

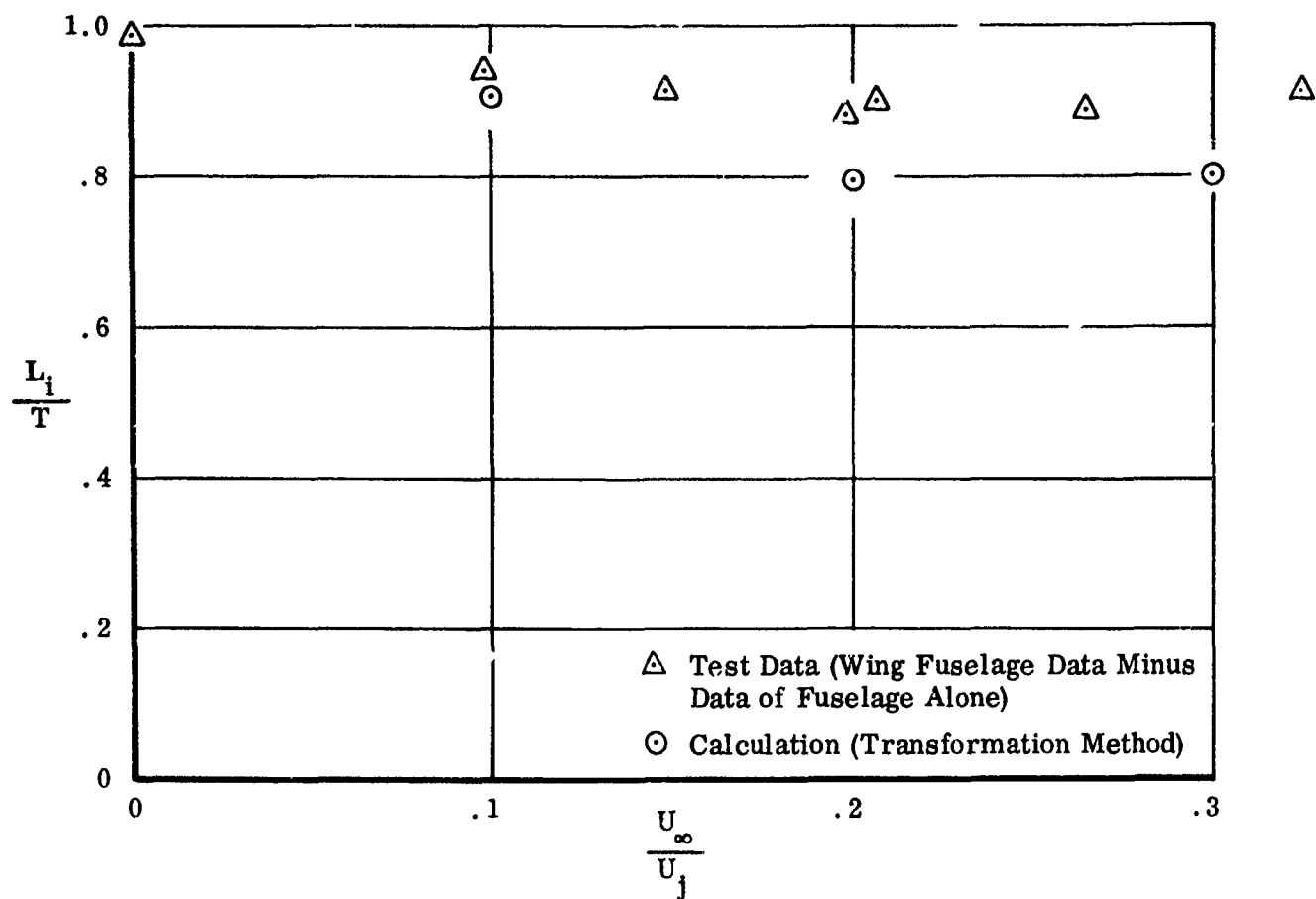


FIGURE 22. POWER-EFFECT LIFT FOR WING WITH LIFT JET

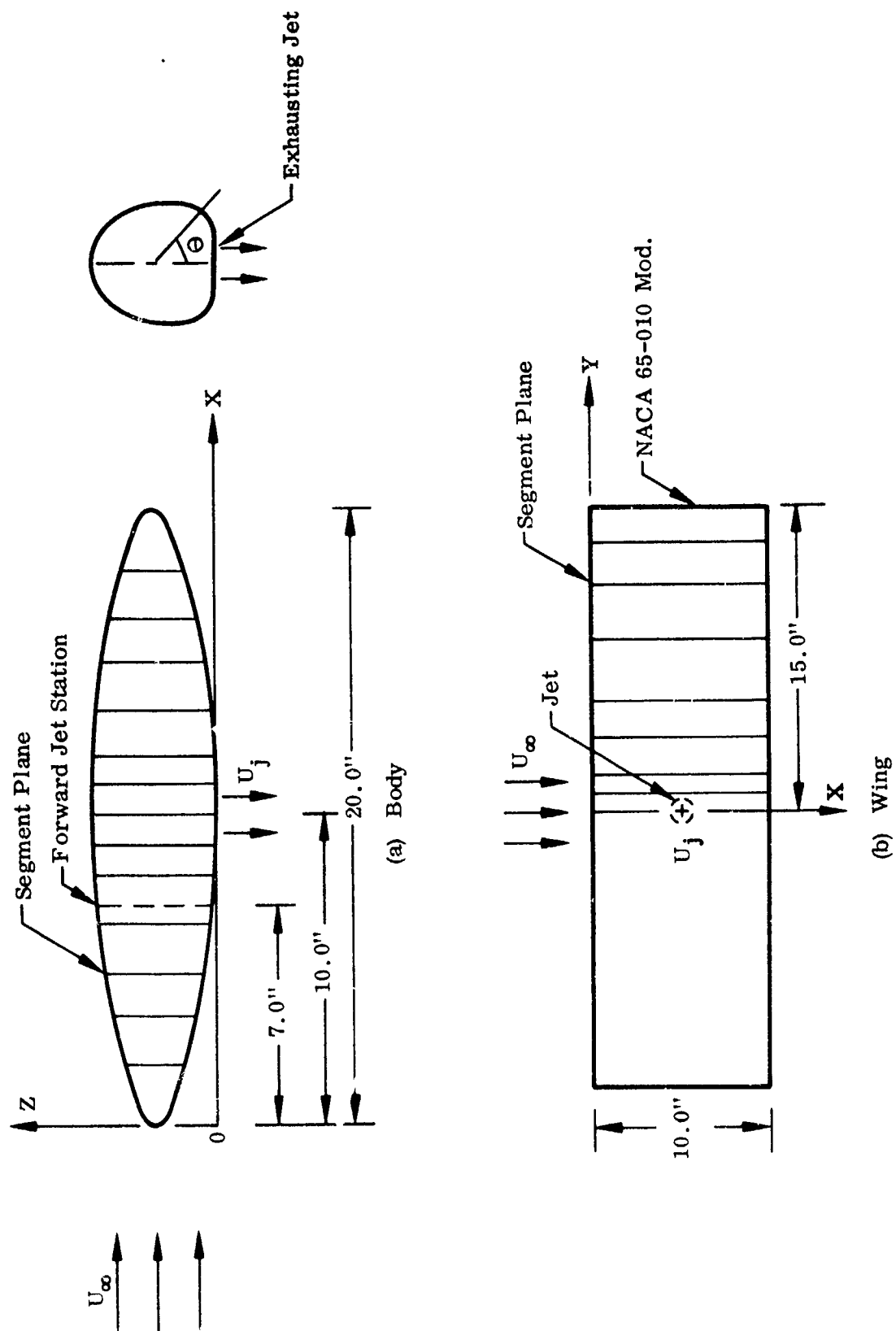


FIGURE 23. CONFIGURATIONS TESTED AT NOROTROP

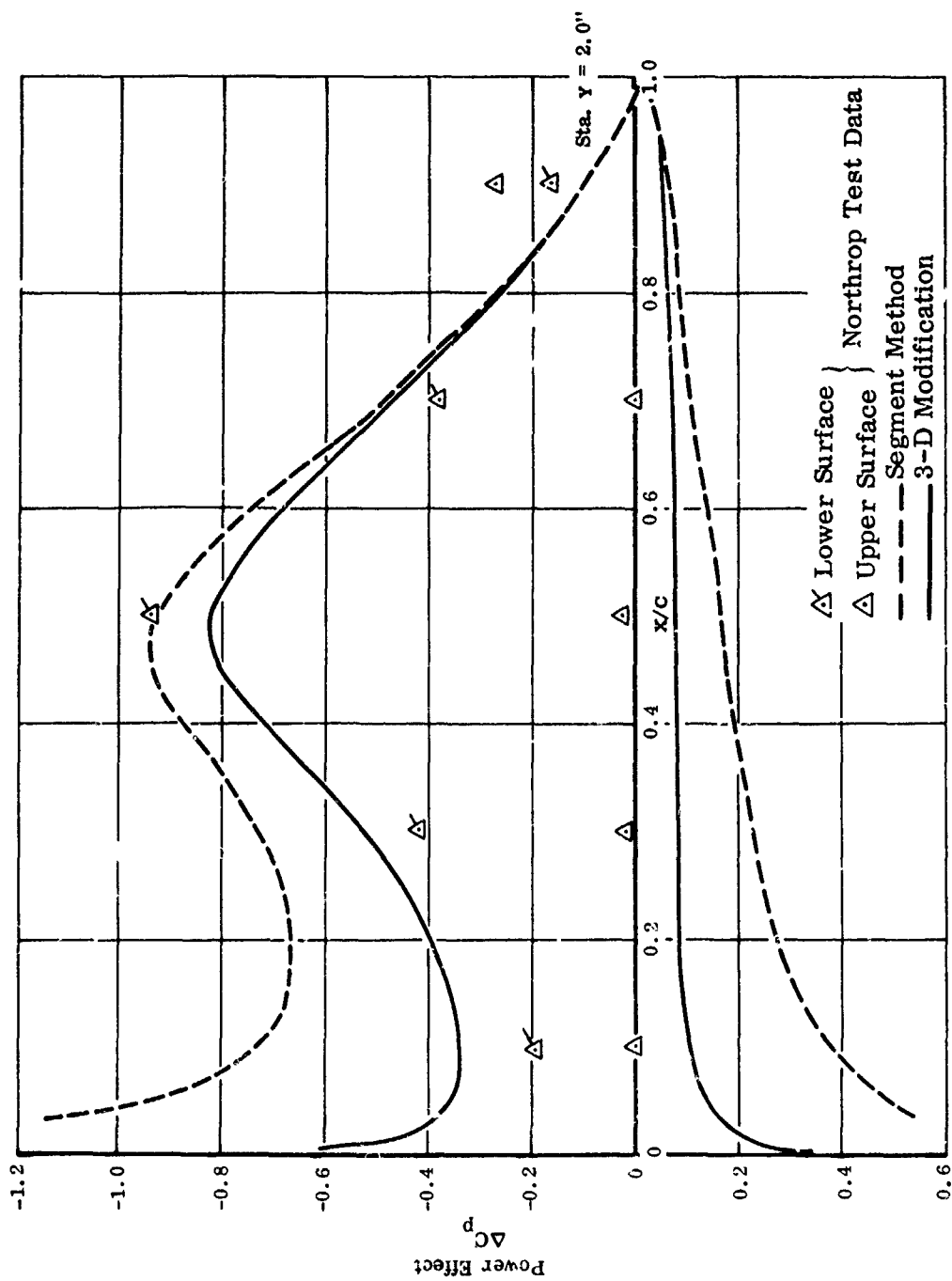


FIGURE 24. POWER-EFFECT PRESSURE COEFFICIENTS ON NORTROP WING AT STATION $Y = 2.0''$

$U_\infty/U_j = 0.1$, $\alpha = \beta = 0^\circ$, Two Midspan Jets at $X/C = 0.5$ and 0.8

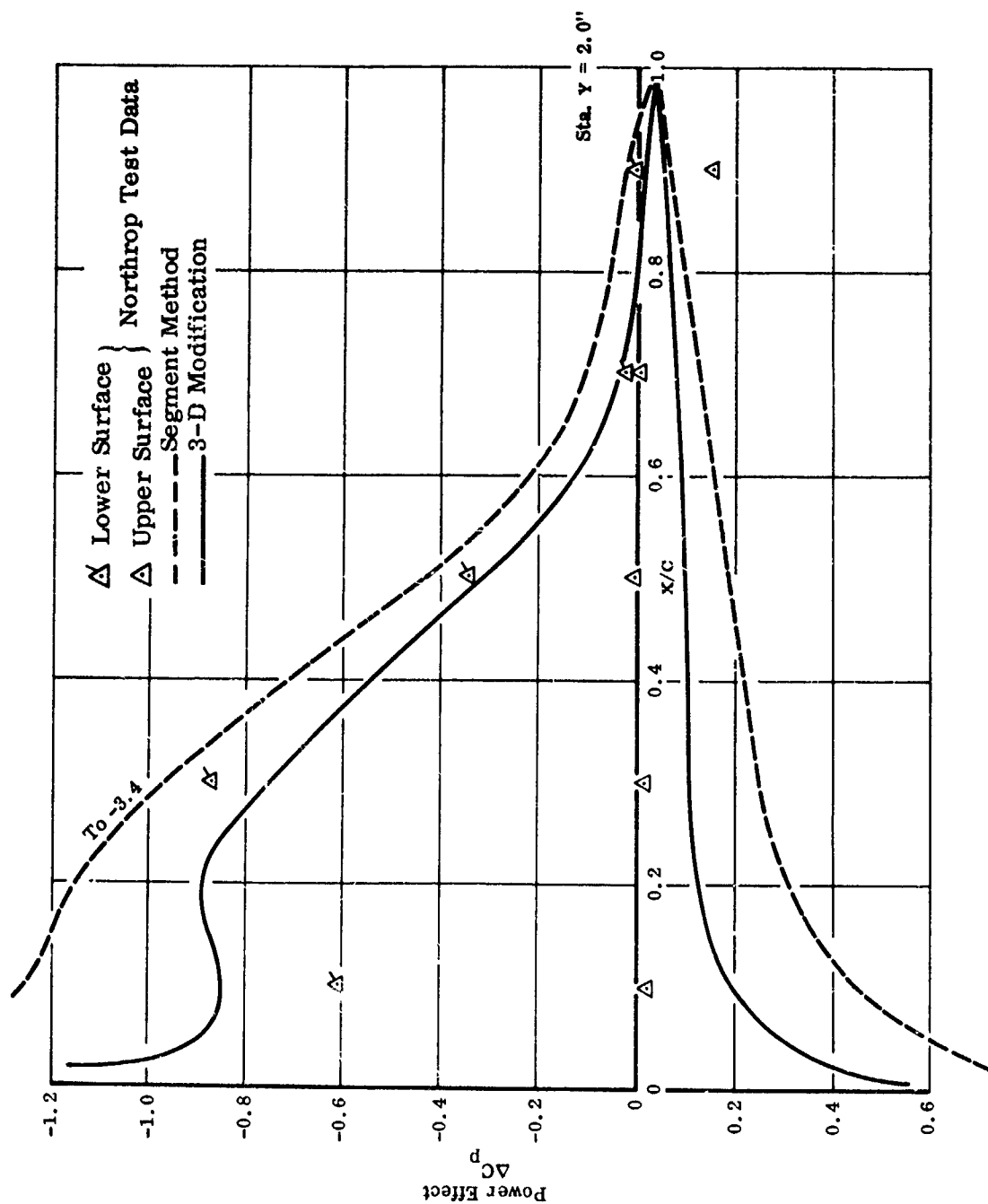


FIGURE 25. POWER-EFFECT PRESSURE COEFFICIENTS ON NORTHROP WING AT STATION $Y = 2.0''$

$U_\infty/U_j = 0.1$, $\alpha = \beta = 0^\circ$, Two Midspan Jets at $X/C = 0.2$ and 0.5

iterations may not be warranted. In practice, one iteration is what is usually needed. Two iterations have, nevertheless, been carried out in some selected problems and also in the sample problem here. This is more for demonstration purpose than for utility.

The present computer program is, in a formal sense, capable of treating both power-on and power-off problems. However, for the power-off case, the wing tips exert a much larger influence upon the flow property than in the case when power effects are being calculated. This important three-dimensional effect has not been adequately accounted for by the present method and the calculations from it are likely to be less accurate. Therefore, the lifting surface theory is recommended under such circumstances.

5. APPLICATION OF LIFTING SURFACE THEORY TO WING

Lifting Surface theory may be utilized to determine the load distribution and aerodynamic coefficients for a given arbitrary planform and specified downwash distribution. The Lifting Surface computer program evaluates power effects on the wing by considering a known, jet-induced downwash distribution.

There are three main components to the program which may be used together in one continuous operation or independently. The downwash control point matrix $[D]$ is generated in the first part of the program, its least squares inverse $[D]^\psi$ is generated in the second part of the program. The pressure distribution produced by the specified downwash matrix $[W]$ is computed by the third component of the program. The downwash control point matrix and its inverse depend only on the planform, the location of the downwash control points and the number of terms in the loading series. Both matrices are independent of the downwash distribution. Once the inverse is computed it forms an input to the third component of the program, where the pressure distribution is computed. Thus $[D]^\psi$ may be retained in punched card form and then used as input for computing the pressure distribution due to specified downwash distributions. The inverse need not be recomputed as long as the planform, location of downwash control points and the size of the pressure loading series remain unchanged.

The Lifting Surface program is a modified version of the computer program for designing and analyzing subsonic lifting surfaces documented in Reference 12. The design options have been eliminated. The capability to calculate pressure distributions produced by a specified cambered surface has also been deleted.

a. Sample Problem Computation

For the sample problem being considered the Lifting Surface program is now used to determine the load distribution and aerodynamic coefficients on the wing, produced by the jet-induced downwash computed in Section II.3.

Figure 26 shows details of the planform of the wing and indicates the location of downwash control points. Figure 26 is identical to Figure 8 of Section II.3, except that all dimensions are now based on a semi-span of unity.

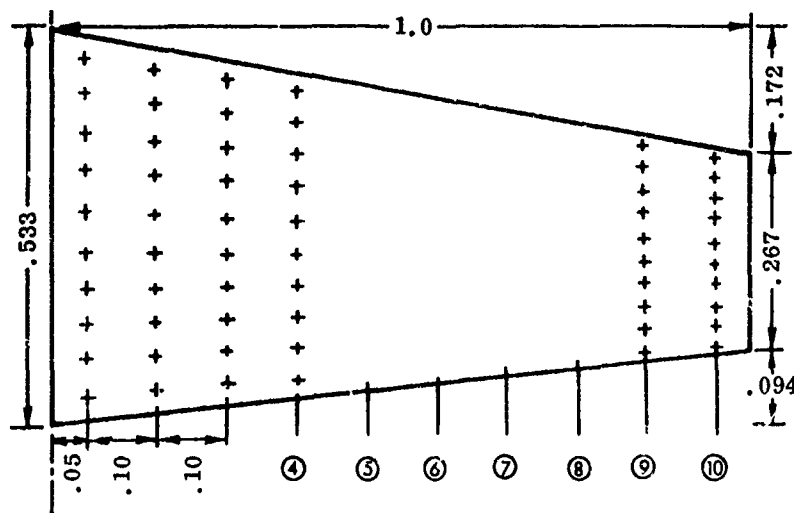


FIGURE 26. DOWNWASH CONTROL POINTS ON WING

(1) Input for Sample Problem

The input cards required for the sample problem are shown in Figure 27. Since all three main components of the program, discussed in detail above, are being executed in one continuous operation, some duplication of input data occurs.

Card 1 lists two control indices, specifying which of the three major components of the program are to be executed. The combination of $ISTART = 1$, $ISTOP = 3$ will execute all three major components. Consequently, the program will start by computing the downwash control matrix $[D]$, will find the inverse $[D]^{-1}$ and will compute the load distribution and aerodynamic coefficients.

Card 2 is a title card.

Card 3 lists the number of spanwise stations on semispan where downwash control points are to be located, $NS = 10$. It specifies the number of spanwise modes to be used in the pressure loading series, $M = 6$ and the number of chordwise modes, $N = 8$. The input control index $NEED = 1$ indicates that the first chordwise mode, i.e., $\cot \theta/2$ mode, is to be used in the computations. The number of leading and trailing edge flaps are specified with $NFLAP = 0$. The next two integers are print and punch controls for the downwash control matrix $[D]$. With $NPR = 0$, $NPU = 0$, no printed or punched output on $[D]$ will be generated. The print control $NAY = 0$ specifies that no intermediate print is to be generated during the computation of $[D]$. The number of leading edge discontinuities is specified as $N\theta LED = 2$, and the number of trailing edge discontinuities, $N\theta TED = 2$, is indicated.

[illegible]

DOWNWASH MATRIX **[W]** GENERATED
AS PUNCHED OUTPUT IN SECTION II. 3. b

FIGURE 27. (Concluded)

Card 4 indicates that the chordwise locations of the downwash control points must be specified through input cards at each spanwise station by listing $SPACE = 0$. It also lists the Mach number, $FMACH = 0.$, and defines the root-semichord $F = .2667$.

Cards 5 and 6 list the spanwise locations of the downwash control points.

Card 7 may be left blank for a wing with no leading or trailing edge flaps.

Card 8 specifies the tangents of the sweepback angles of the leading edges of the geometric regions.

Card 9 specifies the tangents of the sweepback angles of the trailing edges of the geometric regions.

Card 10 lists the spanwise locations of the leading edge discontinuities.

Card 11 lists the spanwise locations of the trailing edge discontinuities.

Card 12 specifies the number of downwash control points at each spanwise station.

Cards 13 – 22 list the chordwise locations of the downwash control points at each spanwise station (in percent of local chord).

This completes the input required for the first main component of the program, which computes the downwash control point matrix $[D]$.

Card 23 is a title card for the next main component of the program.

Card 24 lists the number of rows in the downwash control point matrix or the number of control points contained in $[D]$, $NROW = 100$. It specifies the number of columns in $[D]$, $NCOL = 36$. This is the product of the chordwise and spanwise pressure modes. The control index $NREAD = 0$ indicates that the second main component of the program is being executed in a continuous operation and hence $[D]$ will be read from a scratch tape, rather than input cards. With $NPR = 0$, $NPU = 0$, no printed or punched output will be obtained for $[D]^\psi$, the inverse of the downwash control point matrix. The print control $NAY = 0$ specifies that no intermediate print is to be generated during the computation of $[D]^\psi$.

This completes the input for the second main component of the program, which inverts the downwash control point matrix $[D]$ to obtain $[D]^\psi$.

Card 25 is a title card for the third main component of the program which computes the load distribution and aerodynamic coefficients for a specified downwash matrix.

Card 26 lists the number of chordwise modes used in the pressure loading series, $N = 6$, and the number of spanwise modes, $M = 6$. It specifies the number of spanwise stations where downwash control points are located, $NS = 10$, and specifies the number of rows in the downwash control point matrix, $NR\theta W = 100$. It specifies the number of spanwise stations where the chordwise pressure loading distribution is to be calculated, $NETA = 6$. It lists the number of wing discontinuities, $NDISC = 2$ and the number of leading and trailing edge flaps, $NFLAP = 0$. The intermediate print control is again $NAY = 0$. It also specifies the number of chordwise points at which the pressure loading is to be computed, $NPSI = 10$.

Card 27 lists the number of angles of attack to be treated, $NALFA = 1$. It also specifies the number of EPSLN's to be read later, $NEPSLN = 1$. The input control $NEED = 1$ indicates that the first chordwise mode, i.e., the $\cot \theta/2$ mode, is to be used in the computations. The control index $NREAD1 = 0$ again indicates a continuous operation and thus $[D]$ will be read from a scratch tape rather than from input cards. The next control integer, $NREAD2 = 1$ indicates that the downwash matrix $[W]$ is read from input cards. The number of downwash distributions to be analyzed is specified with $NW = 1$.

Card 28 specifies the root semi-chord, $F = .2667$. It indicates that the chordwise locations of the downwash control points are specified through input cards at each spanwise station by listing $SPACE = 0$. It lists the spanwise location of the edge of the fuselage, $YF = 0$. It indicates how the points at which the pressure loading is calculated are located chordwise, by giving the chordwise spacing $DPSI = .1$.

Card 29 lists the spanwise coordinates of the downwash control point stations.

Card 30 specifies the spanwise locations where the pressure loading is to be computed.

Card 31 lists the angle of incidence between the centerline of the fuselage and wing root chord in degrees, $EPSLN = 0$.

Card 32 specifies the angle of attack in degrees, $ALFA = 0$.

Card 33 may be left blank for a wing with no leading or trailing edge flaps.

Card 34 specifies the chord at each spanwise discontinuity.

Card 35 gives the location of each spanwise discontinuity.

Card 36 lists the distance from root leading edge to the leading edge at each spanwise discontinuity.

Card 37 specifies the number of downwash control points at each spanwise station.

Cards 38 — 57 specify the tangent of the downwash angle at every control point. Cards 38 — 57 are the downwash matrix $[W]$ generated in Section II.3 and shown in tabulated form in Figure 11 of Section II.3.

(2) Output for Sample Problem

With the choice of the punch controls described above, only printed output is obtained.

Figure 28(a) shows a composite of the printout generated by the first main component of the program (CHAIN 1, 8) which computes the downwash control point matrix.

Figure 28(b) shows the printout generated by the second main component of the program (CHAIN 6, 8) which inverts the downwash control point matrix $[D]$. The determinant of the unit matrix is printed out as a check on numerical accuracy.

Figure 28(c) shows the output from the third main component of the program (CHAIN 7, 8) which calculates the pressure loading and aerodynamic coefficients.

Geometric parameters of the wing are shown in Figure 28(c) and are all identified. Aerodynamic coefficients and the pressure loading calculated at the spanwise stations specified are shown in Figure 28(c). Again all computed variables are identified.

b. Applicability and Limitations

The program is applicable to continuous surfaces of arbitrary planform and no interference effects such as slots, ground effects, large dihedral angles or end plates are included. The program does contain provisions for body effects.

Downwash control points must not be located at or near the leading edge, since the cotangent elements of $[D]$ would become excessively large and dominate the solution for the pressure coefficient matrix $[A]$. Due to the computing techniques utilized, downwash control points must not be located at discontinuities in the planform and at flap hinge lines.

CHAIN (1,8)

CALCULATION OF DOWNWASH CONTROL POINT MATRIX FOR SAMPLE PROBLEM

NO. OF SPANWISE MODES = 6

NO. OF CHORDWISE MODES = 6

NO. OF FLAP MODES = 0

COTANGENT MODE, NEED = 1

POSITION OF FLAP 1 = 0.0

100 DOWNWASH CONTROL POINTS MACH NO.=0.0

DOWNWASH CONTROL POINTS	1	TO	10	Y=	0.49999997E-01
DOWNWASH CONTROL POINTS	11	TO	20	Y=	0.14999998E 00
DOWNWASH CONTROL POINTS	21	TO	30	Y=	0.25000000E 00
DOWNWASH CONTROL POINTS	31	TO	40	Y=	0.34999996E 00
DOWNWASH CONTROL POINTS	41	TO	50	Y=	0.44999999E 00
DOWNWASH CONTROL POINTS	51	TO	60	Y=	0.54999995E 00
DOWNWASH CONTROL POINTS	61	TO	70	Y=	0.64999998E 00
DOWNWASH CONTROL POINTS	71	TO	80	Y=	0.75000000E 00
DOWNWASH CONTROL POINTS	81	TO	90	Y=	0.84999996E 00
DOWNWASH CONTROL POINTS	91	TO	100	Y=	0.94999999E 00

FIGURE 28(a). LIFTING SURFACE THEORY PROGRAM PRINTED OUTPUT FOR SAMPLE PROBLEM

CHAIN (5,6)

INVERT DOWNWASH CONTROL POINT MATRIX FOR SAMPLE PROBLEM

DETERMINANT OF UNIT MATRIX = 0.10000000 01

FIGURE 28(b). (Continued)

CHAIN (7.4)

CALCULATION OF PRESSURE LOADING DISTRIBUTION FOR SAMPLE PROBLEM

NO 300Y

GEOMETRIC PARAMETERS

AVERAGE CHORD, CAVE = 0.430130

MEAN AERODYNAMIC CHORD, C_{BAR} = 0.414381

LOCATION OF 1/4 C_{BAR}, X_{BAR} = 0.180132

SPANWISE LOCATION OF C_{BAR}, Y_{BAR} = 0.444514

RESULTS FOR ALPHA = 0.0 , AND EPSILON = 0.0 DEGREES

LIFT COEFFICIENT, C_L = -0.11013

MOMENT COEFFICIENT, C_M = -0.00069

INDUCED DRAG COEFFICIENT, C_{DI} = 0.00095

PRESSURE LOADING DISTRIBUTION, PR

SPAN =	0.1000	0.2500	0.3880	0.5250	0.8000	0.9500
FRACTION OF CHORD						
0.1000	-0.2422	-0.2237	-0.1915	-0.1576	-0.0481	-0.0501
0.2000	-0.1884	-0.1703	-0.1437	-0.1185	-0.0649	-0.0377
0.3000	-0.1639	-0.1499	-0.1285	-0.1073	-0.0605	-0.0275
0.4000	-0.1360	-0.1262	-0.1098	-0.0922	-0.0520	-0.0231
0.5000	-0.1072	-0.1013	-0.0896	-0.0756	-0.0419	-0.0190
0.6000	-0.0834	-0.0811	-0.0737	-0.0629	-0.0350	-0.0162
0.7000	-0.0659	-0.0667	-0.0630	-0.0549	-0.0319	-0.0147
0.8000	-0.0493	-0.0526	-0.0517	-0.0461	-0.0282	-0.0129
0.9000	-0.0272	-0.0301	-0.0307	-0.0279	-0.0167	-0.0084
1.0000	-0.0000	-0.0000	-0.0000	-0.0000	0.0000	-0.0000

LOCAL SEMICHORD, C/2

0.2533 0.2333 0.2150 0.1967 0.1601 0.1401

CL C/CAVE

-0.1841 -0.1645 -0.1356 -0.1051 -0.0508 -0.0221

C_M C**2/CAVE C_{BAR}

-0.0132 -0.0052 0.0008 0.0044 0.0050 0.0028

C_D*C/CAVE

0.0029 0.0019 0.0009 0.0003 -0.0000 -0.0000

FIGURE 28(c). (Concluded)

c. Additional Calculations and Comparison with Test Data

Once the inverse of the downwash control point matrix has been obtained for a particular wing planform, it is a relatively easy task to obtain the power induced aerodynamics for a range of downwash distribution corresponding to different power conditions. Figures 29a through 29g show calculations for the test model, described in Appendix I, compared with test data for a number of power configurations, velocity ratios and angles of attack.

The interference lift for the vectored thrust, forward position, 90° nozzle deflection angle is shown in Figure 29a for a range of velocity ratios. The wing calculations show that, for all velocity ratios, the induced lift L_i (lift with power on minus lift with power off) is less than for the static case that is, $U_\infty = 0$. In contrast the test data for wing plus body indicate that there is a lift augmentation at the higher velocity ratios. For nozzle deflection angles of 45° (Figure 29b), although there is now no positive jet interference lift at the higher velocity ratios, the induced lift from the test data is nearly constant for $.3 \leq U_\infty / U_{j0} \leq .5$, whereas the calculations indicate the induced lift decreases as the velocity ratio increases.

For both the above cases the induced lift was determined from the test data using the inlet plugged as the unpowered case. With the inlet open the mainstream flow through the ejector produces a "power" effect which can be quite large as indicated in Appendix I.

The body alone lift, with power on, for the vectored thrust, forward position, 90° nozzle deflection angle is shown in Figure 29c. Since this configuration was not tested with the inlets plugged, it is not possible to determine the induced lift. However, due to model symmetry, it is reasonable to assume that the power off plugged inlet lift will be quite small and so that the induced lift graph for the body alone configuration will be very similar to Figure 29c.

The positive lift arises due to power induced uploads on the nacelles and body ahead of the jet exits. If this lift increment is subtracted from the wing-body test data, we get very good agreement with the wing calculations.

Figures 29d and 29e show comparisons between the calculations and test data for the aft nozzle positions with two vectoring angles. For the aft position the body alone power effects are expected to be smaller than for the forward position due to the jet exhausts being farther removed from the nacelles. The agreement between test and calculations is seen to be extremely good for all velocity ratios.

Figure 29f shows calculations of the induced lift on the wing with the lift jet operating at a velocity ratio of .20 for a range of α . For $\alpha \leq 8^\circ$, L_i/T and hence

C_{Li} (induced lift coefficient), is effectively independent of α . For larger α the calculated induced lift is still approximately constant whereas the test data shows a sudden increase in induced lift. This is due to a change in the stalling characteristics for the wing, deduced from the pressure measurements, brought about by the jet induced flow field producing a downwash over the wing for this particular jet arrangement and velocity ratio.

This result identifies an area in which care must be taken in using the prediction methods. It has been assumed that one can calculate power effects and add these to the unpowered aerodynamics of the vehicle. This procedure of superposition appears to be justified for the linear range of α , but must not be used for nonlinear α . Instead, these two effects must be considered together for nonlinear α . It is possible that the induced flow field due to the power could be included in the nonlinear wing aerodynamics procedure presented in Section VII of Volume I but this has not been studied under the present investigation.

Similar observations may be made for the vectored thrust configuration. Calculations and test data are shown in Figure 29g.

Calculations of pitching moment due to power effects show that there is a nose up pitching moment for body alone, the magnitude of which does not change noticeably with the addition of the wing. This result is in agreement with the calculations.

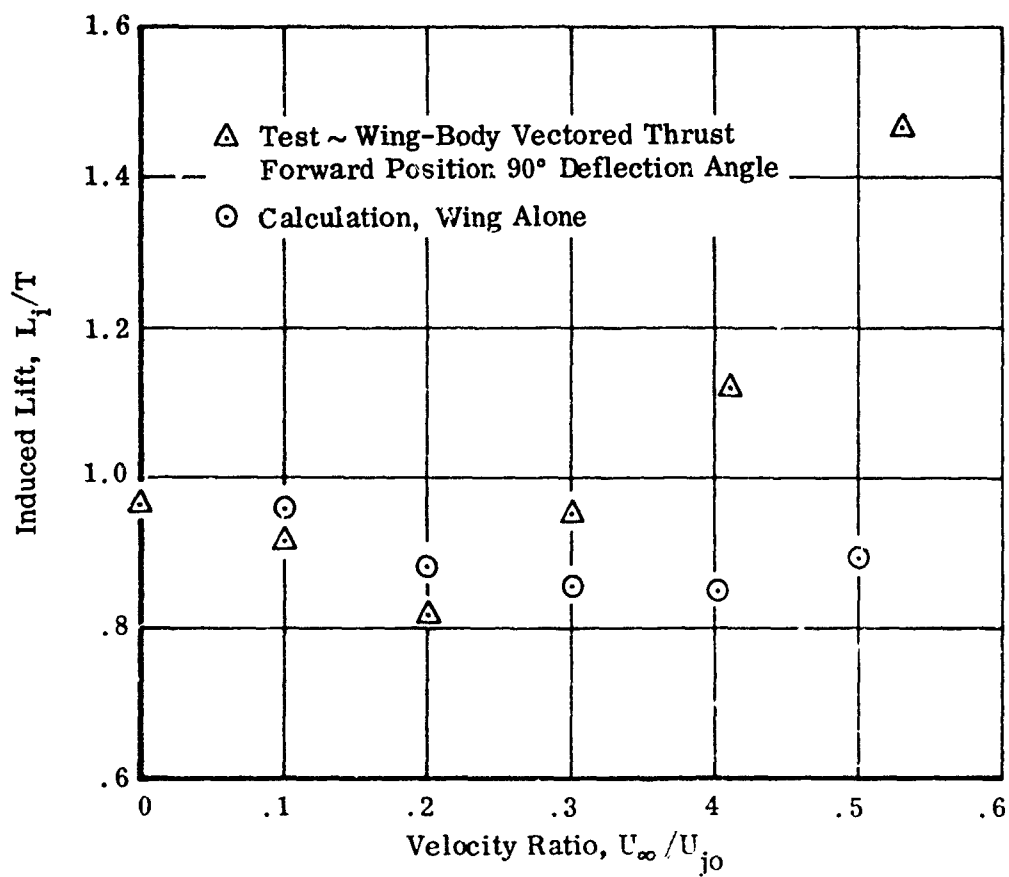


FIGURE 29a. INTERFERENCE LIFT FOR VECTORED THRUST,
 FORWARD POSITION, 90° DEFLECTION ANGLE, $\alpha = \beta = 0$

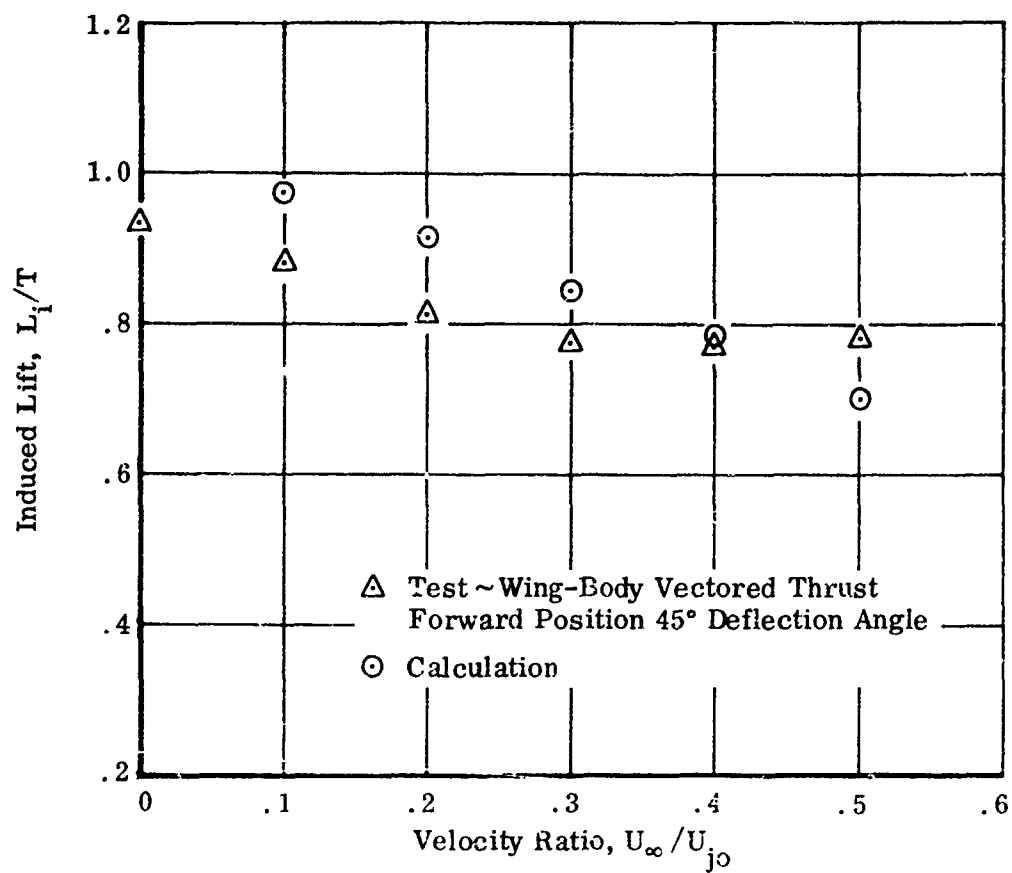


FIGURE 29b. INTERFERENCE LIFT FOR VECTORED THRUST,
FORWARD POSITION, 45° DEFLECTION ANGLE, $\alpha = \beta = 0$

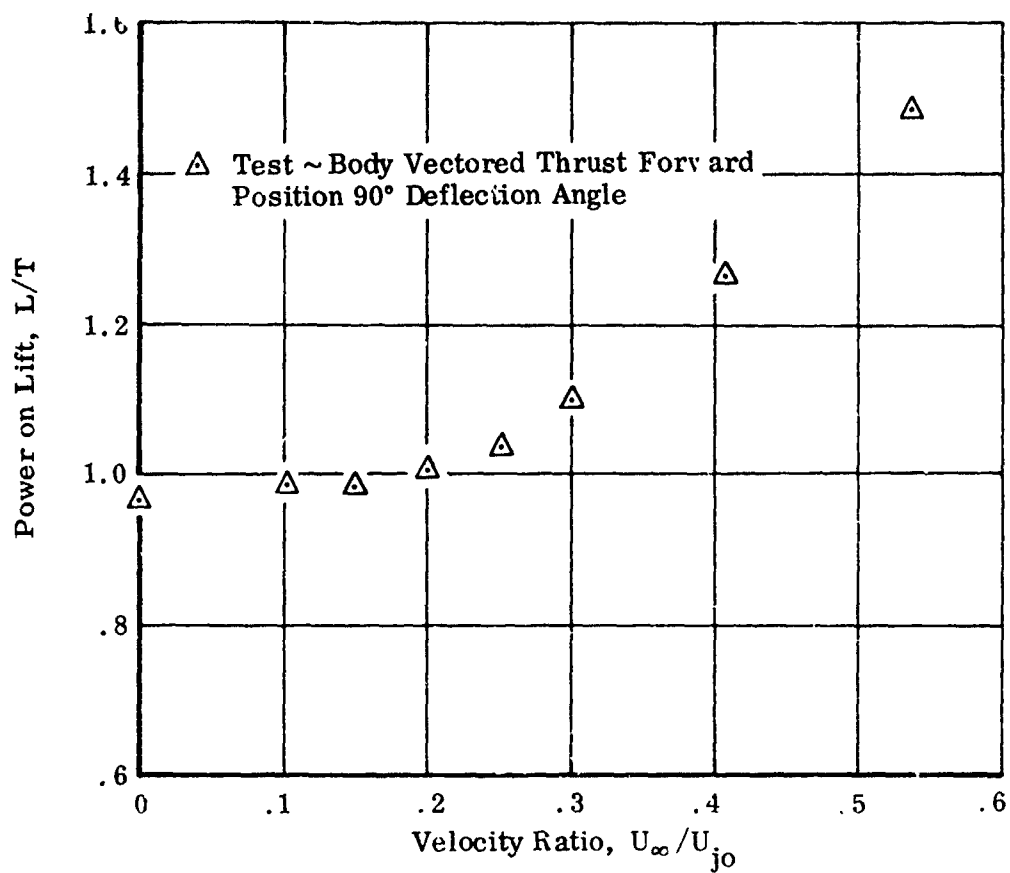


FIGURE 29c. LIFT FOR VECTORED THRUST, FORWARD POSITION, 90° DEFLECTION ANGLE, $\alpha = \beta = 0$

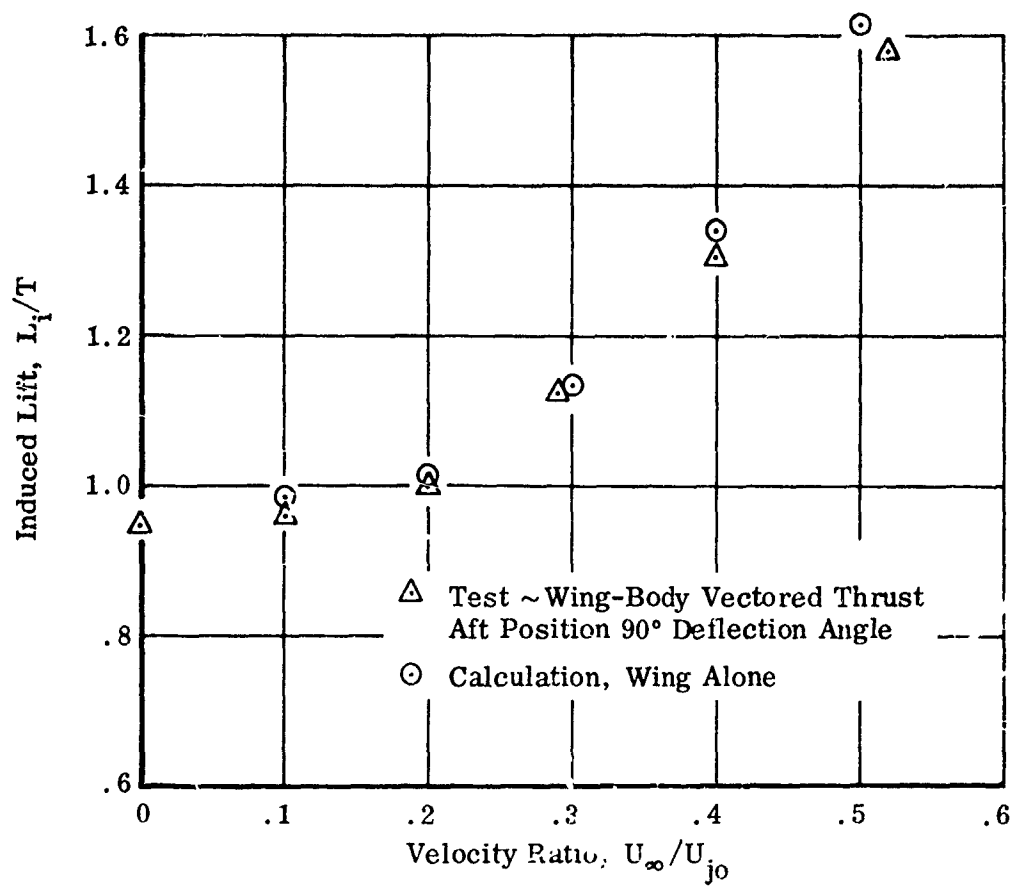


FIGURE 29d. INTERFERENCE LIFT FOR VECTORED THRUST,
 AFT POSITION, 90° DEFLECTION ANGLE, $\alpha = \beta = 0$

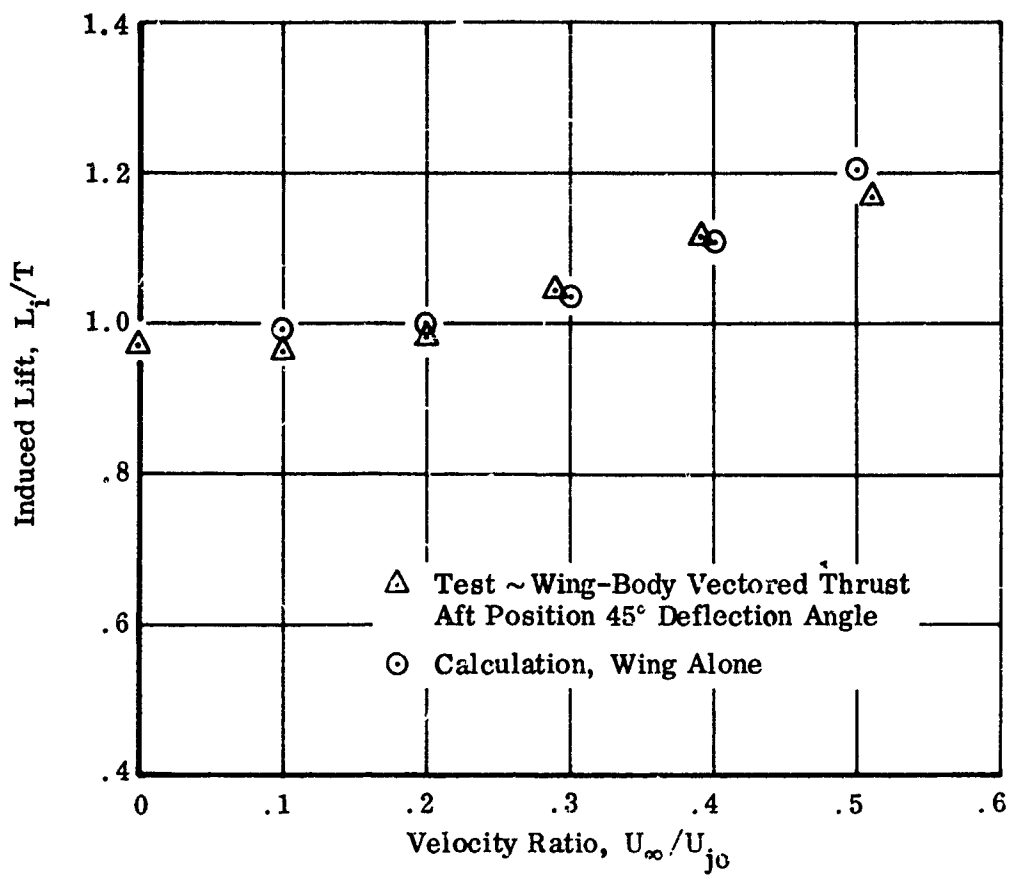


FIGURE 29e. INTERFERENCE LIFT FOR VECTORED THRUST,
AFT POSITION, 45° DEFLECTION ANGLE, $\alpha = \beta = 0$

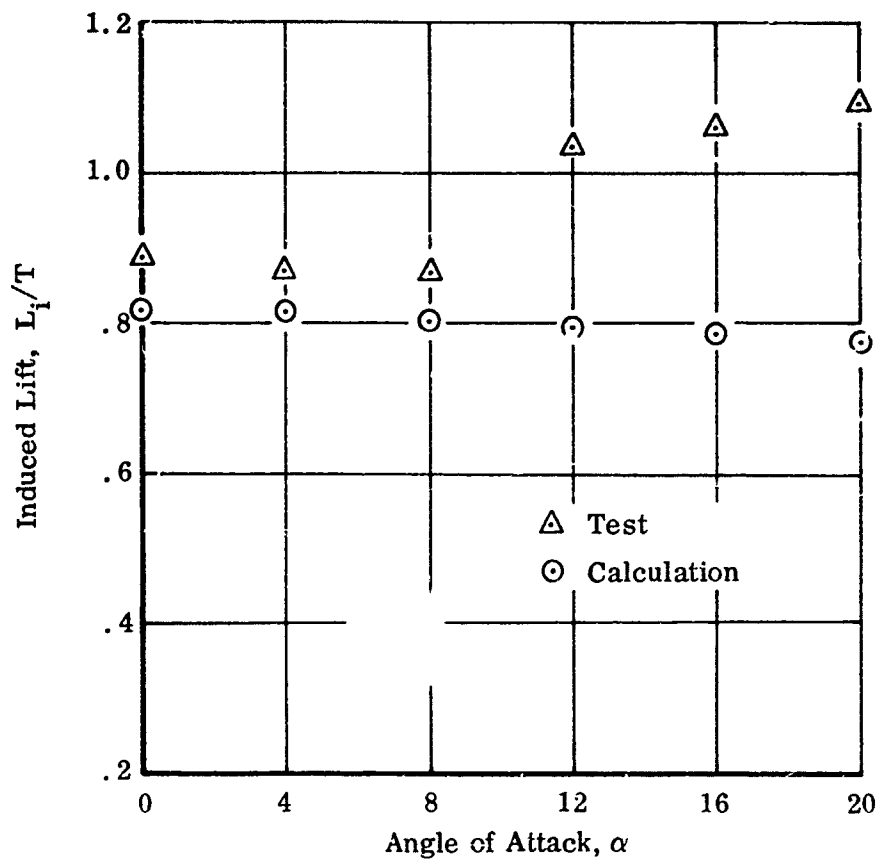


FIGURE 29f. INDUCED LIFT VERSUS ANGLE OF ATTACK,
LIFT JET ($U_\infty/U_{j0} = .20$), $\beta = 0$

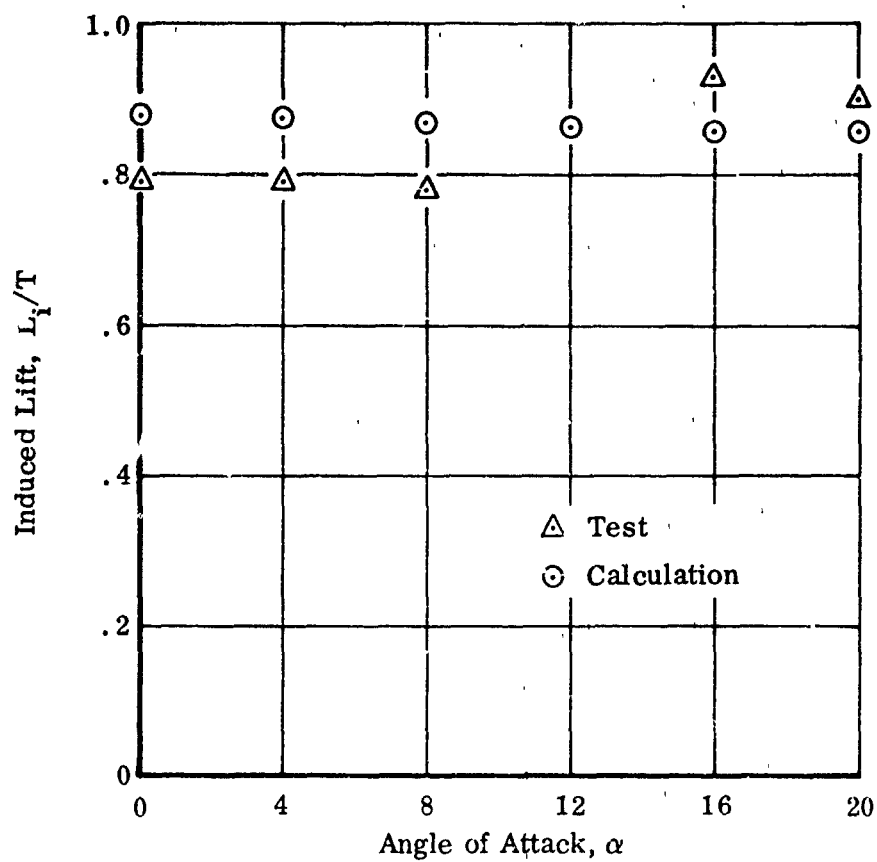


FIGURE 29g. INDUCED LIFT VERSUS ANGLE OF ATTACK,
VECTORED THRUST, FORWARD POSITION, 90°
DEFLECTION ANGLE ($U_\infty/U_{j0} = .20$), $\beta = 0$

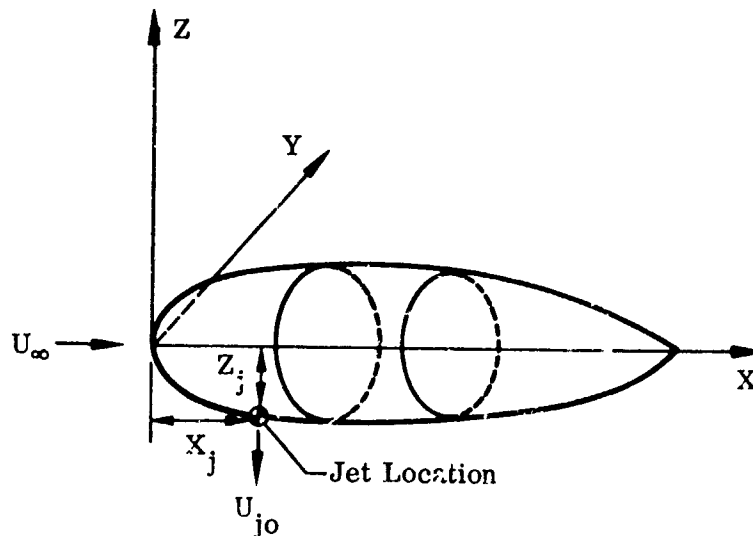
SECTION III

POWER EFFECTS ON THE FUSELAGE

The calculation of the jet induced loads on a fuselage is accomplished by using the transformation method with the disturbance velocities at the surface of the body calculated by the jet program. To use the transformation method, it is necessary to map the body at different body stations. This section describes the application of these methods to the calculation of fuselage loads.

1. SAMPLE PROBLEM

To demonstrate the application of the methods, the fuselage of the wind tunnel test model which was tested during this investigation will be used. This fuselage is described in Appendix I of this volume. A sketch of the model fuselage with coordinate system is shown below.



The power and flight conditions which must be specified to complete the problem description are as follows:

Jet location (single jet issuing from the fuselage):

$$X_j = 208 \text{ inches}$$

$$Y_j = 0$$

$$Z_j = -30.8 \text{ inches}$$

$$\text{Jet diameter} = 22.5 \text{ inches}$$

$$\text{Jet velocity ratio } \frac{U}{U_{jo}} = 0.2$$

Flight Conditions:

$$\alpha = 0$$

$$\beta = 0$$

All the above dimensions are ten times wind tunnel model dimensions, as will be the case throughout this section.

Jet inclination angles:

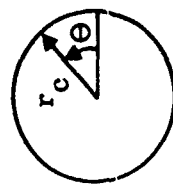
The jet will be taken to be exhausting along the negative Z direction for the sample problem.

2. APPLICATION OF THE MAPPING METHOD

A complete description of the fuselage will not be given here since this is not necessary to describe the application of the mapping method. Instead, a complete treatment of one section of the body will be given, this being sufficient to demonstrate application of the method.

Figure 29 shows the section of the wind tunnel test model body at station 264.25 together with terminology for mapping into a circle. This section has been rotated 90° counterclockwise so that the axis of symmetry is along the X-axis with the bottom of the section cutting the positive X-axis. This coordinate system is not related to the original fuselage coordinate system but is in the terminology used in the mapping program. This location of the section is the proper one for the mapping method, and the mapping coefficients obtained with this orientation are in the correct form for the transformation method. Figure 30 shows the inputs to the mapping computer program required to obtain a mapping of this section.

The first card contains four integers. The first of these numbers specifies the number of points specified about the section. The second number specifies the number of corners around the section (for a symmetrical section this would represent the number of pairs of corners except for corners on the X-axis), which for this section is



Mapping Circle

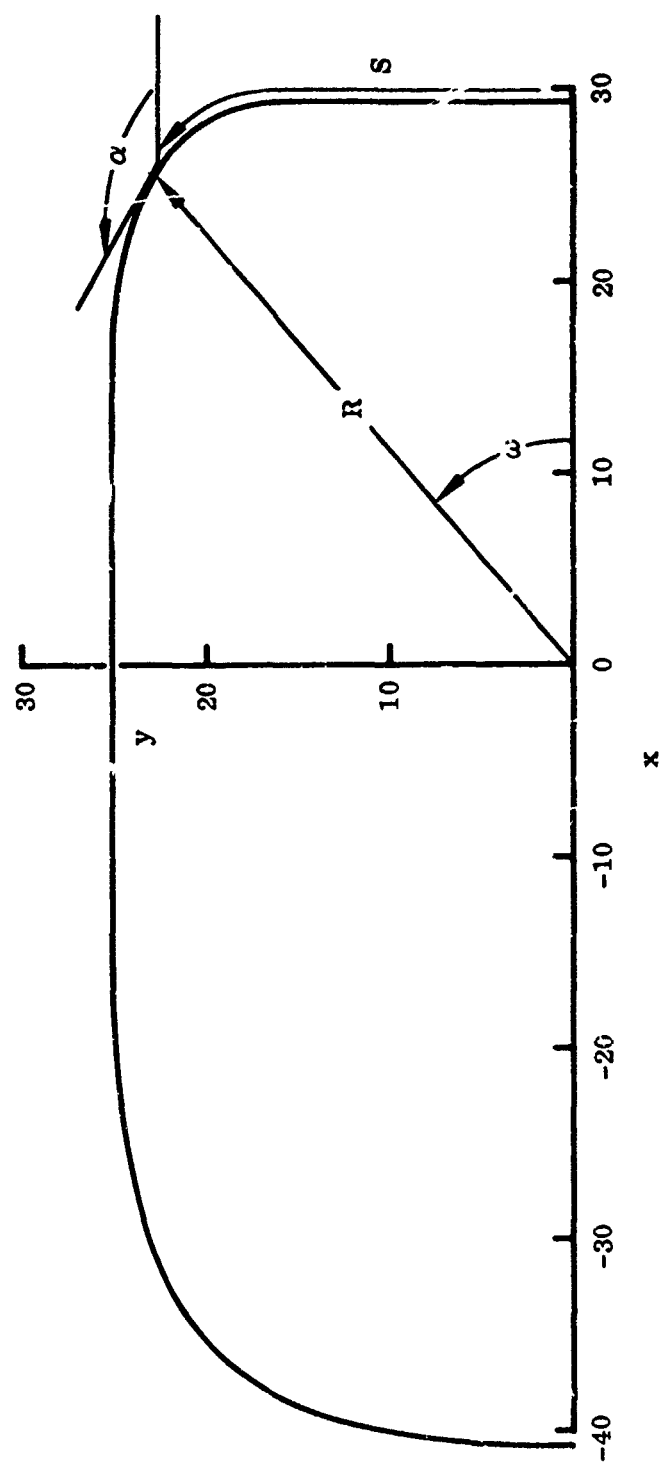


FIGURE 30. STATION 264.25 OF TEST MODEL FUSELAGE

zero. The third number represents the number of terms in the expansions for the potential and for the mapping function. The last number on this card specifies that the section being mapped is symmetrical.

Cards 2 through 6 specify the X-coordinates of the (in this case) 37 points being taken about the section starting on the positive X-axis and ending on the negative X-axis. Cards 7 through 11 specify the Y-coordinates of these same points on the section.

Since there are no corners to be specified on this section, the next number (on card 12) specifies what shift is desired to translate the body along the X-axis. In this case there is no need to shift the section location as it is sufficiently well centered.

Card 13 specifies inputs needed to specify parameters for the numerical integration of the mapping function obtained. The first two numbers specify the X- and Y- locations of the initial point of the mapping.

The next three numbers specify the angular range (about the mapping circle) of points to be obtained on the section, and the approximate spacings to be obtained. In this case it is specified that points from 0° to 180° around the mapping circle are to be calculated and are at an interval size of 5° .

Card 14 specifies a similar set of parameters for the analytically integrated mapping. It specifies that 37 points are to be obtained with a spacing of 5° of theta and that the points are to start at $\theta = 0^\circ$.

Figure 31 shows the output of the mapping program. These outputs have been described in Section II.2 and so will not be further explained here.

Figure 32 shows a plot of the mapping as obtained by analytical integration. A comparison of Figure 32 and Figure 29 shows that the mapped section must be shifted 4.42 inches in the negative X direction to give the best fit. This, then, is the value of the constant term in the mapping.

The complete tabulation of coefficients for the wind tunnel test model body with canopy off are shown in Table II. The values of dr_c/dx , the rate of change of the mapping circle radius with body station, have been obtained by graphical differentiation of r_c plotted versus x . In addition to the coefficients tabulated in Table II, the initial mapping coefficient a_{-1} , required as input to the jet program, is equal to 1.0 for all the fuselage stations.

COMPUTATIONS FOR S AND ALPHA VERSUS THETA.

X	Y	R	S	V	ALPHA	OMEGA	THETA
0.29300E 02	0.0	0.29300E 02	0.0	0.23437E-01	0.90000E 02	0.0	0.0
0.29300E 02	0.29951E 01	0.29453E 02	0.29951E 01	0.23461E-01	0.90300E 02	0.58366E 01	0.40005E 01
0.29300E 02	0.59849E 01	0.29906E 02	0.59849E 01	0.24582E-01	0.90000E 02	0.11551E 02	0.80756E 01
0.29300E 02	0.89848E 01	0.30647E 02	0.89848E 01	0.27908E-01	0.90000E 02	0.17048E 02	0.12523E 02
0.29300E 02	0.11980E 02	0.31655E 02	0.11980E 02	0.32614E-01	0.90000E 02	0.22238E 02	0.17686E 02
0.29300E 02	0.14975E 02	0.32305E 02	0.14975E 02	0.36064E-01	0.90423E 02	0.27071E 02	0.23582E 02
0.29212E 02	0.17964E 02	0.34293E 02	0.17969E 02	0.36681E-01	0.99152E 02	0.31589E 02	0.29817E 02
0.27955E 02	0.20648E 02	0.34754E 02	0.20969E 02	0.37472E-01	0.14923E 03	0.36450E 02	0.36137E 02
0.25666E 02	0.22557E 02	0.34170E 02	0.23964E 02	0.38991E-01	0.14923E 03	0.41311E 02	0.42661E 02
0.22938E 02	0.23784E 02	0.33043E 02	0.26961E 02	0.39790E-01	0.16147E 03	0.46037E 02	0.49410E 02
0.20041E 02	0.24535E 02	0.31580E 02	0.29956E 02	0.38162E-01	0.16914E 03	0.50757E 02	0.56108E 02
0.17075E 02	0.24945E 02	0.30229E 02	0.32951E 02	0.33229E-01	0.17487E 03	0.55508E 02	0.62244E 02
0.14085E 02	0.25096E 02	0.28778E 02	0.35946E 02	0.26503E-01	0.17895E 03	0.60697E 02	0.67344E 02
0.11090E 02	0.25100E 02	0.27441E 02	0.38941E 02	0.21492E-01	0.18044E 03	0.66162E 02	0.71389E 02
0.80952E 01	0.25100E 02	0.26373E 02	0.41936E 02	0.20983E-01	0.17977E 03	0.72124E 02	0.74945E 02
0.51004E 01	0.25100E 02	0.25613E 02	0.44930E 02	0.23460E-01	0.18011E 03	0.78512E 02	0.78736E 02
0.21055E 01	0.25100E 02	0.25188E 02	0.47925E 02	0.22509E-01	0.17997E 03	0.85203E 02	0.82742E 02
0.88936E 00	0.25100E 02	0.25116E 02	0.51142E 02	0.21112E-01	0.18003E 03	0.87969E 02	0.84257E 02
-0.38842E 01	0.25100E 02	0.25399E 02	0.53915E 02	0.20147E-01	0.17999E 03	0.98795E 02	0.89613E 02
-0.63791E 01	0.25100E 02	0.26026E 02	0.56510E 02	0.22882E-01	0.18000E 03	0.10532E 03	0.93304E 02
-0.98739E 01	0.25100E 02	0.26972E 02	0.59055E 02	0.22280E-01	0.18000E 03	0.11147E 03	0.97210E 02
-0.12869E 02	0.25100E 02	0.28207E 02	0.62900E 02	0.20449E-01	0.18000E 03	0.11714E 03	0.10084E 03
-0.15863E 02	0.25100E 02	0.29692E 02	0.65894E 02	0.21111E-01	0.18025E 03	0.12229E 03	0.10434E 03
-0.18858E 02	0.25048E 02	0.31353E 02	0.68887E 02	0.24378E-01	0.19195E 03	0.12697E 03	0.10819E 03
-0.21847E 02	0.24874E 02	0.33106E 02	0.71884E 02	0.28682E-01	0.18481E 03	0.13129E 03	0.11272E 03
-0.24923E 02	0.24535E 02	0.34902E 02	0.74879E 02	0.32319E-01	0.18848E 03	0.13533E 03	0.11795E 03
-0.27761E 02	0.23963E 02	0.36673E 02	0.77874E 02	0.34407E-01	0.19392E 03	0.13920E 03	0.12366E 03
-0.30617E 02	0.23064E 02	0.39332E 02	0.80870E 02	0.35066E-01	0.20161E 03	0.14300E 03	0.12961E 03
-0.33291E 02	0.21719E 02	0.39749E 02	0.83868E 02	0.34901E-01	0.21241E 03	0.14687E 03	0.13559E 03
-0.35620E 02	0.19839E 02	0.40772E 02	0.86868E 02	0.34486E-01	0.22565E 03	0.15089E 03	0.14152E 03
-0.37446E 02	0.17608E 02	0.41320E 02	0.89867E 02	0.34072E-01	0.23879E 03	0.15499E 03	0.14738E 03
-0.39609E 02	0.14770E 02	0.41464E 02	0.92865E 02	0.33584E-01	0.24929E 03	0.15913E 03	0.15316E 03
-0.40159E 02	0.11904E 02	0.41353E 02	0.95861E 02	0.32862E-01	0.25671E 03	0.16327E 03	0.15884E 03
-0.40465E 02	0.89611E 01	0.41147E 02	0.98855E 02	0.31887E-01	0.26185E 03	0.16741E 03	0.16437E 03
-0.40652E 02	0.59845E 01	0.40925E 02	0.10185E 03	0.30843E-01	0.26546E 03	0.17158E 03	0.16972E 03
-0.40700E 02	0.29944E 01	0.40762E 02	0.10485E 03	0.30031E-01	0.26804E 03	0.17578E 03	0.17491E 03
-0.40700E 02	0.0	0.40700E 02	0.10784E 03	0.29725E-01	0.27006E 03	0.17999E 03	0.18000E 03

FIGURE 32. OUTPUT OF MAPPING FUNCTION PROGRAM AT TEST FUSELAGE STATION 264.25

SECTION MAPPING BY NUMERICAL INTEGRATION.

X	Y	THETA
0.29352E 02	0.36200E 01	0.84908E-01
0.29477E 02	0.70875E 01	0.16982E 00
0.29596E 02	0.10282E 02	0.25472E 00
0.29600E 02	0.13133E 02	0.33963E 00
0.29391E 02	0.15626E 02	0.42454E 00
0.28895E 02	0.17731E 02	0.50945E 00
0.28077E 02	0.19635E 02	0.59436E 00
0.26934E 02	0.21216E 02	0.67926E 00
0.25475E 02	0.22534E 02	0.76417E 00
0.23707E 02	0.23584E 02	0.84908E 00
0.21620E 02	0.24364E 02	0.93399E 00
0.19196E 02	0.24876E 02	0.10189E 01
0.16414E 02	0.25153E 02	0.11038E 01
0.13270E 02	0.25250E 02	0.11887E 01
0.97872E 01	0.25233E 02	0.12736E 01
0.60171E 01	0.25169E 02	0.13585E 01
0.20378E 01	0.25109E 02	0.14434E 01
-0.20582E 01	0.25082E 02	0.15283E 01
-0.61745E 01	0.25094E 02	0.16132E 01
-0.10220E 02	0.25130E 02	0.16982E 01
-0.14112E 02	0.25160E 02	0.17831E 01
-0.17782E 02	0.25141E 02	0.18680E 01
-0.21179E 02	0.25020E 02	0.19729E 01
-0.24269E 02	0.24742E 02	0.20378E 01
-0.27041E 02	0.24253E 02	0.21227E 01
-0.29503E 02	0.23512E 02	0.22076E 01
-0.31676E 02	0.22494E 02	0.22925E 01
-0.33589E 02	0.21196E 02	0.23774E 01
-0.35261E 02	0.19633E 02	0.24623E 01
-0.36704E 02	0.17828E 02	0.25472E 01
-0.37917E 02	0.15807E 02	0.26321E 01
-0.38896E 02	0.13585E 02	0.27170E 01
-0.39643E 02	0.11173E 02	0.28020E 01
-0.40173E 02	0.85806E 01	0.28863E 01
-0.40515E 02	0.58260E 01	0.29748E 01
-0.40701E 02	0.29467E 01	0.30567E 01
-0.40760E 02	-0.10836E-02	0.31416E 01

FIGURE 32. (Continued)

RADIUS OF MAPPING CIRCLE = 0.33317E 02

REAL PARTS OF COEFFICIENTS.

0.00000E 03 -0.80102E 03 -0.11475E 06 -0.54775E 06 0.17340E 07 -0.11485E 09 -0.70960E 10
-0.60582E 11 -0.20472E 13

IMAGINARY PARTS OF COEFFICIENTS.

0.0 0.0 0.0 0.0 0.0 0.0 0.0
0.0 0.0

FIGURE 32. (Continued)

MAPPING OF SECTION WITH CORNERS REMOVED.

X	Y
33.74065	0.0
33.79533	3.71916
33.92583	7.27334
34.04285	10.53344
34.03062	13.42824
33.78172	15.94495
33.22249	18.11038
32.32132	19.96355
31.07805	21.53214
29.50369	22.32333
27.60135	23.83009
25.35806	24.54831
22.75081	24.99301
19.76187	25.20651
16.39557	25.25409
12.68871	25.20993
8.71039	25.14067
4.55337	25.09227
0.32129	25.08478
-3.88293	25.11311
-7.96487	25.15170
-11.84319	25.15948
-15.45312	25.08385
-18.74998	24.86530
-21.71240	24.44403
-24.34244	23.76903
-26.66010	22.80710
-28.69418	21.54808
-30.47015	20.00362
-32.00211	18.19855
-33.29158	16.15981
-34.33445	13.90728
-35.13164	11.45243
-35.69736	8.80503
-36.06100	5.98449
-36.25879	3.02955
-36.32085	0.00042

FIGURE 32. (Concluded)

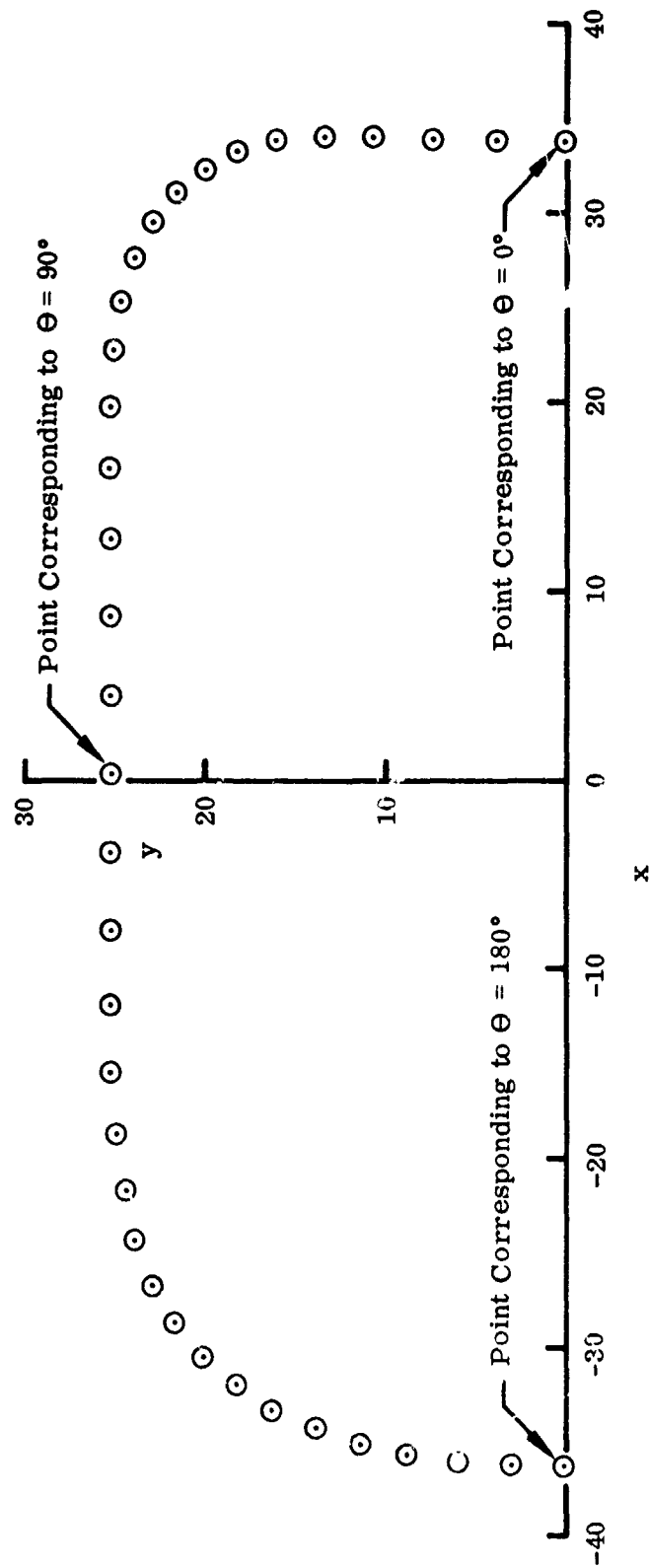


FIGURE 33. MAPPING OF FUSELAGE AT STATION 264.25

TABLE II. COEFFICIENTS OF MAPPING FOR FUSELAGE

F/S S/A	r_c	dr_c/dx	a_0	a_1	a_2	a_3	a_4	a_5	a_6	a_7	a_8	a_9
25.7	10.2633	.285	7.8008	$.71436 \times 10^1$	$-.46764 \times 10^1$	$-.17220 \times 10^3$	$.69240 \times 10^3$	$.14727 \times 10^2$	$-.21603 \times 10^5$	$.40889 \times 10^5$	$.21969 \times 10^6$	$-.38224 \times 10^7$
41	15.0898	.274	5.1774	$.25764 \times 10^2$	$-.73365 \times 10^2$	$-.63894 \times 10^3$	$-.17548 \times 10^4$	$.43300 \times 10^5$	$.11580 \times 10^6$	$-.49521 \times 10^7$	$-.19394 \times 10^8$	$.59975 \times 10^9$
73	21.7262	.176	1.9762	$.81113 \times 10^2$	$-.3189 \times 10^3$	$-.40341 \times 10^4$	$-.45148 \times 10^5$	$.38924 \times 10^6$	$.47368 \times 10^7$	$-.11093 \times 10^9$	$-.89304 \times 10^9$	$.17429 \times 10^{11}$
94	25.1396	.142	-.45742	$.12664 \times 10^2$	$-.62289 \times 10^3$	$-.10198 \times 10^5$	$-.12042 \times 10^6$	$.63980 \times 10^6$	$.19652 \times 10^8$	$-.42390 \times 10^9$	$-.53246 \times 10^{10}$	$.11100 \times 10^{12}$
115	28.3436	.1155	-2.7841	$.17304 \times 10^3$	$-.88554 \times 10^3$	$-.23602 \times 10^5$	$-.24410 \times 10^6$	$.52265 \times 10^6$	$.28524 \times 10^8$	$-.12650 \times 10^{10}$	$-.27246 \times 10^{11}$	$.33738 \times 10^{12}$
143.5	30.7743	.077	-3.553	$.19969 \times 10^3$	$-.10054 \times 10^4$	$-.47881 \times 10^5$	$-.45438 \times 10^6$	$-.48116 \times 10^6$	$-.38244 \times 10^8$	$-.37311 \times 10^{10}$	$-.66089 \times 10^{11}$	$-.25037 \times 10^{12}$
169.5	31.9933	.054	-3.4023	$.19745 \times 10^3$	$-.98524 \times 10^3$	$-.72717 \times 10^5$	$-.55979 \times 10^6$	$.98070 \times 10^5$	$-.11108 \times 10^9$	$-.57747 \times 10^{10}$	$-.79340 \times 10^{11}$	$-.97576 \times 10^{12}$
185.5	33.0565	.04	-3.1494	$.18810 \times 10^3$	$-.1441 \times 10^4$	$-.10515 \times 10^6$	$-.66067 \times 10^6$	$.17509 \times 10^7$	$-.97966 \times 10^8$	$-.55082 \times 10^{10}$	$-.48035 \times 10^{11}$	$-.10264 \times 10^{13}$
211.5	33.9764	.001	-3.4023	$.17811 \times 10^3$	$-.13119 \times 10^4$	$-.13530 \times 10^6$	$-.61693 \times 10^6$	$.29750 \times 10^7$	$-.50522 \times 10^8$	$-.50994 \times 10^{10}$	$-.27398 \times 10^{11}$	$-.24533 \times 10^{13}$
234.25	33.317	-.03	-1.42	$.16565 \times 10^3$	$-.80102 \times 10^3$	$-.11475 \times 10^6$	$-.54775 \times 10^6$	$.17340 \times 10^7$	$-.11485 \times 10^9$	$-.70960 \times 10^{10}$	$-.60582 \times 10^{11}$	$-.20872 \times 10^{13}$
26	31.0699	-.0503	-7.44 5	$.12136 \times 10^3$	$-.14940 \times 10^3$	$-.62063 \times 10^5$	$-.18956 \times 10^6$	$.40965 \times 10^7$	$-.48139 \times 10^8$	$-.36282 \times 10^{10}$	$.79756 \times 10^{10}$	$.46619 \times 10^{11}$
240	29.5153	-.0635	-9.4064	$.9946 \times 10^2$	$.11392 \times 10^3$	$-.41363 \times 10^5$	$-.13665 \times 10^6$	$.29437 \times 10^7$	$-.18782 \times 10^9$	$-.18358 \times 10^{10}$	$.19634 \times 10^{11}$	$.45817 \times 10^{12}$
374	27.5112	-.074	-11.8762	$.47583 \times 10^2$	$.27331 \times 10^3$	$-.24738 \times 10^5$	$-.13019 \times 10^6$	$.15003 \times 10^7$	$.57690 \times 10^7$	$-.93720 \times 10^9$	$.13366 \times 10^{10}$	$.23796 \times 10^{12}$
414	23.7772	-.135	-14.6391	$.25525 \times 10^2$	$.13394 \times 10^3$	$-.14122 \times 10^5$	$-.69219 \times 10^5$	$.43107 \times 10^6$	$.37599 \times 10^7$	$-.24462 \times 10^9$	$-.96070 \times 10^8$	$.31622 \times 10^{11}$
450	17.5796	-.185	-17.6552	$.24497 \times 10^2$	$.80204 \times 10^2$	$-.30498 \times 10^4$	$-.15568 \times 10^5$	$.79269 \times 10^5$	$.42978 \times 10^6$	$-.20739 \times 10^8$	$-.54266 \times 10^8$	$.22970 \times 10^{10}$
497	8.213	-.206	-21.2522	$.13116 \times 10^2$	$.80401 \times 10^1$	$-.11905 \times 10^3$	$-.32560 \times 10^3$	$.76206 \times 10^3$	$.16588 \times 10^4$	$-.34590 \times 10^5$	$.90360 \times 10^3$	$.11027 \times 10^7$

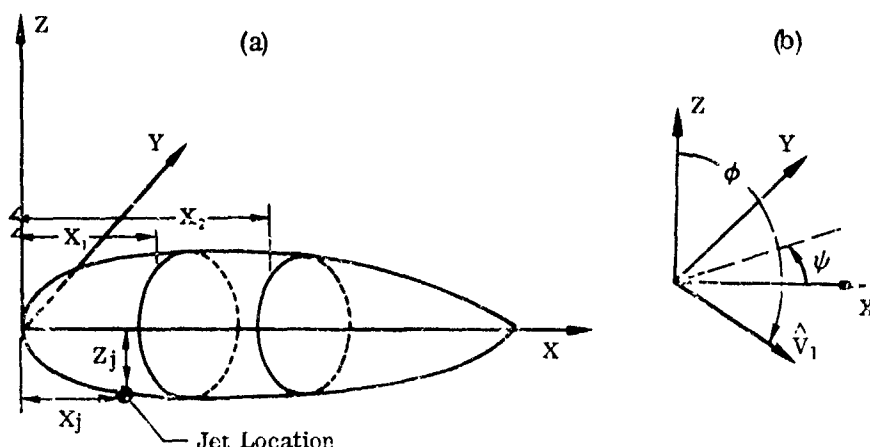
3. APPLICATION OF JET FLOW FIELD THEORY TO FUSELAGE

The purpose of the Jet Flow Field theory, when used in conjunction with the Transformation Method, is to predict jet-induced velocity components at the control points on the fuselage required by the Transformation Method to evaluate power effects. This is accomplished by executing the Jet Flow Field program to generate required data for the Transformation Method in the form of punched data cards. To insure compatibility with the Transformation Method, the control points on the fuselage where induced velocity components are to be computed are specified by utilizing the mapping coefficients for the fuselage cross sections obtained in Section III.2. The punched output is generated in a manner providing a continuous block of input data to the Transformation Method computer program. Both of the above points will be described in greater detail in the discussion of the sample problem computations.

It should also be noted that the application of the Jet Flow Field program to provide data to the Transformation Method program for the computation of power effects on the fuselage, differs only slightly from its application to computing power effects on the wing, discussed in Section II.3. Consequently, much of the discussion below will parallel that of Section II.3.

a. Sample Problem Computation

For the sample problem being considered, the Jet Flow Field program is now used to compute the jet-induced velocities at the 16 fuselage stations described in Section III.2. A sketch of the fuselage and the location of the jet with respect to the input/output coordinate system is shown below. The jet exhaust angles ϕ and ψ are also defined.



(1) Input for Sample Problem

The input cards required for the sample problem are tabulated in Figure 34.

Card 1 lists three control indices. The first one, $MULT = 1$, indicates that a single jet configuration is being treated. The second one, $IGEOM = 2$, specifies that control points on fuselage cross sections will be generated utilizing the mapping coefficients obtained. The third control index, $IPUNCH = 1$, generates the punched output for the Transformation Method program.

Card 2 specifies angle of attack, $\alpha = 0$ and angle of sideslip, $\beta = 0$.

Card 3 controls the number of steps and the step size in the numerical integration of the equations of motion for the jet path. For the sample problem, 90 steps with a step size of .4 (jet exit diameters) are chosen.

Cards 4 and 5 contain information about the jet. The jet location, in the coordinate system of Figure 33, is $X = 208.$, $Y = 0$, $Z = -30.8$. The jet exhaust angles ϕ and ψ , defined in Figure 33(b), are 180 and 0 degrees, respectively. The jet exit diameter, $d_o = 22.5$ and the velocity ratio, $U_\infty/U_{jo} = .2$.

Card 6 may be left blank for single jet computations. For a multiple-jet configuration it would be used to control the geometry of the jet resulting from the intersection of two other jets.

The remaining input cards provide data to generate the control points at which jet-induced velocities are to be evaluated. These control points, in order to insure compatibility with the Transformation Method, are generated by utilizing the mapping coefficients and mapping circle radii obtained for the 16 fuselage stations of the sample problem. The number of control points generated at each fuselage station is governed by the input variable, $NTHT$, which is the number of increments $\Delta\theta$ into which the mapping circle (or mapping semicircle if only half the fuselage is to be mapped at each station) is to be divided in the Transformation Method computer program. Since the flow is symmetric ($\beta = 0$), computations will be carried out for only half the body. Consequently, the number of control points at each fuselage station will be $NTHT + 1$.

Card 7 specifies that $NTHT$, the number of equal increments $\Delta\theta$ into which the mapping semicircle is divided, is 18, which will generate 19 control points at each fuselage station. It defines the number of fuselage stations $NS = 16$. It also defines the number of terms used in the mapping expansion, $NCOEF = 11$, and through the control index $NSYM = 0$ indicates that computations are to be effected for only half the fuselage at each station.

The data in cards 8-55 are taken from Table II, which is determined in Section III.2.

Cards 8-10 provide the data from which the fuselage cross section at the first station can be generated by the computer program. Card 8 specifies the location of the station, $X = 23.7$, the mapping circle radius $R = 10.2633$, and the rate of change of R with X , $DRDX = .285$.

Cards 9 and 10 list the real parts of the coefficients to be used in the mapping expansion (thus only symmetrical fuselages may be treated).

Cards 11-55 are similar data blocks for fuselage stations $X = 41., 73., 94., 118., 143.5, 162.5, 185.5, 221.5, 264.5, 316., 343., 374., 411., 450.,$ and $497.$

Note: The rate of change of the mapping circle radius with distance along the fuselage, $DRDX$, is not required for any of the computations performed by the Jet Flow Field program. It will, however, be required by the Transformation Method program, and is read as part of the input so that it may be punched out in the proper sequence in the data package to be provided to the Transformation Method program.

(2) Output for Sample Problem

For the sample problem being considered, both printed and punched outputs are obtained.

● Printed Output

Figure 35(a) shows the first page of printout. The jet configuration being treated is identified both by appropriate heading and by printout of pertinent input information. Input controlling the numerical integration procedure is also displayed. Figure 35(b) shows a partial printout of computed jet centerline information. The coordinates of the jet centerline are identified. The nondimensionalized jet speed U_j/U_{j0} and the nondimensionalized major diameter of the ellipse representing the cross section of the jet, d/d_0 , are also printed out. These properties are printed out at each integration interval as specified on card 3 of the input. The variables $XCOORD$ and DIA show a monotonic increase over this region, while $UJ = U_j/U_{j0} \sim 1$ once the jet speed U_j approaches the freestream speed U_∞ . Figure 35(c) shows the printout for the jet-induced velocity components at the first fuselage station specified, $X = 23.7$. The coordinates of the 19 control points at the station are identified. For this symmetric flow sample problem, only the positive half of the fuselage station is generated. The induced

*** SINGLE JET CONFIGURATION ***

XJET	YJET	ZJET	PHI	PSI	U/UJO
208.0000	0.0	-30.8000	180.0000	0.0	0.2000

ANGLE OF ATTACK = 0.0
 ANGLE OF SIDESLIP = 0.0

NUMBER OF STEPS IN INTEGRATION = 90
 INTEGRATION INTERVAL = 0.40 JET EXIT DIAMETERS

FIGURE 35(a). INPUT PARAMETERS FOR SAMPLE PROBLEM

** SINGLE JET CENTERLINE **

XCOORD	YCOORD	ZCOORD	UJ	DIA
208.00	0.0	-30.80	1.000	1.00
208.10	0.0	-39.80	0.948	1.18
208.44	0.0	-48.80	0.893	1.45
209.10	0.0	-57.80	0.833	1.90
210.26	0.0	-66.80	0.760	2.64
212.10	0.0	-75.80	0.688	2.93
214.71	0.0	-84.80	0.626	3.23
218.18	0.0	-93.80	0.573	3.55
222.60	0.0	-102.80	0.528	3.88
228.11	0.0	-111.80	0.489	4.23
234.83	0.0	-120.80	0.456	4.60
242.92	0.0	-129.80	0.427	4.98
252.59	0.0	-138.80	0.402	5.37
264.06	0.0	-147.80	0.381	5.77
277.60	0.0	-156.80	0.363	6.18
293.52	0.0	-165.80	0.347	6.60
312.22	0.0	-174.80	0.333	7.03
334.13	0.0	-183.80	0.321	7.47
359.77	0.0	-192.80	0.311	7.92
399.78	0.0	-201.80	0.301	8.38
424.86	0.0	-210.80	0.293	8.86
465.87	0.0	-219.80	0.285	9.34
513.81	0.0	-228.80	0.278	9.85
569.84	0.0	-237.80	0.272	10.37
635.36	0.0	-246.80	0.266	10.91
711.98	0.0	-255.80	0.261	11.47

FIGURE 35(b). JET CENTERLINE FOR SAMPLE PROBLEM

*** INDUCED VELOCITIES ON BODY ***

X	Y	Z	U	V	W
23.700	0.0	-18.691	-0.44731E-04	0.0	0.93589E-02
23.700	1.731	-18.452	-0.29299E-04	0.74342E-04	0.93522E-02
23.700	3.392	-18.003	0.17127E-04	0.14471E-03	0.93320E-02
23.700	4.929	-17.252	0.93755E-04	0.20799E-03	0.92982E-02
23.700	6.300	-16.217	0.19770E-03	0.26181E-03	0.92517E-02
23.700	7.462	-14.928	0.32468E-03	0.30423E-03	0.91937E-02
23.700	8.375	-13.417	0.47016E-03	0.33399E-03	0.91253E-02
23.700	9.013	-11.720	0.62943E-03	0.35036E-03	0.90481E-02
23.700	9.359	-9.879	0.79768E-03	0.35398E-03	0.89638E-02
23.700	9.414	-7.930	0.97076E-03	0.34585E-03	0.88739E-02
23.700	9.211	-5.925	0.11440E-02	0.32832E-03	0.87802E-02
23.700	8.797	-3.952	0.13102E-02	0.30427E-03	0.86867E-02
23.700	9.190	-2.130	0.14593E-02	0.27544E-03	0.85993E-02
23.700	7.363	-0.557	0.15857E-02	0.24165E-03	0.85234E-02
23.700	6.282	0.728	0.16860E-02	0.20212E-03	0.84616E-02
23.700	4.954	1.724	0.17521E-02	0.15697E-03	0.84140E-02
23.700	3.424	2.435	0.18155E-02	0.10731E-03	0.83802E-02
23.700	1.751	2.860	0.18469E-02	0.54512E-04	0.83602E-02
23.700	-0.000	3.090	0.18572E-02	-0.10974E-08	0.83536E-02

*** INDUCED VELOCITIES ON BODY ***

X	Y	Z	U	V	W
497.000	0.0	11.592	-0.38669E-02	0.0	-0.36283E-01
497.000	1.248	11.710	-0.38559E-02	-0.32777E-03	-0.36249E-01
497.000	2.428	12.065	-0.38229E-02	-0.63462E-03	-0.36148E-01
497.000	3.472	12.672	-0.37675E-02	-0.90060E-03	-0.35979E-01
497.000	4.344	13.559	-0.36882E-02	-0.11144E-02	-0.35736E-01
497.000	5.048	14.731	-0.35858E-02	-0.12762E-02	-0.35424E-01
497.000	5.593	16.153	-0.34644E-02	-0.13892E-02	-0.35053E-01
497.000	5.977	17.783	-0.33283E-02	-0.14552E-02	-0.34638E-01
497.000	6.220	19.576	-0.31835E-02	-0.14815E-02	-0.34193E-01
497.000	6.361	21.449	-0.30356E-02	-0.14813E-02	-0.33738E-01
497.000	6.404	23.268	-0.28954E-02	-0.14592E-02	-0.33306E-01
497.000	6.283	24.923	-0.27713E-02	-0.14038E-02	-0.32923E-01
497.000	5.925	26.387	-0.26646E-02	-0.13014E-02	-0.32593E-01
497.000	5.323	27.673	-0.25732E-02	-0.11519E-02	-0.32310E-01
497.000	4.520	28.773	-0.24969E-02	-0.96575E-03	-0.32074E-01
497.000	3.553	29.651	-0.24371E-02	-0.75149E-03	-0.31889E-01
497.000	2.448	30.287	-0.23945E-02	-0.51400E-03	-0.31757E-01
497.000	1.246	30.676	-0.23697E-02	-0.26051E-03	-0.31677E-01
497.000	-0.000	30.808	-0.23600E-02	0.91033E-08	-0.31650E-01

FIGURE 35(c). INDUCED VELOCITY COMPONENTS AT STATIONS 23.7 AND 497.

velocity components U , V , W , all nondimensionalized by U_∞ , are printed out for each control point. Figure 35(c) also shows the printout for the last fuselage station considered in this problem, $X = 497$. Similar printouts are obtained for the other intermediate stations specified as part of the input.

● Punched Output

The punched output for the sample problem is shown in tabulated form in Figure 36. The output data block for the first fuselage station is identified. The first card lists the fuselage station $X = 23.7$, the mapping radius $R = 10.2633$ and the rate of change of R with X , $DRDX = .285$. The next two cards list the real parts of the coefficients used in the mapping expansion. Cards 4-7 list the induced velocity components in the X -direction for each of the 19 control points at fuselage station $X = 23.7$. The induced velocity components in the Y -direction are listed on cards 8-11 and cards 12-15 specify the induced velocity components in the Z -direction. Data blocks of this type, each consisting of 15 cards, follow for each of the other 15 fuselage stations specified as part of the input. The punched output is identified in columns 73-80. The fuselage station number is shown in columns 75-77. Sequence numbers for each station appear in columns 78-80. The letters U , V , W and column 74 identify the velocity components listed on the data cards.

Note: From the tabulations of Figure 36 it is apparent that the first three data cards of the data generated for each fuselage station represent an exact duplication of input cards described previously. They are generated as part of the punched output so that a more complete data block for the Transformation Method program may be obtained without additional card handling.

b. Applicability and Limitations

See discussion on applicability and limitations in Section II.3.

118.000000	28.343547	0.113500							5
0.100000E-01	-0.27841E-01	0.17304E-03	-0.48554E-03	-0.23607E-05	-0.24410E-06				5 1
0.52264E-06	0.28524E-08	-0.12650E-10	-0.27246E-11	0.33738E-12					5 2
-0.36275E-02	-0.13715E-02	-0.25885E-02	-0.12652E-02	0.53032E-03	0.26146E-02	U			5 1
0.48162E-02	0.70119E-02	0.40868E-02	0.10838E-01	0.12125E-01	0.12988E-01	U			5 2
0.13557E-01	0.13734E-01	0.14161E-01	0.14285E-01	0.14344E-01	0.14376E-01	U			5 3
0.14385E-01						U			5 4
0.0	0.18667E-02	0.34320E-02	0.45124E-02	0.50735E-02	0.51665E-02	V			5 1
0.48657E-02	0.42722E-02	0.35423E-02	0.28371E-02	0.22340E-02	0.17250E-02	V			5 2
0.12871E-02	0.42349E-03	0.64212E-03	0.42908E-03	0.26071E-03	0.12162E-03	V			5 3
-0.60669E-08						V			5 4
0.35500E-01	0.35318E-01	0.34773E-01	0.33859E-01	0.32577E-01	0.30963E-01	W			5 1
0.29061E-01	0.26861E-01	0.24367E-01	0.21770E-01	0.19364E-01	0.17328E-01	W			5 2
0.15607E-01	0.14135E-01	0.12734E-01	0.12043E-01	0.11132E-01	0.11060E-01	W			5 3
0.10431E-01						W			5 4
143.500000	30.764297	0.077000							6
0.100000E-01	-0.35530E-01	0.19777E-03	-0.10054E-04	-0.47481E-05	-0.45438E-06				6 1
-0.48116E-06	-0.38244E-08	-0.37311E-10	-0.66049E-11	-0.25037E-12					6 2
-0.51658E-02	-0.45729E-02	-0.27456E-02	0.36324E-03	0.44463E-02	0.28012E-02	U			6 1
0.12881E-01	0.16485E-01	0.19386E-01	0.21302E-01	0.22242E-01	0.22509E-01	U			6 2
0.22416E-01	0.22159E-01	0.21854E-01	0.21573E-01	0.21356E-01	0.21222E-01	U			6 3
0.21176E-01						U			6 4
0.0	0.54082E-02	0.90235E-02	0.11817E-01	0.12449E-01	0.11833E-01	V			6 1
0.10319E-01	0.52673E-02	0.61336E-02	0.43165E-02	0.29537E-02	0.19802E-02	V			6 2
0.12902E-02	0.40821E-03	0.48372E-03	0.27492E-03	0.14384E-03	0.60530E-04	V			6 3
-0.19024E-08						V			6 4
0.60778E-01	0.59572E-01	0.58074E-01	0.55569E-01	0.52788E-01	0.47857E-01	W			6 1
0.43142E-01	0.37719E-01	0.32265E-01	0.26734E-01	0.21787E-01	0.18237E-01	W			6 2
0.15373E-01	0.13187E-01	0.11550E-01	0.10380E-01	0.96024E-02	0.91580E-02	W			6 3
0.90127E-02						W			6 4
143.500000	31.993286	0.054000							7
0.100000E-01	-0.34023E-01	0.19745E-03	-0.48524E-03	-0.72717E-05	-0.55479E-06				7 1
0.48077E-05	-0.11108E-07	-0.57747E-10	-0.79340E-11	-0.97578E-12					7 2
-0.77011E-02	-0.52508E-02	-0.40610E-03	0.89661E-02	0.17500E-01	0.25021E-01	U			7 1
0.30747E-01	0.34635E-01	0.36611E-01	0.36678E-01	0.35455E-01	0.33766E-01	U			7 2
0.32136E-01	0.30766E-01	0.29687E-01	0.28879E-01	0.28333E-01	0.28030E-01	U			7 3
0.27435E-01						U			7 4
0.0	0.15283E-01	0.25505E-01	0.29494E-01	0.28666E-01	0.24923E-01	V			7 1
0.19723E-01	0.14085E-01	0.90177E-02	0.52611E-02	0.28735E-02	0.14165E-02	V			7 2
0.59207E-03	0.13225E-03	-0.48881E-04	-0.18236E-03	-0.16364E-03	-0.98536E-04	V			7 3
0.74411E-08						V			7 4
0.10149E-00	0.99479E-01	0.94320E-01	0.87100E-01	0.78284E-01	0.68594E-01	W			7 1
0.58611E-01	0.48239E-01	0.37687E-01	0.28150E-01	0.20680E-01	0.15376E-01	W			7 2
0.11780E-01	0.93019E-02	0.76105E-02	0.64535E-02	0.57121E-02	0.53119E-02	W			7 3
0.51883E-02						W			7 4
145.500000	33.056488	0.040000							8
0.100000E-01	-0.31494E-01	0.18814E-03	-0.12441E-04	-0.10515E-05	-0.68047E-06				8 1
0.17304E-07	-0.77466E-08	-0.55082E-10	-0.48035E-11	-0.10264E-13					8 2
-0.46774E-01	-0.11666E-01	0.43733E-01	0.76264E-01	0.70342E-01	0.93574E-01	U			8 1
0.70661E-01	0.33775E-01	0.74253E-01	0.60909E-01	0.59241E-01	0.48502E-01	U			8 2
0.43744E-01	0.40495E-01	0.38290E-01	0.36816E-01	0.35717E-01	0.35456E-01	U			8 3
0.35326E-01						U			8 4
0.0	0.86061E-01	0.10842E-00	0.75773E-01	0.73747E-01	0.52446E-01	V			8 1
0.13678E-01	0.18480E-01	0.19745E-02	0.21466E-02	0.55754E-03	0.16695E-02	V			8 2
-0.20364E-02	-0.20321E-02	-0.18152E-02	-0.14670E-02	-0.10319E-02	-0.53451E-03	V			8 3
0.17985E-07						V			8 4
0.25421E-00	0.22664E-00	0.17605E-00	0.13894E-00	0.10774E-00	0.86314E-01	W			8 1
0.65463E-01	0.46682E-01	0.29528E-01	0.16548E-01	0.41981E-02	0.32824E-02	W			8 2
0.43977E-03	0.12560E-02	0.23742E-02	0.30174E-02	0.34488E-02	0.36735E-02	W			8 3
-0.47428E-02						W			8 4

FIGURE 3C. (Continued)

221.500000	33.976395	C.001000		9
0.10000E 01-C.34023E 01	0.17811E 03-C.13119E 04-0.13530E 06-0.61693E 06			9 1
0.29753E 07-C.05222E 08-0.50994E 10-C.27399E 11-0.24583E 13				9 2
-0.1893E 09-C.11113E-01	0.14261E 00 0.17738E 00 0.17187E 00 0.15512E 00	U		9 1
0.13494E 00 0.11325E 00 0.42790E-01	0.74725E-01 0.61530E-01 0.52540E-01	U		9 2
0.46531E-01 0.47643E-01 0.40251E-01	0.38727E-01 0.37483E-01 0.3754E-01	U		9 3
0.37474E-01		U		9 4
0.0	-0.31484E 07-0.28674E 00-0.21581E 00-0.15163E 00-0.12109E 00	V		9 1
-0.37204E-01-0.58280E-01-0.37028E-01-0.24011E-01-0.16484E-01-0.12511E-01		V		9 2
-0.49345E-02-0.40717E-02-0.44785E-02-0.49468E-02-0.3431E-02-0.17582E-02		V		9 3
0.43002E-07		V		9 4
-0.1641E 00-0.55326E 00-0.33054E 00-0.22020E 00-0.16483E 00-0.13310E 00		W		9 1
-0.11077E 00-0.49958E-01-0.75170E-01-0.54321E-01-0.43333E-01-0.36241E-01		W		9 2
-0.31463E-01-0.29277E-01-0.27801E-01-0.26994E-01-0.26549E-01-0.26594E-01		W		9 3
-0.26615E-01		W		9 4
264.200000	33.316925	-C.030000		10
0.10200E 01-0.44290E 01 0.16565E 03-0.80102E 03-0.11475E 06-0.54775E 06				10 1
0.17342E 07-0.11485E 09-0.75960E 10-0.60587E 11-0.27027E 13				10 2
-0.13191E-01-0.11062E-01-0.56679E-02 0.13507E-02 0.45044E-02 0.14706E-01	U			10 1
0.19605E-01 0.23409E-01 0.26109E-01 0.27473E-01 0.27623E-01 0.27072E-01	U			10 2
0.26284E-01 0.25546E-01 0.24946E-01 0.24599E-01 0.24215E-01 0.24076E-01	U			10 3
0.24034E-01		U		10 4
0.0	-0.26718E-01-0.46978E-01-0.58125E-01-0.61110E-01-0.58112E-01	V		10 1
-0.51032E-01-0.41761E-01-0.32529E-01-0.24993E-01-0.19544E-01-0.15756E-01	V			10 2
-0.1304E-01-0.10767E-01-0.86910E-02-0.66440E-02-0.45522E-02-0.23537E-02	V			10 3
0.1961E-07		V		10 4
-0.1766E 00-0.17578E 00-0.16803E 00-0.15698E 00-0.14406E 00-0.13078E 00	W			10 1
-0.11767E 00-0.10416E 00-0.90142E-01-0.76846E-01-0.65694E-01-0.57306E-01	W			10 2
-0.51504E-01-0.47756E-01-0.45420E-01-0.44020E-01-0.43316E-01-0.43105E-01	W			10 3
-0.43292E-01		W		10 4
316.000000	31.069885	-C.050300		11
0.10000E 01-0.74475E 01 0.12156E 03-0.14940E 03-0.62063E 05-0.18956E 06				11 1
0.40985E 07-0.48139E 08-0.36282E 10 0.79756E 10 0.46619E 11				11 2
-0.97733E-02-0.93924E-02-0.82796E-02-0.45307E-02-0.43245E-02-0.19135E-02	U			11 1
0.48052E-03 0.27504E-02 0.48486E-02 0.66741E-02 0.50734E-02 0.70620E-02	U			11 2
0.96554E-02 0.99966E-02 0.10188E-01 0.10290E-01 0.10333E-01 0.10342E-01	U			11 3
0.10341E-01		U		11 4
0.0	-0.42478E-02-0.15257E-01-0.20242E-01-0.23027E-01-0.23846E-01	V		11 1
-0.23056E-01-0.21080E-01-0.11490E-01-0.15916E-01-0.13749E-01-0.11997E-01	V			11 2
-0.10446E-01-0.48937E-02-0.72065E-02-0.55767E-02-0.48191E-02-0.19564E-02	V			11 3
0.68995E-07		V		11 4
-0.10435E 00-0.10358E 00-0.10129E 00-0.97611E-01-0.92812E-01 0.87308E-01	W			11 1
-0.91484E-01-0.75491E-01-0.69345E-01-0.63267E-01-0.57763E-01-0.53371E-01	W			11 2
-0.50016E-01-0.47718E-01-0.46129E-01-0.45073E-01-0.44469E-01-0.44217E-01	W			11 3
-0.44153E-01		W		11 4
343.000000	29.515289	-0.063500		12
0.10000E 01-0.94054E 01 0.89946E 02 0.11392E 03-0.41363E 05-0.13665E 06				12 1
0.29437E 07-0.18782E 08-0.18358E 10 0.19634E 11 0.45817E 12				12 2
-0.87337E-02-0.84853E-02-0.77818E-02-0.67046E-02-0.53241E-02-0.37312E-02	U			12 1
-0.20634E-02-0.43540E-03 0.11069E-02 0.25149E-02 0.36914E-02 0.45658E-02	U			12 2
0.51596E-02 0.55513E-02 0.58110E-02 0.59755E-02 0.60660E-02 0.61055E-02	U			12 3
0.61157E-02		U		12 4
0.0	-0.53084E-02-0.10011E-01-0.13592E-01-0.15802E-01-0.16736E-01	V		12 1
-0.16648E-01-0.15770E-01-0.14371E-01-0.12825E-01-0.11431E-01-0.10218E-01	V			12 2
-0.90288E-02-0.77409E-02-0.63468E-02-0.48793E-02-0.33354E-02-0.17006E-02	V			12 3
0.56991E-07		V		12 4
-0.84867E-01-0.84305E-01-0.82705E-01-0.80231E-01-0.77008E-01-0.73190E-01	W			12 1
-0.69038E-01-0.64776E-01-0.60475E-01-0.56227E-01-0.52341E-01-0.49162E-01	W			12 2
-0.46790E-01-0.45079E-01-0.43847E-01-0.43007E-01-0.42509E-01-0.42273E-01	W			12 3
-0.42208E-01		W		12 4

FIGURE 36. (Continued)

374.000000	27.511200	-0.074000							13
0.10000E 01	-0.11876E 02	0.47583E 02	0.27331E 03	-0.24758E 05	-0.13019E 06				13 1
0.15000E 07	0.57690E 07	-0.93720E 09	0.13366E 10	0.23796E 12					13 2
-0.74791E-02	-0.73363E-02	-0.69224E-02	-0.62661E-02	-0.53993E-02	-0.43770E-02				U 13 1
-0.32797E-02	-0.21715E-02	-0.10868E-02	-0.75036E-04	0.78717E-03	0.14511E-02				U 13 2
0.19323E-02	0.22798E-02	0.25302E-02	0.26988E-02	0.27994E-02	0.28508E-02				U 13 3
0.28666E-02									U 13 4
0.0	-0.35475E-02	-0.67314E-02	-0.92490E-02	-0.10753E-01	-0.11873E-01				V 13 1
-0.1211E-01	-0.11806E-01	-0.11111E-01	-0.10271E-01	-0.94451E-02	-0.86155E-02				V 13 2
-0.76843E-02	-0.66130E-02	-0.54367E-02	-0.41850E-02	-0.28538E-02	-0.14478E-02				V 13 3
0.49305E-07									V 13 4
-0.68847E-01	-0.68493E-01	-0.57466E-01	-0.65834E-01	-0.63665E-01	-0.61077E-01				W 13 1
-0.58241E-01	-0.55294E-01	-0.52301E-01	-0.49376E-01	-0.46748E-01	-0.44616E-01				W 13 2
-0.42997E-01	-0.41778E-01	-0.40867E-01	-0.40235E-01	-0.39850E-01	-0.39649E-01				W 13 3
-0.39587E-01									W 13 4
411.000000	23.677185	-0.135000							14
0.10000E 01	-0.14639E 02	0.25525E 02	0.13394E 03	-0.14122E 05	-0.69219E 05				14 1
0.43107E 06	0.37599E 07	-0.24462E 09	-0.96070E 08	0.31622E 11					14 2
-0.61602E-02	-0.60934E-02	-0.58935E-02	-0.55605E-02	-0.50993E-02	-0.45301E-02				U 14 1
-0.38866E-02	-0.31999E-02	-0.24978E-02	-0.18218E-02	-0.12260E-02	-0.74554E-03				U 14 2
-0.37829E-03	-0.10029E-03	-0.10727E-03	-0.25195E-03	-0.34119E-03	-0.38728E-03				U 14 3
0.40127E-03									U 14 4
0.0	-0.22508E-02	-0.42863E-02	-0.59365E-02	-0.71171E-02	-0.78301E-02				V 14 1
-0.81212E-02	-0.80595E-02	-0.77556E-02	-0.73417E-02	-0.68921E-02	-0.63861E-02				V 14 2
-0.57664E-02	-0.50152E-02	-0.41590E-02	-0.32221E-02	-0.22084E-02	-0.11250E-02				V 14 3
0.41558E-07									V 14 4
-0.55335E-01	-0.55154E-01	-0.54611E-01	-0.53713E-01	-0.52474E-01	-0.50944E-01				W 14 1
-0.49202E-01	-0.47322E-01	-0.45364E-01	-0.43434E-01	-0.41685E-01	-0.40238E-01				W 14 2
-0.39109E-01	-0.38241E-01	-0.37585E-01	-0.37124E-01	-0.36939E-01	-0.36693E-01				W 14 3
-0.36649E-01									W 14 4
450.000000	17.579895	-0.185000							15
0.10000E 01	-0.17655E 02	0.24497E 02	0.80204E 02	-0.30498E 04	-0.15568E 05				15 1
0.79269E 05	0.42978E 06	-0.20739E 08	-0.54266E 08	0.22970E 10					15 2
-0.50665E-02	-0.50323E-02	-0.49296E-02	-0.47563E-02	-0.45123E-02	-0.42061E-02				U 15 1
-0.38549E-02	-0.34739E-02	-0.30757E-02	-0.26824E-02	-0.23256E-02	-0.20268E-02				U 15 2
-0.17850E-02	-0.15886E-02	-0.14319E-02	-0.13150E-02	-0.12358E-02	-0.11895E-02				U 15 3
-0.11740E-02									U 15 4
0.0	-0.11399E-02	-0.21879E-02	-0.30684E-02	-0.37438E-02	-0.42133E-02				V 15 1
-0.44870E-02	-0.45798E-02	-0.45331E-02	-0.44080E-02	-0.42341E-02	-0.39872E-02				V 15 2
-0.36328E-02	-0.31724E-02	-0.26342E-02	-0.20373E-02	-0.13888E-02	-0.70277E-03				V 15 3
0.24030E-07									V 15 4
-0.45345E-01	-0.45247E-01	-0.44951E-01	-0.44455E-01	-0.43758E-01	-0.42884E-01				W 15 1
-0.41880E-01	-0.40786E-01	-0.39635E-01	-0.38486E-01	-0.37432E-01	-0.36540E-01				W 15 2
-0.35814E-01	-0.35221E-01	-0.34746E-01	-0.34391E-01	-0.34150E-01	-0.34009E-01				W 15 3
-0.33962E-01									W 15 4
497.000000	8.212999	-0.206000							16
0.10000E 01	-0.21252E 02	0.13116E 02	0.80401E 01	-0.11905E 03	-0.32960E 03				16 1
0.76206E 03	0.16588E 04	-0.34590E 05	0.90360E 03	0.11027E 07					16 2
-0.38669E-02	-0.38559E-02	-0.38229E-02	-0.37675E-02	-0.36882E-02	-0.35858E-02				U 16 1
-0.34644E-02	-0.33288E-02	-0.31835E-02	-0.30356E-02	-0.28954E-02	-0.27713E-02				U 16 2
-0.26646E-02	-0.25732E-02	-0.24969E-02	-0.24371E-02	-0.23945E-02	-0.23687E-02				U 16 3
-0.23600E-02									U 16 4
0.0	-0.32777E-03	-0.63462E-03	-0.90060E-03	-0.11144E-02	-0.12762E-02				V 16 1
-0.13892E-02	-0.14552E-02	-0.14815E-02	-0.14813E-02	-0.14592E-02	-0.14038E-02				V 16 2
-0.13014E-02	-0.11519E-02	-0.96575E-03	-0.75149E-03	-0.51400E-03	-0.26051E-03				V 16 3
0.91033E-08									V 16 4
-0.36283E-01	-0.36249E-01	-0.36148E-01	-0.35979E-01	-0.35736E-01	-0.35424E-01				W 16 1
-0.35053E-01	-0.34638E-01	-0.34193E-01	-0.33738E-01	-0.33306E-01	-0.32923E-01				W 16 2
-0.32593E-01	-0.32310E-01	-0.32074E-01	-0.31889E-01	-0.31757E-01	-0.31677E-01				W 16 3
-0.31650E-01									W 16 4

FIGURE 36. (Concluded)

4. APPLICATION OF TRANSFORMATION METHOD TO FUSELAGE

This section bears close resemblance to the discussion in Section II.4 of "Application of Transformation Method to Wing." A finite wing is also a three-dimensional body but it has a distinctive property of generating lift in a uniform stream. Thus, by ignoring a part of the computer program which is concerned with circulation, the power effects on a fuselage are calculated in a manner similar to that for a wing.

a. Inputs to Transformation Method for Sample Problem

All the input data for this sample problem are shown in Figure 37. The punched outputs from the jet flow field program again make up the major portion of the input. Two cards must also precede this basic input block to specify various flow indices, and none, two or four cards may follow this block, depending on the options.

Card 1 and Card 2 denote the same number of flow indices as those on Cards 1 and 2 in the previous section on application to a wing. The meaning of each input is also the same, except that the number of quantities of the following indices are different. The classification index (IGECM) is now equal to 2 to denote a fuselage, the number of iterations (JSTOP) is 1, the number of stations (NSTA) is 16, the computation index (NSYM) is 0 to indicate the existence of a plane of symmetry, and the number of angular increments from 0 to π (MTHET) is 18.

Cards 3 through 242 contain the punched output data furnished by the jet flow field program, which include the X coordinate, the mapping coefficients, and the induced velocity components for stations 1 through 16. There are 15 cards for every station.

Card 243 specifies the station number immediately preceding the exhausting jet.

Card 244 refers to the X coordinate of the fuselage tail.

Card 245 lists in order the number of jets, the jet exit diameter, X coordinate of the center of gravity, and the reference length for nondimensionalizing computed moments.

Card 246 denotes in order the Y coordinate of the nose, Z coordinate of the nose; X coordinate, Y coordinate and Z coordinate of the tail.

b. Outputs from Transformation Method for Sample Problem

Figure 38 lists directly or indirectly a portion of the input data on cards 1 through 242.

Figure 39 establishes the correspondence between the angular increments of the mapping circle and their corresponding geometric locations at every fuselage station. The first column gives the angular increments in degrees.

Figure 40 shows the pressure coefficient distribution at each station after application of the segment method. Since these coefficients are tabulated against angular increments only, cross reference to Figure 39 is needed in order to establish pressure distributions in the physical plane.

Figure 41 is also a table for the pressure distribution similar to the one in Figure 40 but after the three-dimensional modification has been introduced.

Figure 42 gives the parameters used in the three-dimensional modification and in the computation of forces and moments, originally read in as input data on Cards 243 through 246. The computed forces (normalized to the thrust) and moments (normalized by the thrust and reference length) on the fuselage after one iteration are also tabulated in the same figure.

Some of the computed results of this sample problem have been compared with the available wind tunnel test data and are shown in Figures 43(a) through 43(d). The power-effect pressure distributions in these figures are representative for fuselages with a lift jet in a uniform flow. The typical feature of this class may be described as follows: The power effect in the fore part of the fuselage is generally very small, as seen in Figure 43(a). As we approach the lift jet, there is a small region in the front where the power effect is positive (Figure 43(b)). The negative power effect then decreases rapidly and its magnitude becomes very large in the immediate neighborhood of the jet but tapers off to a constant level in the distance of one or two jet diameters. This constant level of power effect is in general quite high and prevails over the entire back part of the fuselage (Figures 43(c) and 43(d)). Thus, it contributes a major portion of the forces and moments. The origin of this effect is due mostly to the wake formed behind the lift jet. Its prediction lies beyond the scope of the present method. Consequently, the discrepancy between the calculation and the test data in this region is large.

When the sideslip angle is not zero, the jet wake region does not completely enfold the back portion of the fuselage. The comparison between the prediction and the test becomes more favorable as may be seen in Figures 44(a) to 44(c).

Further calculations and wind tunnel test data are compared in Figures 45 and 46. The body referred to in Figure 46 is the one tested at Northrop prior to the present contract (see Figure 23 in Section II. 4).

2000 COMPUTATION

OPTIONS SPECIFIED FOR THIS RUN ARE

1. THREE DIMENSIONAL MODIFICATION OF 1 ITERATION
2. POWER EFFECT ONLY

```

NSTA= 16  N= 11  NFOUR= 20  NSYN= 0  MTHET= 18  IRECT= 1  IFORCE= 1
UJ= 0.200  ALPHA= 0.0  BETA= 0.0

STATION= 23.699597  RADIUS= 10.263370  DERIV= 0.285000

GEOMETRY COEFFICIENT *A* FOR STATION 1
0.100000E 01  0.780000E 01  0.714360E 01  -0.172200E 03  0.692400E 03
0.147270E 02  -0.216030E 05  0.408890E 05  0.219690E 06  -0.382240E 07

VELOCITY COMPONENT *U* AT STATION 1
-0.44731E-04  -0.29299E-04  0.11127E-04  0.93755E-04  0.19770E-03  0.32468E-03
0.47016E-03  0.62943E-03  0.79768E-03  0.97076E-03  0.11440E-02  0.13102E-02
0.14598E-02  0.15857E-02  0.16860E-02  0.17521E-02  0.19155E-02  0.18469E-02
0.18572E-02

VELOCITY COMPONENT *V* AT STATION 1
0.0  0.74342E-04  0.14471E-03  0.20799E-03  0.26181E-03  0.30423E-03
0.33389E-03  0.35038E-03  0.35398E-03  0.34585E-03  0.32832E-03  0.30427E-03
0.27544E-03  0.24165E-03  0.20212E-03  0.15697E-03  0.10731E-03  0.54512E-04
-0.10974E-08

VELOCITY COMPONENT *W* AT STATION 1
0.93589E-02  0.93522E-02  0.93320E-02  0.92982E-02  0.92517E-02  0.91937E-02
0.91253E-02  0.90491E-02  0.89638E-02  0.88739E-02  0.87802E-02  0.86867E-02
0.85993E-02  0.85234E-02  0.84416E-02  0.84140E-02  0.83802E-02  0.83602E-02
0.83336E-02

STATION= 41.000000  RADIUS= 15.089800  DERIV= 0.254000

```

FIGURE 38. PARTIAL LIST OF INPUT DATA FOR SAMPLE FUSELAGE

TABLE FOR FUSELAGE GEOMETRY

THETA O.J	X= 23.70			X= 41.00			X= 73.00			X= 94.00		
	Y(I)	Z(I)	Y(I)	Y(I)	Z(I)	Y(I)	Y(I)	Z(I)	Y(I)	Y(I)	Z(I)	Z(I)
0.0	0.0	-0.18601E 02	0.0	0.0	-0.22211E 02	0.0	0.0	-0.26239E 02	0.0	0.0	-0.27860E 02	0.0
10.00	0.17307E 01	-0.12454E J2	0.24615E 01	0.24615E 01	-0.21992E 02	0.36290E 01	0.36290E 01	-0.25973E 02	0.42943E 01	0.42943E 01	-0.27600E 02	0.0
20.00	0.33915E 01	-0.18003E 02	0.48337E 01	0.48337E 01	-0.21318E 02	0.70475E 01	0.70475E 01	-0.25152E 02	0.82859E 01	0.82859E 01	-0.26776E 02	0.0
30.00	0.49291E 01	-0.17252E 02	0.70168E 01	0.70168E 01	-0.20208E 02	0.10086E 02	0.10086E 02	-0.23725E 02	0.11741E 02	0.11741E 02	-0.25276E 02	0.0
40.00	0.63004E 01	-0.16217E 02	0.89361E 01	0.89361E 01	-0.18666E 02	0.12644E 02	0.12644E 02	-0.21645E 02	0.14553E 02	0.14553E 02	-0.22984E 02	0.0
50.00	0.74621E 01	-0.14928E 02	0.10549E 02	0.10549E 02	-0.16725E 02	0.14677E 02	0.14677E 02	-0.18923E 02	0.16697E 02	0.16697E 02	-0.19876E 02	0.0
60.00	0.83752E 01	-0.13417E 02	0.11794E 02	0.11794E 02	-0.14448E 02	0.16119E 02	0.16119E 02	-0.15592E J2	0.18143E 02	0.18143E 02	-0.15982E 02	0.0
70.00	0.90129E 01	-0.11720E 02	0.12609E 02	0.12609E 02	-0.11863E 02	0.16968E 02	0.16968E 02	-0.11657E 02	0.18917E 02	0.18917E 02	-0.11298E 02	0.0
80.00	0.93580E 01	-0.94782E 01	0.13018E 02	0.13018E 02	-0.89704E 01	0.17354E 02	0.17354E 02	-0.71713E 01	0.19220E 02	0.19220E 02	-0.58934E 01	0.0
90.00	0.94143E 01	-0.79298E 01	0.13131E 02	0.13131E 02	-0.58727E 01	0.17454E 02	0.17454E 02	-0.23861E 01	0.19302E 02	0.19302E 02	-0.11547E 00	0.0
100.00	0.92113E 01	-0.59251E 01	0.12993E 02	0.12993E 02	-0.27953E 01	0.17266E 02	0.17266E 02	-0.23109E 01	0.19134E 02	0.19134E 02	0.55073E 01	0.0
110.00	0.87972E 01	-0.39520E 01	0.12510E 02	0.12510E 02	-0.71674E-01	0.16589E 02	0.16589E 02	0.66608E 01	0.18401E 02	0.18401E 02	0.10647E 02	0.0
120.00	0.81901E 01	-0.21296E 01	0.11587E 02	0.11587E 02	0.26857E 01	0.15269E 02	0.15269E 02	0.10654E 02	0.16901E 02	0.16901E 02	0.15421E 02	0.0
130.00	0.73626E 01	-0.55655E 00	0.10256E 02	0.10256E 02	0.50562E 01	0.13384E 02	0.13384E 02	0.14338E 02	0.14784E 02	0.14784E 02	0.19855E 02	0.0
140.00	0.62817E 01	0.72769E 00	0.86160E 01	0.86160E 01	0.71195E 01	0.11124E 02	0.11124E 02	0.17619E 02	0.12314E 02	0.12314E 02	0.23804E 02	0.0
150.00	0.49539E 01	0.17239E 01	0.67169E 01	0.67169E 01	0.87795E 01	0.85964E 01	0.85964E 01	0.20317E 02	0.95697E 01	0.95697E 01	0.26997E 02	0.0
160.00	0.34241E 01	0.24354E 01	0.45914E 01	0.45914E 01	0.99959E 01	0.58457E 01	0.58457E 01	0.22317E 02	0.65371E 01	0.65371E 01	0.29321E 02	0.0
170.00	0.17507E 01	0.28600E 01	0.30003E 01	0.30003E 01	0.10757E 02	0.29489E 01	0.29489E 01	0.23562E 02	0.33016E 01	0.33016E 01	0.30762E 02	0.0
180.00	0.63475E-05	0.28600E 01	0.83717E-05	0.83717E-05	0.11021E 02	0.10631E-04	0.10631E-04	0.23989E 02	0.11900E-04	0.11900E-04	0.31260E 02	0.0
190.00	-0.17507E 01	0.28600E 01	-0.23211E 01	-0.23211E 01	0.10757E 02	-0.29489E 01	-0.29489E 01	0.20317E 02	-0.33016E 01	-0.33016E 01	0.30762E 02	0.0
200.00	-0.34241E 01	0.24354E 01	-0.45914E 01	-0.45914E 01	0.99959E 01	-0.58456E 01	-0.58456E 01	0.22317E 02	-0.65371E 01	-0.65371E 01	0.29321E 02	0.0
210.00	-0.49539E 01	0.17239E 01	-0.67169E 01	-0.67169E 01	0.87795E 01	-0.85964E 01	-0.85964E 01	0.20317E 02	-0.95697E 01	-0.95697E 01	0.26997E 02	0.0
220.00	-0.62817E 01	0.72769E 00	-0.86160E 01	-0.86160E 01	0.71195E 01	-0.11124E 02	-0.11124E 02	0.17619E 02	-0.12314E 02	-0.12314E 02	0.23804E 02	0.0
230.00	-0.73626E 01	-0.55655E 00	-0.10256E 02	-0.10256E 02	0.50562E 01	-0.13384E 02	-0.13384E 02	0.14338E 02	-0.14784E 02	-0.14784E 02	0.19855E 02	0.0
240.00	-0.81901E 01	-0.21296E 01	-0.11587E 02	-0.11587E 02	0.26857E 01	-0.15269E 02	-0.15269E 02	0.10654E 02	-0.16901E 02	-0.16901E 02	0.15421E 02	0.0
250.00	-0.87972E 01	-0.39520E 01	-0.12510E 02	-0.12510E 02	-0.71674E-01	-0.16589E 02	-0.16589E 02	0.66608E 01	-0.18401E 02	-0.18401E 02	0.10647E 02	0.0
260.00	-0.92113E 01	-0.59251E 01	-0.12993E 02	-0.12993E 02	-0.27953E 01	-0.17266E 02	-0.17266E 02	0.23109E 01	-0.19134E 02	-0.19134E 02	0.55073E 01	0.0
270.00	-0.94143E 01	-0.79298E 01	-0.13131E 02	-0.13131E 02	-0.58727E 01	-0.17454E 02	-0.17454E 02	-0.23861E 01	-0.19302E 02	-0.19302E 02	-0.11547E 00	0.0
280.00	-0.93580E 01	-0.94782E 01	-0.13018E 02	-0.13018E 02	-0.89704E 01	-0.17354E 02	-0.17354E 02	-0.71713E 01	-0.19220E 02	-0.19220E 02	-0.58934E 01	0.0
290.00	-0.90129E 01	-0.11720E 02	-0.12609E 02	-0.12609E 02	-0.11863E 02	-0.16968E 02	-0.16968E 02	-0.11657E 02	-0.18917E 02	-0.18917E 02	-0.11298E 02	0.0
300.00	-0.83752E 01	-0.13417E 02	-0.11794E 02	-0.11794E 02	-0.14448E 02	-0.16119E 02	-0.16119E 02	-0.15592E 02	-0.18143E 02	-0.18143E 02	-0.15982E 02	0.0
310.00	-0.74621E 01	-0.4928E 02	-0.10549E 02	-0.10549E 02	-0.16725E 02	-0.14677E 02	-0.14677E 02	-0.18923E 02	-0.16697E 02	-0.16697E 02	-0.19876E 02	0.0
320.00	-0.63004E 01	-0.16217E 02	-0.89361E 01	-0.89361E 01	-0.18666E 02	-0.12644E 02	-0.12644E 02	-0.21645E 02	-0.14553E 02	-0.14553E 02	-0.22984E 02	0.0
330.00	-0.49291E 01	-0.17252E 02	-0.70168E 01	-0.70168E 01	-0.20208E 02	-0.10086E 02	-0.10086E 02	-0.23725E 02	-0.11741E 02	-0.11741E 02	-0.25276E 02	0.0
340.00	-0.33915E 01	-0.18003E 02	-0.48337E 01	-0.48337E 01	-0.21318E 02	-0.70475E 01	-0.70475E 01	-0.25152E 02	-0.82859E 01	-0.82859E 01	-0.26776E 02	0.0
350.00	-0.17307E 01	-0.18601E 02	-0.24615E 01	-0.24615E 01	-0.21992E 02	-0.36290E 01	-0.36290E 01	-0.25973E 02	-0.42943E 01	-0.42943E 01	-0.27860E 02	0.0

FIGURE 39. CORRESPONDENCE BETWEEN ANGULAR INCREMENTS OF MAPPING CIRCLES AND CARTESIAN COORDINATES OF FUSELAGE SECTIONS

TABLE FOR FUSELAGE GEOMETRY

THETA	Y(I)	Z(I)	Y(I)	Z(I)	Y(I)	Z(I)	Y(I)	Z(I)	Y(I)	Z(I)	Y(I)	Z(I)
0.0	0.0	-0.29108E 02	0.0	-0.30200E 02	0.0	-0.30676E 02	0.0	-0.30826E 02	0.0	-0.30938E 02	0.0	-0.30983E 02
10.00	0.50473E 01	-0.28923E 02	0.60031E 01	-0.30238E 02	0.66114E 01	-0.30826E 02	0.71582E 01	-0.30826E 02	0.71582E 01	-0.30938E 02	0.71582E 01	-0.30983E 02
20.00	0.95866E 01	-0.28225E 02	0.11082E 02	-0.29863E 02	0.12119E 02	-0.30796E 02	0.13272E 02	-0.30796E 02	0.13272E 02	-0.30826E 02	0.13272E 02	-0.30826E 02
30.00	0.13535E 02	-0.26715E 02	0.14991E 02	-0.28667E 02	0.16252E 02	-0.29718E 02	0.17921E 02	-0.29718E 02	0.17921E 02	-0.30280E 02	0.17921E 02	-0.30280E 02
40.00	0.16338E 02	-0.24196E 02	0.18001E 02	-0.26049E 02	0.19351E 02	-0.27215E 02	0.21223E 02	-0.27215E 02	0.21223E 02	-0.28236E 02	0.21223E 02	-0.28236E 02
50.00	0.18583E 02	-0.20686E 02	0.20265E 02	-0.22265E 02	0.21614E 02	-0.23449E 02	0.23347E 02	-0.23449E 02	0.23347E 02	-0.24793E 02	0.23347E 02	-0.24793E 02
60.00	0.20042E 02	-0.16247E 02	0.21674E 02	-0.17435E 02	0.22946E 02	-0.18527E 02	0.23382E 02	-0.18527E 02	0.23382E 02	-0.19904E 02	0.23382E 02	-0.19904E 02
70.00	0.201745E 02	-0.10847E 02	0.22269E 02	-0.11472E 02	0.23413E 02	-0.13234E 02	0.23582E 02	-0.13234E 02	0.23582E 02	-0.13521E 02	0.23582E 02	-0.13521E 02
80.00	0.20377E 01	-0.45547E 01	0.22248E 02	-0.46690E 01	0.23451E 02	-0.50023E 01	0.24420E 02	-0.50023E 01	0.24420E 02	-0.58448E 01	0.24420E 02	-0.58448E 01
90.00	0.21059E 02	0.21804E 01	0.22504E 02	0.30352E 01	0.23458E 02	0.29427E 01	0.24302E 02	0.29427E 01	0.24302E 02	0.25228E 01	0.24302E 02	0.25228E 01
100.00	0.20933E 02	0.87084E 01	0.22438E 02	0.10339E 02	0.23438E 02	0.10738E 02	0.24289E 02	0.10738E 02	0.24289E 02	0.10788E 02	0.10738E 02	0.10788E 02
110.00	0.20212E 02	0.14680E 02	0.20218E 02	0.17017E 02	0.23098E 02	0.17829E 02	0.24101E 02	0.17829E 02	0.24101E 02	0.18279E 02	0.17829E 02	0.18279E 02
120.00	0.18675E 02	0.20160E 02	0.20570E 02	0.22979E 02	0.22077E 02	0.23969E 02	0.23310E 02	0.23969E 02	0.23310E 02	0.24637E 02	0.23969E 02	0.24637E 02
130.00	0.16919E 02	0.25206E 02	0.18492E 02	0.28220E 02	0.20170E 02	0.29128E 02	0.21570E 02	0.29128E 02	0.21570E 02	0.29783E 02	0.29128E 02	0.29783E 02
140.00	0.13897E 02	0.29592E 02	0.15746E 02	0.32652E 02	0.17362E 02	0.33357E 02	0.18775E 02	0.33357E 02	0.18775E 02	0.33689E 02	0.33357E 02	0.33689E 02
150.00	0.33052E 02	0.33052E 02	0.10902E 02	0.36156E 02	0.13784E 02	0.36672E 02	0.15049E 02	0.36672E 02	0.15049E 02	0.36980E 02	0.36672E 02	0.36980E 02
160.00	0.74751E 01	0.35545E 02	0.85823E 01	0.38673E 02	0.96006E 01	0.39022E 02	0.10565E 02	0.39022E 02	0.10565E 02	0.39117E 02	0.39022E 02	0.39117E 02
170.00	0.37135E 01	0.37110E 02	0.43839E 01	0.40191E 02	0.49463E 01	0.40387E 02	0.54717E 01	0.40387E 02	0.54717E 01	0.40311E 02	0.40387E 02	0.40311E 02
180.00	0.15898E-04	0.37658E 02	0.15883E-04	0.40700E 02	0.17981E 01	0.40826E 02	0.19404E-04	0.40826E 02	0.19404E-04	0.40631E 02	0.40826E 02	0.40631E 02
190.00	0.371735E 01	0.37110E 02	-0.43839E 01	0.40191E 02	-0.49463E 01	0.40387E 02	-0.54717E 01	0.40387E 02	-0.54717E 01	0.40311E 02	0.40387E 02	0.40311E 02
200.00	0.74751E 01	0.35545E 02	0.85823E 01	0.38673E 02	0.96006E 01	0.39022E 02	0.10565E 02	0.39022E 02	0.10565E 02	0.39117E 02	0.39022E 02	0.39117E 02
210.00	0.10902E 02	0.33052E 02	0.12415E 02	0.36156E 02	0.13784E 02	0.36672E 02	0.15049E 02	0.36672E 02	0.15049E 02	0.36980E 02	0.36672E 02	0.36980E 02
220.00	0.13897E 02	0.29592E 02	0.15746E 02	0.32652E 02	0.17362E 02	0.33357E 02	0.18775E 02	0.33357E 02	0.18775E 02	0.33689E 02	0.33357E 02	0.33689E 02
230.00	0.16919E 02	0.25206E 02	0.18492E 02	0.28220E 02	0.20170E 02	0.29128E 02	0.21570E 02	0.29128E 02	0.21570E 02	0.29783E 02	0.29128E 02	0.29783E 02
240.00	0.18675E 02	0.20160E 02	0.20570E 02	0.22979E 02	0.22077E 02	0.23969E 02	0.23310E 02	0.23969E 02	0.23310E 02	0.24637E 02	0.23969E 02	0.24637E 02
250.00	0.14680E 02	0.14680E 02	0.21880E 02	0.17017E 02	0.23098E 02	0.17829E 02	0.24101E 02	0.17829E 02	0.24101E 02	0.18279E 02	0.17829E 02	0.18279E 02
260.00	0.87084E 01	-0.22438E 02	0.22438E 02	0.10339E 02	-0.23438E 02	0.10738E 02	-0.24289E 02	0.10738E 02	-0.24289E 02	0.10788E 02	0.10738E 02	0.10788E 02
270.00	0.21059E 02	0.21804E 01	0.22504E 02	0.30352E 01	0.23458E 02	0.29427E 01	0.24302E 02	0.29427E 01	0.24302E 02	0.25228E 01	0.24302E 02	0.25228E 01
280.00	0.20933E 02	0.87084E 01	0.22438E 02	0.10339E 02	0.23438E 02	0.10738E 02	0.24289E 02	0.10738E 02	0.24289E 02	0.10788E 02	0.10738E 02	0.10788E 02
290.00	0.20212E 02	0.14680E 02	0.20218E 02	0.17017E 02	0.23098E 02	0.17829E 02	0.24101E 02	0.17829E 02	0.24101E 02	0.18279E 02	0.17829E 02	0.18279E 02
300.00	0.18675E 02	-0.45547E 01	0.22248E 02	-0.46690E 01	0.23451E 02	-0.50023E 01	0.24420E 02	-0.50023E 01	0.24420E 02	-0.58448E 01	0.24420E 02	-0.58448E 01
310.00	0.20745E 02	-0.10847E 02	0.22269E 02	-0.11472E 02	0.23413E 02	-0.13234E 02	0.23582E 02	-0.13234E 02	0.23582E 02	-0.13521E 02	0.23582E 02	-0.13521E 02
320.00	0.20042E 02	-0.16247E 02	0.21674E 02	-0.17435E 02	0.22946E 02	-0.18527E 02	0.23382E 02	-0.18527E 02	0.23382E 02	-0.19904E 02	0.23382E 02	-0.19904E 02
330.00	0.201745E 02	-0.10847E 02	0.22269E 02	-0.11472E 02	0.23413E 02	-0.13234E 02	0.23582E 02	-0.13234E 02	0.23582E 02	-0.13521E 02	0.23582E 02	-0.13521E 02
340.00	0.20377E 01	-0.45547E 01	0.22248E 02	-0.46690E 01	0.23451E 02	-0.50023E 01	0.24420E 02	-0.50023E 01	0.24420E 02	-0.58448E 01	0.24420E 02	-0.58448E 01
350.00	0.21059E 02	0.21804E 01	0.22504E 02	0.30352E 01	0.23458E 02	0.29427E 01	0.24302E 02	0.29427E 01	0.24302E 02	0.25228E 01	0.24302E 02	0.25228E 01
360.00	0.20933E 02	0.87084E 01	0.22438E 02	0.10339E 02	0.23438E 02	0.10738E 02	0.24289E 02	0.10738E 02	0.24289E 02	0.10788E 02	0.10738E 02	0.10788E 02
370.00	0.20212E 02	0.14680E 02	0.20218E 02	0.17017E 02	0.23098E 02	0.17829E 02	0.24101E 02	0.17829E 02	0.24101E 02	0.18279E 02	0.17829E 02	0.18279E 02
380.00	0.18675E 02	0.20160E 02	0.20570E 02	0.22979E 02	0.22077E 02	0.23969E 02	0.23310E 02	0.23969E 02	0.23310E 02	0.24637E 02	0.23969E 02	0.24637E 02
390.00	0.16919E 02	0.25206E 02	0.18492E 02	0.28220E 02	0.20170E 02	0.29128E 02	0.21570E 02	0.29128E 02	0.21570E 02	0.29783E 02	0.29128E 02	0.29783E 02
400.00	0.13897E 02	0.29592E 02	0.15746E 02	0.32652E 02	0.17362E 02	0.33357E 02	0.18775E 02	0.33357E 02	0.18775E 02	0.33689E 02	0.33357E 02	0.33689E 02
410.00	0.33052E 02	0.33052E 02	0.10902E 02	0.36156E 02	0.13784E 02	0.36672E 02	0.15049E 02	0.36672E 02	0.15049E 02	0.36980E 02	0.36672E 02	0.36980E 02
420.00	0.74751E 01	0.35545E 02	0.85823E 01	0.38673E 02	0.96006E 01	0.39022E 02	0.10565E 02	0.39022E 02	0.10565E 02	0.39117E 02	0.39022E 02	0.39117E 02
430.00	0.37135E 01	0.37110E 02	0.43839E 01	0.40191E 02	0.49463E 01	0.40387E 02	0.54717E 01	0.40387E 02	0.54717E 01	0.40311E 02	0.40387E 02	0.40311E 02
440.00	0.15898E-04	0.37658E 02	0.15883E-04	0.40700E 02	0.17981E 01	0.40826E 02	0.19404E-04	0.40826E 02	0.19404E-04	0.40631E 02	0.40826E 02	0.40631E 02
450.00	0.371735E 01	0.37110E 02	-0.43839E 01	0.40191E 02	-0.49463E 01	0.40387E 02	-0.54717E 01	0.40387E 02	-0.54717E 01	0.40311E 02	0.40387E 02	0.40311E 02
460.00	0.74751E 01	0.35545E 02	0.85823E 01	0.38673E 02	0.96006E 01	0.39022E 02	0.10565E 02	0.39022E 02	0.10565E 02	0.39117E 02	0.39022E 02	0.39117E 02
470.00	0.10902E 02	0.33052E 02	0.12415E 02	0.36156E 02	0.13784E 02	0.36672E 02	0.15049E 02	0.36672E 02	0.15049E 02	0.36980E 02	0.36672E 02	0.36980E 02
480.00	0.13897E 02	0.29592E 02	0.15746E 02	0.32652E 02	0.17362E 02	0.33357E 02	0.18775E 02	0.33357E 02	0.18775E 02	0.33689E 02	0.33357E 02	0.33689E 02
490.00	0.16919E 02	0.25206E 02	0.18492E 02	0.28220E 02	0.20170E 02	0.29128E 02	0.21570E 02	0.29128E 02	0.21570E 02	0.29783E 02	0.29128E 02	0.29783E 02
500.00	0.13897E 02	0.29592E 02	0.15746E 02	0.32652E 02	0.17362E 02	0.33357E 02	0.18775E 02	0.33357E 02	0.18775E 02	0.33689E 02	0.33357E 02	0.33689E 02
510.00	0.33052E 02	0.33052E 02	0.10902E 02	0.36156E 02	0.13784E 02	0.36672E 02	0.15049E 02	0.36672E 02	0.15049E 02	0.36980E 02	0.36672E 02	0.36980E 02
520.00	0.74751E 01	0.35545E 02	0.85823E 01	0.38673E 02	0.96006E 01	0.39022E 02	0.10565E 02	0.39022E 02	0.10565E 02	0.39117E 02	0.39022E 02	0.39117E 02
530.00	0.37135E 01	0.37110E 02	0.43839E 01	0.40191E 02	0.49463E 01	0.40387E 02	0.54717E 01	0.40387E 02	0.54717E 01	0.40311E 02	0.40387E 02	0.40311E 02
540.00	0.15898E-04	0.37658E 02	0.15883E-04	0.40700E 02	0.17981E 01	0.40826E 02	0.19404E-04	0.40826E 02	0.19404E-04	0.40631E 02	0.40826E 02	0.40631E 02
550.00	0.371735E 01	0.37110E 02	-0.43839E 01	0.40191E 02	-0.49463E 01	0.40387E 02	-0.54717E 01	0.40387E 02	-0.54717E 01	0.40311E 02	0.40387E 02	0.40311E 02
560.00	0.74751E 01	0.35545E 02	0.85823E 01	0.38673E 02	0.96006E 01	0.39022E 02	0.10565E 02	0.39022E 02	0.10565E 02	0.39117E 02	0.39022E 02	0.39117E 02
570.00	0.10902E 02	0.33052E 02	0.12415E 02	0.36156E 02	0.13784E 02	0.36672E 02	0.15049E 02	0.36672E 02	0.15049E 02	0.36980E 02	0.36672E 02	0.36980E 02
580.00	0.13897E 02	0.29592E 02	0.15746E 02	0.32652E 02	0.17362E 02	0.33357E 02	0.18775E 02	0.33357E 02	0.18775E 02	0.33689E 02	0.33357E 02	0.33689E 02
590.00	0.16919E 02	0.25206E 02	0.18492E 02	0.28220E 02	0.20170E 02	0.29128E 02	0.21570E 02	0.29128E				

FIGURE 39. (Continued)

TABLE FOR FUSELAGE GEOMETRY

THETA	X=221.50			X=264.25			X=316.00			X=343.00		
	Y(I)	Z(I)	V(I)	Y(I)	Z(I)	V(I)	Y(I)	Z(I)	V(I)	Y(I)	Z(I)	V(I)
0.0	0.0	-0.30646E 02	0.0	-0.29321E 02	-0.25076E 02	0.0	-0.25076E 02	-0.25076E 02	0.0	-0.21568E 02	-0.21568E 02	0.0
10.00	0.75264E 01	-0.30800E 02	0.77733E 01	-0.29506E 02	-0.24931E 02	0.59833E 01	0.59833E 01	-0.24931E 02	0.54233E 01	-0.21370E 02	-0.21370E 02	0.0
20.00	0.14033E 02	-0.30910E 02	0.13428E 02	-0.29611E 02	-0.24836E 02	0.11367E 02	0.11367E 02	-0.24836E 02	0.10483E 02	-0.20461E 02	-0.20461E 02	0.0
30.00	0.19066E 02	-0.30293E 02	0.18110E 02	-0.28803E 02	-0.24658E 02	0.15832E 02	0.15832E 02	-0.24658E 02	0.14829E 02	-0.18928E 02	-0.18928E 02	0.0
40.00	0.22623E 02	-0.29488E 02	0.21532E 02	-0.26658E 02	-0.24330E 02	0.19350E 02	0.19350E 02	-0.24330E 02	0.18289E 02	-0.16626E 02	-0.16626E 02	0.0
50.00	0.24764E 02	-0.275280E 02	0.23830E 02	-0.21811E 02	-0.23704E 02	0.21978E 02	0.21978E 02	-0.23704E 02	0.20923E 02	-0.14928E 02	-0.14928E 02	0.0
60.00	0.25623E 02	-0.20456E 02	0.24993E 02	-0.18331E 02	-0.22704E 02	0.23704E 02	0.23704E 02	-0.22704E 02	0.22818E 02	-0.08454E 01	-0.08454E 01	0.0
70.00	0.25620E 02	-0.13914E 02	0.25255E 02	-0.11976E 02	-0.21795E 02	0.24559E 02	0.24559E 02	-0.21795E 02	0.23964E 02	-0.3131E 0	-0.3131E 0	0.0
80.00	0.25339E 02	-0.59610E 01	0.25141E 02	-0.42903E 01	-0.24795E 02	0.24795E 02	0.24795E 02	-0.24795E 02	0.24454E 02	0.29722E 01	0.29722E 01	0.0
90.00	0.25162E 02	0.27114E 01	0.25085E 02	0.40988E 01	-0.24815E 02	0.24815E 02	0.24815E 02	-0.24815E 02	0.24607E 02	0.96547E 01	0.96547E 01	0.0
100.00	0.25130E 02	0.11312E 02	0.25152E 02	0.12385E 02	-0.24840E 02	0.24840E 02	0.24840E 02	-0.24840E 02	0.24654E 02	0.16322E 02	0.16322E 02	0.0
110.00	0.25024E 02	0.19142E 02	0.25084E 02	0.19873E 02	-0.24662E 02	0.24662E 02	0.24662E 02	-0.24662E 02	0.24414E 02	0.22304E 02	0.22304E 02	0.0
120.00	0.24429E 02	0.25711E 02	0.24444E 02	0.26133E 02	-0.23804E 02	0.23804E 02	0.23804E 02	-0.23804E 02	0.23416E 02	0.27309E 02	0.27309E 02	0.0
130.00	0.22880E 02	0.30876E 02	0.22807E 02	0.31080E 02	-0.21916E 02	0.21916E 02	0.21916E 02	-0.21916E 02	0.21397E 02	0.31434E 02	0.31434E 02	0.0
140.00	0.20145E 02	0.34808E 02	0.20004E 02	0.34808E 02	-0.18487E 02	0.18487E 02	0.18487E 02	-0.18487E 02	0.18428E 02	0.34810E 02	0.34810E 02	0.0
150.00	0.16323E 02	0.37690E 02	0.16160E 02	0.37712E 02	-0.15196E 02	0.15196E 02	0.15196E 02	-0.15196E 02	0.14685E 02	0.37407E 02	0.37407E 02	0.0
160.00	0.11593E 02	0.39555E 02	0.11452E 02	0.39552E 02	-0.10681E 02	0.10681E 02	0.10681E 02	-0.10681E 02	0.10271E 02	0.39172E 02	0.39172E 02	0.0
170.00	0.60666E 01	0.40488E 02	0.59841E 01	0.40481E 02	-0.55413E 01	0.55413E 01	0.55413E 01	-0.55413E 01	0.52992E 01	0.40137E 02	0.40137E 02	0.0
180.00	0.22204E-04	0.40746E 02	0.21890E-04	0.40741E 02	-0.20207E-04	0.20207E-04	0.20207E-04	-0.20207E-04	0.19276E-04	0.40488E 02	0.40488E 02	0.0
190.00	-0.60666E 01	0.40488E 02	-0.59841E 01	0.40481E 02	-0.55413E 01	0.55413E 01	0.55413E 01	-0.55413E 01	0.52992E 01	0.40137E 02	0.40137E 02	0.0
200.00	-0.11593E 02	0.39555E 02	-0.11452E 02	0.39552E 02	-0.10681E 02	0.10681E 02	0.10681E 02	-0.10681E 02	0.10271E 02	0.39172E 02	0.39172E 02	0.0
210.00	-0.16323E 02	0.37690E 02	-0.16160E 02	0.37712E 02	-0.15196E 02	0.15196E 02	0.15196E 02	-0.15196E 02	0.14685E 02	0.37407E 02	0.37407E 02	0.0
220.00	-0.20145E 02	0.34808E 02	-0.20004E 02	0.34808E 02	-0.18487E 02	0.18487E 02	0.18487E 02	-0.18487E 02	0.18428E 02	0.34810E 02	0.34810E 02	0.0
230.00	-0.22880E 02	0.30876E 02	-0.22807E 02	0.31080E 02	-0.21916E 02	0.21916E 02	0.21916E 02	-0.21916E 02	0.21397E 02	0.31434E 02	0.31434E 02	0.0
240.00	-0.24429E 02	0.25711E 02	-0.24444E 02	0.26133E 02	-0.23804E 02	0.23804E 02	0.23804E 02	-0.23804E 02	0.23416E 02	0.27309E 02	0.27309E 02	0.0
250.00	-0.25024E 02	0.19142E 02	-0.25084E 02	0.19873E 02	-0.24662E 02	0.24662E 02	0.24662E 02	-0.24662E 02	0.24414E 02	0.22304E 02	0.22304E 02	0.0
260.00	-0.25130E 02	0.11312E 02	-0.25152E 02	0.12385E 02	-0.24840E 02	0.24840E 02	0.24840E 02	-0.24840E 02	0.24654E 02	0.16322E 02	0.16322E 02	0.0
270.00	-0.25162E 02	0.27114E 01	-0.25085E 02	0.40988E 01	-0.24815E 02	0.24815E 02	0.24815E 02	-0.24815E 02	0.24607E 02	0.96547E 01	0.96547E 01	0.0
280.00	-0.25339E 02	-0.59610E 01	-0.25141E 02	-0.42903E 01	-0.24795E 02	0.24795E 02	0.24795E 02	-0.24795E 02	0.24454E 02	0.29722E 01	0.29722E 01	0.0
290.00	-0.25620E 02	-0.13914E 02	-0.25255E 02	-0.11976E 02	-0.21795E 02	0.21795E 02	0.21795E 02	-0.21795E 02	0.23964E 02	-0.3131E 01	-0.3131E 01	0.0
300.00	-0.25623E 02	-0.20456E 02	-0.24993E 02	-0.18331E 02	-0.22704E 02	0.22704E 02	0.22704E 02	-0.22704E 02	0.22818E 02	-0.84545E 01	-0.84545E 01	0.0
310.00	-0.24764E 02	-0.25280E 02	-0.23830E 02	-0.23181E 02	-0.21978E 02	0.21978E 02	0.21978E 02	-0.21978E 02	0.20923E 02	-0.12938E 02	-0.12938E 02	0.0
320.00	-0.22623E 02	-0.28488E 02	-0.21532E 02	-0.26658E 02	-0.19350E 02	0.19350E 02	0.19350E 02	-0.19350E 02	0.18289E 02	-0.16426E 02	-0.16426E 02	0.0
330.00	-0.19066E 02	-0.30293E 02	-0.18110E 02	-0.28803E 02	-0.15832E 02	0.15832E 02	0.15832E 02	-0.15832E 02	0.14829E 02	-0.18928E 02	-0.18928E 02	0.0
340.00	-0.14033E 02	-0.30910E 02	-0.13428E 02	-0.29611E 02	-0.11367E 02	0.11367E 02	0.11367E 02	-0.11367E 02	0.10483E 02	-0.20461E 02	-0.20461E 02	0.0
350.00	-0.75264E 01	-0.30800E 02	-0.72733E 01	-0.29506E 02	-0.24931E 02	0.59833E 01	0.59833E 01	-0.24931E 02	0.54233E 01	-0.21370E 02	-0.21370E 02	0.0

FIGURE 39. (Continued)

TABLE FOR FUSELAGE GEOMETRY

THEIA	Y(I)	Z(I)	Y(I)	Z(I)	X=411.00	Y(I)	Z(I)	Y(I)	Z(I)	X=450.00	Y(I)	Z(I)	Y(I)	Z(I)	X=497.00
0.0	0.0	-0.16370E 02	0.0	-0.16370E 02	-0.91041E 01	0.0	-0.91041E 01	0.0	-0.98371E 00	-0.68371E 00	0.0	-0.68371E 00	0.0	-0.68371E 00	0.11592E 02
10.00	0.50530E 01	-0.16098E 02	0.44958E 01	-0.16098E 02	-0.89022E 01	0.30877E 01	-0.89022E 01	0.30877E 01	-0.68588E 00	-0.68588E 00	0.12482E 01	-0.68588E 00	0.12482E 01	-0.68588E 00	0.11710E 02
20.00	0.97831E 01	-0.15251E 02	0.86765E 01	-0.15251E 02	-0.82477E 01	0.59845E 01	-0.82477E 01	0.59845E 01	-0.70348E-01	-0.70348E-01	0.24277E 01	-0.70348E-01	0.24277E 01	-0.70348E-01	0.12065E 02
30.00	0.13907E 02	-0.13712E 02	0.12303E 02	-0.13712E 02	-0.70090E 01	0.85365E 01	-0.70090E 01	0.85365E 01	0.10302E 01	0.10302E 01	0.34719E 01	0.10302E 01	0.34719E 01	0.10302E 01	0.12672E 02
40.00	0.17293E 02	-0.11314E 02	0.15288E 02	-0.11314E 02	-0.50425E 01	0.10676E 02	-0.50425E 01	0.10676E 02	0.26905E 01	0.26905E 01	0.44444E 01	0.26905E 01	0.44444E 01	0.26905E 01	0.13559E 02
50.00	0.19969E 02	-0.80000E 01	0.17583E 02	-0.80000E 01	-0.25926E 01	0.12408E 02	-0.25926E 01	0.12408E 02	0.49177E 01	0.49177E 01	0.50684E 01	0.49177E 01	0.50684E 01	0.49177E 01	0.14731E 02
60.00	0.21965E 02	-0.38597E 01	0.19276E 02	-0.38597E 01	0.11989E 01	0.13733E 02	0.11989E 01	0.13733E 02	0.76484E 01	0.76484E 01	0.55932E 01	0.76484E 01	0.55932E 01	0.76484E 01	0.16153E 02
70.00	0.23269E 02	0.10144E 01	0.20383E 02	0.10144E 01	0.53658E 01	0.14641E 02	0.53658E 01	0.14641E 02	0.10822E 02	0.10822E 02	0.59775E 01	0.10822E 02	0.59775E 01	0.10822E 02	0.17731E 02
80.00	0.23992E 02	0.65501E 01	0.21034E 02	0.65501E 01	0.10049E 02	0.15188E 02	0.10049E 02	0.15188E 02	0.14369E 02	0.14369E 02	0.62196E 01	0.14369E 02	0.62196E 01	0.14369E 02	0.19576E 02
90.00	0.24392E 02	0.12474E 02	0.21405E 02	0.12474E 02	0.15120E 02	0.15622E 02	0.15120E 02	0.15622E 02	0.18098E 02	0.18098E 02	0.62196E 01	0.18098E 02	0.62196E 01	0.18098E 02	0.21449E 02
100.00	0.24549E 02	0.18240E 02	0.21520E 02	0.18240E 02	0.19987E 02	0.15622E 02	0.19987E 02	0.15622E 02	0.21695E 02	0.21695E 02	0.64036E 01	0.21695E 02	0.64036E 01	0.21695E 02	0.23268E 02
110.00	0.24201E 02	0.23364E 02	0.21162E 02	0.23364E 02	0.24331E 02	0.15335E 02	0.24331E 02	0.15335E 02	0.24917E 02	0.24917E 02	0.62827E 01	0.24917E 02	0.62827E 01	0.24917E 02	0.24923E 02
120.00	0.22991E 02	0.27723E 02	0.20069E 02	0.27723E 02	0.28054E 02	0.14434E 02	0.28054E 02	0.14434E 02	0.27723E 02	0.27723E 02	0.59232E 01	0.27723E 02	0.59232E 01	0.27723E 02	0.26387E 02
130.00	0.20818E 02	0.31431E 02	0.18166E 02	0.31431E 02	0.31220E 02	0.12998E 02	0.31220E 02	0.12998E 02	0.30171E 02	0.30171E 02	0.53234E 01	0.30171E 02	0.53234E 01	0.30171E 02	0.27673E 02
140.00	0.17821E 02	0.36521E 02	0.15552E 02	0.36521E 02	0.33846E 02	0.11058E 02	0.33846E 02	0.11058E 02	0.32247E 02	0.32247E 02	0.45202E 01	0.32247E 02	0.45202E 01	0.32247E 02	0.28773E 02
150.00	0.14132E 02	0.36906E 02	0.12336E 02	0.36906E 02	0.35869E 02	0.87140E 01	0.35869E 02	0.87140E 01	0.33880E 02	0.33880E 02	0.35528E 01	0.33880E 02	0.35528E 01	0.33880E 02	0.29651E 02
160.00	0.98255E 01	0.38549E 02	0.85862E 01	0.38549E 02	0.37256E 02	0.60193E 01	0.37256E 02	0.60193E 01	0.35043E 02	0.35043E 02	0.24476E 01	0.35043E 02	0.24476E 01	0.35043E 02	0.30287E 02
170.00	0.50390E 01	0.39504E 02	0.44111E 01	0.39504E 02	0.38048E 02	0.30692E 01	0.38048E 02	0.30692E 01	0.35745E 02	0.35745E 02	0.12460E 01	0.35745E 02	0.12460E 01	0.35745E 02	0.30676E 02
180.00	0.18280E-04	0.39819E 02	0.16017E-04	0.39819E 02	0.38304E 02	0.11110E-04	0.38304E 02	0.11110E-04	0.35983E 02	0.35983E 02	0.45074E-05	0.35983E 02	0.45074E-05	0.35983E 02	0.30808E 02
190.00	-0.50390E 01	0.39504E 02	-0.44111E 01	0.39504E 02	0.38048E 02	-0.30692E 01	0.38048E 02	-0.30692E 01	0.35745E 02	0.35745E 02	-0.12460E 01	0.35745E 02	-0.12460E 01	0.35745E 02	0.30676E 02
200.00	-0.98255E 01	0.38549E 02	-0.85862E 01	0.38549E 02	0.37256E 02	-0.60193E 01	0.37256E 02	-0.60193E 01	0.35043E 02	0.35043E 02	-0.24476E 01	0.35043E 02	-0.24476E 01	0.35043E 02	0.30287E 02
210.00	-0.14132E 02	0.36906E 02	-0.12336E 02	0.36906E 02	0.35869E 02	-0.87140E 01	0.35869E 02	-0.87140E 01	0.33880E 02	0.33880E 02	-0.35528E 01	0.33880E 02	-0.35528E 01	0.33880E 02	0.29651E 02
220.00	-0.17821E 02	0.34521E 02	-0.15552E 02	0.34521E 02	0.33846E 02	-0.11058E 02	0.33846E 02	-0.11058E 02	0.32247E 02	0.32247E 02	-0.45202E 01	0.32247E 02	-0.45202E 01	0.32247E 02	0.28773E 02
230.00	-0.20818E 02	0.31431E 02	-0.18166E 02	0.31431E 02	0.31220E 02	-0.12998E 02	0.31220E 02	-0.12998E 02	0.30171E 02	0.30171E 02	-0.53234E 01	0.30171E 02	-0.53234E 01	0.30171E 02	0.27673E 02
240.00	-0.22991E 02	0.27723E 02	-0.20069E 02	0.27723E 02	0.28054E 02	-0.14434E 02	0.28054E 02	-0.14434E 02	0.27723E 02	0.27723E 02	-0.59232E 01	0.27723E 02	-0.59232E 01	0.27723E 02	0.26387E 02
250.00	-0.24201E 02	0.23364E 02	-0.21162E 02	0.23364E 02	0.24331E 02	-0.15335E 02	0.24331E 02	-0.15335E 02	0.24917E 02	0.24917E 02	-0.62827E 01	0.24917E 02	-0.62827E 01	0.24917E 02	0.24923E 02
260.00	-0.24549E 02	0.18240E 02	-0.21520E 02	0.18240E 02	0.24331E 02	-0.15622E 02	0.24331E 02	-0.15622E 02	0.21695E 02	0.21695E 02	-0.64036E 01	0.21695E 02	-0.64036E 01	0.21695E 02	0.23268E 02
270.00	-0.24392E 02	0.12474E 02	-0.21405E 02	0.12474E 02	0.15120E 02	-0.15524E 02	0.15120E 02	-0.15524E 02	0.18098E 02	0.18098E 02	-0.62196E 01	0.18098E 02	-0.62196E 01	0.18098E 02	0.21449E 02
280.00	-0.23992E 02	0.65501E 01	-0.21034E 02	0.65501E 01	0.10099E 02	-0.15188E 02	0.10099E 02	-0.15188E 02	0.14369E 02	0.14369E 02	-0.62196E 01	0.14369E 02	-0.62196E 01	0.14369E 02	0.19576E 02
290.00	-0.23269E 02	0.10144E 01	-0.20383E 02	0.10144E 01	0.53658E 01	-0.14641E 02	0.53658E 01	-0.14641E 02	0.10822E 02	0.10822E 02	-0.59775E 01	0.10822E 02	-0.59775E 01	0.10822E 02	0.17731E 02
300.00	-0.21965E 02	-0.38597E 01	-0.19276E 02	-0.38597E 01	0.11989E 01	-0.13733E 02	0.11989E 01	-0.13733E 02	0.76484E 01	0.76484E 01	-0.55932E 01	0.76484E 01	-0.55932E 01	0.76484E 01	0.16153E 02
310.00	-0.19969E 02	-0.80000E 01	-0.17583E 02	-0.80000E 01	-0.25926E 01	-0.12408E 02	-0.25926E 01	-0.12408E 02	0.91177E 01	0.91177E 01	-0.50684E 01	0.91177E 01	-0.50684E 01	0.91177E 01	0.14731E 02
320.00	-0.17293E 02	-0.11314E 02	-0.15288E 02	-0.11314E 02	-0.50425E 01	-0.10676E 02	-0.50425E 01	-0.10676E 02	0.26905E 01	0.26905E 01	-0.44444E 01	0.26905E 01	-0.44444E 01	0.26905E 01	0.13559E 02
330.00	-0.13907E 02	-0.13712E 02	-0.12303E 02	-0.13712E 02	-0.70090E 01	-0.85365E 01	-0.70090E 01	-0.85365E 01	0.10302E 01	0.10302E 01	-0.34719E 01	0.10302E 01	-0.34719E 01	0.10302E 01	0.12672E 02
340.00	-0.97831E 01	-0.15251E 02	-0.86755E 01	-0.15251E 02	-0.82477E 01	-0.59845E 01	-0.82477E 01	-0.59845E 01	-0.70348E-01	-0.70348E-01	-0.24277E 01	-0.70348E-01	-0.24277E 01	-0.70348E-01	0.12665E 02
350.00	-0.50530E 01	-0.16098E 02	-0.44958E 01	-0.16098E 02	-0.89022E 01	-0.30877E 01	-0.89022E 01	-0.30877E 01	-0.68588E 00	-0.68588E 00	-0.12482E 01	-0.68588E 00	-0.12482E 01	-0.68588E 00	0.11710E 02

FIGURE 39. (Concluded)

PRESSURE COEFFICIENTS AT FUSELAGE, SEGMENT METHOD.

THETA	X= 23.73 RB= 10.26 ORDX= 0.28	X= 41.00 RB= 15.09 ORDX= 0.25	X= 73.00 RB= 21.73 ORDX= 0.18	X= 94.00 RB= 25.14 ORDX= 0.14	X= 118.00 RB= 28.34 ORDX= 0.11	X= 143.50 RB= 30.74 ORDX= 0.08	X= 163.50 RB= 31.99 ORDX= 0.05
0.0	0.89460E-04	0.11067E-02	0.37235E-02	0.50061E-02	0.72418E-02	0.10305E-01	0.19341E-01
10.00	0.46660E-04	0.10216E-02	0.30695E-02	0.46430E-02	0.65088E-02	0.84047E-02	0.78212E-02
20.00	-0.80734E-04	0.77425E-03	0.24582E-02	0.15341E-02	0.41355E-02	0.17115E-02	-0.14982E-01
30.00	-0.28591E-03	0.38243E-03	0.14618E-02	0.17013E-02	0.13890E-03	-0.96059E-02	-0.47713E-01
40.00	-0.55198E-03	-0.12251E-03	0.19644E-03	-0.55088E-03	-0.43031E-02	-0.18941E-01	-0.64977E-01
50.00	-0.86098E-03	-0.70119E-03	-0.11879E-02	-0.28564E-02	-0.44224E-02	-0.26114E-01	-0.71591E-01
60.00	-0.11922E-02	-0.13214E-02	-0.25987E-02	-0.51167E-02	-0.12174E-01	-0.31635E-01	-0.73988E-01
70.00	-0.15294E-02	-0.19406E-02	-0.40246E-02	-0.73868E-02	-0.15778E-01	-0.36510E-01	-0.75877E-01
80.00	-0.18628E-02	-0.25679E-02	-0.55214E-02	-0.97633E-02	-0.19420E-01	-0.41078E-01	-0.77191E-01
90.00	-0.21881E-02	-0.32258E-02	-0.70369E-02	-0.12085E-01	-0.22691E-01	-0.44324E-01	-0.76108E-01
100.00	-0.25108E-02	-0.38725E-02	-0.84245E-02	-0.14080E-01	-0.25173E-01	-0.45931E-01	-0.73071E-01
110.00	-0.28273E-02	-0.44421E-02	-0.95675E-02	-0.15600E-01	-0.26792E-01	-0.46254E-01	-0.69307E-01
120.00	-0.31166E-02	-0.49020E-02	-0.10459E-01	-0.16709E-01	-0.27774E-01	-0.45865E-01	-0.65768E-01
130.00	-0.33463E-02	-0.52829E-02	-0.11191E-01	-0.17581E-01	-0.28399E-01	-0.45179E-01	-0.62803E-01
140.00	-0.35013E-02	-0.55979E-02	-0.11724E-01	-0.18247E-01	-0.28767E-01	-0.44422E-01	-0.60441E-01
150.00	-0.36015E-02	-0.58303E-02	-0.12246E-01	-0.18717E-01	-0.28935E-01	-0.43748E-01	-0.58698E-01
160.00	-0.36670E-02	-0.59874E-02	-0.12545E-01	-0.19017E-01	-0.28979E-01	-0.43230E-01	-0.57098E-01
170.00	-0.37054E-02	-0.60812E-02	-0.12713E-01	-0.19164E-01	-0.28982E-01	-0.42912E-01	-0.56057E-01
180.00	-0.37181E-02	-0.61129E-02	-0.12766E-01	-0.19209E-01	-0.28980E-01	-0.42803E-01	-0.55653E-01
190.00	-0.37054E-02	-0.60812E-02	-0.12713E-01	-0.19164E-01	-0.28982E-01	-0.42912E-01	-0.56057E-01
200.00	-0.36670E-02	-0.59874E-02	-0.12545E-01	-0.19017E-01	-0.28979E-01	-0.43230E-01	-0.57098E-01
210.00	-0.36015E-02	-0.58303E-02	-0.12246E-01	-0.18717E-01	-0.28935E-01	-0.43748E-01	-0.58698E-01
220.00	-0.35013E-02	-0.55979E-02	-0.11724E-01	-0.18247E-01	-0.28767E-01	-0.44422E-01	-0.60441E-01
230.00	-0.33463E-02	-0.52829E-02	-0.11191E-01	-0.17581E-01	-0.28399E-01	-0.45179E-01	-0.62803E-01
240.00	-0.31166E-02	-0.49020E-02	-0.10459E-01	-0.16709E-01	-0.27774E-01	-0.45865E-01	-0.65768E-01
250.00	-0.28273E-02	-0.44421E-02	-0.95675E-02	-0.15600E-01	-0.26792E-01	-0.46254E-01	-0.69307E-01
260.00	-0.25108E-02	-0.38725E-02	-0.84245E-02	-0.14080E-01	-0.25173E-01	-0.45931E-01	-0.73071E-01
270.00	-0.21881E-02	-0.32258E-02	-0.70369E-02	-0.12085E-01	-0.22691E-01	-0.44324E-01	-0.76108E-01
280.00	-0.18628E-02	-0.25679E-02	-0.55214E-02	-0.97633E-02	-0.19420E-01	-0.41078E-01	-0.77191E-01
290.00	-0.15294E-02	-0.19406E-02	-0.40246E-02	-0.73868E-02	-0.15778E-01	-0.36510E-01	-0.75877E-01
300.00	-0.11922E-02	-0.13214E-02	-0.25987E-02	-0.51166E-02	-0.12174E-01	-0.31635E-01	-0.73988E-01
310.00	-0.86098E-03	-0.70119E-03	-0.11879E-02	-0.28564E-02	-0.44224E-02	-0.26114E-01	-0.71591E-01
320.00	-0.55198E-03	-0.12251E-03	0.19644E-03	-0.55088E-03	-0.43031E-02	-0.18941E-01	-0.64977E-01
330.00	-0.28591E-03	0.38243E-03	0.14618E-02	0.17013E-02	0.13890E-03	-0.96059E-02	-0.47713E-01
340.00	-0.80734E-04	0.77425E-03	0.24582E-02	0.35341E-02	0.41355E-02	0.17115E-02	-0.14982E-01
350.00	0.46660E-04	0.10216E-02	0.30695E-02	0.46430E-02	0.65088E-02	0.84047E-02	0.78212E-02

FIGURE 40. POWER-EFFECT PRESSURE COEFFICIENTS ON SAMPLE FUSELAGE
AFTER APPLICATION OF SEGMENT METHOD

PRESSURE COEFFICIENTS AT FUSELAGE, SEGMENT METHOD.

THETA	X=185.50		X=221.50		X=264.25		X=314.00		X=343.00		X=374.00		X=411.00	
	RB= 33.06	DRDX= 0.04	RB= 33.98	DRDX= 0.00	RB= 33.32	DRDX= -0.03	RB= 31.07	DRDX= -0.05	RB= 29.57	DRDX= -0.06	RB= 27.51	DRDX= -0.07	RB= 25.68	DRDX= -0.13
0.0	0.91351E-01		0.34268E 00		0.26704E-01		0.19451E-01		0.17391E-01		0.14902E-01		0.12882E-01	
10.00	-0.13480E-01		-0.45446E 00		-0.14264E-01		-0.16516E-01		-0.15915E-01		-0.13774E-01		-0.11680E-01	
20.00	-0.18973E 00		-0.10174E 01		-0.27928E-01		-0.64914E-02		-1.96381E-02		-0.10239E-01		-0.98947E-02	
30.00	-0.31241E 00		-0.11534E 01		-0.10586E 00		-0.11062E-01		-0.57774E-03		-0.47657E-02		-0.60834E-02	
40.00	-0.31499E 00		-0.10004E 01		-0.15176E 00		-0.25630E-01		-0.10195E-01		-0.14332E-02		-0.21035E-02	
50.00	-0.25572E 00		-0.63370E 00		-0.13420E 00		-0.29711E-01		-0.13370E-01		-0.47041E-02		-0.21641E-03	
60.00	-0.21089E 00		-0.39195E 00		-0.96176E-01		-0.26834E-01		-0.13402E-01		-0.57279E-02		-0.89973E-03	
70.00	-0.18160E 00		-0.27483E 00		-0.75065E-01		-0.22235E-01		-0.12295E-01		-0.55459E-02		-0.71976E-03	
80.00	-0.15668E 00		-0.21043E 00		-0.68151E-01		-0.20765E-01		-0.11499E-01		-0.53813E-02		-0.75374E-03	
90.00	-0.13339E 00		-0.16411E 00		-0.65334E-01		-0.21294E-01		-0.12030E-01		-0.60324E-02		-0.13893E-02	
100.00	-0.11418E 00		-0.13400E 00		-0.63383E-01		-0.22990E-01		-0.13609E-01		-0.75941E-02		-0.21491E-02	
110.00	-0.99791E-01		-0.11360E 00		-0.61274E-01		-0.24747E-01		-0.15459E-01		-0.90444E-02		-0.31692E-02	
120.00	-0.89729E-01		-0.10065E 00		-0.59408E-01		-0.25914E-01		-0.16337E-01		-0.93614E-02		-0.39388E-02	
130.00	-0.82901E-01		-0.92714E-01		-0.57072E-01		-0.25913E-01		-0.15764E-01		-0.84786E-02		-0.32391E-02	
140.00	-0.78179E-01		-0.85089E-01		-0.53825E-01		-0.23743E-01		-0.14554E-01		-0.75076E-02		-0.23814E-02	
150.00	-0.75076E-01		-0.80946E-01		-0.51314E-01		-0.22397E-01		-0.13506E-01		-0.66800E-02		-0.16470E-02	
160.00	-0.73136E-01		-0.77705E-01		-0.49613E-01		-0.21425E-01		-0.12762E-01		-0.61090E-02		-0.11337E-02	
170.00	-0.72177E-01		-0.76656E-01		-0.48866E-01		-0.20932E-01		-0.12379E-01		-0.58234E-02		-0.87692E-02	
180.00	-0.71904E-01		-0.76358E-01		-0.48657E-01		-0.20769E-01		-0.12264E-01		-0.57414E-02		-0.80270E-02	
190.00	-0.72177E-01		-0.76657E-01		-0.48866E-01		-0.20332E-01		-0.12379E-01		-0.58234E-02		-0.87692E-02	
200.00	-0.73136E-01		-0.77706E-01		-0.49613E-01		-0.21425E-01		-0.12762E-01		-0.61090E-02		-0.11337E-02	
210.00	-0.75076E-01		-0.80940E-01		-0.51314E-01		-0.23743E-01		-0.14554E-01		-0.75076E-02		-0.16470E-02	
220.00	-0.78179E-01		-0.85084E-01		-0.53824E-01		-0.25913E-01		-0.15764E-01		-0.84786E-02		-0.23814E-02	
230.00	-0.82901E-01		-0.92709E-01		-0.57072E-01		-0.25913E-01		-0.15764E-01		-0.84786E-02		-0.23814E-02	
240.00	-0.89729E-01		-1.0066E 00		-0.59409E-01		-0.27990E-01		-0.16337E-01		-0.93614E-02		-0.39388E-02	
250.00	-0.99791E-01		-0.11361E 00		-0.61280E-01		-0.27990E-01		-0.16337E-01		-0.93614E-02		-0.39388E-02	
260.00	-0.11418E 00		-0.13400E 00		-0.63383E-01		-0.27990E-01		-0.16337E-01		-0.93614E-02		-0.39388E-02	
270.00	-0.13400E 00		-0.16412E 00		-0.65335E-01		-0.27990E-01		-0.16337E-01		-0.93614E-02		-0.39388E-02	
280.00	-0.15668E 00		-0.21042E 00		-0.68150E-01		-0.27990E-01		-0.16337E-01		-0.93614E-02		-0.39388E-02	
290.00	-0.18159E 00		-0.27482E 00		-0.75058E-01		-0.27990E-01		-0.16337E-01		-0.93614E-02		-0.39388E-02	
300.00	-0.21089E 00		-0.39195E 00		-0.96176E-01		-0.27990E-01		-0.16337E-01		-0.93614E-02		-0.39388E-02	
310.00	-0.25572E 00		-0.63368E 00		-0.13420E 00		-0.27990E-01		-0.16337E-01		-0.93614E-02		-0.39388E-02	
320.00	-0.31498E 00		-0.10002E 01		-0.15175E 00		-0.27990E-01		-0.16337E-01		-0.93614E-02		-0.39388E-02	
330.00	-0.31238E 00		-0.11532E 01		-0.10585E 00		-0.27990E-01		-0.16337E-01		-0.93614E-02		-0.39388E-02	
340.00	-0.18974E 00		-0.10174E 01		-0.27990E-01		-0.27990E-01		-0.16337E-01		-0.93614E-02		-0.39388E-02	
350.00	-0.13483E-01		-0.45442E 00		0.14283E-01		0.16515E-01		0.15915E-01		0.13774E-01		0.11680E-01	

FIGURE 40. (Continued)

PRESSURE COEFFICIENTS AT FUSELAGE, SEGMENT METHOD.

THETA	X=450.00		X=497.00		X=
	RB=	DRDX=	RB=	DRDX=	RB=
	0.18	-0.18	0.21	-0.21	DRDX=
0.0	0.10107E-01		0.77184E-02		
10.00	0.97202E-02		0.74562E-02		
20.00	0.84870E-02		0.67084E-02		
30.00	0.64151E-02		0.51882E-02		
40.00	0.43020E-02		0.45956E-02		
50.00	0.29291E-02		0.40956E-02		
60.00	0.21971E-02		0.38320E-02		
70.00	0.19841E-02		0.37167E-02		
80.00	0.18518E-02		0.36355E-02		
90.00	0.13705E-02		0.34009E-02		
100.00	0.50350E-03		0.29530E-02		
110.00	-0.30925E-03		0.24793E-02		
120.00	-0.32121E-03		0.23078E-02		
130.00	0.28413E-03		0.27092E-02		
140.00	0.94034E-03		0.31712E-02		
150.00	0.15546E-02		0.37167E-02		
160.00	0.20156E-02		0.42363E-02		
170.00	0.22682E-02		0.45996E-02		
180.00	0.23466E-02		0.47142E-02		
190.00	0.22692E-02		0.45896E-02		
200.00	0.20157E-02		0.42363E-02		
210.00	0.15547E-02		0.37167E-02		
220.00	0.94049E-03		0.31712E-02		
230.00	0.28424E-03		0.27092E-02		
240.00	-0.32113E-03		0.23878E-02		
250.00	-0.30939E-03		0.24792E-02		
260.00	0.50342E-03		0.29530E-02		
270.00	0.13704E-02		0.34009E-02		
280.00	0.18518E-02		0.36355E-02		
290.00	0.19842E-02		0.37157E-02		
300.00	0.21971E-02		0.38320E-02		
310.00	0.29291E-02		0.40956E-02		
320.00	0.43021E-02		0.45957E-02		
330.00	0.64151E-02		0.55681E-02		
340.00	0.84849E-02		0.67083E-02		
350.00	0.97202E-02		0.74662E-02		

FIGURE 40. (Concluded)

PRESSURE COEFFICIENTS AT FUSELAGE, THREE DIMENSIONAL MODIFICATION OF 1 ITERATION.

	X= 21.70 RB= 10.26 THETA DROX= 0.28	X= 41.00 RB= 15.09 DROX= 0.25	X= 73.00 RB= 21.73 DROX= 0.18	X= 94.00 RB= 25.14 DROX= 0.14	X= 116.00 RB= 28.34 DROX= 0.11	X= 143.50 RB= 30.76 DROX= 0.08	X= 163.50 RB= 31.99 DROX= 0.06
0.0	0.89460E-04	0.11067E-02	-0.12178E-01	-0.23009E-01	-0.59330E-01	-0.16672E 00	-0.26107E 00
10.00	0.46660E-04	0.10216E-02	-0.12798E-01	-0.23196E-01	-0.56032E-01	-0.16625E 00	-0.26460E 00
20.00	-0.80734E-04	0.77425E-03	-0.12656E-01	-0.23760E-01	-0.50768E-01	-0.16370E 00	-0.26475E 00
30.00	-0.28591E-03	0.38243E-03	-0.13225E-01	-0.24434E-01	-0.50111E-01	-0.16355E 00	-0.26104E 00
40.00	-0.55198E-03	-0.12515E-03	-0.13921E-01	-0.25600E-01	-0.50073E-01	-0.16278E 00	-0.26400E 00
50.00	-0.86098E-03	-0.70119E-03	-0.14646E-01	-0.26594E-01	-0.50290E-01	-0.16400E 00	-0.26311E 00
60.00	-0.11222E-02	-0.13214E-02	-0.15321E-01	-0.27270E-01	-0.50597E-01	-0.16276E 00	-0.26338E 00
70.00	-0.12294E-02	-0.19406E-02	-0.15906E-01	-0.27623E-01	-0.50712E-01	-0.16183E 00	-0.26493E 00
80.00	-0.18628E-02	-0.25679E-02	-0.16359E-01	-0.27518E-01	-0.51251E-01	-0.16190E 00	-0.26590E 00
90.00	-0.21881E-02	-0.32258E-02	-0.16614E-01	-0.26816E-01	-0.48238E-01	-0.16268E 00	-0.26590E 00
100.00	-0.23108E-02	-0.38725E-02	-0.16645E-01	-0.25602E-01	-0.47504E-01	-0.16768E-01	-0.11937E 00
110.00	-0.28273E-02	-0.44421E-02	-0.16500E-01	-0.24300E-01	-0.46919E-01	-0.16597E-01	-0.97061E-01
120.00	-0.31166E-02	-0.49020E-02	-0.16241E-01	-0.22836E-01	-0.43764E-01	-0.16276E-01	-0.81231E-01
130.00	-0.33463E-02	-0.52829E-02	-0.15915E-01	-0.21337E-01	-0.26939E-01	-0.16091E-01	-0.66714E-01
140.00	-0.35013E-02	-0.55979E-02	-0.15561E-01	-0.19910E-01	-0.22805E-01	-0.16699E-01	-0.53578E-01
150.00	-0.36015E-02	-0.58303E-02	-0.15223E-01	-0.18710E-01	-0.19602E-01	-0.16556E-01	-0.42837E-01
160.00	-0.36670E-02	-0.59874E-02	-0.14959E-01	-0.17821E-01	-0.17339E-01	-0.16597E-02	-0.35024E-01
170.00	-0.37054E-02	-0.60812E-02	-0.14782E-01	-0.17263E-01	-0.15930E-01	-0.16611E-02	-0.30321E-01
180.00	-0.37181E-02	-0.61129E-02	-0.14720E-01	-0.17069E-01	-0.15441E-01	-0.16677E-02	-0.26101E-01
190.00	-0.37054E-02	-0.60812E-02	-0.14782E-01	-0.17263E-01	-0.15930E-01	-0.16621E-02	-0.30321E-01
200.00	-0.36670E-02	-0.59874E-02	-0.14959E-01	-0.17821E-01	-0.17339E-01	-0.16597E-02	-0.30321E-01
210.00	-0.36015E-02	-0.58303E-02	-0.15223E-01	-0.18710E-01	-0.19602E-01	-0.16556E-01	-0.42837E-01
220.00	-0.35013E-02	-0.55979E-02	-0.15561E-01	-0.19910E-01	-0.22805E-01	-0.16699E-01	-0.53578E-01
230.00	-0.33463E-02	-0.52829E-02	-0.15915E-01	-0.21337E-01	-0.26939E-01	-0.16091E-01	-0.66714E-01
240.00	-0.31166E-02	-0.49020E-02	-0.16241E-01	-0.22836E-01	-0.31724E-01	-0.16597E-01	-0.81231E-01
250.00	-0.28273E-02	-0.44421E-02	-0.16500E-01	-0.24300E-01	-0.36919E-01	-0.16597E-01	-0.97061E-01
260.00	-0.25108E-02	-0.38725E-02	-0.16645E-01	-0.25602E-01	-0.42504E-01	-0.16268E-01	-0.11937E 00
270.00	-0.21881E-02	-0.32258E-02	-0.16614E-01	-0.26816E-01	-0.48238E-01	-0.16268E-01	-0.16268E 00
280.00	-0.18628E-02	-0.25679E-02	-0.16359E-01	-0.27518E-01	-0.51251E-01	-0.16190E 00	-0.16590E 00
290.00	-0.15294E-02	-0.19406E-02	-0.15906E-01	-0.27623E-01	-0.50712E-01	-0.16183E 00	-0.16590E 00
300.00	-0.11922E-02	-0.13214E-02	-0.15321E-01	-0.27270E-01	-0.50597E-01	-0.16276E 00	-0.26338E 00
310.00	-0.86098E-03	-0.70119E-03	-0.14646E-01	-0.26594E-01	-0.50290E-01	-0.16400E 00	-0.26311E 00
320.00	-0.55198E-03	-0.12515E-03	-0.13921E-01	-0.25600E-01	-0.50073E-01	-0.16278E 00	-0.26400E 00
330.00	-0.28591E-03	0.38243E-03	-0.13225E-01	-0.24434E-01	-0.50111E-01	-0.16355E 00	-0.26104E 00
340.00	-0.80734E-04	0.77425E-03	-0.12656E-01	-0.23760E-01	-0.50768E-01	-0.16370E 00	-0.26475E 00
350.00	0.46660E-04	0.10216E-02	-0.12798E-01	-0.23196E-01	-0.56032E-01	-0.16625E 00	-0.26460E 00

FIGURE 41. POWER-EFFECT PRESSURE COEFFICIENTS ON
SAMPLE FUSELAGE AFTER ONE ITERATION

PRESSURE COEFFICIENTS AT FUSELAGE, THREE DIMENSIONAL MODIFICATION OF 1 ITERATION.

X=450.00 X=497.00 X=

 P3= 17.58 RB= 6.21 RB=

 THETA DRDX= -0.18 DRDX= -0.21 DRDX=

0.0	0.10107E-01	0.77184E-02
10.00	0.97202E-02	0.74662E-02
20.00	0.84870E-02	0.6704 E-02
30.00	0.64153E-02	0.56887E-02
40.00	0.43027E-02	0.45956E-02
50.00	0.29291E-02	0.40956E-02
60.00	0.21971E-02	0.38320E-02
70.00	0.19441E-02	0.37167E-02
80.00	0.18518E-02	0.36355E-02
90.00	0.13705E-02	0.34009E-02
100.00	0.50350E-03	0.29530E-02
110.00	-0.30925E-03	0.24793E-02
120.00	-0.32121E-03	0.23878E-02
130.00	0.28413E-03	0.27092E-02
140.00	0.94044E-03	0.31712E-02
150.00	0.15546E-02	0.37167E-02
160.00	0.20154E-02	0.42363E-02
170.00	0.22682E-02	0.45896E-02
180.00	0.23466E-02	0.47142E-02
190.00	0.22682E-02	0.45896E-02
200.00	0.20157E-02	0.42363E-02
210.00	0.15547E-02	0.37167E-02
220.00	0.94049E-03	0.31712E-02
230.00	0.28424E-03	0.27092E-02
240.00	-0.32113E-03	0.23878E-02
250.00	-0.30939E-03	0.24792E-02
260.00	0.50342E-03	0.29530E-02
270.00	0.13704E-02	0.34009E-02
280.00	0.18518E-02	0.36355E-02
290.00	0.19842E-02	0.37167E-02
300.00	0.21971E-02	0.38320E-02
310.00	0.29291E-02	0.40956E-02
320.00	0.43027E-02	0.45956E-02
330.00	0.64153E-02	0.56887E-02
340.00	0.84870E-02	0.67043E-02
350.00	0.97202E-02	0.74662E-02

FIGURE 41. (Concluded)

PARAMETERS USED IN 3D MODIFICATION OF FUSELAGE COMPUTATION IDIS= 4 NJET= 8 LENGTH OF FUSELAGE= 517.000
 PARAMETERS USED IN FORCE AND MOMENT COMPUTATION LJET OF DIAMETER= 22.500 XCG= 238.200 REFERENCE LENGTH= 83.500
 COORDINATES OF NOSE X= 0.0 Y= 0.0 Z= -10.000 COORDINATES OF TAIL X= 517.000 Y= 0.0 Z= 24.900

***FORCES AND MOMENTS**

X-FORCE Y-FORCE Z-FORCE
 C.114E-02 0.552E-06 -0.122E-01

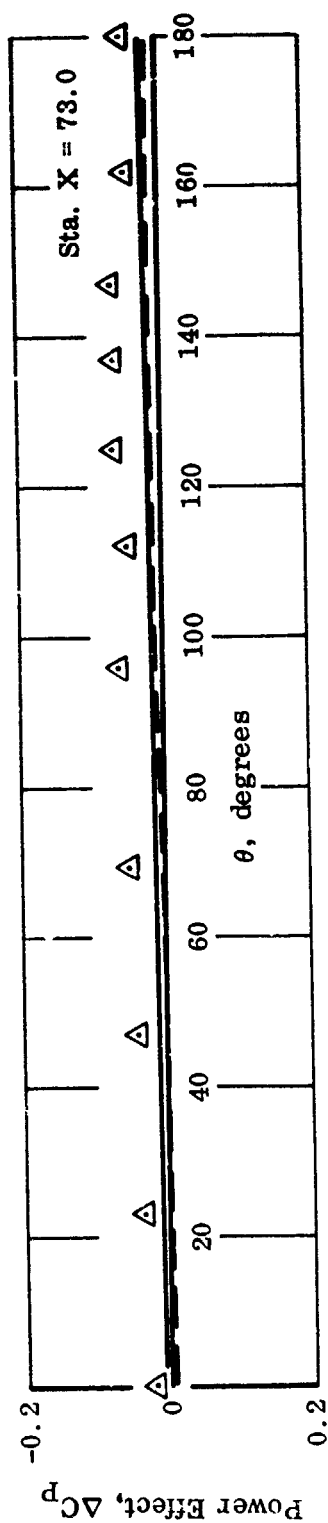
PITCHING MOMENT COMPUTED ABOUT AXIS THRU C.G.= 0.585E-03

YAWING MOMENT COMPUTED ABOUT AXIS THRU C.G.= 0.973E-07

END OF BODY COMPUTATION

FIGURE 42. FORCES AND MOMENTS ON SAMPLE FUSELAGE
 BY TRANSFORMATION METHOD

Δ Test Data
 --- Segment Method
 — 3-D Modification



The relationship between θ and fuselage station geometry is given in Figure 39.

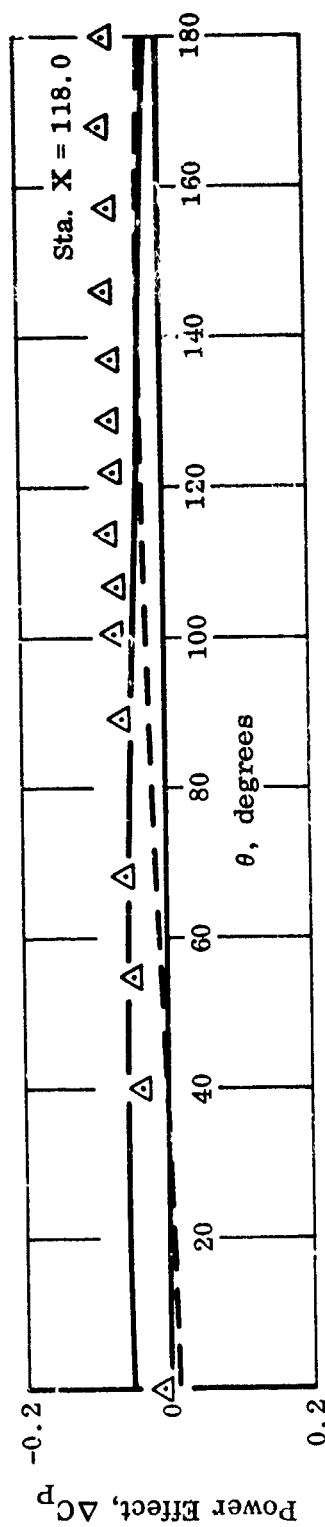
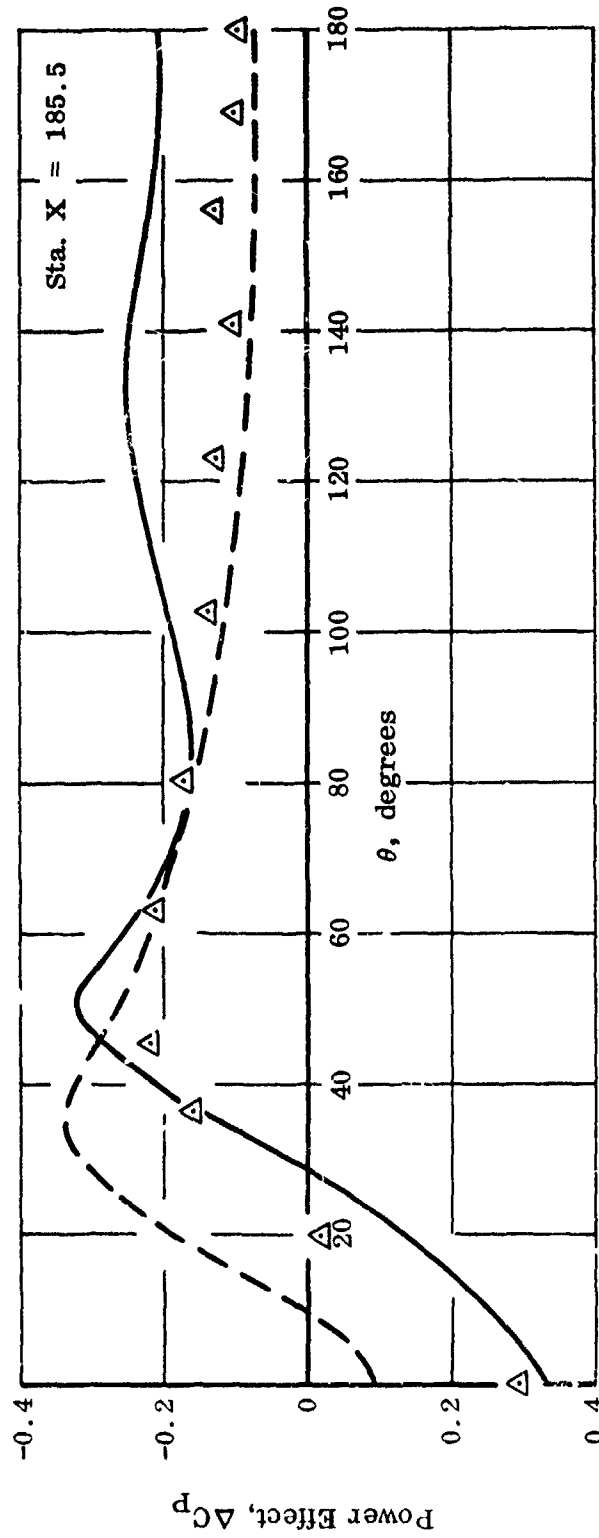


FIGURE 43a. POWER-EFFECT PRESSURE COEFFICIENTS ON SAMPLE FUSELAGE AT STATIONS $X = 73.0$ AND $X = 118.0$

$$U_{\infty}/U_j = 0.2, \alpha = \beta = 0^\circ, \text{ Lift Jet}$$

Δ Test Data
 --- Segment Method
 — 3-D Modification

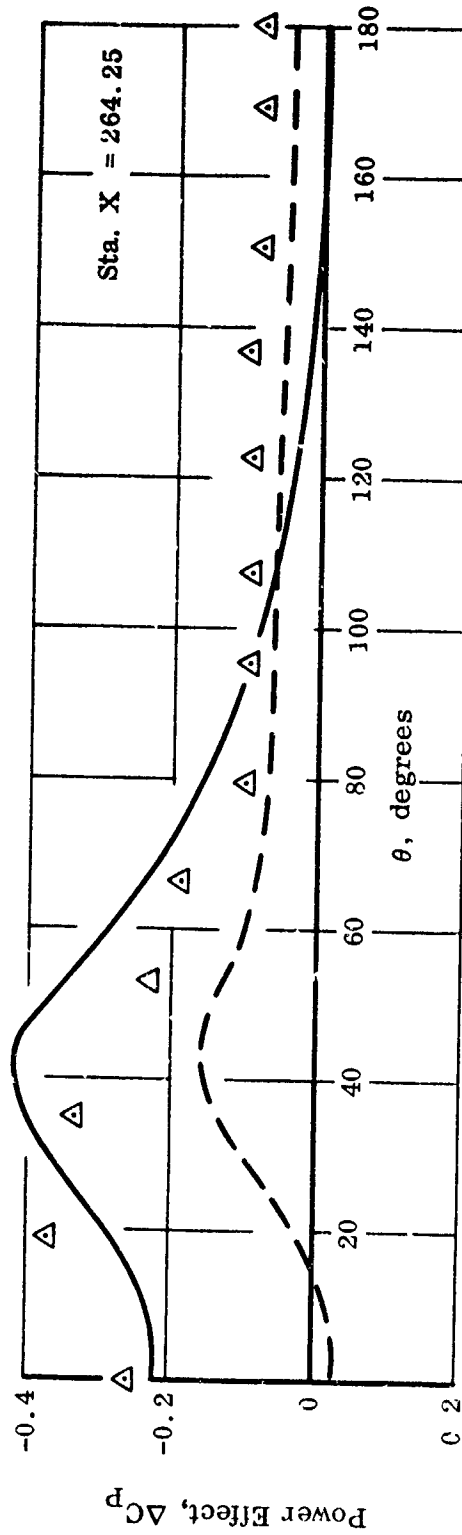


The relationship between θ and fuselage station geometry is given in Figure 39.

FIGURE 43b. POWER-EFFECT PRESSURE COEFFICIENTS ON SAMPLE FUSELAGE AT STATION X = 185.5

$$U_{\infty}/U_j = 0.2, \alpha = \beta = 0^\circ, \text{ Lift Jet}$$

Δ Test Data
 --- Segment Method
 — 3-D Modification

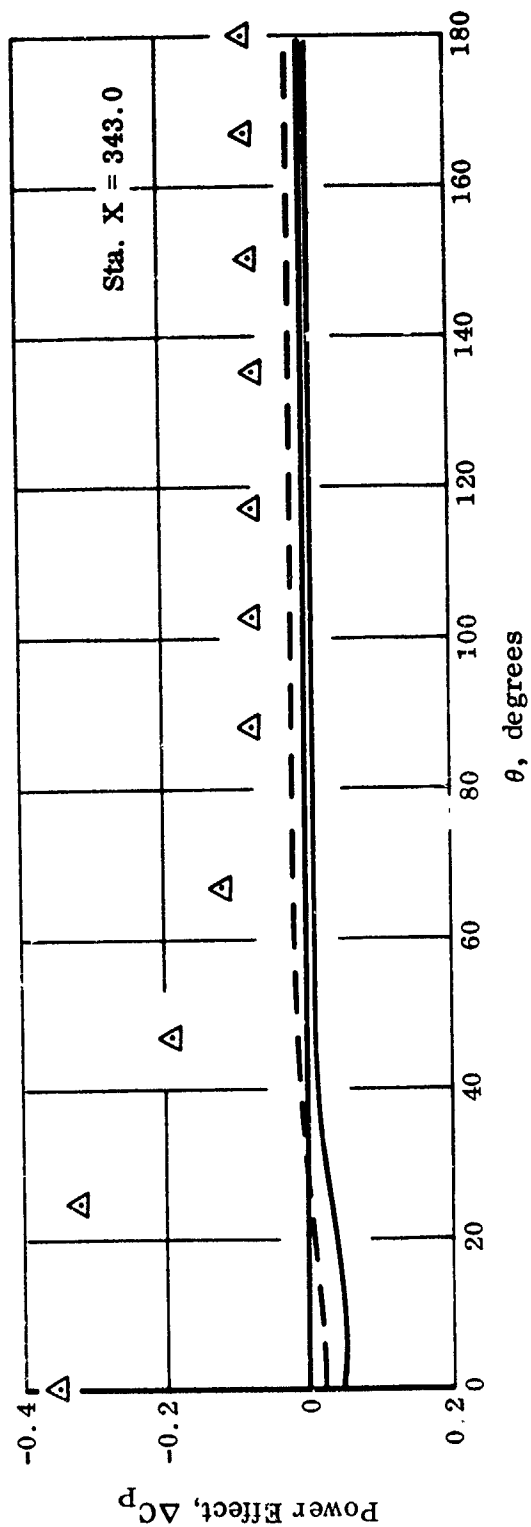


The relationship between θ and fuselage station geometry is given in Figure 39.

FIGURE 43c. POWER-EFFECT PRESSURE COEFFICIENTS ON SAMPLE FUSELAGE AT STATION X = 264.25

$$U_{\infty}/U_j = 0.2, \alpha = \beta = 0^\circ, \text{ Lift Jet}$$

Δ Test Data
 --- Segment Method
 — 3-D Modification

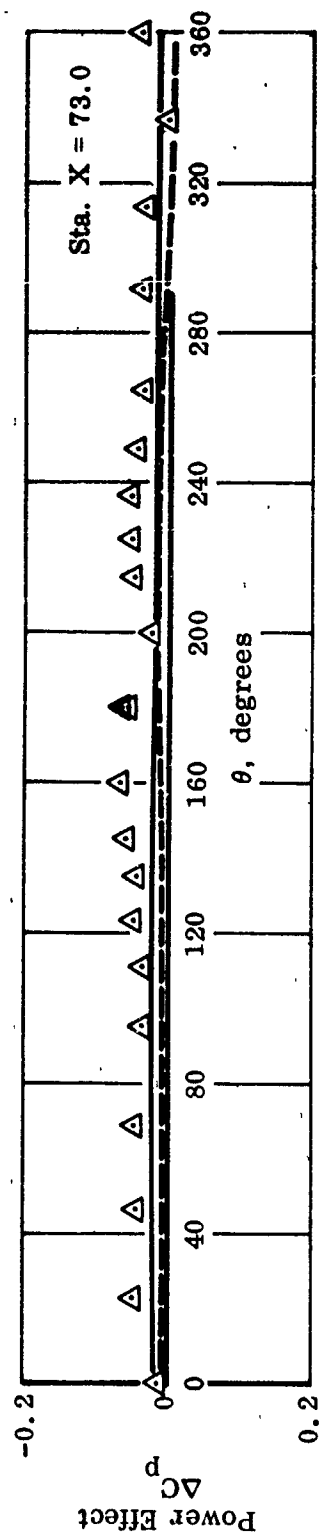


The relationship between ρ and fuselage station geometry is given in Figure 39.

FIGURE 43d. POWER-EFFECT PRESSURE COEFFICIENTS ON SAMPLE FUSELAGE AT STATION X = 343.0

$$U_\infty / U_j = 0.2, \alpha = \beta = 0^\circ, \text{ Lift Jet}$$

Δ Test Data
 --- Segment Method
 — 3-D Modification



The relationship between θ and fuselage station geometry is given in Figure 39.

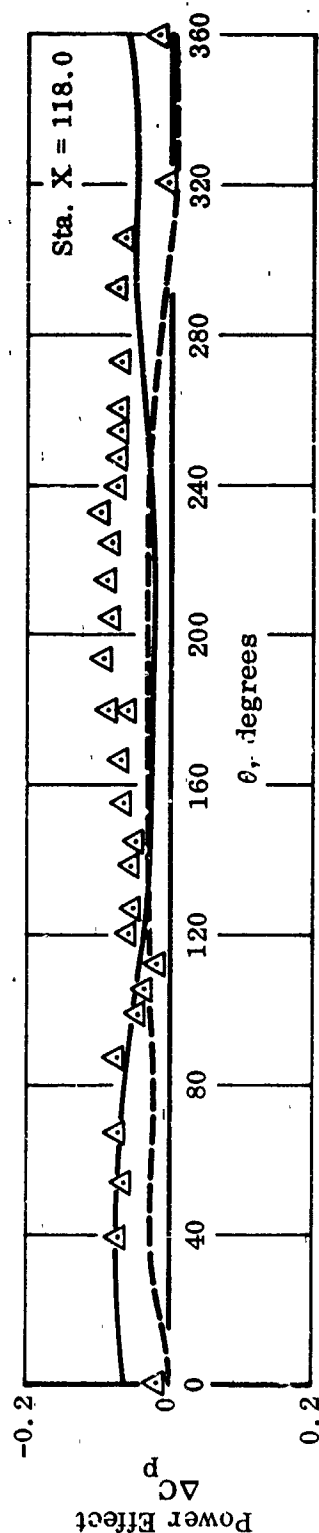
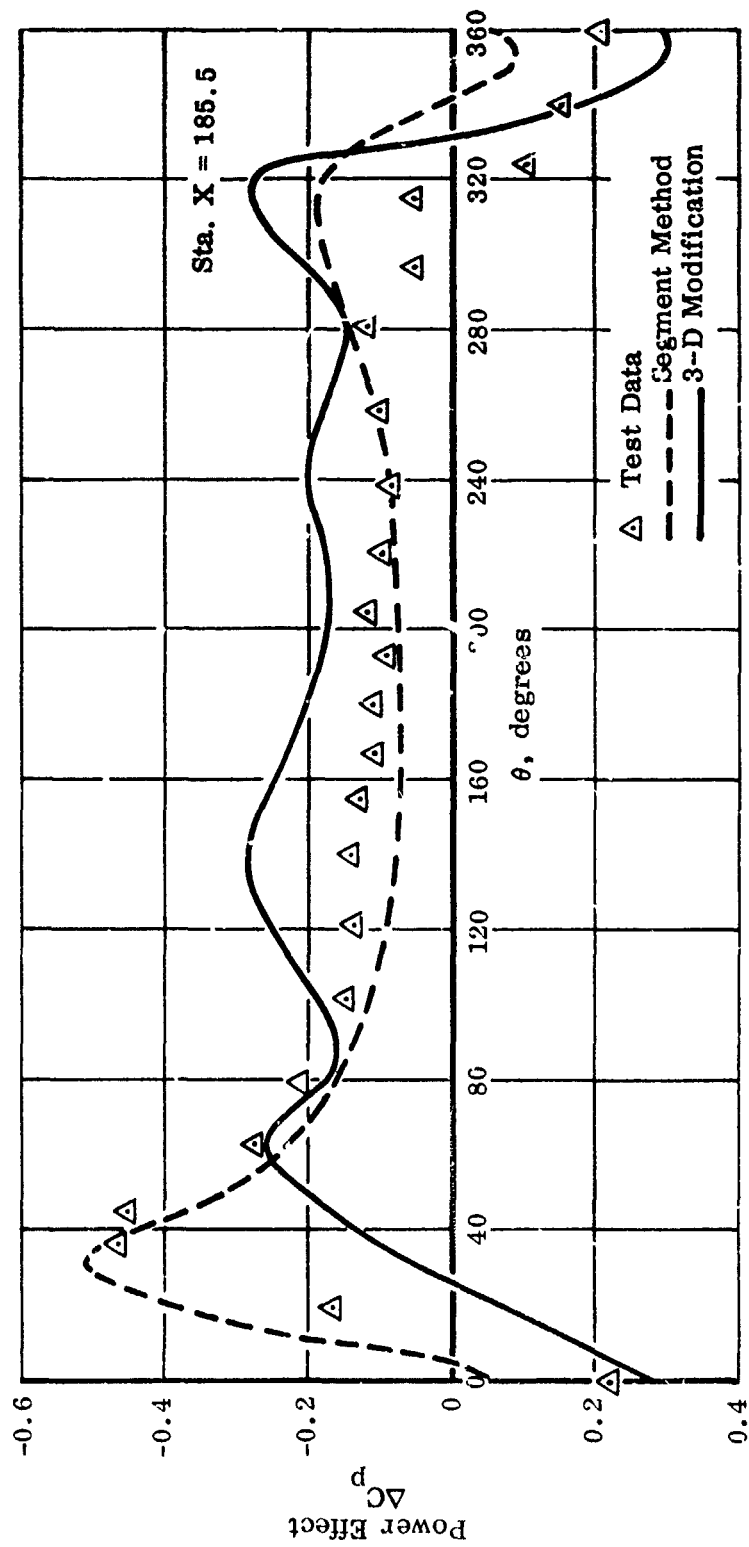


FIGURE 44a. POWER-EFFECT PRESSURE COEFFICIENTS ON FUSELAGE
AT STATIONS X = 73.0 AND X = 118.0

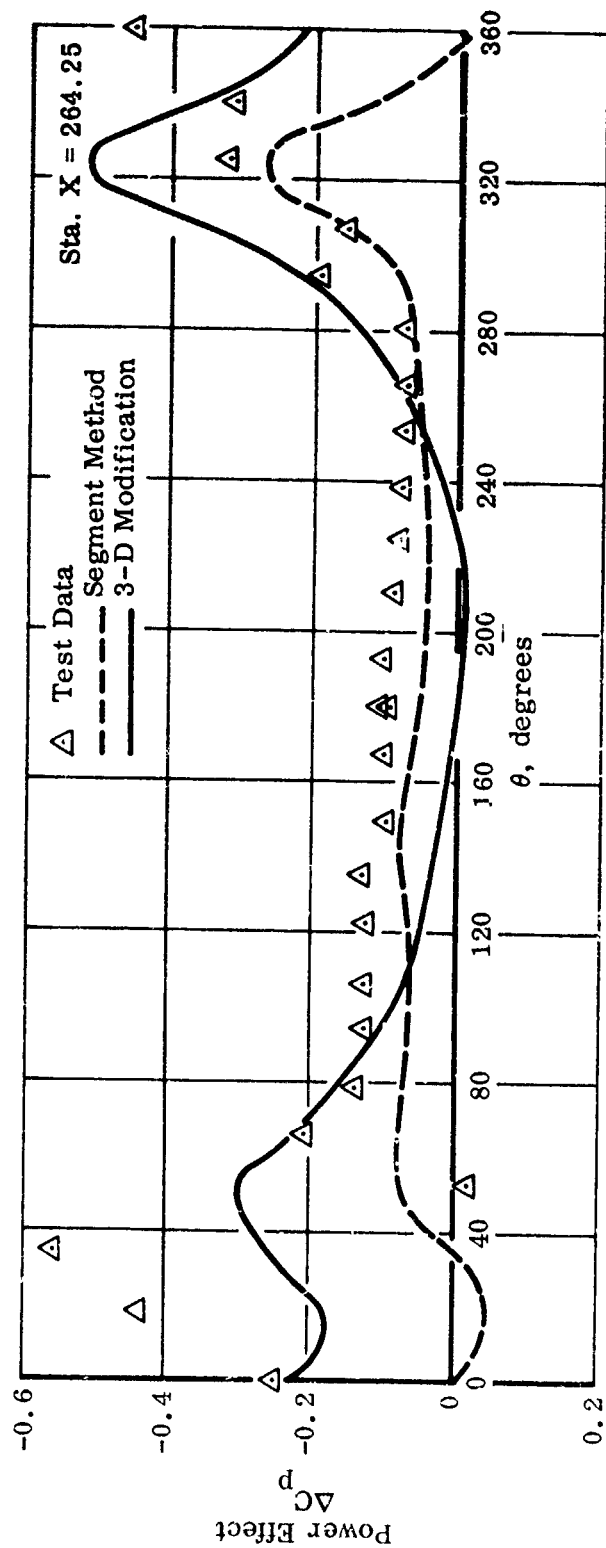
$U_\infty/U_j = 0.2$, $\alpha = 0^\circ$, $\beta = 10^\circ$, Lift Jet



The relationship between θ and fuselage station geometry is given in Figure 39.

FIGURE 44b. POWER-EFFECT PRESSURE COEFFICIENT ON FUSELAGE
AT STATION X = 185.5

$$U_\infty / U_j = 0.2, \quad \alpha = 0^\circ, \quad \beta = 10^\circ, \quad \text{Lift Jet}$$



The relationship between θ and fuselage station geometry is given in Figure 39.

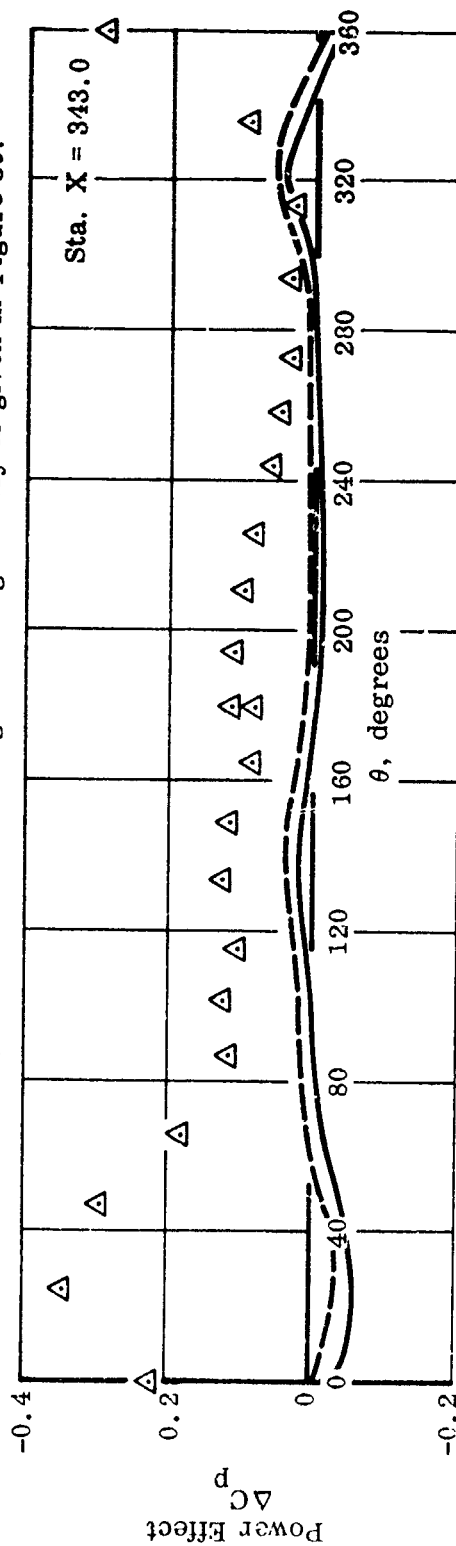


FIGURE 44c. POWER-EFFECT PRESSURE COEFFICIENTS ON FUSELAGE
AT STATIONS X = 264.25 AND X = 343.0

$U_\infty/U_j = 0.2$, $\alpha = 0^\circ$, $\beta = 10^\circ$, Lift Jet

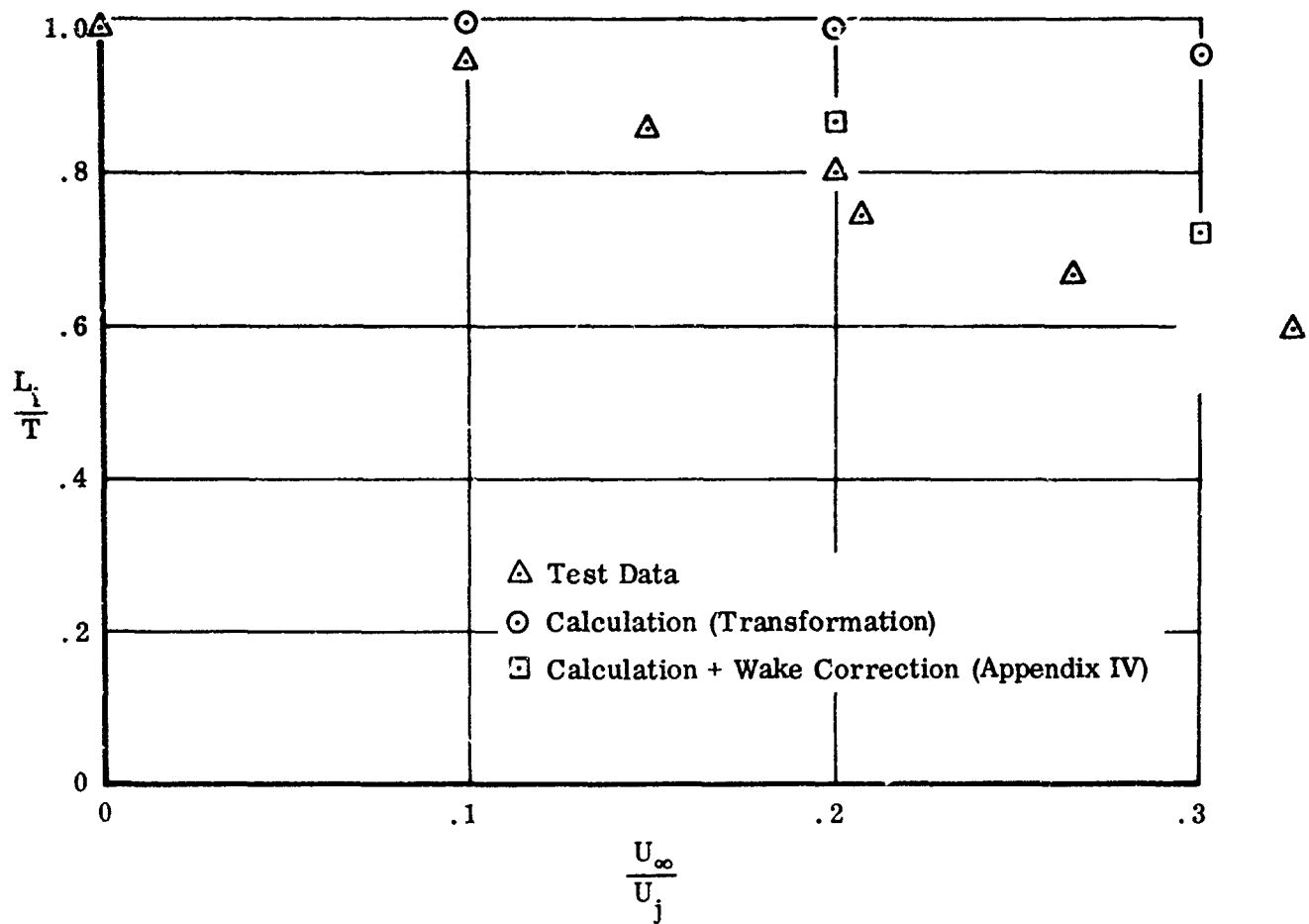


FIGURE 45. POWER-EFFECT LIFT FOR FUSELAGE ALONE WITH LIFT JET

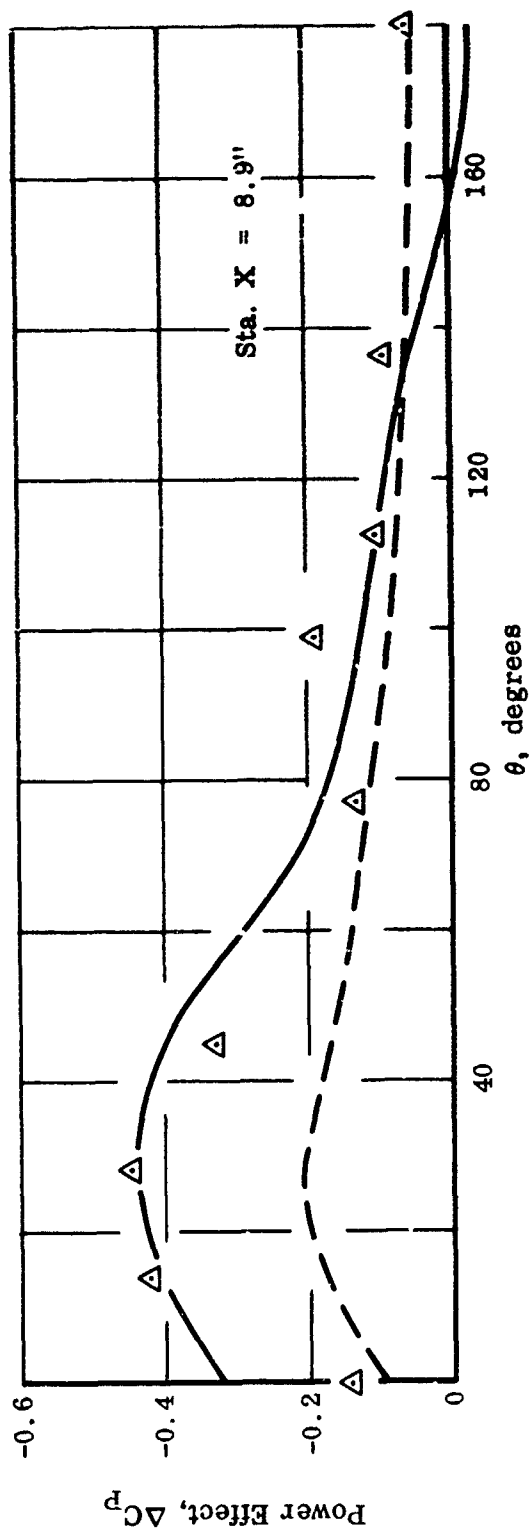
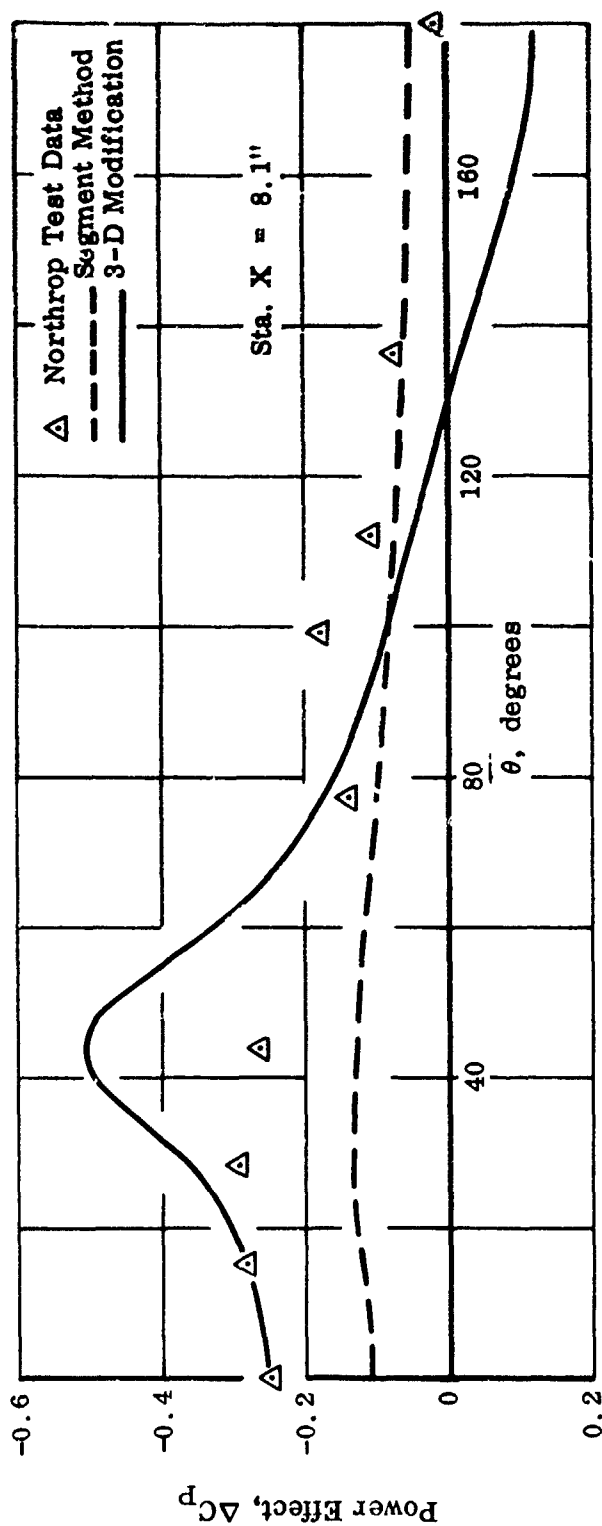


FIGURE 46a. POWER-EFFECT PRESSURE COEFFICIENTS ON NORTHROP
BODY AT STATIONS X = 8.1 AND X = 8.9

$U_\infty/U_j = 0.1$, $\alpha = \beta = 0^\circ$, Center Jet at X = 10.0

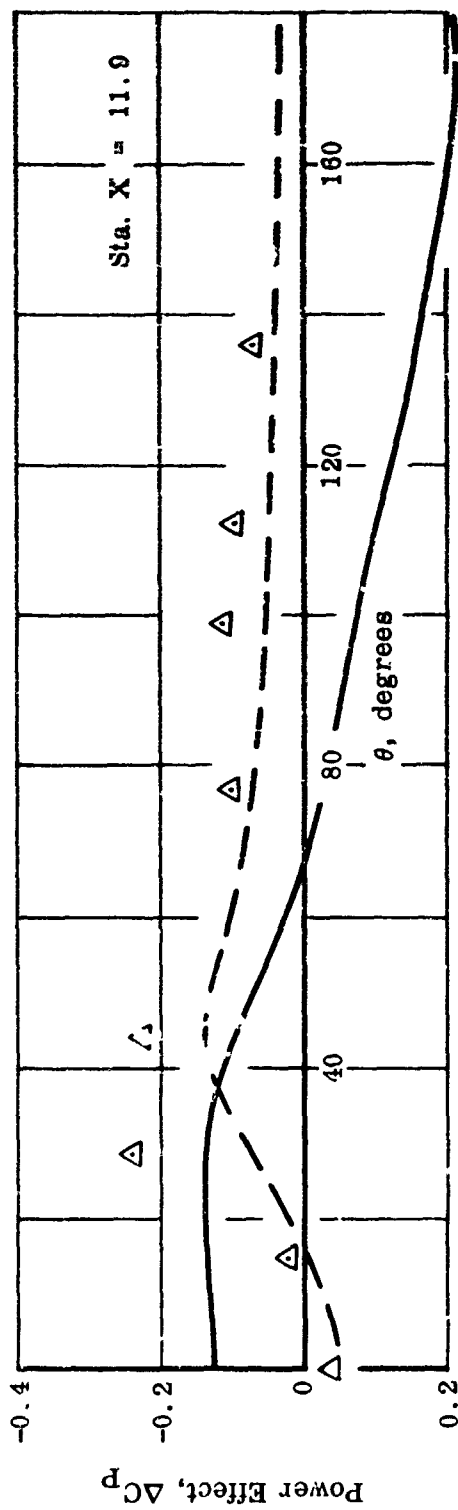
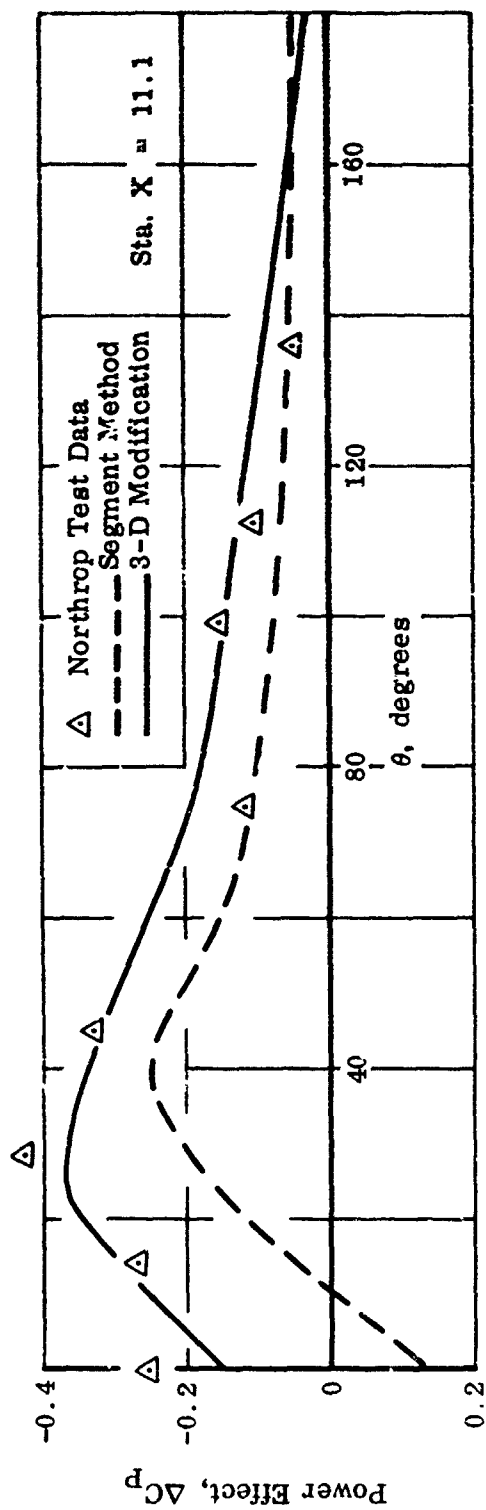


FIGURE 46b. POWER-EFFECT PRESSURE COEFFICIENTS ON NORTROP
 BODY AT STATIONS $X = 11.1$ AND $X = 11.9$

$U_\infty/U_j = 0.1$, $\alpha = \beta = 0^\circ$, Center Jet at $X = 10.0$

c. Method Applicability and Limitations

As pointed out in the beginning of this section, the method for predicting power effect on a fuselage is very similar to that of a wing. However, for the sample problems considered in this Volume, there are two differences between fuselage and wing computations. The first one is the formation of a wake behind the exhausting jet which engulfs a large portion of the fuselage and is a fundamental problem. The second difference is computational, and may be briefly described as follows: The induced velocities usually undergo very large changes across the jet, as discussed previously. These are most noticeable in the mainstream direction, which is also the longitudinal direction of a fuselage without sideslip. When we invoke numerical differentiations in the longitudinal direction to determine the strength of the residual sources and sinks, these large variations generally magnify the intensity of the sources and sinks and may cause erratic behavior in the final results. This irregularity usually gets worse when higher iterations are carried out, even though some smoothing of the input data is applied. For this reason, two iterations were not performed. To compare the case of a wing, we notice that the largest variation in the induced velocities exists in the mainstream direction and does not traverse any of the wing stations. In addition, the computational procedure automatically smooths out some of the large variations in the mainstream direction by integration for the "boundary functions" (see Volume I, Section IV, for details) and the subsequent expansion in a Fourier series.

Since the power effect on a fuselage, disregarding the wake, contributes only a fraction to the total power-effect forces and moments, some uncertainty in prediction may be tolerable. Based on this assumption, the segment method is useful since it includes some of the three-dimensional effects that are already present in the jet flow field and gives fairly reasonable results in most cases.

As in the case for a wing, the present computer program is also capable of treating the power-on and power-off problems in a formal sense. However, the three-dimensional effects due to the nose and the tail of the fuselage are not included.

In the examples calculated so far, no smoothing procedure was used for the input data.

SECTION IV

POWER EFFECTS ON CONTROL SURFACES

To predict the aerodynamics of a V/STOL aircraft it is necessary to be able to predict the effects of power on the horizontal and vertical tail surfaces. This power effect can be attributed primarily to an induced flow angle at the tail location. Having a method of predicting the power induced flow angle it is then possible to estimate the aerodynamic forces and moments induced on the tail surfaces by the exiting jet. This section will describe how to obtain the jet induced flow angles at the location of the tail surfaces.

1. SAMPLE PROBLEM

The sample problem to demonstrate the calculation of the downwash at the tail will be the wind tunnel test model described in Appendix I, with the lift jet operating. The jet parameters and the flight conditions are the same as specified in Section III, except that here three values of U_{∞}/U_{j0} will be considered .1, .2, and .3.

Power induced downwash and sideslip will be computed at the test rake location:

$$x = 44.23 \text{ inches}$$

$$y = -6.75 \text{ inches}$$

Dimensions in model scale

$$z = .9, 2.9, 4.9, 6.9, 8.9, 10.9, 12.9 \text{ inches}$$

2. APPLICATION OF JET FLOW FIELD PROGRAM TO CONTROL SURFACES

The use of the jet flow field program consists of specifying the points at which jet induced velocity components are to be computed, details of jet location and the flight variables. A description of sample input and output for the jet flow field program has been given in Section II.3. The application of the jet flow field program to the tail problem differs only in the location of the control points.

In this example the downwash and sidewash angles will be computed at the rake location instead of the vertical or horizontal tail location since test data exists for the rake location.

Figures 47 and 48 show a comparison of power induced downwash and sidewash obtained by the jet program and compared with wind tunnel test data for the body alone with the rake attached. The theory will not account for the presence of a body or a wing so it must be assumed that these components can be ignored in calculating the power induced angles. The agreement shown in the figure can be considered satisfactory considering the scatter in the test data.

3. CALCULATION OF POWER INDUCED FORCES AND MOMENTS ON CONTROL SURFACES

To calculate the incremental force and moments induced on the tail it is necessary to estimate the $C_{L\alpha}$ of the surface in the presence of the fuselage (and other tail panels) and the centroid of the panel load. These values may be estimated by empirical methods such as are to be found in DATCOM. When these values are known, the jet induced downwash and sidewash can be used to estimate an incremental angle of attack or sideslip on the surface in question. From these values it is possible to estimate power induced forces and moments on the tail surfaces. Some estimates of this nature have been made for the wind tunnel test model of this study but the accuracy with which the incremental forces and moments can be measured from the test data precludes any conclusions as to method accuracy. The comparisons made do show, however, that such estimates are of the right order of magnitude.

○ Theory
 △ Test - BJ

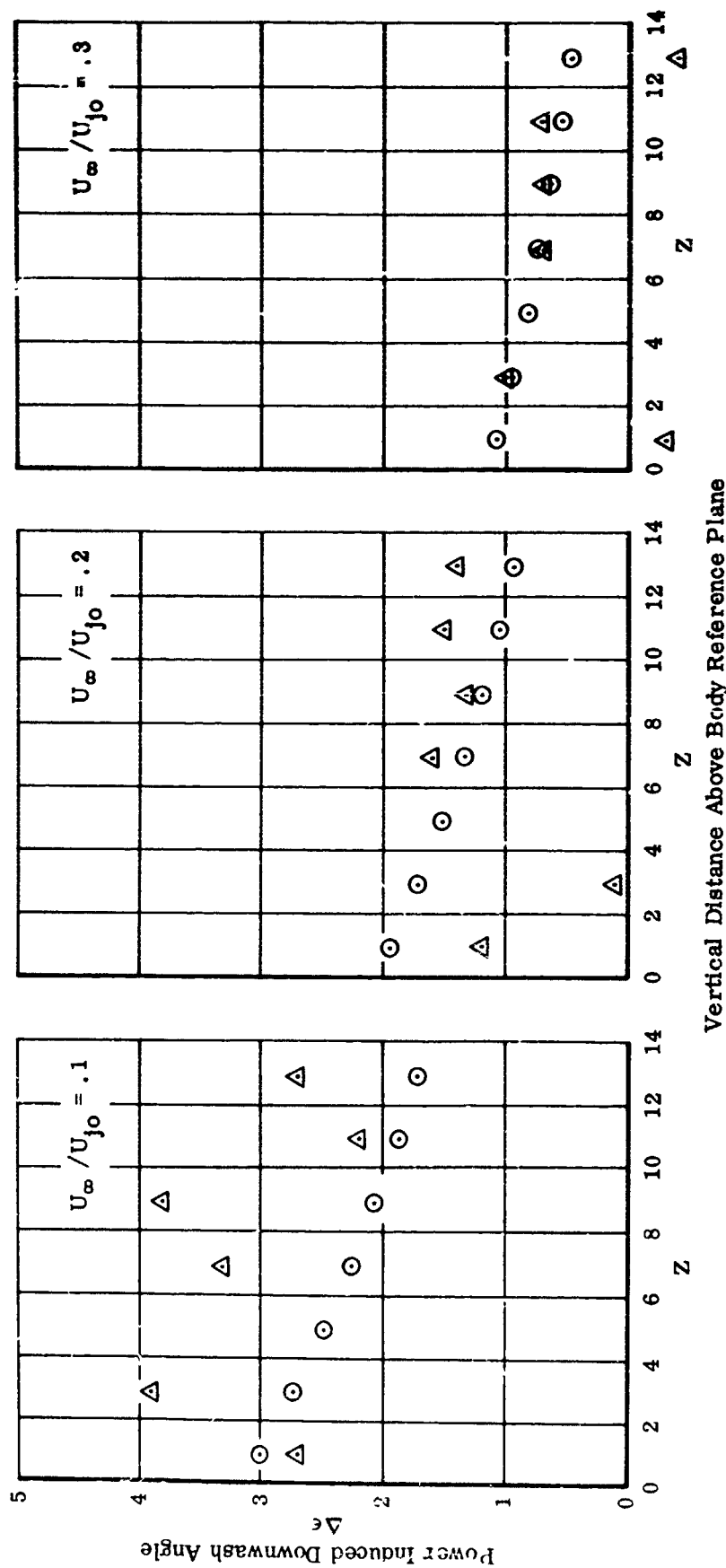


FIGURE 47. LIFT JET POWER INDUCED DOWNWASH AT RAKE LOCATION

○ Theory
 △ Test
 (31C-305)

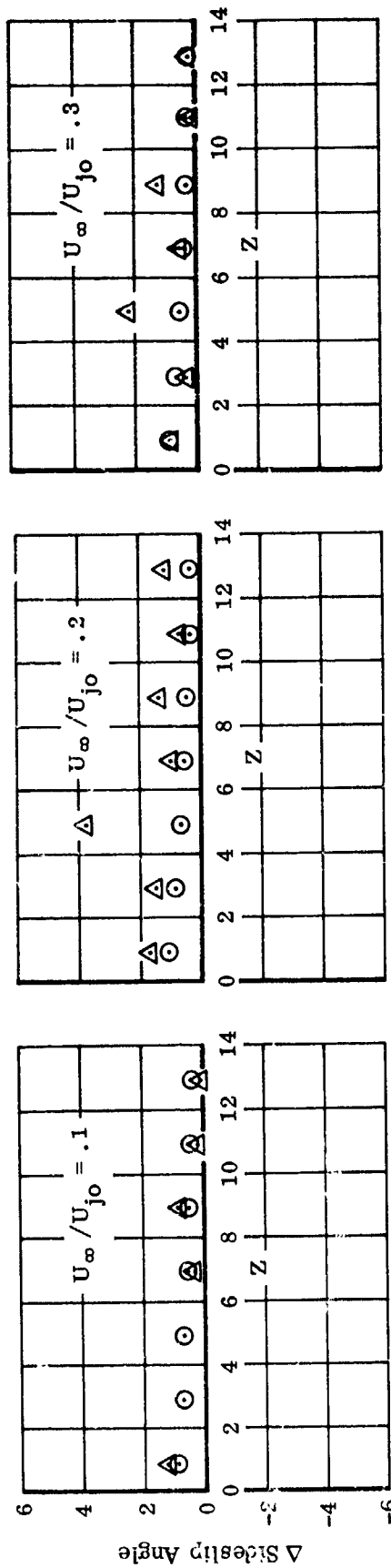


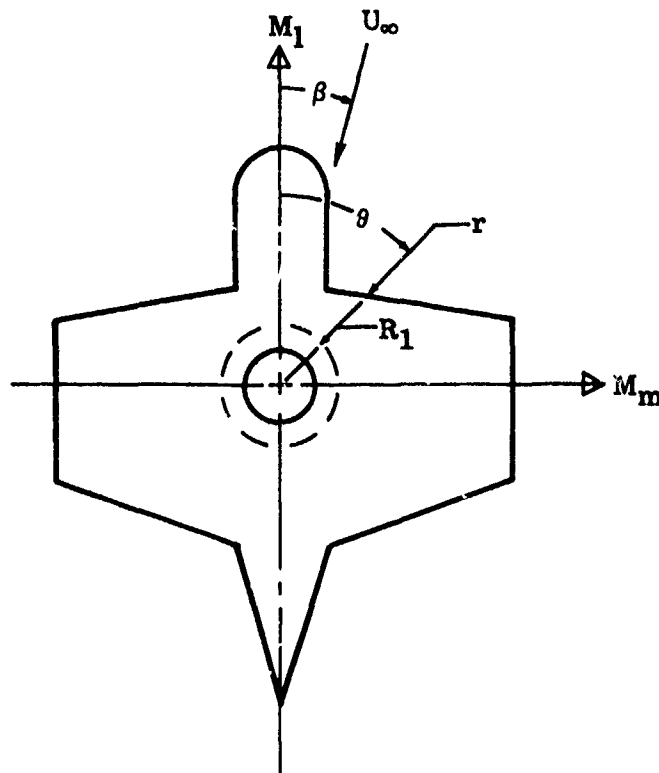
FIGURE 48. LIFT JET POWER INDUCED SIDEWASH AT RAKE LOCATION

SECTION V

APPLICATION OF INLET METHOD

The method of force and moment estimation for normal inlets described in Volume I, Section V, consists of three parts. The inlet induced forces are two parts, lip forces which act in the immediate vicinity of the inlet, and surface forces which act at greater distances. The third part consists of a description of the net thrust of the propulsive device causing the inlet flow. An approximation for a lift fan has been derived, but data obtained from test could be used in place of the model.

The inlet method may be applied to a wide variety of configurations. This versatility is a direct result of the empirical nature of the model. Because of this empirical nature, some comment is required on selection of the parameters used in the equations summarized below.



$$\left(\begin{array}{c} \text{inlet +} \\ \text{net fan thrus.} \end{array} \right) = \left(\begin{array}{c} \text{inlet lip} \\ \text{forces} \end{array} \right) + \left(\begin{array}{c} \text{surface} \\ \text{forces} \end{array} \right) + \left(\begin{array}{c} \text{net fan} \\ \text{forces} \end{array} \right)$$

Lip Forces:

$$L_L = \frac{\rho}{2} A_f \left[U_f^2 (1 - A_f / 4\pi R_1^2) + U_\infty^2 (\eta - k^2) \right]$$

$$D_L = \rho A_f U_f U_\infty$$

$$M_{Lb} = -\rho A_f U_f U_\infty (R_1/2) \sin \beta$$

$$M_{mL} = \rho A_f U_f U_\infty (R_1/2) \cos \beta$$

Surface Forces:

$$L_S = \frac{\rho}{2} U_\infty U_f \frac{A_f}{\pi} \left[\cos \beta \int_0^{2\pi} \ln \left| \frac{r}{R_1} \right| \cos \theta d\theta + \sin \beta \int_0^{2\pi} \ln \left| \frac{r}{R_1} \right| \sin \theta d\theta \right] + \frac{\rho}{4} U_f^2 \left(\frac{A_f}{2\pi R_1} \right)^2 \int_0^{2\pi} [1 - (R_1/r)^2] d\theta$$

$$M_{mS} = \frac{\rho}{2} U_\infty U_f \frac{A_f R_1}{\pi} \left[\cos \beta \int_0^{2\pi} [(r/R_1) - 1] \cos^2 \theta d\theta + \sin \beta \int_0^{2\pi} [(r/R_1) - 1] \cos \theta \sin \theta d\theta \right] + \frac{\rho}{2} U_f^2 \frac{(A_f/2\pi)^2}{R_1} \int_0^{2\pi} (1 - R_1/r) \cos \theta d\theta$$

$$M_{LS} = \frac{\rho}{2} U_\infty U_f \frac{A_f R_1}{\pi} \left[\cos \beta \int_0^{2\pi} (1 - r/R_1) \cos \theta \sin \theta d\theta + \sin \beta \int_0^{2\pi} (1 - r/R_1) \sin^2 \theta d\theta \right] + \frac{\rho}{2} U_f^2 \frac{(A_f/2\pi)^2}{R_1} \int_0^{2\pi} [(R_1/r) - 1] \sin \theta d\theta$$

Fan Flow and Force:

$$U_f = \left[(C_t U_t^2 + (\gamma - K^2) U_\infty^2) / (1 + C_o S_{cB} / A_f) \right]^{0.5}$$

$$T_f = \frac{\rho}{2} A_f \frac{C_t}{1 + C_o S_{cB} / A_f} U_t^2 - \frac{\rho}{2} (\gamma - K^2) \frac{C_o S_{cB}}{1 + C_o S_{cB} / A_f} U_\infty^2$$

Summation:

$$L = L_L + L_S + T_f$$

$$D = D_L$$

$$M_L = M_{LL} + M_{LS}$$

$$M_m = M_{mL} + M_{mS}$$

1. SELECTION OF PARAMETERS

a. Inlet Method

In the application of the inlet method, judgement must be used in determining the boundaries of the surface upon which the inlet is assumed to have an effect. The magnitude of the pitching moment due to forward velocity as well as the magnitude and sign of the static moment is a direct function of the size and distribution of the effective area. In simple cases such as the presence of an inlet in the surface of a rectangular wing, it is obvious that the entire surface should be considered in the calculations. In more complicated situations it is presently thought that the area considered for each inlet be defined by a radius measured from the centroid of the inlet to the nearest edge of the body or the nearest barrier to flow, such as a sharp corner. Lift forces are concentrated in the immediate vicinity of the inlet and are not so greatly affected by the definition of the effective area.

The radius R_1 , used to separate the area on which "lip" forces act from the area on which "surface" forces act, is completely arbitrary. The value of R_1 does not affect the final result of the calculation which contains the sum of "lip" and "surface" forces. In a particular calculation it may be convenient to make R_1 correspond to the

actual inlet size or to make R_1 a larger value and minimize the value of the surface force integrals.

Although the integrals appearing in the surface force equations are easily adapted to machine computation, graphical integration or a finite summation using a worksheet such as that shown in Table 3 has been found to be satisfactory. Because the forces are concentrated in the immediate vicinity of the inlet, large angular increments may often be used with little loss in accuracy. For configurations with more than one inlet, the present procedure is to superimpose the effects of the individual inlets without consideration of interaction between inlets.

b. Fan Flow Model

In application of the fan flow model, values of the parameters η and K must be selected. These parameters appear only in the combination $\eta - K^2$ and this combined parameter should be in the range ± 1 .

For deep inlets K may be assumed to be zero. For very thin inlets the value of K will approach unity. Reference (2) shows that $K = 0.7$ for a relatively deep fan-in-wing installation.

The dynamic head recovery factor η varies from near unity for deep inlets (3) to zero for thin inlets (4). Even for deep inlets, the value of η will fall quite rapidly with forward speed if no flow turning device is present.

The parameter C_t is obtained by fitting static thrust versus RPM curves for a particular fan after values have been selected for $\eta - K^2$ and $C_D S_{CB}$.

2. EXAMPLES OF APPLICATION

The analytical models are applied to several configurations and indicate characteristics consistent with the data. It is not possible to completely verify the analysis as it is not presently possible to separate the effect of the propulsive wake, present in the data, from the effect of the inlet flow, and it is not yet possible to calculate the exit effect with complete confidence for these configurations. No sample calculations are shown because of the relative simplicity of the model, but the selection of the empirical parameters is indicated.

Although a large amount of data is available for both lift-jet and lift-fan configurations, only lift fan data is considered. Lift-jet inlet effects are relatively small due to the lower mass flows and this may result in inlet force variations of the

same order as data scatter ⁽⁵⁾. The amount of usable data available is further reduced by the presence of a high degree of wind tunnel wall interference in some tests.

The methods have been applied to four configurations:

1. fan-in-nacelle ⁽⁶⁾
2. fan-in-fuselage ⁽³⁾
3. fan-in-wing ⁽⁴⁾
4. 1/6-scale XV5A ⁽⁷⁾

a. Fan Flow Calculations

Reference (3) and Reference (4) have been used to substantiate the propulsion model. The static thrust versus RPM curves were fitted for both the fan-in-fuselage and fan-in-wing configurations. Using the value of C_t so obtained, fan flow versus forward velocity was calculated and is compared to experimental values in Figure 50. Both curves are reasonably well predicted.

It should be noted that in matching the static thrust curve, the parameter actually obtained is the combination $(C_t / 1 + C_{DS_{CB}}/A_f)$, not C_t . Therefore, variation of the value of $C_{DS_{CB}}$ does not affect the static values produced by the equations but only varies the apparent value of C_t and the effects of translational velocity through the parameter combination $(\eta - K^2 / 1 + C_{DS_{CB}}/A_f)$. Thus, it may be possible to fit data while using values for individual parameters which are in error.

b. Fan-in-Nacelle

The fan-in-nacelle model of Reference (6) is indicated in Figure 49. The twelve inch fan was electrically driven and was not equipped with inlet devices or exit vanes to aid in turning the flow. The model was reversed in the wind tunnel and the fan was tested in both leading and trailing positions.

The results yielded by the empirical model are shown in Figures 51 and 52; no exit effects are included in the calculated curves, which include inlet effect, net fan thrust, and unpowered aerodynamics. Available data for similar inlets indicate that the dynamic head recovery factor can be expected to decrease rapidly as free stream velocity increases from the static conditions. Therefore, curves for both total loss and complete recovery are shown. The parameter K was assumed to be zero.

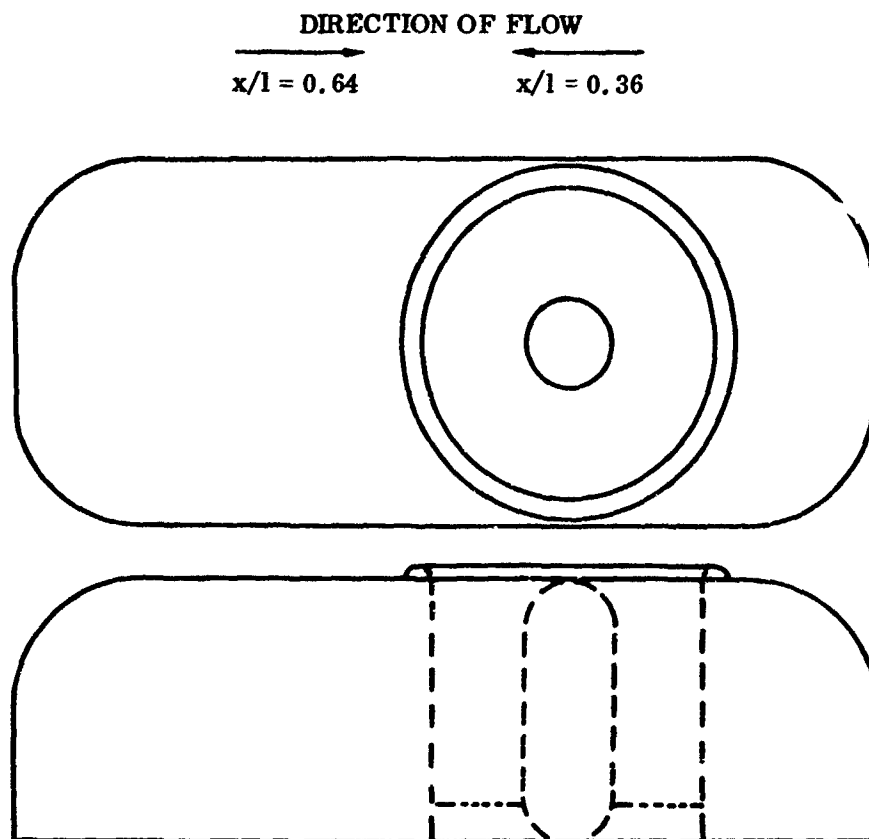


FIGURE 49. FAN-IN-NACELLE CONFIGURATION

The method reflects the change in flow direction as seen in the lift data. Lift forces are reasonably well predicted by assuming high recovery at low speeds and low recovery at high speeds. Drag is also well predicted. The lack of accuracy in the moment prediction may be due to uncertainties in the unpowered aerodynamics, exit effects not included in the predictions, or errors in the selection of the propulsion parameters. Increased fan flow rates would improve overall correlation, but arbitrary changes in propulsion parameters would yield little additional information.

c. Fan-in-Fuselage

The full-scale fan-in-fuselage model of Reference (3) was a shoulder wing configuration of aspect ratio five. The single fan was mounted vertically in the fuselage with the fan axis passing through the wing quarter chord and moment center. A single semicircular vane was placed behind the leading edge of the inlet to improve pressure recovery and inhibit separation. Only tail-off, flap-retracted data are considered.

In the application of the empirical method, the depth of the inlet led to the assumption that the flow is axial to the fan; data shows that pressure recovery of the inlet is nearly complete. Therefore, the parameter $\eta - K^2$ is assumed to be unity.

The diameter of the assumed circular inlet was chosen to contain the intersection of the actual inlet and the fuselage. The projected planform of the wing-body was used in calculating induced surface forces. Inlet sealed data was used to represent power-off terms.

The results of the calculations and data are shown in Figures 53 and 54. Figure 53 compares fan flow rate and fan rotor thrust. Figure 54 shows lift, drag and moment coefficients. It can be seen that drag is best predicted and pitching moment least well predicted. This may, however, be due to the lack of fan exit effects in the analytical predictions.

NASA TN-D-2560 identifies the presence of wind tunnel wall interference in this test and noting that uncorrected data is presented here, removal of the interference would be expected to improve lift correlation. The effect on the moment correlation is not known.

d. Fan-in-Wing

Calculations were also made for the one-sixth scale model of the XV-5A reported in Reference (7). The configuration of the test model was gear down, flaps down, and tail off. The model moment center is ahead of the fan axis.

In the application of the model, the parameter $\eta - K^2$ is assumed to be zero. The assumed inlet size closely matches that of the actual inlets which are nearly circular. Each fan is assumed to produce induced forces only on the wing panel in which it is mounted. Data obtained with inlet and exit sealed are used to predict power-off effects.

The results are presented in Figures 55, 56 and 57. The empirical prediction is presented both with and without power-off aerodynamics. Fan exit effects present in the test are not included in the empirical predictions. The forces and moments for this test were nondimensionalized by the use of the "slipstream" dynamic pressure q^s , where:

$$q^s = 0.5 \rho_\infty U_\infty^2 + L_o / A_F$$

$$L_o = \text{static lift at constant RPM}$$

$$A_F = \text{total fan area}$$

Again, drag force is best predicted and moment least well predicted. The addition of exit effects to the prediction should improve the moment correlation and may improve the lift prediction. The use of exit open, power-off data would improve the moment prediction at the expense of lift prediction, due to disturbance of flow on the lower wing surface.

TABLE 3
INLET-SURFACE FORCE AND MOMENT CALCULATIONS

1	2	3	4	5	6	7	8	9	10	11	12
θ	$\Delta\theta$	R/R_1	$\ln R/R_1$	$\cos\theta$	$\sin\theta$	F_1	$F_1\Delta\theta$	F_2	$F_2\Delta\theta$	F_3	$F_3\Delta\theta$
						4×5	7×2	4×3	9×2	$3^2 - 1$	11×2

1	2	3	4	5	6	7	8	9	10	11	12
θ	$\Delta\theta$	R/R_1	$R/R_1 - 1$	$\cos\theta$	$\sin\theta$	M_1	$M_1\Delta\theta$	M_2	$M_2\Delta\theta$	M_3	$M_3\Delta\theta$
						4×5^2	7×2	$4 \times 5 \times 6$	9×2	$4 \times 5/3$	11×2

1	2	3	4	5	6	7	8	9	10	11	12
θ	$\Delta\theta$	R/R_1	$R/R_1 - 1$	$\cos\theta$	$\sin\theta$	L_1	$L_1\Delta\theta$	L_2	$L_2\Delta\theta$	L_3	$L_3\Delta\theta$
						$4 \times 5 \times 6$	7×2	4×6^2	9×2	$4 \times 6/3$	11×2

$$L_s = 0.5\rho U_\infty U_{f\pi} \frac{A_f}{\pi} (\Sigma F_1 \Delta\theta \cos\beta + \Sigma F_2 \Delta\theta \sin\beta) - 0.25(A_f/2\pi R_1)^2 \rho U_f^2 \Sigma F_3 \Delta\theta$$

$$M_s = 0.5\rho U_\infty U_{f\pi} \frac{A_f R_1}{\pi} (\Sigma M_1 \Delta\theta \cos\beta + \Sigma M_2 \Delta\theta \sin\beta) + 0.5\rho U_{fR_1}^2 (A_f/2\pi)^2 \Sigma M_3 \Delta\theta$$

$$M_s = -0.5\rho U_\infty U_{f\pi} \frac{A_f R_1}{\pi} (\Sigma L_1 \Delta\theta \cos\beta + \Sigma L_2 \Delta\theta \sin\beta) - 0.5\rho U_{fR_1}^2 (A_f/2\pi)^2 \Sigma L_3 \Delta\theta$$

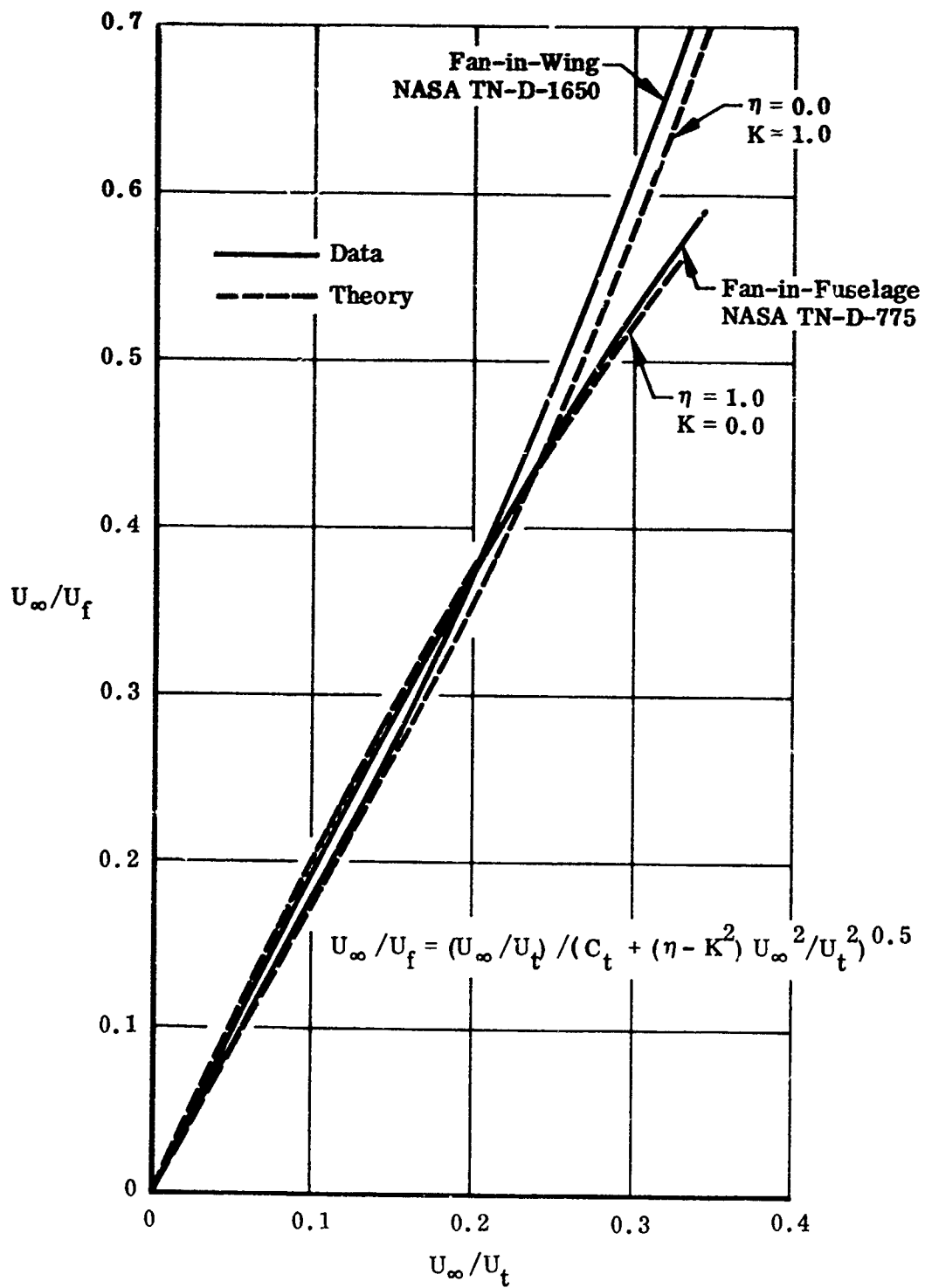


FIGURE 50. FAN FLOW PARAMETERS

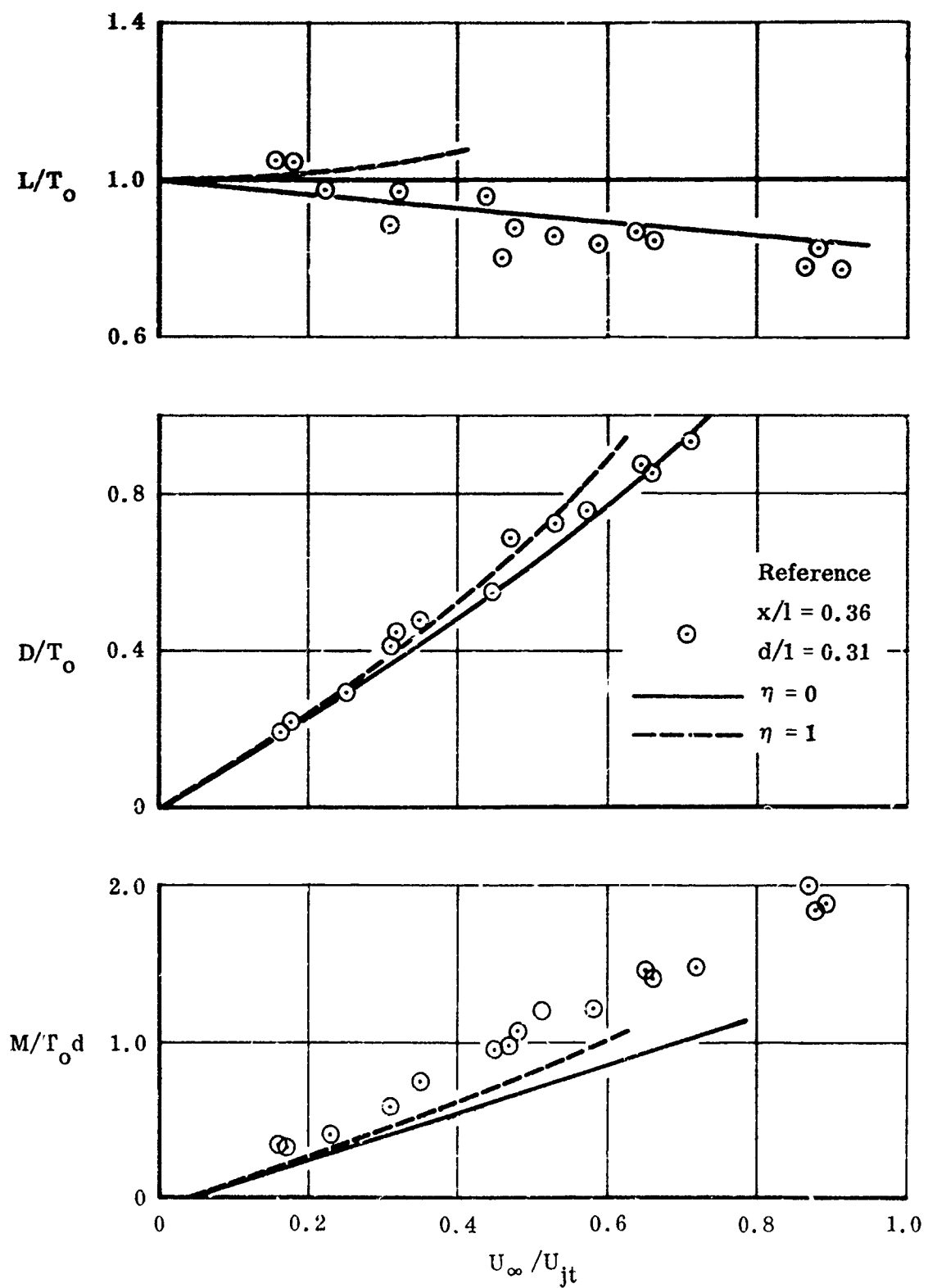


FIGURE 51. FAN-IN-NACELLE, INLET LEADING

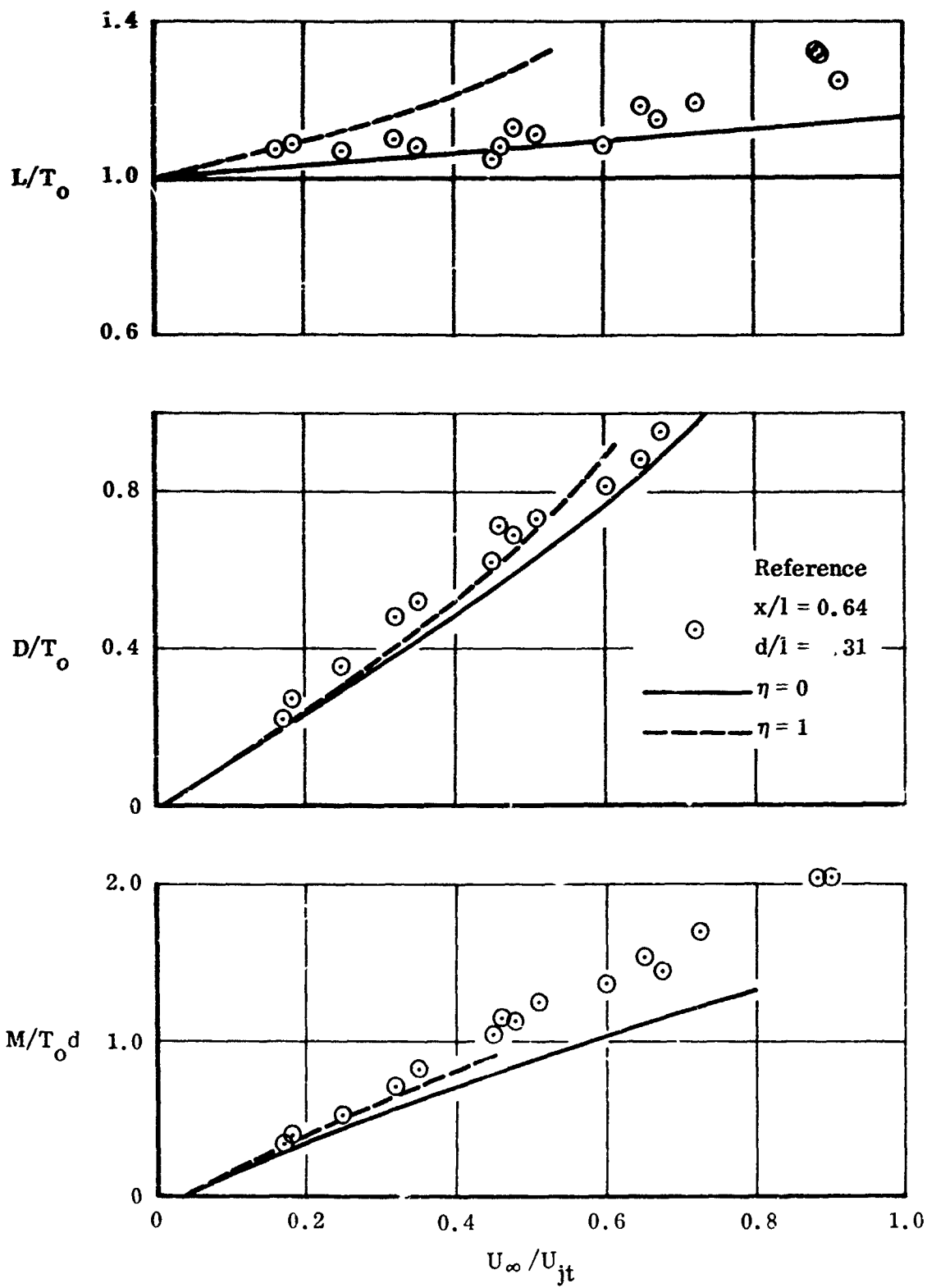


FIGURE 52. FAN-IN-NACELLE, INLET TRAILING

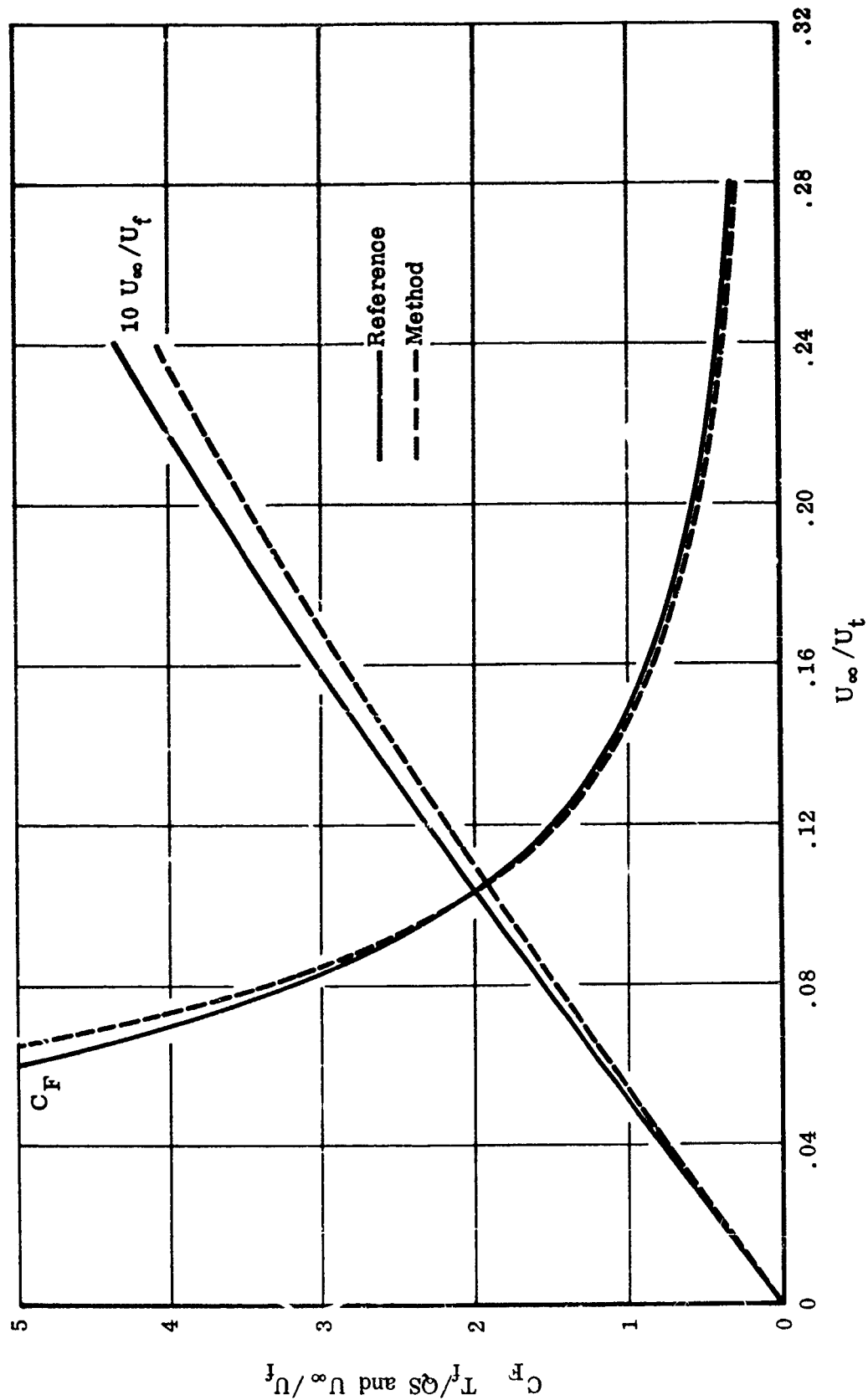


FIGURE 53. FAN-IN-FUSELAGE, PROPULSION PARAMETERS

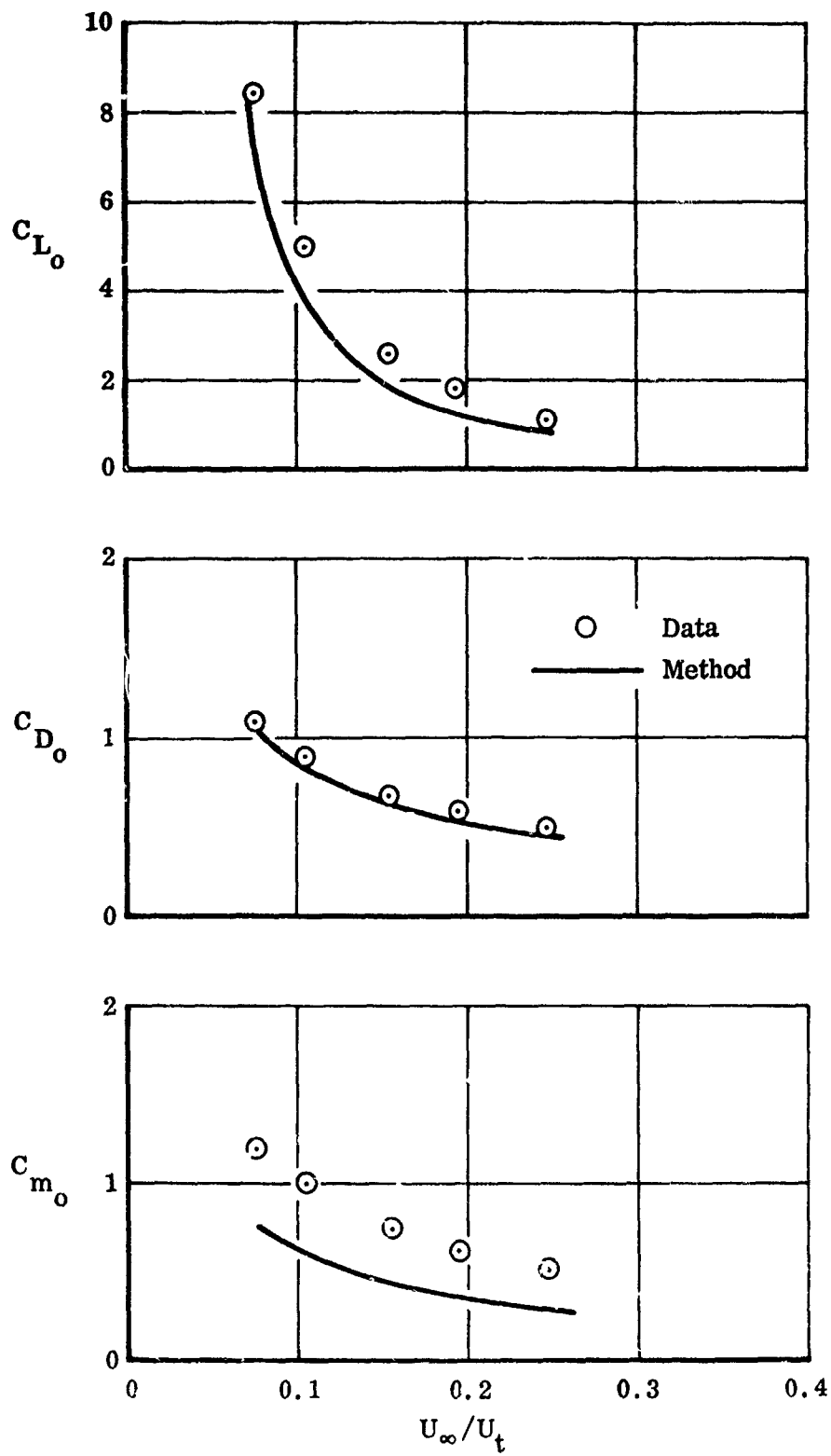


FIGURE 54. FAN-IN-FUSELAGE

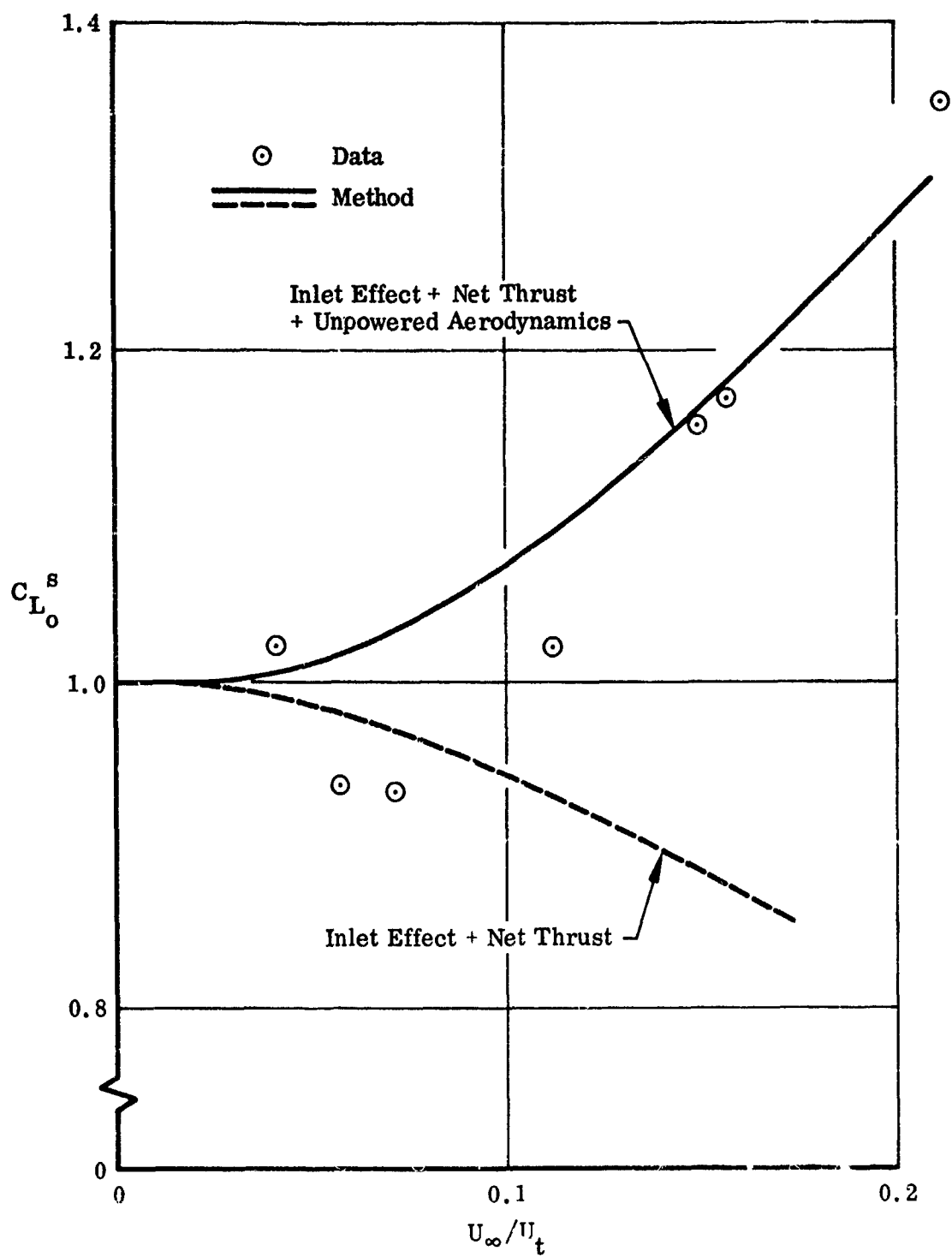


FIGURE 55. 1/6-SCALE XV-5A, FAN-IN-WING, LIFT FORCE

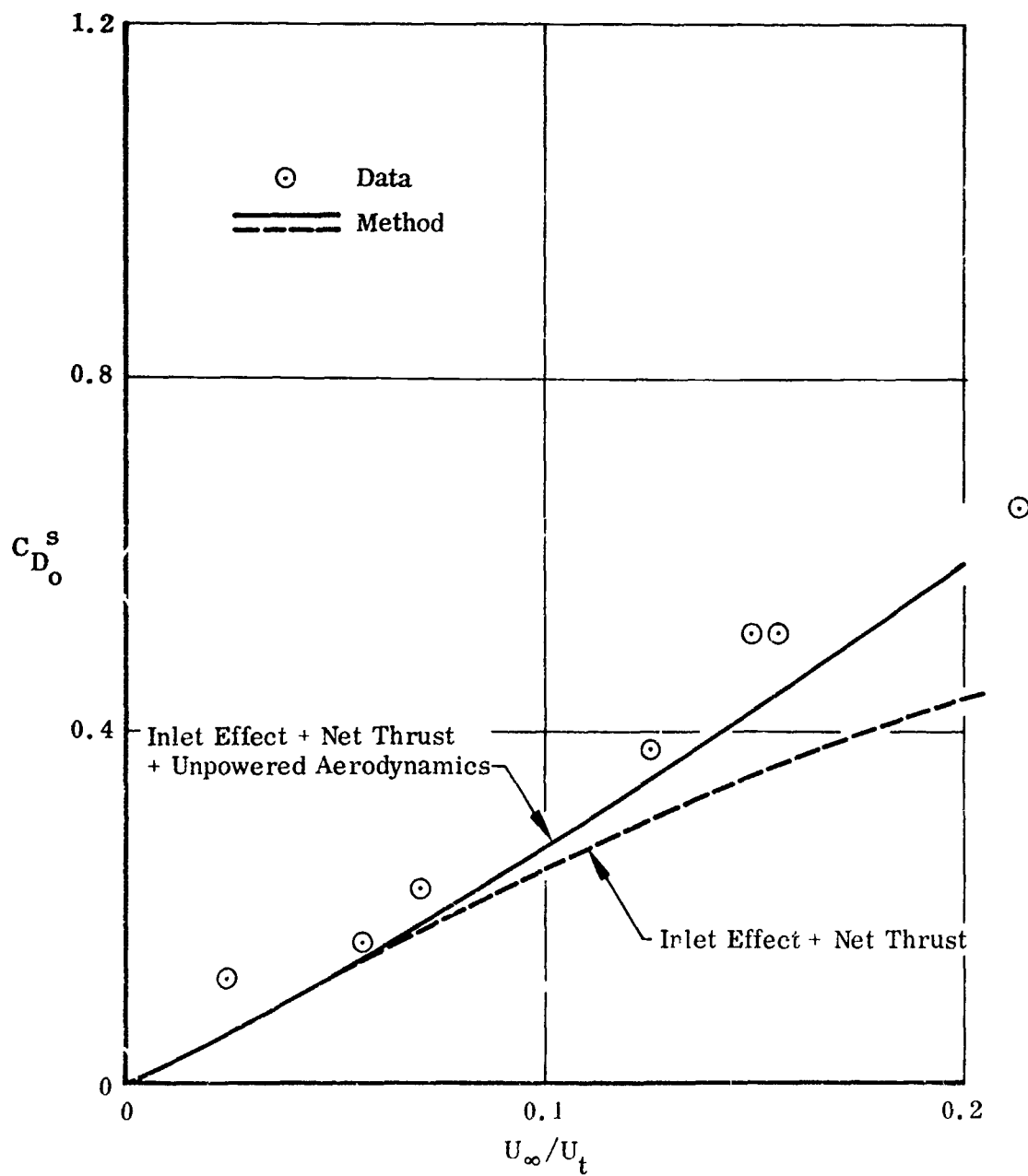


FIGURE 56. 1/6-SCALE XV-5A, FAN-IN-WING, DRAG FORCE

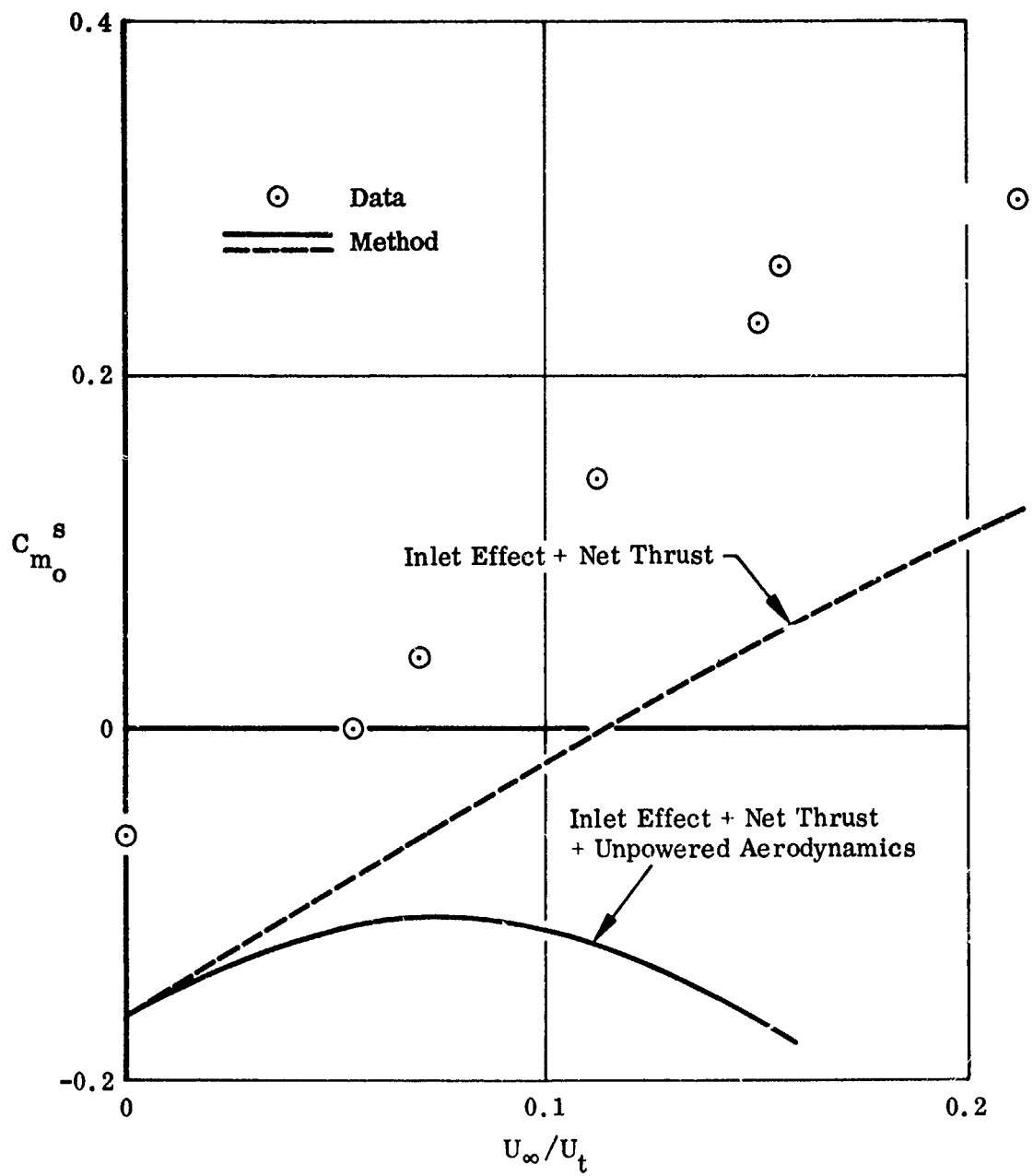


FIGURE 57. 1/6-SCALE XV-5A, FAN-IN-WING, PITCHING MOMENT

SECTION VI

NONLINEAR BODY AERODYNAMICS

The body aerodynamics are computed by combining slender body theory with viscous crossflow effects to obtain nonlinear coefficients at high angles of attack and sideslip. The method, described in Volume I, has been programmed for the computer with the linear and the viscous components of the aerodynamic coefficients printed out separately. The computer program requires that the mapping of the body cross sections be known. This mapping is obtainable by means of the mapping method described in Sections II and III. A simplified method of obtaining inputs to the computer program is also described which permits more ready calculation of body aerodynamics by bypassing the mapping of the body cross sections.

1. SAMPLE PROBLEM

To illustrate the use of the nonlinear body aerodynamics program the wind tunnel test model body described in Appendix I will be used. The aerodynamic coefficients and rotary derivatives will be calculated for this body through an angle of attack and angle of sideslip range.

a. Description of Body Coordinate System

The axis system used to describe the body is shown in Figure 58. The coordinates are body axes with the x-axis aligned along the body. The exact location of the x-axis is chosen to permit the body cross sections to be obtained in planes perpendicular to this axis. The exact location of the origin is not restricted to be at the body nose but may be chosen to suit the user. The axis system chosen consists of a right hand system with the x-axis directed aft, the y-axis to the right and the z-axis upward.

The flight conditions for the static coefficients are specified as a resultant angle of attack α and a roll angle ϕ . The resultant angle of attack is the angle between the freestream direction and the x-axis and is always defined as positive. The roll angle is then specified as the angle between the freestream component in the y-z plane and the body vertical plane (x-z plane) as shown in Figure 58.

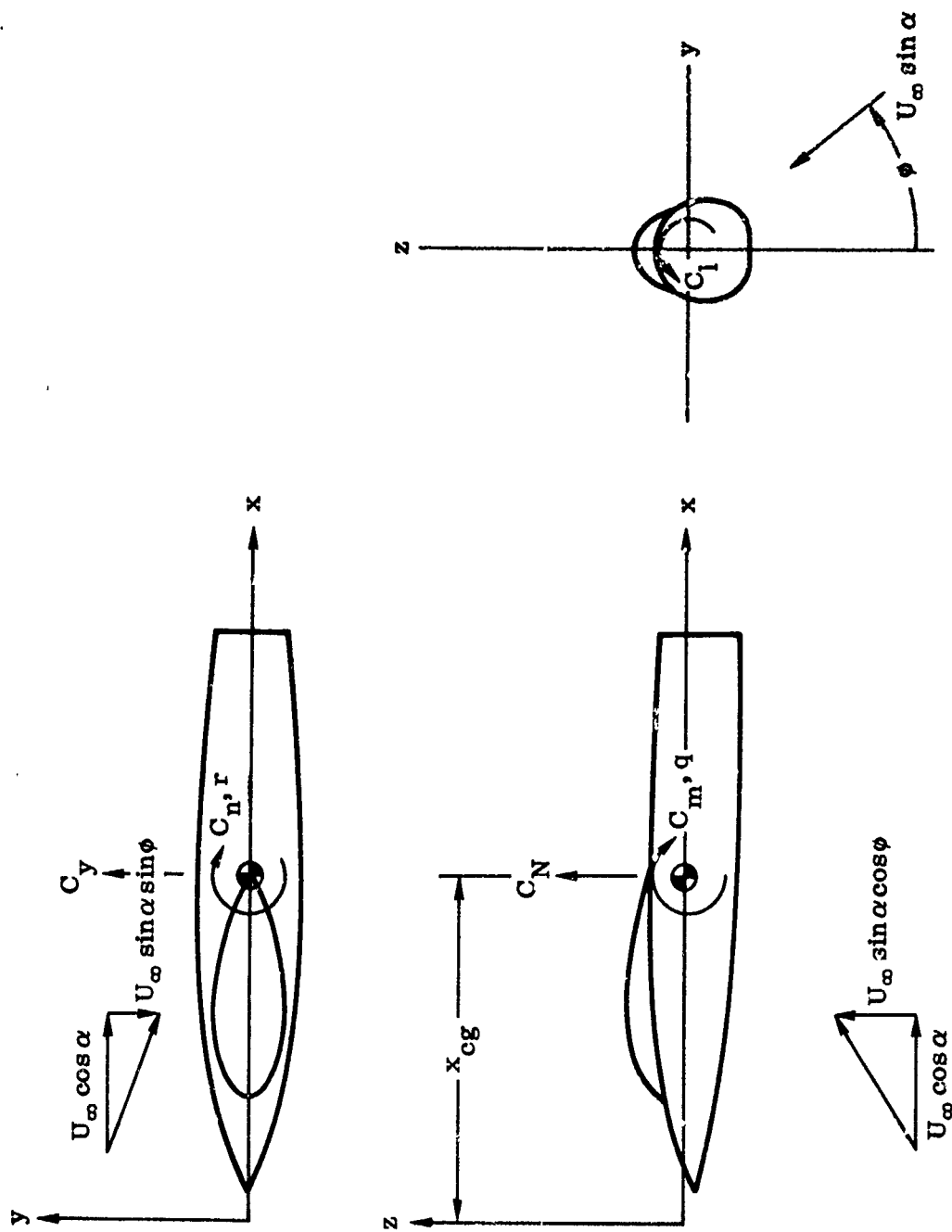


FIGURE 58. SIGN CONVENTION FOR BODY AERODYNAMIC COEFFICIENTS

Of the rotary velocities p is not considered of importance for a body and so is not included in the computation. The rotary components q and r are specified in body axes with q as a vector in the direction of the positive y -axis and r as a vector in the direction of the negative z axis. This convention was chosen to be consistent with the terminology of Reference 6.

A reference length l_r , reference area S_r and a center of gravity location x_{cg} are specified. All of the force coefficients are based on the same reference area. Pitching, yawing and rolling moment coefficients are defined on the reference area and the reference length specified. This differs from the conventional way of defining the moments. The reference point about which the moments are taken is the specified center of gravity location which is located on the x -axis. The effects of including rotary velocities assume that the center of rotations of q and r are at x_{cg} .

The force and moment coefficients are in body axes as shown in Figure 58, C_N positive along the positive z -axis, C_m positive for a moment pitching the nose up. C_y is positive in the positive y direction and C_n positive for a nose right moment. Rolling moment coefficient C_l is defined positive counterclockwise the moment being specified about the x -axis. No attempt has been made to incorporate the axial force coefficient as the method used is not suitable for that purpose.

b. Body Description for Nonlinear Force and Moment Program

To use the computer program for aerodynamic coefficients the body must be described for a series of sections taken perpendicular to the x -axis. It is not necessary to take the sections chosen at equal intervals but the spacing should be relatively uniform with more sections being taken in regions where the cross sectional parameters are changing rapidly.

The section inputs include both the geometrical variables S and dS/dx and the coefficients of the mapping function and their derivatives. It is therefore necessary to know the mapping of each of the sections being inputted. Although it is necessary to include mapping coefficients, the nature of the slender body theory is such that only the first few coefficients are of primary significance. For this reason it is possible to approximate the coefficients of the mapping function and still retain reasonable accuracy. Therefore, methods are presented for obtaining the mapping coefficients accurately and an easier approximate method which retains the more significant coefficients.

The coefficients as obtained by the mapping program must be modified before they are suitable for use with the nonlinear body aerodynamics program and the method of modification will be described. The simplified method of obtaining coefficients for the mapping function will also be described and a complete set of inputs to the program will be given for this simplified method.

c. Modification of Mapping Function for Body Aerodynamics Program

Equation (1) of Section II is not in the proper form for use with the body aerodynamics program. When this equation is rewritten to include the constant term, i.e., to locate the section

$$Z = \zeta + a_0 + ib_0 + \frac{a_1 + ib_1}{\zeta} + \frac{a_2 + ib_2}{\zeta^2} + \dots + \frac{a_n + ib_n}{\zeta^n} \quad (3)$$

the section is located and mapped as shown in Figure 59(a). For the body aerodynamics program the section is rotated as shown in Figure 59(b) and the mapping is commenced at a different point on the section. In addition, instead of basing the mapping on a circle of radius r_c , the mapping is rewritten to base the new mapping on the unit circle coordinate $\sigma = e^{i\theta}$. The final form of the mapping is then:

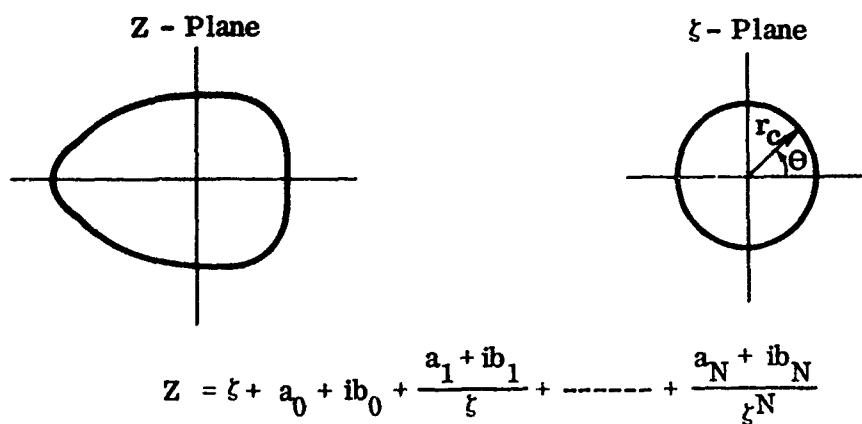
$$Z = r_c \sigma + c_0 + id_0 + \frac{c_1 + id_1}{\sigma} + \frac{c_2 + id_2}{\sigma^2} + \dots + \frac{c_n + id_n}{\sigma^n} \quad (4)$$

where these coefficients are related to the coefficients of Equation (3) by the relation

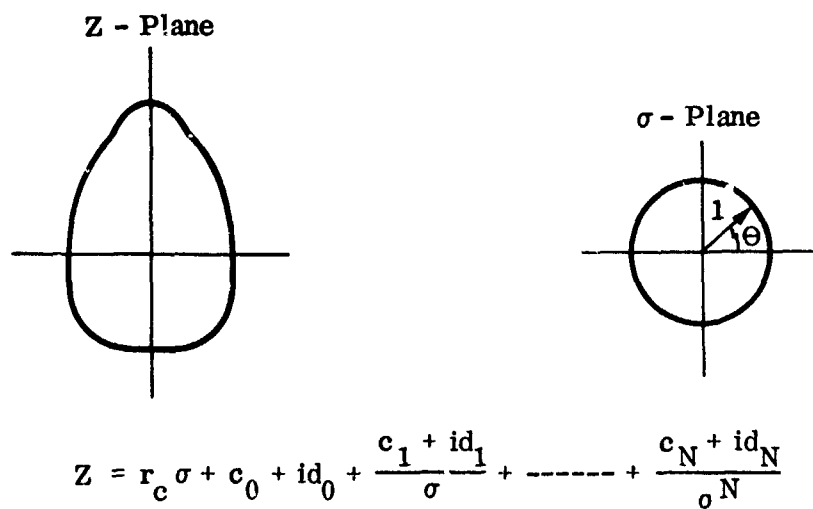
$$c_n + id_n = \frac{(-i)^{n+1}}{r_c^n} (a_n + ib_n) \quad (5)$$

For a symmetrical shape this reduces to the relation

$$\begin{aligned} Z &= r_c \sigma - ia_0 - \frac{a_1}{r_c \sigma} + \frac{ia_2}{r_c^2 \sigma^2} + \frac{a_3}{r_c^3 \sigma^3} - \frac{ia_4}{r_c^4 \sigma^4} - \dots \\ &= r_c \sigma + id_0 + \frac{c_1}{\sigma} + \frac{id_2}{\sigma^2} + \frac{c_3}{\sigma^3} + \frac{id_4}{\sigma^4} + \dots \end{aligned} \quad (6)$$



a. Original Mapping Relation



b. Final Mapping Relation

FIGURE 59. CHANGE OF MAPPING FUNCTION FOR BODY AERODYNAMICS PROGRAM

d. Simplified Handbook Method for Obtaining Coefficients

Since it is desired to use the body aerodynamics program for preliminary design type work it is, where possible, desirable to avoid the complexity of obtaining the mapping function. It is possible to do this for the usual fuselage shapes encountered and still retain sufficient accuracy for preliminary design purposes.

The actual fuselage is replaced by an equivalent body in which the sections are replaced by equivalent ellipses keeping the same body camber. This replaces the mapping of Equation (6) above with the truncated mapping

$$Z = r_c \sigma + i d_0 + \frac{c_1}{\sigma} \quad (7)$$

This expression retains the most critical terms in the mapping as far as obtaining the body aerodynamics and it is possible to approximate the three coefficients r_c , d_0 and c_1 .

Defining a to be half of the maximum vertical dimension of the true cross section and b to be half the maximum lateral dimension of the section, it is possible to approximate r_c and c_1 by the expressions

$$r_c = \frac{a+b}{2} \quad (8)$$

$$c_1 = \frac{b-a}{2} \quad (9)$$

the results being reasonably accurate for fuselages which do not depart too far from the elliptical. The coefficient d_0 can be replaced by the centroid of the sectional area.

The remainder of the inputs required for the slender body portion of the computer program are quantities which can be obtained directly from the body geometry, such as the cross sectional areas and its derivative with respect to x .

e. Viscous Cross Flow Input

The computer program also requires that a cross flow drag coefficient be input for both the components of flow in the vertical plane and the lateral plane.

The viscous crossflow terms can be obtained by using the drag coefficients of an infinite two-dimensional elliptical cylinder at each body station, the character of the ellipse changing according to the maximum dimensions of the body as described above.

These drag coefficients can be obtained using the drag coefficient given in Reference 9 for two dimensional subcritical ellipses and given by

$$C_D = .015 \left(1 + \frac{c}{t}\right) + 1.1 \frac{t}{c} \quad (10)$$

where t = maximum dimension perpendicular to crossflow

c = maximum dimension parallel to crossflow

A coefficient is computed for a crossflow velocity component in the vertical direction in one case and a second coefficient is computed for a crossflow component in the lateral plane. These two coefficients are then multiplied by the maximum dimensions perpendicular to the flow direction for the input parameters.

2. SAMPLE COMPUTATIONS FOR TEST BODY

Table IV shows a set of computations for r_c and c_1 for the wind tunnel test model of this study. The computations are straightforward involving no difficulties. The major inconvenience in developing the inputs for the program is in obtaining S and the derivatives of each of the coefficients with respect to body station. There is no conceptual difficulty involved but the required integration for the body cross sectional area and the centroid location and the graphical differentiations needed to obtain dS/dx , dr_c/dx , dd_0/dx and dc_1/dx is tedious. If necessary, computer programs can be written to do the necessary integration and differentiations but such programs are not included here.

a. Sample Inputs for Force and Moment Program

Figure C0 shows a sample set of inputs for the body aerodynamics program. The data are for the wind tunnel test model body of this study contract with the canopy off.

Card 1 specifies the maximum number of mapping coefficients for any section input (maximum of 12) and the number of stations for which section data is input (maximum of 40).

Cards 2-4 give the station locations of the input sections, maximum of 40. The remainder of the cards must be in units consistent with these numbers. The stations input must not include the nose location nor the tail section if these stations have zero area and mapping circle radius.

Cards 5-7 contain the radii of the mapping circle at the input stations.

Cards 8-10 give the values of $\frac{dr_c}{dx}$ for the same stations.

Cards 11-13 are the cross sectional areas S of the sections.

Cards 14-16 are the values of dS/dx .

Cards 17-19 give the values of the side viscous crossflow drag coefficient per unit length times the maximum vertical dimension at the section.

Cards 20-22 give the vertical viscous crossflow drag coefficient times the maximum lateral section dimension.

Cards 23-76 consist of sets of three cards for each of the input sections (in this case 18 sets). The first card of this set contains two numbers. The first of these specifies the number of mapping coefficients of the given section. If the number specified is zero, the program uses the number given on Card 1. The number given

TABLE IV. COMPUTATIONS FOR WIND TUNNEL
TEST MODEL

x	y/2	z-	z+	r _c	c _i
7.25	4.25	-14.1	-5.6	4.25	0
23.7	9.2	-18.7	3.1	10.05	-.85
41.0	13.1	-22.2	11.0	14.85	-1.75
73.0	17.4	-26.25	24.0	21.2625	-3.8625
94.0	19.25	-27.95	31.35	24.45	-5.2
118.0	21.0	-29.2	37.75	27.2375	-6.2375
143.5	22.45	-30.2	40.7	28.95	-6.5
163.5	23.45	-30.55	40.7	29.5375	-6.0875
185.5	24.3	-30.8	40.7	30.025	-5.725
221.5	25.05	-30.6	40.7	30.35	-5.3
264.25	25.1	-29.3	40.7	30.05	-4.95
316.0	24.8	-25.0	40.7	28.825	-4.025
343.0	24.6	-21.5	40.4	27.775	-3.175
374.0	24.45	-16.3	39.75	26.2375	-1.7875
411.0	21.5	-9.1	38.3	22.6	-1.10
450.0	15.6	-.85	35.95	17.0	-1.4
497.0	6.4	11.6	30.8	8.0	-1.6
512.0	3.545	16.11	27.5	4.62	-1.075

1	72500E 01	.23700E 02	.42000E 02	.73000E 02	.94000E 02	.11800E 03
2	19350E 03	.16350E 03	.18550E 03	.22150E 03	.26925E 03	.31600E 03
3	34300E 03	.37400E 03	.41100E 03	.45000E 03	.49700E 03	.51200E 03
4	42500E 01	.10050E 02	.14850E 02	.21263E 02	.24450E 02	.27238E 02
5	28950E 02	.29538E 02	.30125E 02	.30350E 02	.30050E 02	.28825E 02
6	27775E 02	.26238E 02	.22600E 02	.17000E 02	.80000E 01	.46200E 01
7	42000E 00	.31500E 00	.24500E 00	.16700E 00	.13300E 00	.92000E -01
8	47000E -01	.29000E -01	.12000E -01	.00000E 00	-.12000E -01	-.30000E -01
9	45000E -01	.67000E -01	-.11900E 00	-.16600E 00	-.21500E 00	-.23000E 00
10	56700E 02	.32916E 03	.70541E 03	.14328E 04	.18927E 04	.23849E 04
11	28020E 04	.30352E 04	.32438E 04	.34037E 04	.33104E 04	.29404E 04
12	26795E 04	.23517E 04	.17438E 04	.96001E 03	.20310E 03	.59300E 02
13	13800E 02	.19700E 02	.22900E 02	.23600E 02	.21700E 02	.19000E 02
14	15500E 12	.12300E 02	.85000E 01	.14000E 01	-.56000E 01	-.98000E 01
15	10600E 02	.12600E 02	-.19400E 02	-.22000E 02	-.19000E 02	-.77000E 01
16	92450E 01	.23750E 02	.36150E 02	.54600E 02	.64500E 02	.72800E 02
17	76050E 02	.77500E 02	.77800E 02	.77550E 02	.74100E 02	.71500E 02
18	57300E 02	.61000E 02	.51500E 02	.40020E 02	.20870E 02	.12080E 02
19	46600E 01	.10100E 02	.14380E 02	.19090E 02	.21150E 02	.23080E 02
20	24620E 02	.25750E 02	.26650E 02	.27500E 02	.27550E 02	.27220E 02
21	27000E 02	.26800E 02	.23600E 02	.17120E 02	.70250E 01	.37350E 01
22						
23						
24	10000E 02	.00000E 00				
25	14500E 00	.51500E -01				

FIGURE 60. NONLINEAR BODY AERODYNAMICS PROGRAM INPUT DATA FOR SAMPLE PROBLEM

26	0	0	
27	-	77771E 01	- .85000E 00
28		12350E 00	- .51800E-01
29	0	0	
30	-	58050E 01	- .17500E 01
31		11400E 00	- .55500E-01
32	0	0	
33	-	21226E 01	- .38625E 01
34		11450E 00	- .70000E-01
35	0	0	
36		18811E 00	- .52000E 01
37		10900E 00	- .62500E-01
38	0	0	
39		24895E 01	- .62375E 01
40		85000E-01	- .33000E-01
41	0	0	
42		35070E 01	- .65000E 01
43		11500E-01	.65000E-02
44	0	0	
45		35786E 01	- .60875E 01
46	-	70000E-02	.20900E-01
47	0	0	
48		35416E 01	- .57250E 01
49	-	95000E-02	.15000E-01
50	0	0	

FIGURE 60. (Continued)

must not exceed the number on the first card. The second number specifies whether or not the section under consideration is symmetrical or not. If the section is symmetrical, the number 0 is input; otherwise 1. The axis of symmetry is assumed to be the vertical plane.

The second card for each set specifies the coefficients of the mapping function. For a symmetrical section the coefficients input follow the order $d_0, c_1, d_2, c_3, d_4, c_5, \dots$ since the other coefficients are zero. For an unsymmetrical section the coefficients are specified in the order $c_0, d_0, c_1, d_1, c_2, d_2, \dots$ up to the maximum number of pairs specified. The subscript 0 specifies the second coefficient (or coefficient pair), the subscript 1 the third coefficient, etc.

The remaining cards specify the flight conditions under which the coefficients are to be found. Card 77 is a comment card and can contain any pertinent information desired.

Card 78 specifies four numbers: reference length, l_r , reference area S_r , center of gravity (and moment center) location x_{cg} and the incremental step size along the body at which computations are made. The program assumes linearity between the incremental steps here specified so that a reasonably large number of steps are required along the body.

The 79th card specifies, respectively, the number of angles of attack to be computed (maximum of 18), the number of roll angles (maximum of 9), number of pitching velocities (maximum of 9) and number of yawing velocities (maximum of 9).

Cards 80 and 81 specify the angle of attack at which the coefficients are to be evaluated. These angles are in degrees.

Card 82 specifies the roll angles which are to be computed, also in degrees.

Card 83 specifies the desired values of pitching velocity inputs. The number input represents $q l_r / 2U_\infty$ (dimensionless).

Similarly Card 84 specifies yawing velocity inputs specified as $r l_r / 2U_\infty$ (dimensionless).

This completes the input cards needed to compute the nonlinear body aerodynamics. Cards are added or subtracted as necessary to input all the specified data. That is, enough cards are used to input the numbers required and no blank cards are to be input. As an example, the number of stations here specified is 18 which

requires 3 cards to specify each of the first set of parameters. More or less cards would be used depending on the number of stations specified.

b. Sample Outputs from Force and Moment Program

Figure 61 shows the output from the computer program for the inputs listed in Figure 60. The first line written out in the information input on the comment card.

The second line lists the flight conditions $\text{PHI } (\varphi)$, $Q \left(\frac{q_1 r}{2U_\infty} \right)$, and $R \left(\frac{r_1 r}{2U_\infty} \right)$ for which the coefficients are calculated.

After this are tabulated the five coefficients C_n , C_m , C_v , C_n and C_l in that order as functions of angle of attack. The coefficients as written out are separated into a potential component (obtained by slender body theory) and a viscous component (using viscous crossflow). To obtain the coefficient these two components must be added together. The program does not calculate a viscous component to the rolling moment so this is printed out as zero.

When more than one set of flight conditions (other than α) are input this tabulation is repeated.

V/STOL TEST MODEL DATA. 12/2/70.

PHI= 0.0 Q= 0.0 R= 0.0

ALPHA	POTENTIAL	CN	CM	CY	CEX	CRM
0.0	POTENTIAL VISCUS	3.4009E-04 0.0	-2.2614E-02 0.0	0.0 0.0	0.0 0.0	0.0 0.0
5.0000	POTENTIAL VISCUS	2.6681E-04 2.5936E-03	1.2029E-02 -9.2671E-04	0.0 0.0	0.0 0.0	0.0 0.0
10.0000	POTENTIAL VISCUS	1.9059E-04 1.0296E-02	4.5463E-02 -3.6787E-03	0.0 0.0	0.0 0.0	0.0 0.0
15.0000	POTENTIAL VISCUS	1.1375E-04 2.2872E-02	7.8157E-02 -8.1723E-03	0.0 0.0	0.0 0.0	0.0 0.0
20.0000	POTENTIAL VISCUS	3.8622E-05 3.9941E-02	1.0763E-01 -1.4271E-02	0.0 0.0	0.0 0.0	0.0 0.0
25.0000	POTENTIAL VISCUS	-3.2516E-05 6.0983E-02	1.3349E-01 -2.1790E-02	0.0 0.0	0.0 0.0	0.0 0.0
30.0000	POTENTIAL VISCUS	-9.7499E-05 8.5360E-02	1.5496E-01 -3.0499E-02	0.0 0.0	0.0 0.0	0.0 0.0
35.0000	POTENTIAL VISCUS	-1.5435E-04 1.1233E-01	1.7137E-01 -4.0136E-02	0.0 0.0	0.0 0.0	0.0 0.0
40.0000	POTENTIAL VISCUS	-2.0135E-04 1.4107E-01	1.8223E-01 -5.0406E-02	0.0 0.0	0.0 0.0	0.0 0.0
45.0000	POTENTIAL VISCUS	-2.3766E-04 1.7072E-01	1.8720E-01 -6.0499E-02	0.0 0.0	0.0 0.0	0.0 0.0

FIGURE 61. NONLINEAR BODY AERODYNAMICS PROGRAM OUTPUT
DATA FOR SAMPLE PROBLEM

3. COMPARISON WITH TEST DATA

Figure 62 shows the comparison between theory and test for normal force coefficient C_N and pitching moment coefficient, C_m at zero sideslip. The theoretically predicted values of C_N are somewhat low. In particular, the predicted lift curve slope at zero angle of attack is predicted to be zero while the test results show a finite value. The value of C_N at zero angle of attack is also in error. The agreement obtained for the pitching moment can be considered to be good.

Figure 63 shows a comparison between test and theoretical side force C_y and yawing moment C_n . The theoretical side force tends to be somewhat low, and the agreement in yawing moment is somewhat worse than the pitching moment agreement.

The computer program does not calculate the derivatives but it is possible to compute two sets of coefficients at different values of a parameter and obtain the derivative by dividing the difference of the coefficients by the incremental change in the parameter.

Figures 64 and 65 show samples of rotary derivatives obtained using the computer program. No test data is available with which to compare the theoretical results, so it is not possible to predict what accuracy is obtained by the theoretical method.

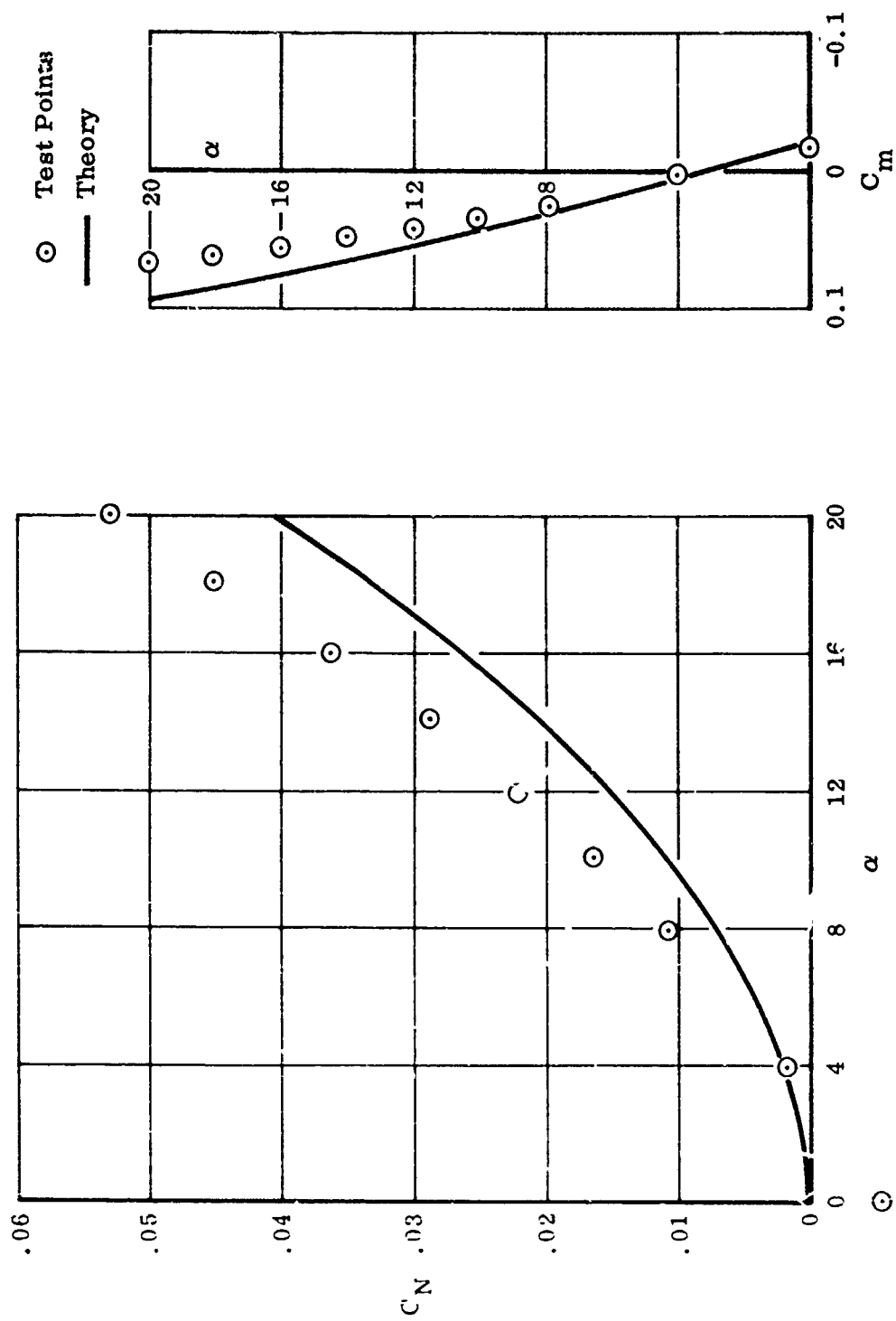


FIGURE 62. THEORY AND TEST CONDITIONS OF C_N AND C_m FOR WIND TUNNEL TEST MODEL FUSELAGE

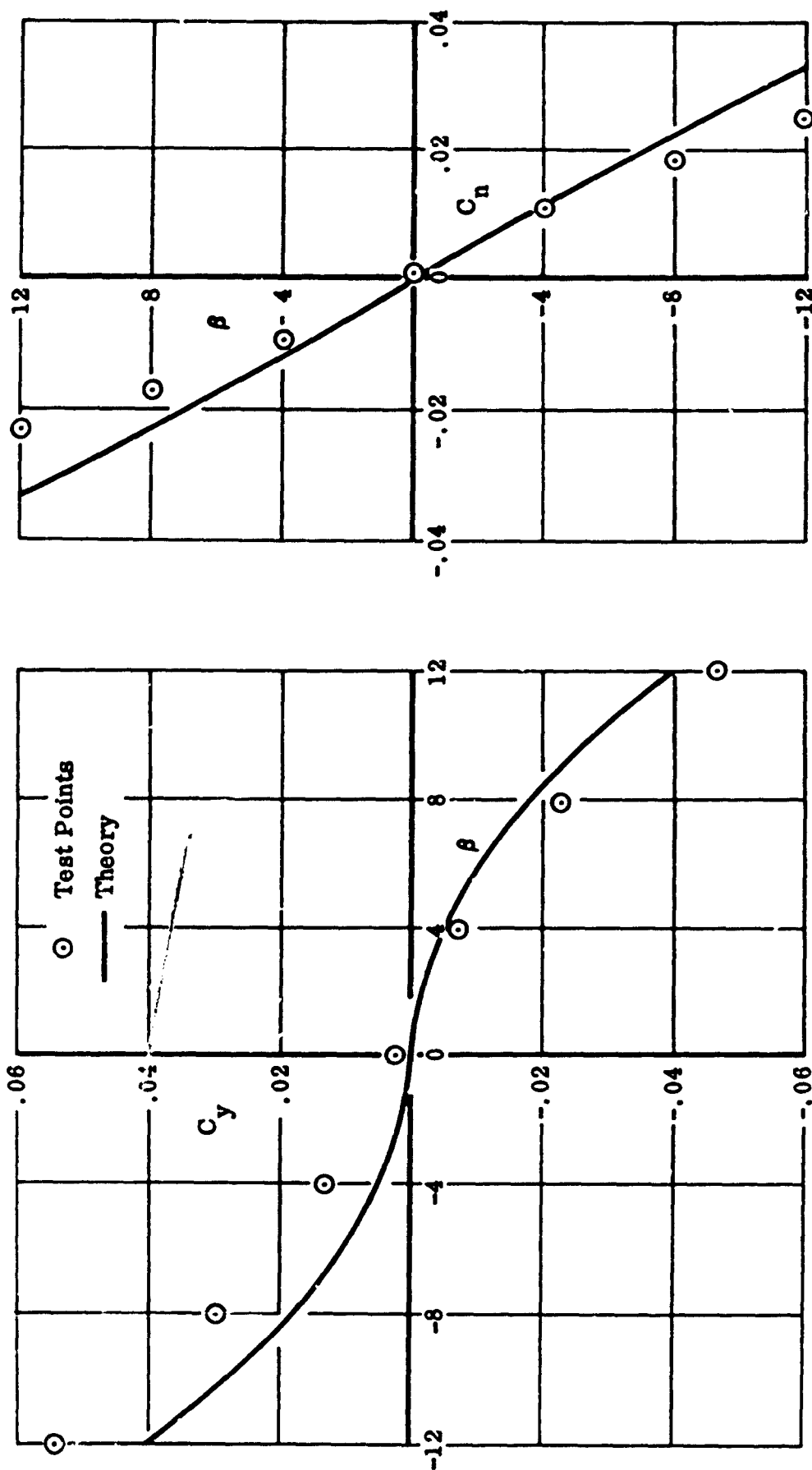


FIGURE 63. THEORY AND TEST COMPARISON OF C_y AND C_n FOR WIND TUNNEL TEST MODEL FUSELAGE

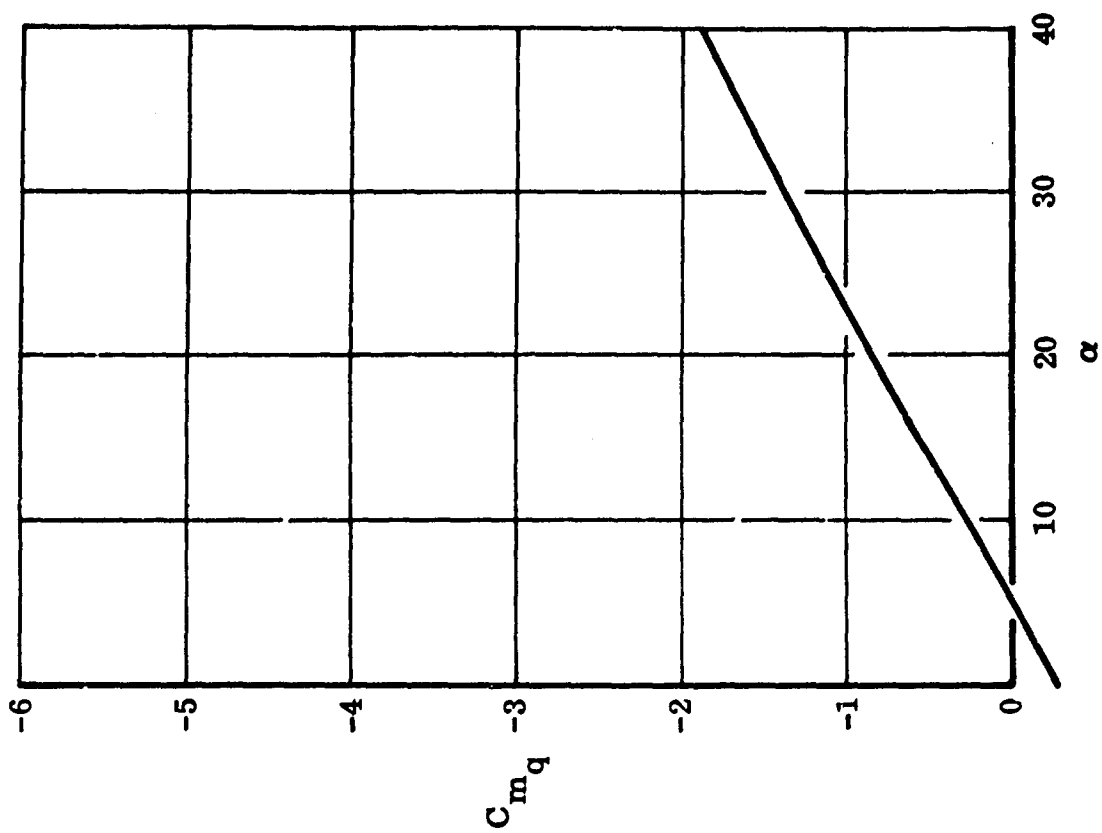
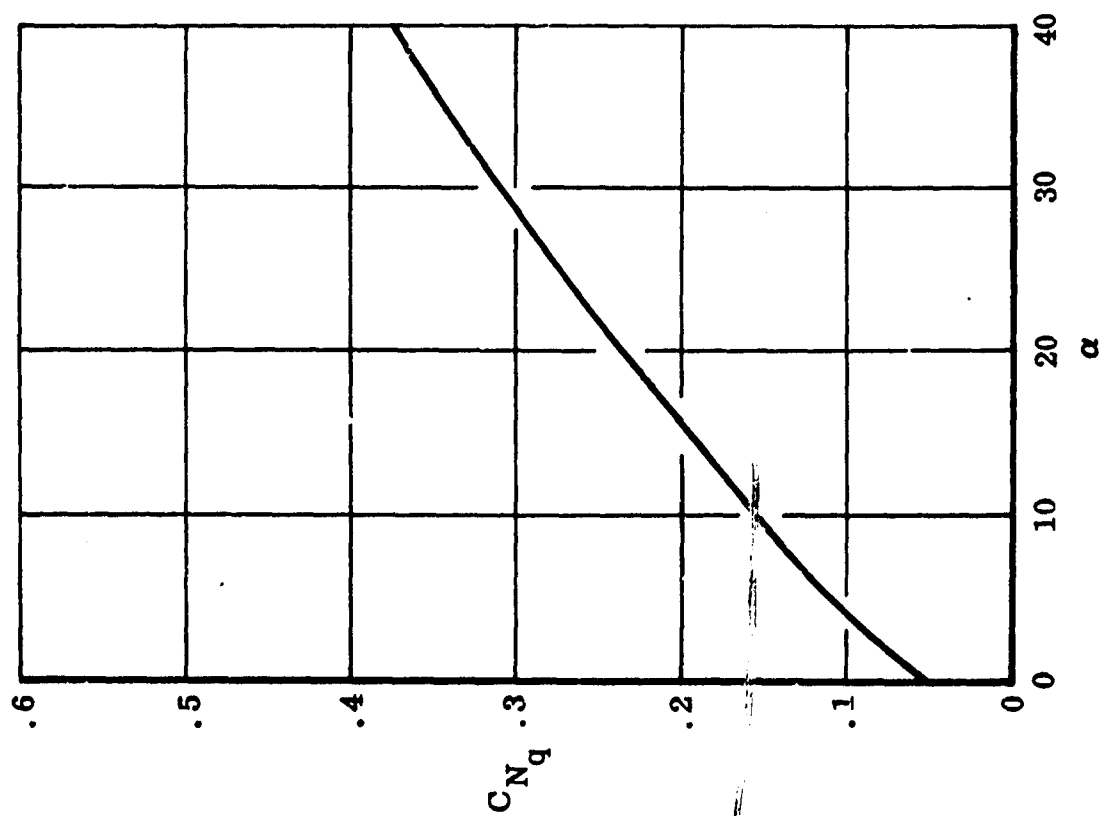


FIGURE 64. COMPUTED C_{Nq} AND C_{mq} FOR WIND TUNNEL TEST MODEL FUSELAGE

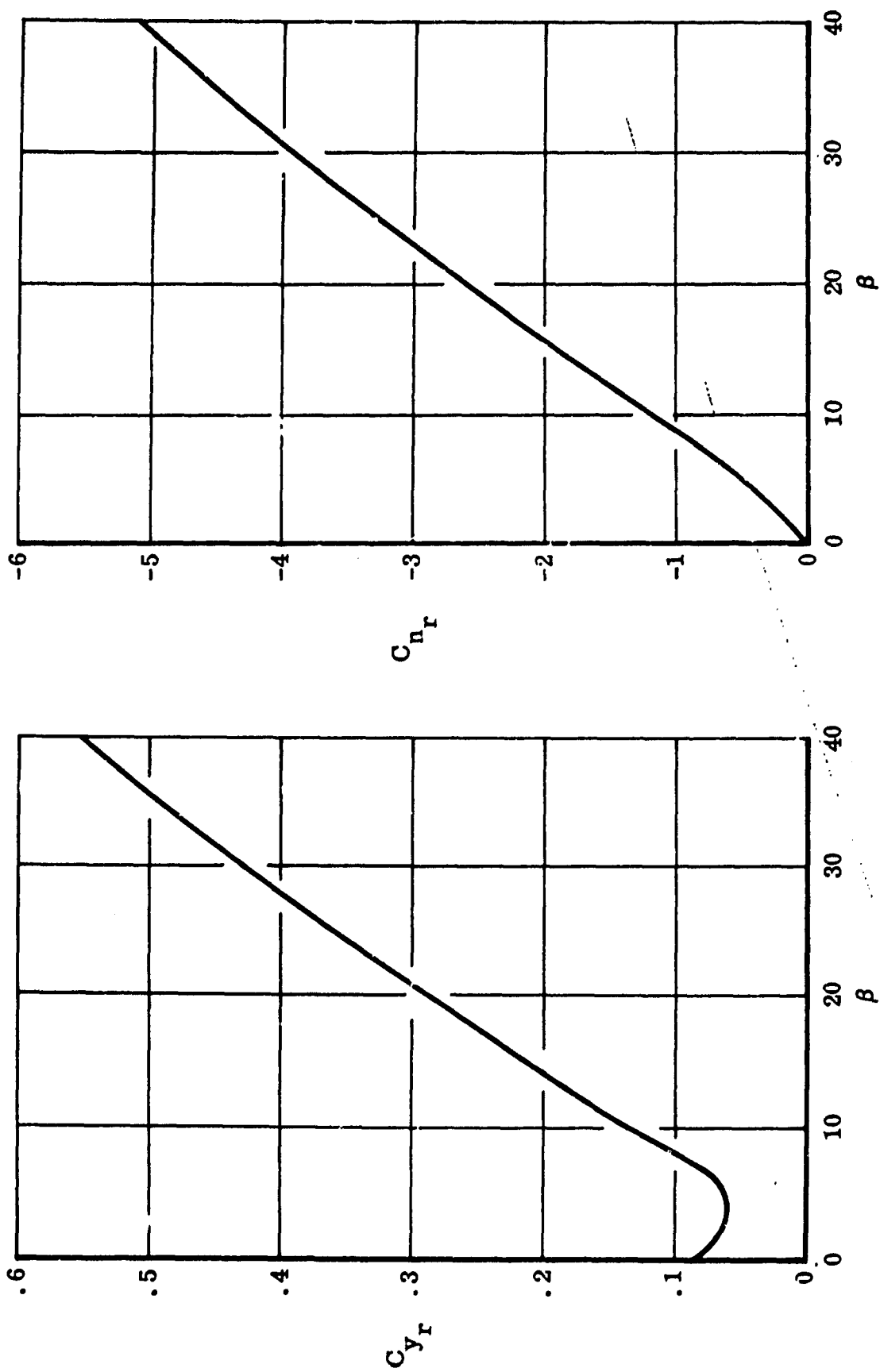


FIGURE 65. COMPUTED C_{y_r} AND C_{n_r} FOR WIND TUNNEL
TEST MODEL FUSELAGE

SECTION VII

NONLINEAR WING AERODYNAMICS

The method used for predicting the nonlinear aerodynamics of wings is that described in Section VII of Volume I. This method has been programmed for the computer and essentially converts the known section characteristics for the wing into finite wing characteristics. First the wing section characteristics have to be identified from available test data. This information is then used to obtain the positions and relative strengths of the two lifting lines. The wing planform and flight condition are included with the section model into the computer program to enable the wing aerodynamics to be determined.

1. SAMPLE PROBLEM

To illustrate the use of the nonlinear wing aerodynamics program the wing for the wind tunnel test model, described in Appendix I, will be used.

The wing planform is shown in Figure 66 with the axes system, lifting lines (discussed later) and downwash control line indicated. The wing employed a NACA 63A010 section.

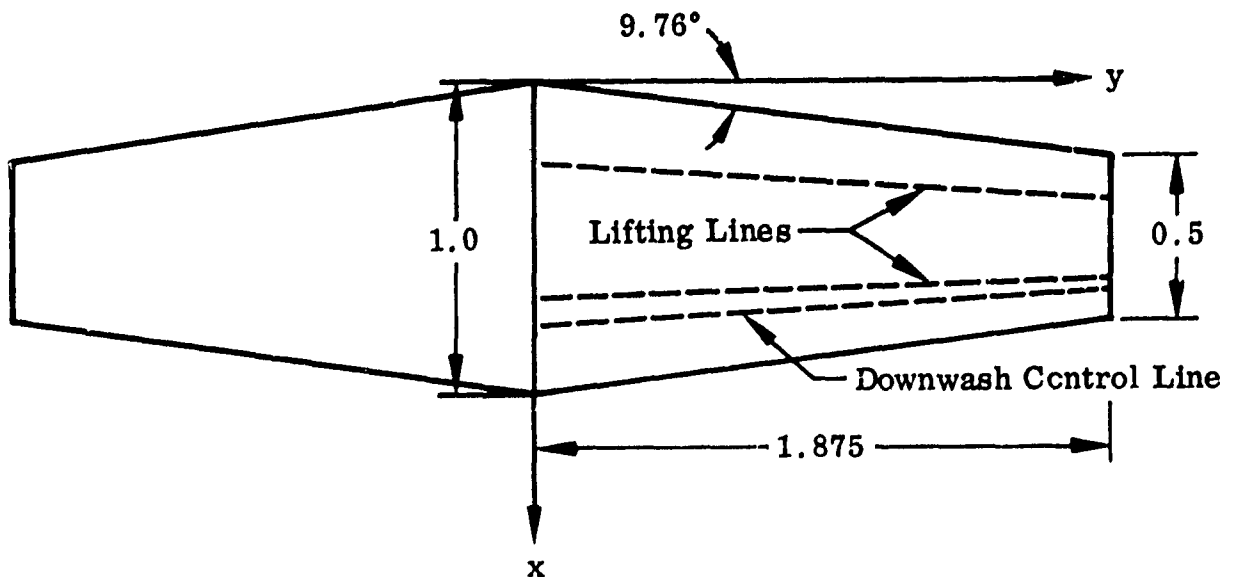


FIGURE 66. WING PLANFORM WITH LIFTING LINES AND DOWNWASH CONTROL LINE SHOWN

The axis system chosen is a right hand system with the x-axis directed aft and the z-axis directed upwards. The flight conditions for the sample problem will be $\alpha = 14^\circ$ and 16° , $\beta = 0^\circ$ with the rotary variables p , q , r all equal to zero.

a. Determination of Section Parameters

The separation characteristics of airfoil sections are a function of the Reynolds Number, R , the flow tending to separate at a lower value of α , for lower values of R . The unpowered runs in the tests described in Appendix I were at a Reynolds Number/foot = 1.3×10^6 . No data could be found for the test model wing section (NACA 63A010) for Reynolds Numbers as low as the test value. However, data for section NACA 64₁-012, with a similar section geometry, for the required values of R has been determined in Reference 10 and is tabulated in Table V.

The drag coefficient for the airfoil at $\alpha = 90^\circ$ is taken to be 2.08 (value for NACA 0012 airfoil) with the line of action passing through the chord center. The leading lifting line, in the mathematical model for the airfoil section, is positioned at the quarter chord position ($C_{m_{1/4}} = 0$ in linear α range). The downwash control point is taken to be at .75 chord. The aft lifting line is now chosen to give a good fit to the section pitching moment while satisfying the boundary condition of no flow through the section at the downwash control station and providing an exact duplication of the section normal force. In this case, by taking the aft lifting line to be located at .70 of the chord, a satisfactory representation to the section characteristics is possible as shown in Table V. The weighting function W_t (weighting of circulation between leading and aft lifting lines) is also shown in Table V. The value of W_t is needed for $\alpha = 0$ and this is determined by extrapolation of the values for larger α .

b. Inputs to Nonlinear Wing Aerodynamics Program for Sample Problem

A sample set of inputs for the nonlinear wing aerodynamics program is shown in Figure 67.

Card 1 specifies the initial value of wing angle of attack α , angle of sideslip β , and the step size in α all in degrees.

Card 2 provides wing planform information in the form of the y-coordinates (relative to the wing root chord), of the wing root and tip chords, wing taper ratio, and the tangent of the leading edge sweep angle.

Card 3 gives in order, the rolling, pitching and yawing velocities.

Card 4 contains the reference length (relative to the wing root chord), the x-

TABLE V. SECTION DATA FOR AIRFOIL SECTION

NACA 64₁-012

TEST			LIFTING LINE METHOD		
α	C_N	$C_{m\ 1/4}$	C_N	$C_{m\ 1/4}$	W_t
0	0	0.0	0.	0.	Indet.
2	0.18	0.0	0.18	0.003	0.974
4	0.36	0.0	0.36	-0.007	0.972
6	0.54	0.0	0.54	-0.013	0.970
7	0.63	-0.004	0.63	-0.016	0.969
8	0.71	-0.008	0.71	-0.020	0.967
9	0.78	-0.010	0.78	-0.025	0.962
10	0.83	-0.015	0.83	-0.032	0.953
12	0.83	-0.060	0.83	-0.051	0.914
14	0.68	-0.095	0.68	-0.079	0.807

and z- coordinates of the center of gravity location.

Card 5 contains the wing section normal force coefficient for $\alpha = 90^\circ$ and the x-coordinate of the intersection of its line of action with the airfoil chord.

Card 6 gives the number of circulation and downwash control points.

Card 7 specifies the number of angle of attacks to be computed and the number of iterations for each α .

Card 8 indicates whether the wing loading is symmetrical about the x-axis, in this case NSYM = 0 indicating symmetry. (NSYM = 1 indicates asymmetrical loading.)

Cards 9 and 10 list the y-coordinates of the circulation control points and downwash control points.

Cards 11, 12 and 13 specify the x-coordinates (relative to chord) and the tangents of the sweep angles for the leading lifting line, the aft lifting line and the line connecting the downwash control points.

Card 14 contains the effective angles of attack for the downwash control point stations. In this case the values have been determined from the previous calculations for $\alpha = 12^\circ$.

Cards 15 and 16 list the values of α in degrees at which the circulation weighting function is tabulated.

Cards 17 and 18 contain the tabulated values of the circulation weighting function determined in this case from Table V.

c. Outputs to Nonlinear Wing Aerodynamics Program for Sample Problem

Figure 68 shows the output from the computer program for the input listed in Figure 67. The flight condition is shown in the form of values for α , β and p , q , r . The spanwise loading and effective angle of attack at the spanwise stations are shown next. The normal force coefficient and the moments about the y- and x-axes follow. This output, excepting the flight condition variables, is repeated for the number of iterations on α (in this case 2).

This set of output is then repeated for the number of α 's input to the program which in this case is two.

d. Method Applicability and Limitations

The method, as presently programmed, is restricted to straight tapered wings. Because the approach uses lifting lines the method is really applicable to large aspect ratio wings and the accuracy of the predictions will not be as good for lower aspect ratio wings. Flaps may be accounted for by changing the

section characteristics for the wing. Calculations of the finite wing aerodynamic characteristics depend on a knowledge of the section characteristics so that in some cases this may be a limitation on the method. The method is programmed to calculate the effects of sideslip and the rotary derivatives although no significant attempt has been made to validate these options.

In typical calculations two iterations are used in the linear range of α and five iterations for nonlinear α . Estimates of the effective angle of attack are determined from previous computations at lower values of α . The initial calculations have usually started with $\alpha = 4^\circ$ and effective alpha equal to 2° .

2. COMPARISON WITH TEST DATA

The calculations shown in Figure 68 are for the test model described in Appendix I. The test data for these conditions for comparison were

$$\alpha = 14^\circ : C_N = .708 \quad , \quad C_{MY} = .365$$

$$\alpha = 16^\circ : C_N = .665 \quad , \quad C_{MY} = .375$$

Further calculations for an aspect ratio 6 wing are shown in Figure 69 compared with the test data of NASA TM 2-27-29A.

Results for Alpha = 14.0000, and Beta = 0.0000 Degrees

P = 0.0

Q = 0.0

R = 0.0

SPANWISE LOADING AND EFFECTIVE ALPHA

Span	.04	.20	.40	.70	.90
Loading	.7948	.717	.5523	.5131	.3498
Effective Alpha	.1506	.1537	.2444	.1474	.1070

Normal force coefficient, $C_N = .73009$

Moment coefficient about Y-axis, $C_{MY} = .35045$

Moment coefficient about X-axis, $C_{MX} = .00000$

SPANWISE LOADING AND EFFECTIVE ALPHA

Span	.04	.20	.40	.70	.90
Loading	.8035	.7123	.5513	.5141	.3548
Effective Alpha	.1571	.1558	.2444	.1514	.1093

Normal force coefficient, $C_N = .73245$

Moment coefficient about Y-axis, $C_{MY} = .35268$

Moment coefficient about X-axis, $C_{MX} = .00000$

Results for Alpha = 16.0000, and Beta = 0.0000 Degrees

P = 0.0

Q = 0.0

R = 0.0

SPANWISE LOADING AND EFFECTIVE ALPHA

Span	.04	.20	.40	.70	.90
Loading	.8905	.7586	.5307	.5479	.3951
Effective Alpha	.1882	.1790	.2793	.1735	.1214

Normal force coefficient, $C_N = .76861$

Moment coefficient about Y-axis, $C_{MY} = .38258$

Moment coefficient about X-axis, $C_{MX} = .00000$

SPANWISE LOADING AND EFFECTIVE ALPHA

Span	.04	.20	.40	.70	.90
Loading	.8875	.7549	.5298	.5470	.3938
Effective Alpha	.1983	.1791	.2793	.1735	.1207

Normal force coefficient, $C_N = .76637$

Moment coefficient about Y-axis, $C_{MY} = .38263$

Moment coefficient about X-axis, $C_{MX} = .00000$

FIGURE 68. SAMPLE OUTPUTS FOR NONLINEAR WING AERODYNAMICS PROGRAM

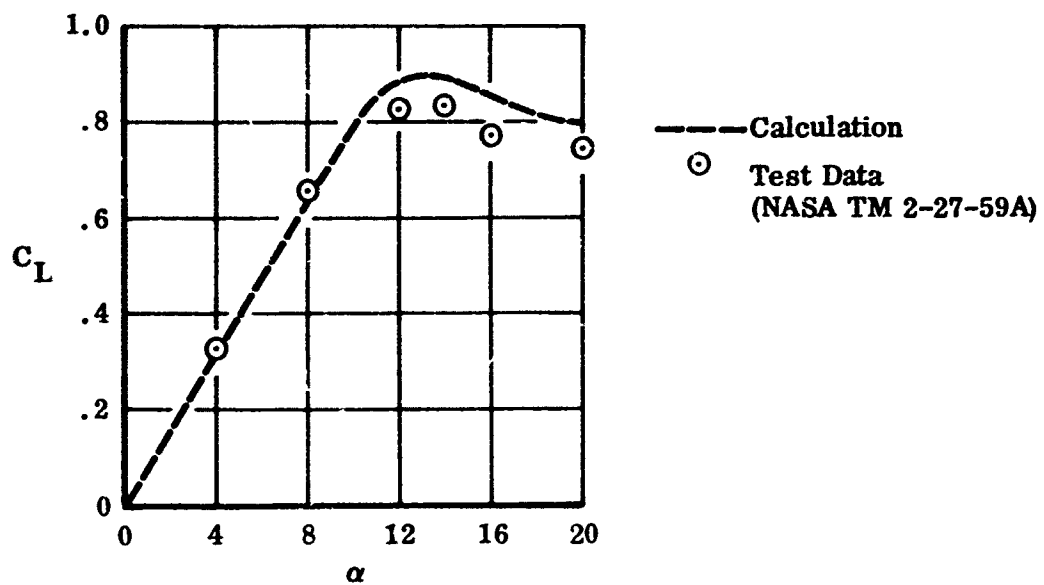


FIGURE 69. WING CALCULATIONS FOR AN ASPECT RATIO 6 WING

APPENDIX I

WIND TUNNEL TESTING OF V/STOL CONFIGURATION MODEL

A model was constructed and tested to supplement the analytical investigation and gain further data for use in validation and improvement of the analytical prediction techniques. The model was configured to resemble a feasible military aircraft but was designed to operate with jets of varied number and location to allow a variety of data to be generated. The test contributes new data because of extensive pressure instrumentation present on the model. These data facilitate identification of the sources of the various induced loads measured during the test.

1. MODEL AND APPARATUS

The model is a shoulder wing configuration equipped with an external airfoil flap and a stabilator mounted on the vertical tail above the fuselage. Two vectored thrust engines are contained in large nacelles mounted beneath the wing adjacent to the fuselage; a single lift engine is mounted within the body and forward of the vectored exits. The general arrangement of the model is shown in the three view drawing of Figure I-1 and the photographs of Figures I-2, I-3, and I-4. Detailed geometrical data are given in Table I-I.

The vectored thrust engines were simulated by ejector type jet engine simulators. Two 3.67-inch diameter nozzles were tested at two longitudinal positions (11 and 111 percent \bar{c}) at nominal deflections of 0, 45, or 90 degrees at the forward location, and 45 or 90 degrees at the aft location. Larger 4.5-inch diameter nozzles were tested in the aft position at a nominal deflection of 90 degrees. Plugs were used to seal the inlets when inlet flow was not desired.

Typical operating curves for the ejectors are shown in Figure I-5. The design of the ejector nozzles produced a relatively nonuniform jet velocity profile, shown in Figure I-6.

Preceding page blank

The lift jet was simulated by a convergent nozzle supplied through a perforated plate. The exit diameter was 2.25 inches. No inlet simulation was provided. The lift jet possessed a relatively uniform exit profile, shown in Figure I-6.

Details of jet exit location and point of application of resultant forces are shown in Table I-II in terms of location along the mean aerodynamic chord and distance below the wing plane.

The engine simulators were driven by cold dry air supplied through a common plenum fed by a flexible metal tube passing through the sting.

Model forces and moments were recorded using a six-component internal balance.

Two hundred and sixty-four pressure taps are present on the left half of the model. They are placed in four groups: a wing pattern, a lower fuselage pattern, a circumferential pattern at five fuselage stations, a nacelle centerline pattern. Lower fuselage and wing pressure patterns are described in Tables I-III and I-IV. Circumferential fuselage and nacelle centerline patterns are shown in Figures I-7 and I-8.

A seven-probe flow angularity rake was sometimes mounted at the tail station in place of the empennage. Its general arrangement may be seen in Figure I-2.

Testing was performed in the NASA Langley V/STOL tunnel which has a test section of 14 X 22 feet.

2. TEST PROCEDURE

Testing of the model was performed in two phases: calibration of balance and engine simulators, and aerodynamic testing within the wind tunnel.

a. Balance Calibration and Corrections

The testing of a powered model requires additional balance calibration and correction beyond that routinely performed during unpowered testing. The air supply balance arrangement used during this test is indicated schematically in Figure I-9.

Although the air supply line is designed to be highly flexible and cause minimum interference with force measurements, corrections must be applied to balance measurements to reflect that portion of the total load which is carried by the line. A series of known loads was applied to the balance-air supply line assembly, and the resultant balance measurements were used to obtain a matrix of linear correction coefficients.

Pressurization of the system caused forces to be exerted on the model by the flexible supply line. These forces were measured and calibrated with the plenum sealed and no nongravitational loads applied to the model. The calibrated forces have been removed from final force data.

The final form of the corrections is shown below. The momentum input due to the supply mass flow was found to be negligible.

$$\tilde{F}_{cor} = \tilde{K} \tilde{F}_{bal} - \tilde{F}_p(P_{sup})$$

where

\tilde{F}_{cor} , a 6x1 matrix of applied loads

\tilde{K} , a 6x6 matrix of correction coefficients

\tilde{F}_{bal} , a 6x1 matrix of loads measured by balance

$\tilde{F}_p(P_{sup})$, a 6x1 matrix of loads applied by the air supply line, calibrated against supply pressure

Additional details concerning the magnitude and accuracy of the corrections may be found in Appendix II.

b. Calibration of Engine Simulators

Each engine simulator-nozzle combination was tested individually to determine direct thrust force and moment applied to the model. The same air supply-balance assembly used during tunnel tests was used for this calibration. A calibrated bell-mouth was used to monitor ejector inlet flow. A limited survey was made of nozzle exit profiles to determine their basic character.

These tests were performed with the units mounted on the bare model plenum to minimize static interference effects by reducing surface area near the exits. Some small interference is of necessity present in the data because of the physical proximity of the external portions of the nozzles and drive system.

Lift jet thrust was calibrated on the basis of total pressure within the nozzle. Ejectors were calibrated as a function of primary nozzle plenum pressure. No corrections were made to ejector calibrations due to forward speed present in the tunnel. Error due to this approximation is examined in Appendix III.

c. Wall Corrections

No corrections were made to the data for possible wall effects. The dimensions of the 14 X 22 foot test section are quite large in comparison to basic model dimensions, and computations, made prior to the test using Heyson's method ⁽¹¹⁾, indicated that wall interference effects would be within the accuracy of the data acquisition system. However, the pitch mechanism used during the test was not capable of maintaining the model at a fixed position within the test section, causing the model to be nearer the floor at the lowest angle of attack tested. An investigation was made to determine if the ground effect of the floor, the nearest surface, was causing any significant effect on the model. The wing-body-nacelle-tail was equipped with the large exits, pitched to a 6 degree angle, and tested at various forward speeds at different heights. An effect was observed at the lowest forward speed tested but not at higher speeds nor statically (see Figure I-10). The minimum model height during normal testing was 42 inches. The nondimensionalized minimum height shown below indicates that the large exits will show the most severe interference at lower angles of attack and low forward speed. The order of magnitude may be one to three percent of total load.

Nozzle	Lift Jet	Small Vector	Large Vector
h/D	13.7	11.4	9.3

d. Test Parameters

The testing of powered models creates a requirement for a parameter relating propulsive and aerodynamic forces. The effective velocity ratio as used in this series of tests is the square root of the ratio of freestream unit momentum flux to mean jet unit momentum flux. It is obtained from the following expression:

$$V/V_J = \left[\frac{\rho_\infty U_\infty^2}{\rho_J U_J^2} \right]^{0.5} = \left[\frac{Q}{T/2A_J} \right]^{0.5}$$

Another parameter, a relative measure of propulsive and aerodynamic forces, is the thrust coefficient - the ratio of thrust to the product of freestream dynamic pressure and wing area.

$$C_T = T/QS$$

The two parameters are related in the manner shown below.

$$V/V_j = \left[\frac{2 A_j / S}{C_T} \right]^{0.5}$$

The effective velocity ratio is used as the prime parameter of this report because it is less related to the geometry of the particular configuration being considered, and it better describes the state of the highly deflected jet.

c. Test Program

The model was constructed such that nacelles, lift engine, wing, and empennage could be mounted on the fuselage in any combination. Complete model buildups were performed for the wing-body-nacelle-tail configuration powered by the two ejectors in the forward position, and for the wing-body-tail powered by the lift jet. Emphasis was placed on the wing-body nacelle powered by the two ejectors with nozzles in the forward or aft position, and the wing-body without nacelles powered by the lift jet.

A standard series of runs was used throughout the test although not all configurations were tested at all conditions. The series, shown in Table I-V, consists of an unpowered angle-of-attack variation, followed by angle-of-attack variation at several velocity ratios, and velocity ratio variation at fixed angles of attack. A similar pattern was adopted for runs involving sideslip. Both force and pressure data were recorded for most runs.

The range of variables tested included angle-of-attack variations of 0 to 20 degrees, angles of sideslip from 0 to ± 12 degrees, and velocity ratios of 0 to .3 for lift jet powered configurations and 0 to .5 for ejector powered configurations. Very limited testing was performed at combined angles of attack and sideslip. Testing was accomplished at dynamic pressures of 0 to 71 psf, resulting in Reynolds numbers of up to 1.5×10^6 per foot.

Dynamic pressure and thrust combinations used to achieve these velocity ratios are listed in Table I-VI. Because of tunnel velocity limits, higher velocity ratios were obtained with the use of reduced thrust. Note that these are nominal values. In general, actual thrust levels were slightly lower than those shown.

A summary of configurations tested is given in Table I-VII.

3. Results

The results of this test are presented in various sections of this report in support of the development and verification of analytical prediction techniques. Complete results will be published in two NASA Technical Memorandums at a later date.

a. Presentation of Results

The force data recorded during the test are presented in several forms:

- (1) Body axis aerodynamic coefficients.
- (2) Stability axis aerodynamic coefficients.
- (3) Forces and moments nondimensionalized by thrust.
- (4) Forces and moments with direct thrust effects removed, nondimensionalized by thrust.
- (5) Forces and moments with direct thrust effects removed, nondimensionalized by dynamic pressure.

In the reduction of aerodynamic coefficients, forces were nondimensionalized by the product of freestream dynamic pressure and wing area. Longitudinal moments were nondimensionalized by the product of freestream dynamic pressure, wing area, and wing mean aerodynamic chord length; lateral moments were nondimensionalized by the product of freestream dynamic pressure, wing area, and wing span.

In the reduction of thrust coefficients, forces were nondimensionalized by the total calibrated thrust of all nozzles operating. Moments were nondimensionalized by the product of total thrust and an effective diameter. The effective diameter is defined as the diameter of a circle equivalent in area to the sum of the exit areas of the operating nozzles.

Thrust removed coefficients were obtained by removing the forces and moments of the operating engine simulators, as determined during static calibration, from the balance measured loads prior to nondimensionalization.

b. Selection of Unpowered Baseline Data

Analysis of the vectored thrust configuration tests has revealed that significant differences exist in unpowered data taken with the ejector inlets open and closed. These differences exceed those directly attributable to vectoring or freestream flow

through the undriven ejectors. When these data are used to obtain an interference effect due to jet operation, two significantly different answers result, dependent on which "unpowered" coefficient is used in the calculations.

$$\begin{bmatrix} \text{interference} \\ \text{effect} \end{bmatrix} = \begin{bmatrix} \text{total} \\ \text{load} \end{bmatrix} - \begin{bmatrix} \text{direct} \\ \text{thrust} \end{bmatrix} + \begin{bmatrix} \text{unpowered} \\ \text{aerodynamics} \end{bmatrix}$$

The effect of the open versus the closed inlet on the power off longitudinal aerodynamic coefficients is shown in Figure I-11 as a function of nozzle deflection angle. Opening of the inlet produces a lift increment of 0.216 with the forward small nozzles deflected 90 degrees. The portion of this increment attributable to momentum change of the free flow passing through the ejectors and nozzles may be found using Figures I-12 and I-13. The unpowered inlet weight flow is found to be 0.46 lbs/sec/ejector producing an estimated vertical force of 2.43 lbs. This is equivalent to a lift coefficient of only 0.018. Thus, the large part of the inlet lift increment cannot be attributed to flow-through momentum, but must be due to interference with the external aerodynamics.

Powered lift data, nondimensionalized by thrust and shown in Figure I-14, do not reflect the significant differences caused by the open inlet in the unpowered data. The difference in powered lift is seen to remain approximately constant at various velocity ratios and, in general, it is small in comparison to the lift loss equivalent to the aerodynamic coefficient increment obtained from power off data. In contrast, the change in inlet mass flow ratio produced by opening the inlet is greater for the powered case than for the unpowered case.

Further examination of the unpowered data, as presented in Figure I-15, indicates that the longitudinal coefficients of the inlet open configurations are functions of nozzle deflection angle while those of the inlet closed configuration are not. This observation in combination with the lack of difference in powered data suggests that the unaccounted inlet increment may be due to the exit interactions of the inlet mass flow as opposed to the variation of the inlet condition per se. This conclusion must be considered tentative, however, because the inlet mass flow ratio as well as the exhaust exit angle are varied by nozzle deflection. An examination of the pressure data for this configuration will give more insight to the cause of the open inlet effect on power off data.

Wing pressure differentials are shown for both inlet conditions in Figure I-16. Opening of the inlets causes a pressure change similar to that produced by a positive angle of attack. Examination of both upper and lower surface pressures at WS 10.55,

Figure I-17, indicates that the effect is present on both surfaces, confirming that opening of the inlets induces a positive angle of attack change of one to two degrees across the wing, and that the effect is not limited to one of the surfaces.

Pressure distributions about the six fuselage stations are shown in Figure I-18. The data are shown as a locus of pressure normals about the local fuselage contour. Lines within the section indicate positive pressures; lines outside the section indicate negative pressures. At interior corners of the body some data have been eliminated for clarity. The effects of the open inlet on fuselage pressures are noted below.

At the most forward station FS 7.3, the pressure change is similar to that which would be produced by a positive angle of attack of approximately two degrees. Changes occur on both upper and lower surfaces.

In front of the nacelles at FS 11.8, pressure changes on the fuselage sides are dominated by apparent changes in nacelle blockage.

Lower fuselage and nacelle pressures are made more positive in front of the nozzles at stations 11.8 and 19.65. Upper surface pressures are not affected at these stations.

Aft of the nozzles and nacelles at FS 26.425, opening of the inlets induces a more negative pressure on the lower fuselage sides; other areas are not strongly affected. No data are available on the upper surface of the fuselage at this station.

At FS 34.30, a more negative pressure is induced about the section due to opening of inlets.

Upper nacelle centerline pressures, shown in Figure I-19, are unaffected except in the vicinity of the inlet lip. Lower surface pressures are made more positive in the vicinity of the exit.

Lower fuselage centerline data, Figure I-20, indicate that opening of the inlets creates more positive pressures ahead of the exit and more negative pressures aft of the exit.

Data from the tail flow angularity rake indicate increased downwash when the inlets are open, Figure I-21.

In summary, opening of the inlets produces:

- (1) An induced positive angle of attack on the wing.
- (2) An induced positive angle of attack at the nose.
- (3) Positive pressure increments on the lower fuselage and nacelle ahead of the exits.
- (4) Negative pressure increments aft of the exits.
- (5) Little effect on upper fuselage pressures.
- (6) Increased downwash at the tail station.

These flow changes are consistent with those associated with jet exit interference effects at high velocity ratios and tend to confirm the initial observation that the "inlet" effect is largely caused by the exit of the inlet flow.

Further confirmation can be gained by observation of lower fuselage centerline pressures for the configuration equipped with the large aft nozzles. It can be seen in Figure I-22 that the largest effect of the open inlet occurs in the vicinity of the exit not the inlet. If the differential lower centerline pressures due to the opening of the inlet are plotted against distance from the exit as in Figure I-23, it is seen that data for the forward small 90 degree nozzle and the aft large 90 degree nozzle show a surprisingly strong correlation.

It is concluded that the proper unpowered data for the vectored thrust configurations are that taken with the inlets closed. Data taken with the inlets open, though the model was unpowered in the sense that no drive pressure was supplied to the ejectors, are in fact power on data at a very high velocity ratio, $V/V_j = 2.9$ for the small forward 90 degree nozzle which has been discussed.

TABLE I-I. MODEL PROPERTIES AND DIMENSIONS

Wing:

Span, b	40.25 in
Area (projected), S	324.00 in ²
Mean aerodynamic chord, \bar{c}	8.35 in
Location of 25% \bar{c}	
F.S.	23.83 in
W.L.	3.555 in
B.L.	\pm 8.94 in
Taper ratio, λ	0.50
Aspect ratio, AR	5.00
Airfoil section	63A010
Leading edge sweep, Λ_{LE}	9.76 deg
Quarter chord sweep, $\Lambda_{c/4}$	5.96 deg

Horizontal Tail:

Span, b_H	22.40 in
Area (projected), S_H	110.72 in ²
Mean aerodynamic chord, \bar{c}_H	5.14 in
Location of 25% \bar{c}_H	
F.S.	44.22 in
W.L.	6.62 in
B.L.	5.00 in
Taper ratio, λ_H50
Aspect ratio, AR_H	4.50
Airfoil section	63A008
Leading edge sweep, Λ_{LEH}	13.40 deg
Quarter chord sweep $\Lambda_{c_{H/4}}$	8.86 deg

Vertical Tail:

Span (centerline), b_v	11.00 in
Span (exposed), b_{ve}	9.00 in
Area (exposed), S_v	71.10 in ²
Mean aerodynamic chord (exposed), \bar{c}_v	8.66 in

TABLE I-I. MODEL PROPERTIES AND DIMENSIONS (CONTINUED)

Location 25% \bar{c}_v

F.S.	43.93 in
W.L.	7.25 in
B.L.	0.00 in
Taper ratio (exposed), λ_v26
Aspect ratio (exposed), AR_v	4.56
Airfoil section	63A008
Leading edge sweep, Λ_{LE_v}	42.9 deg
Quarter chord sweep, $\Lambda_{c_v/4}$	34.0 deg

Flap:

Span, b_F	0.65 wing span
Chord, c_F	0.25 local wing chord
Deflection, δ_F	45.0 deg
Airfoil Section	

FLAP ORDINATES		
x/c	y_u/c	y_b/c
0	.0350	-.0350
.0125	.0544	-.0194
.0250	.0650	-.0150
.0500	.0788	-.0094
.0750	.0888	-.0063
.1000	.0950	-.0013
.1500	.1069	-.0003
.2000	.1138	0
.3000	.1169	0
.4000	.1138	0
.5000	.1050	0
.6000	.0913	0
.7000	.0738	0
.8000	.0525	0
.9000	.0281	0
.9500	.0150	0
1.0000	.0013	0

Overlap	0.01 c
Gap	0.02 c

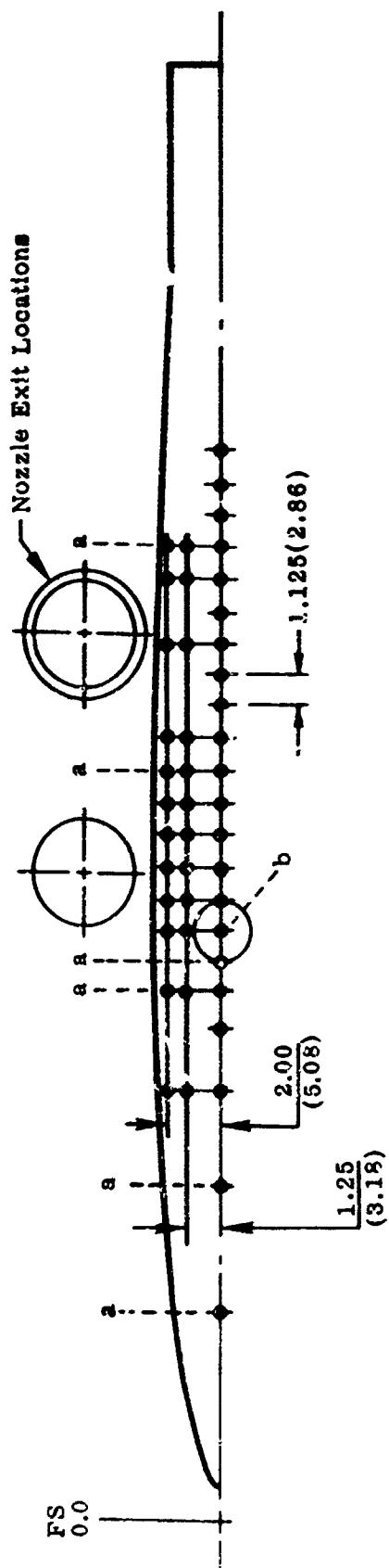
Location of moment center:

F.S.	23.82 in
W.L.	0.00 in
B.L.	0.00 in

TABLE I-II. JET EXIT LOCATION

Diameter in. (cm)	Position	Nominal Deflection degrees	Y/(b/2)	Geometric Center		True Deflection degrees	Line of Force	
				$\Delta X/\bar{c}$	$\Delta Z/D$		$\Delta X/\bar{c}$	$\Delta Z/D$
2.25 (5.72)	—	90	.000	-.112	2.949	90.13	-.135	2.949
3.67 (9.32)	Forward	0	±.251	.068	.743	-1.16	.068	.778
		45	±.251	.036	.938	40.14	.040	.929
		90	±.251	.122	1.410	85.15	.172	1.410
3.67 (9.32)	Aft	45	±.251	1.041	.938	39.09	1.057	.901
		90	±.251	1.127	1.410	85.01	1.160	1.410
4.5 (11.43)	Aft	90	±.251	1.127	1.244	85.46	1.151	1.244

Note: ΔX — Distance aft of leading edge of mean aerodynamic chord
 ΔZ — Distance below wing
D — Nozzle diameter



Port Numbers				
$\frac{X}{L_f}$	Fuselage Station		Butt Line	
	in.	cm	0	1.25 (3.18) (5.04)
.1460	7.300	18.542	a	
.2360	11.800	29.972	a	
.3035	15.175	38.545	128	129
.3485	17.425	44.260	131	
.3710	18.550	47.117	a	
.3935	19.675	49.975	144	
.4160	20.800	52.832	145b	146
.4385	21.925	55.690	148	149
.4610	23.050	58.547	151	152
.4835	24.175	61.404	154	155
.5069	25.300	64.262	157	158
			159	159

Note: a -- See Figure I-7.

b -- Not present when lift jet is mounted.

Port Numbers				
$\frac{X}{L_f}$	Fuselage Station		Butt Line	
	in.	cm	0	1.25 (3.18) (5.04)
.5285	26.425	67.120	a	
.5510	27.550	69.977	175	174
.5715	28.675	72.834	176	175
.5969	29.800	75.692	177	
.6135	30.925	78.550	178	179
.6410	32.050	81.407	181	
.6635	33.175	84.265	182	183
.6860	34.300	87.122	a	
.7085	35.425	89.980	186	
.7310	36.550	92.837	197	
.7535	37.675	95.694	198	

TABLE I-III. LOCATION OF PRESSURE PORTS ON LOWER FUSELAGE

TABLE I-IV. WING PRESSURE PORTS

Chord %	Surface	Port Numbers			
		Spanwise Location $y/(b/2)$			
		0.25*	.39	.52	.80
0.0	-	1	24	47	70
1.0	U	2	25		
	L	13	36		
1.5	U			48	
	L			59	
2.5	U	3	26	49	71
	L	14	37	60	81
5.0	U	4	27	50	72
	L	15	38	61	82
10.0	U	5	28	51	73
	L	16	39	62	83
15.0	U	6	29	52	74
	L	17	40	63	84
25.0	U	7	30	53	75
	L	18	41	64	85
40.0	U	8	31	54	76
	L	19	42	65	86
55.0	U	9	32	55	77
	L	20	43	66	87
70.0	U	10	33	56	78
	L	21	44	67	88
85.0	U	11	34	57	79
	L	22	45	68	89
95.0	U	12	35	58	80
	L	23	46	69	90

Note: U - Upper Surface
L - Lower Surface
* - Nacelle Centerline

TABLE I-V. RUN SEQUENCE

Velocity Ratio	Angle of Attack	Angle of Sideslip
	Degrees	Degrees
Unpowered	0 to 20	0
0.3	0 to 20	0
0.2	0 to 20	0
0.1	0 to 20	0
0 to 0.3/0.5	0	0
0 to 0.3/0.5	10	0
Unpowered	0	-12 to 12
0.3	0	-12 to 12
0.2	0	-12 to 12
0.1	0	-12 to 12
0 to 0.3/0.5	0	-8
0 to 0.3/0.5	0	8

TABLE I-VI TEST CONDITIONS

EJECTORS
3.67-inch D Nozzles

EJECTORS
4.5-inch D Nozzles

LIFT JET
2.25-inch D Nozzle

HIGH THRUST

LOW THRUST

V/V_j	Q	T
	psf	lb
0.00	0.00	140
0.10	4.76	140
0.15	10.71	140
0.20	19.05	140
0.25	29.76	140
0.30	42.86	140
0.40	60.00	110
0.50	60.00	70.5

V/V_j	Q	T
	psf	lb
0.00	0.00	30
0.10	2.86	80
0.15	6.43	80
0.20	11.40	80
0.25	17.86	80
0.30	25.70	80
0.40	45.60	80
0.45	58.00	80
0.50	71.40	80

V/V_j	Q	T
	psf	lb
0.00	0.00	177
0.10	4.00	177
0.20	16.00	177
0.30	36.00	177
0.39	60.00	177

V/V_j	Q	T
	psf	lb
0.00	0.00	80
0.10	14.43	80
0.15	32.60	80
0.20	57.96	80
0.20	26.67	37
0.25	41.66	37
0.30	60.00	37

LIFT JET WITH EJECTORS, 3.67-inch D Nozzles

TOTAL		
V/V_j	Q	T
	psf	lb
0.00	0.00	188
0.09	4.76	188
0.14	10.71	188
0.19	19.05	188
0.24	29.76	188
0.28	42.86	188
0.38	60.00	143
0.50	60.00	84.2

EJECTOR	
V/V_j	T
	lb
0.00	140
0.10	140
0.15	140
0.20	140
0.25	140
0.30	140
0.40	110
0.50	70.5

LIFT JET	
V/V_j	T
	lb
0.00	48
0.07	48
0.11	48
0.15	48
0.19	48
0.22	48
0.32	32.5
0.49	13.7

POWER CONFIGURATION	VEHICLE CONFIGURATION				
	BODY	BODY-WING	BODY-WING-TAIL	BODY-WING-FLAP	BODY-WING-TAIL & FLAP
LIFT JET	AB	AB	AT		
FOR VECTOR DEF 0° 45° 90°	AB	A A AT	A A ABT	A A	A
AFT VECTOR DEF 0° 45° 90°		A AB		A	A
AFT VECTOR 4.5" 90°		A			
LIFT & FOR VECTOR DEF 90°		AB			
LIFT JET & AFT VECTOR DEF 90°		AB			
<p>note: A - longitudinal data E - lateral data T - stabilator effectiveness</p>					

TABLE I-VII. TEST PROGRAM SUMMARY

[illegible]

FIGURE I-1. MODEL GENERAL ARRANGEMENT



FIGURE I-2. WING-BODY-NACELLE WITH TAIL FLOW ANGULARITY
RAKE, POWERED BY SMALL FORWARD NOZZLES

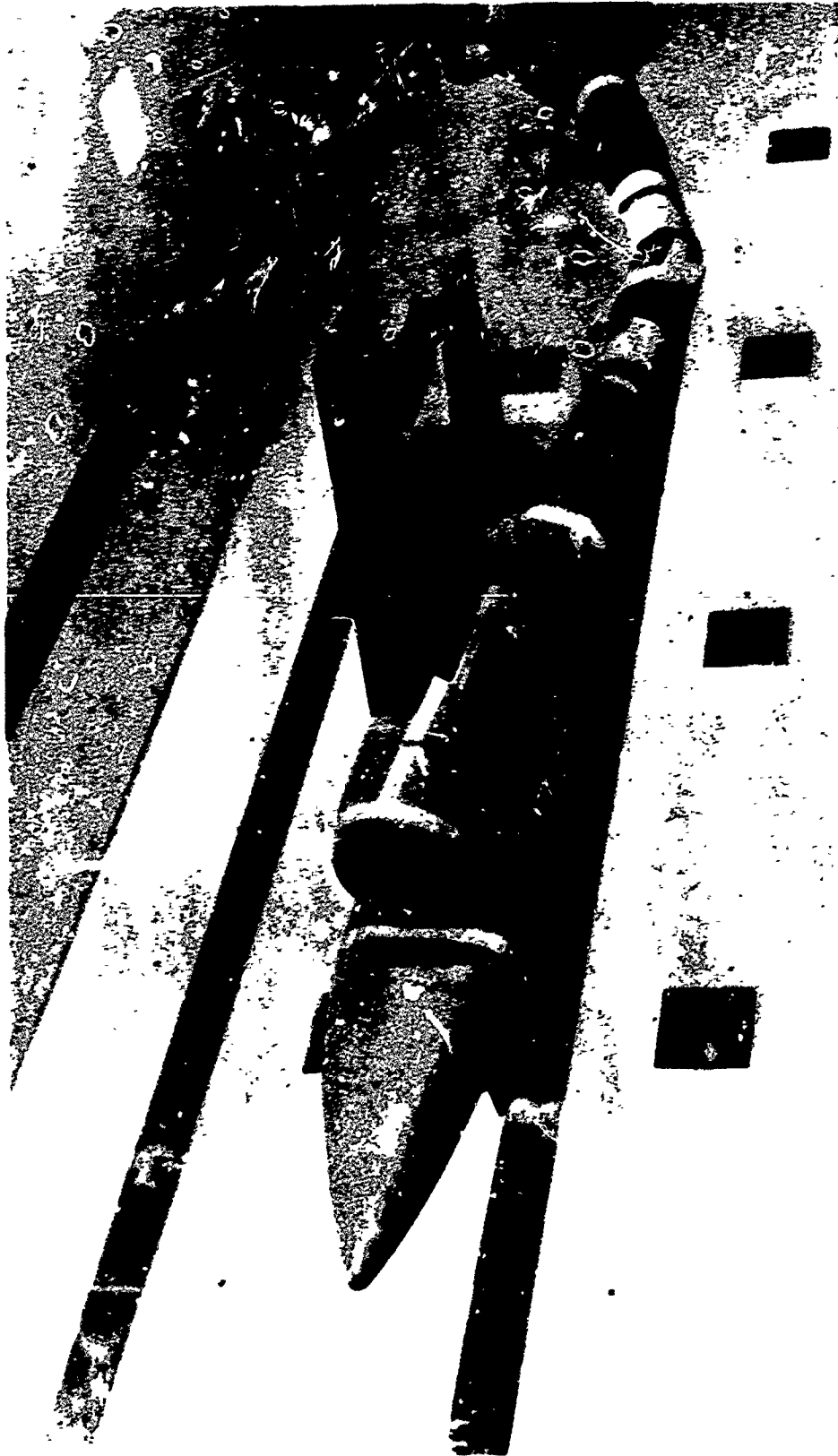


FIGURE I-3. WING-BODY-NACELLE TAIL WITH FLAP, POWERED BY
AFT SMALL NOZZLES



FIGURE I-4. WING-BODY-TAIL, POWERED BY LIFT JET

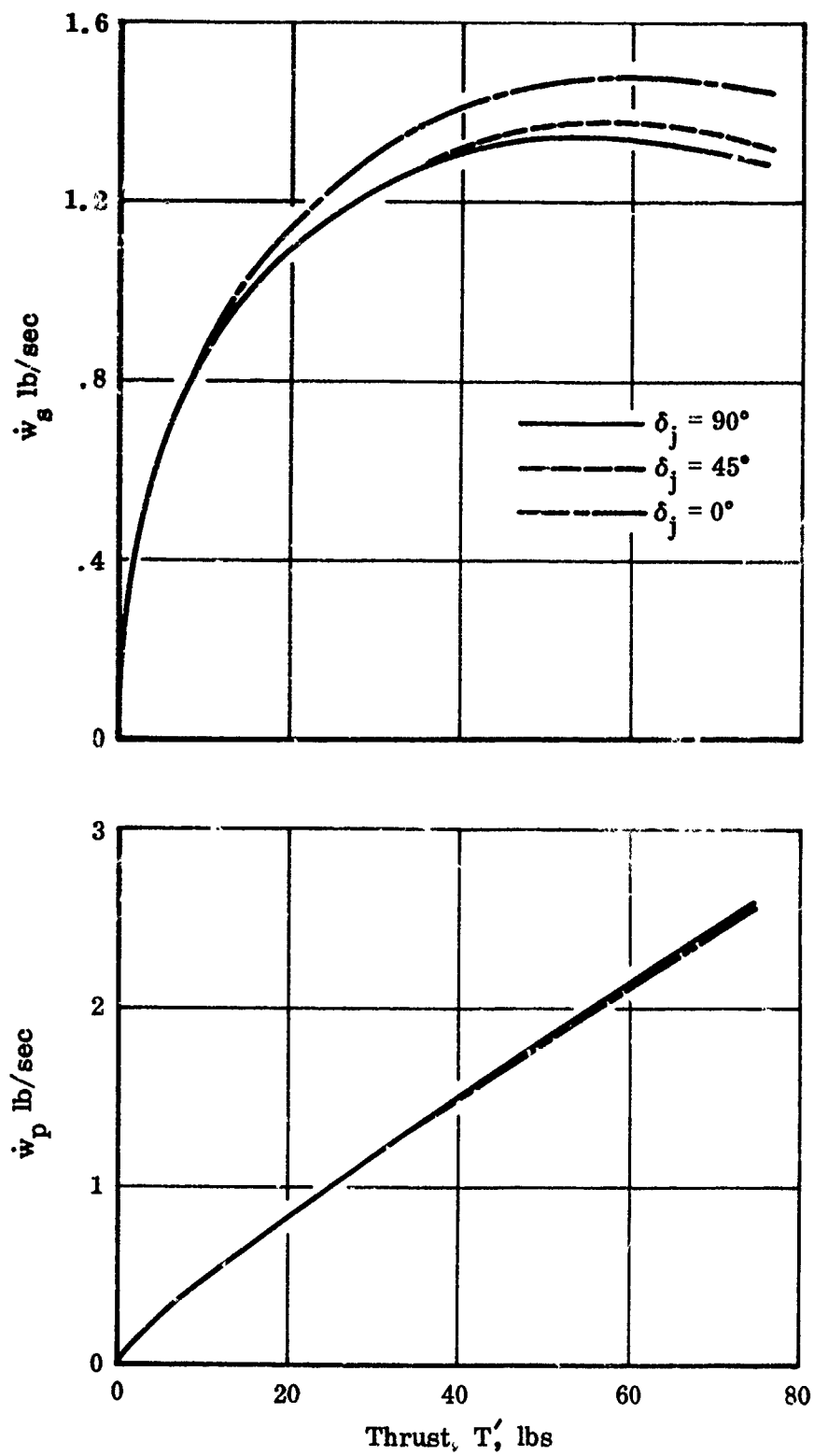


FIGURE I-5. EJECTOR OPERATING CHARACTERISTICS
a. FORWARD SMALL NOZZLES

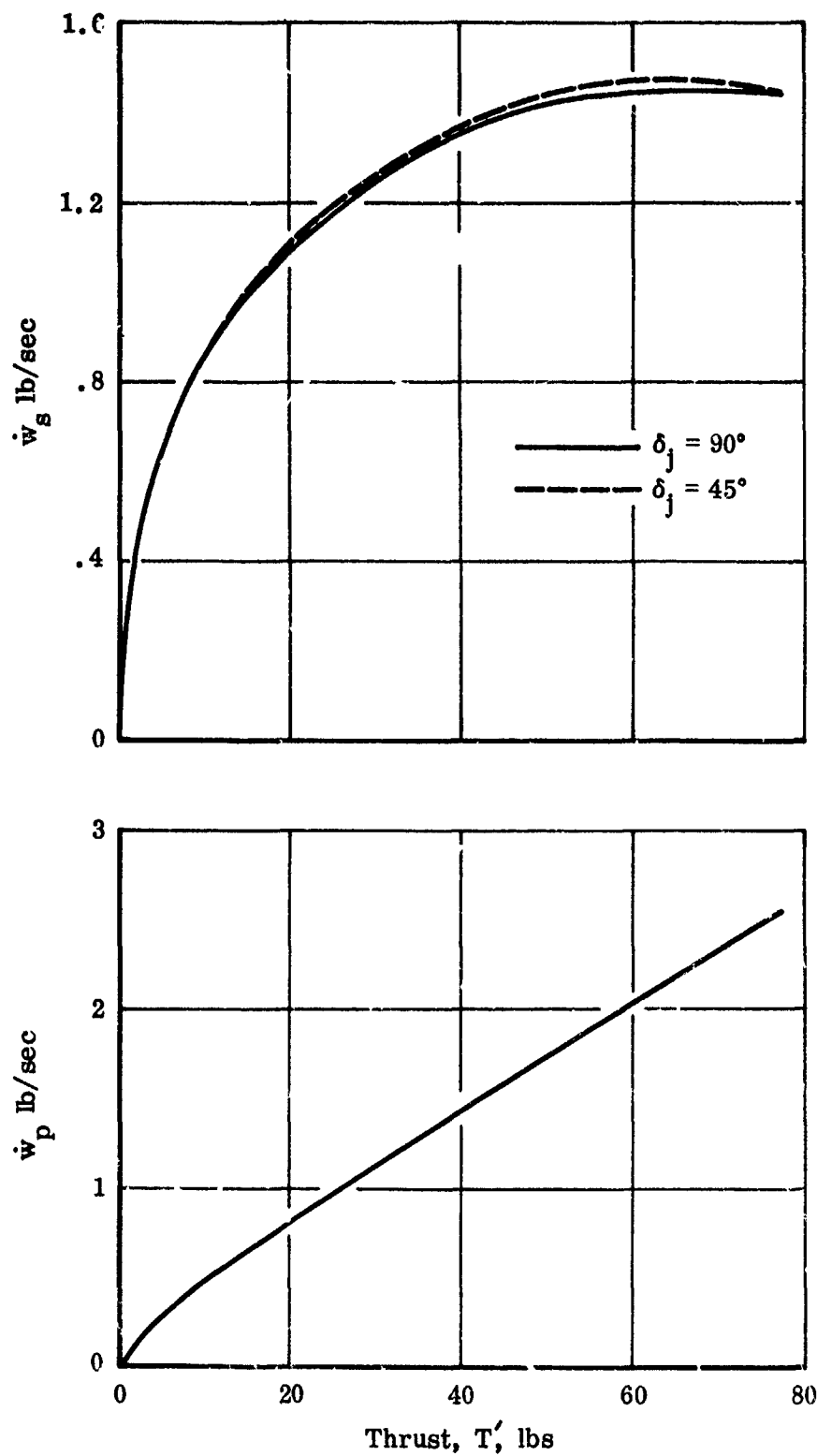


FIGURE I-5 (cont.) EJECTOR OPERATING CHARACTERISTICS
b. AFT SMALL NOZZLES

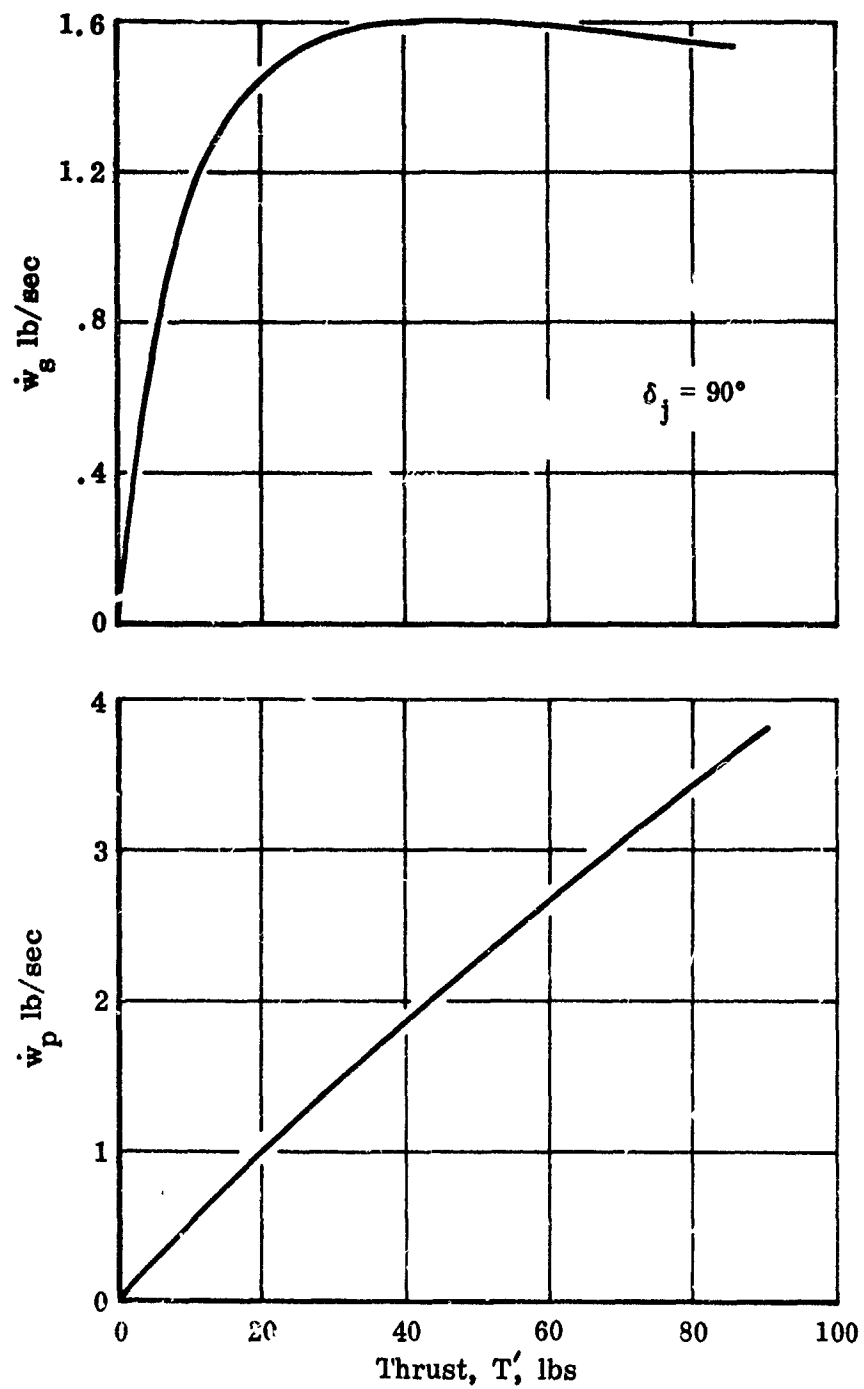


FIGURE I-5 (concluded). EJECTOR OPERATING CHARACTERISTICS
c. AFT LARGE NOZZLES

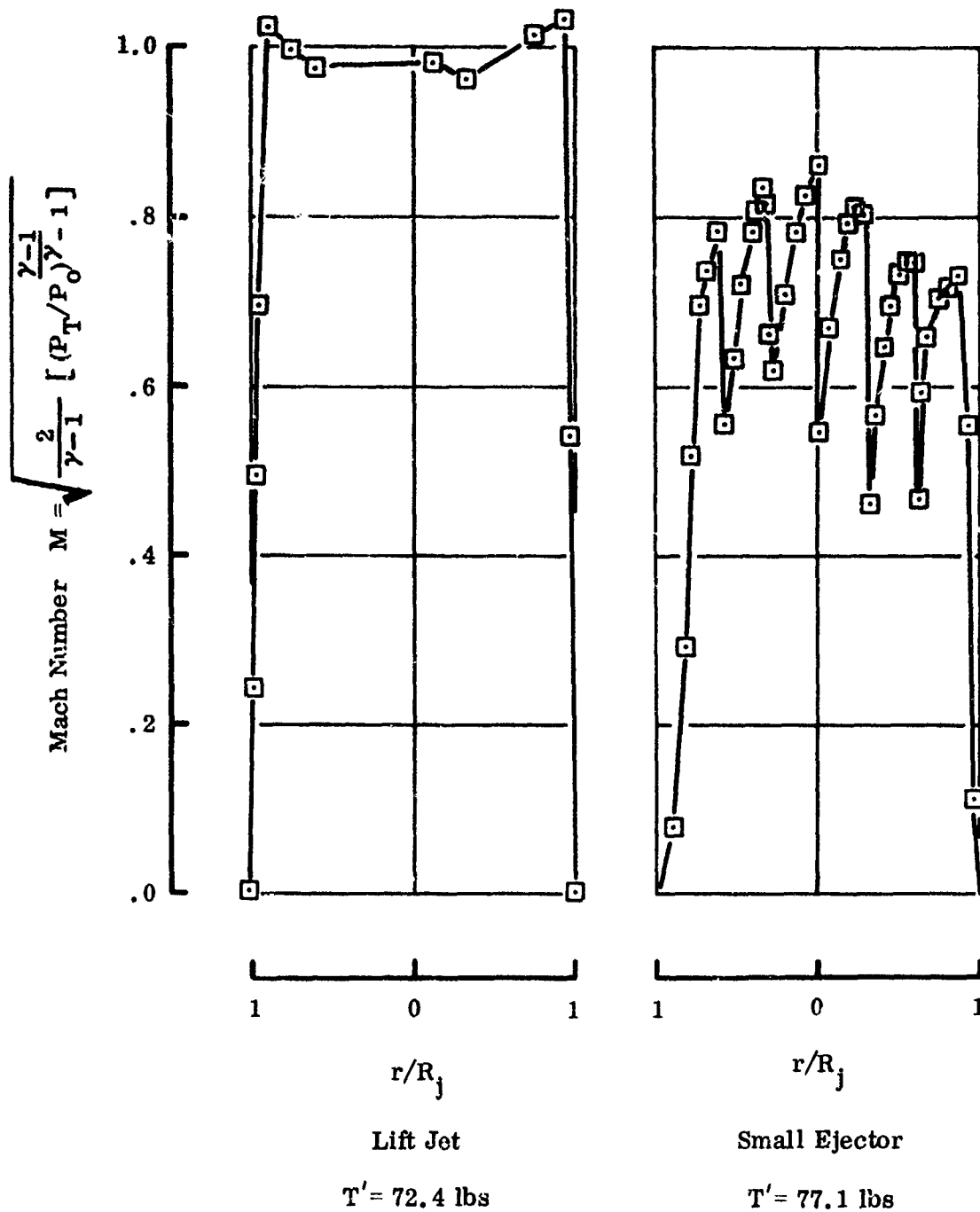
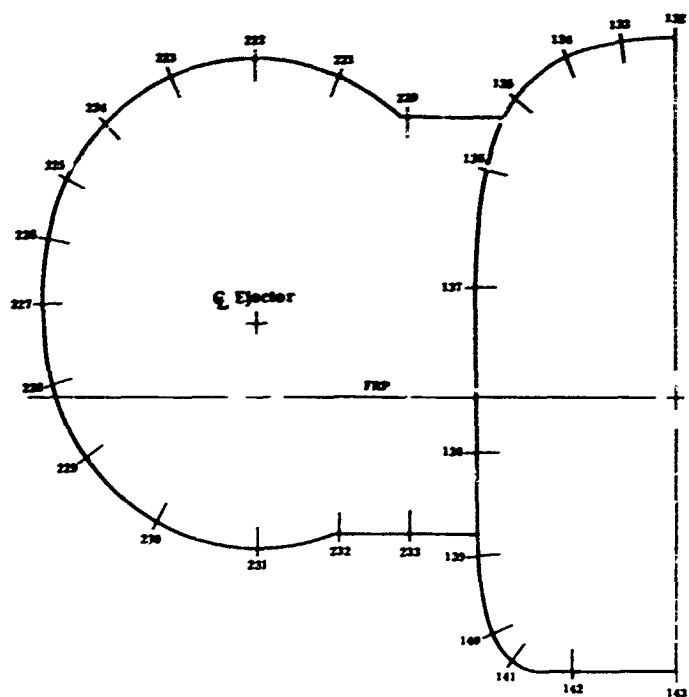
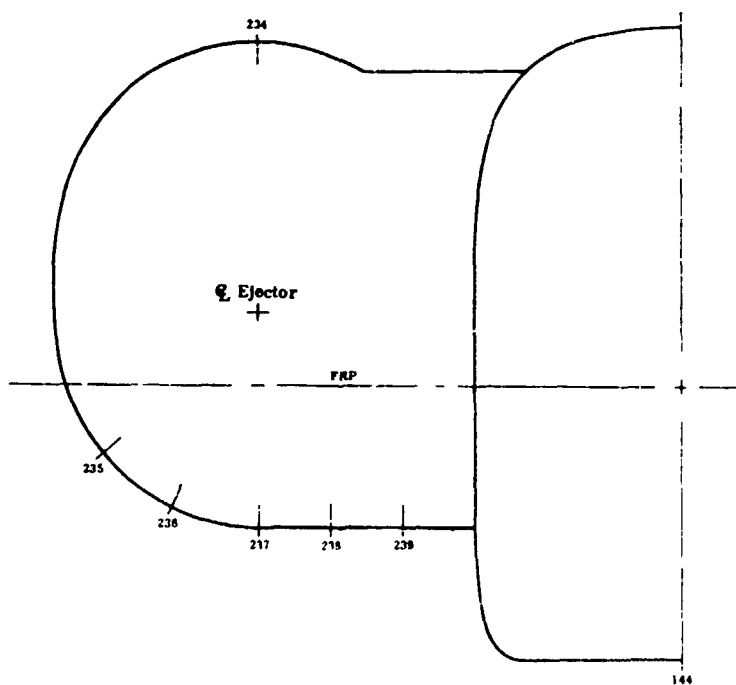


FIGURE I-6. TYPICAL EXIT PROFILES ALONG LONGITUDINAL NOZZLE CENTERLINE



FS 18.55



FS 19.675

FIGURE I-7 (concluded)

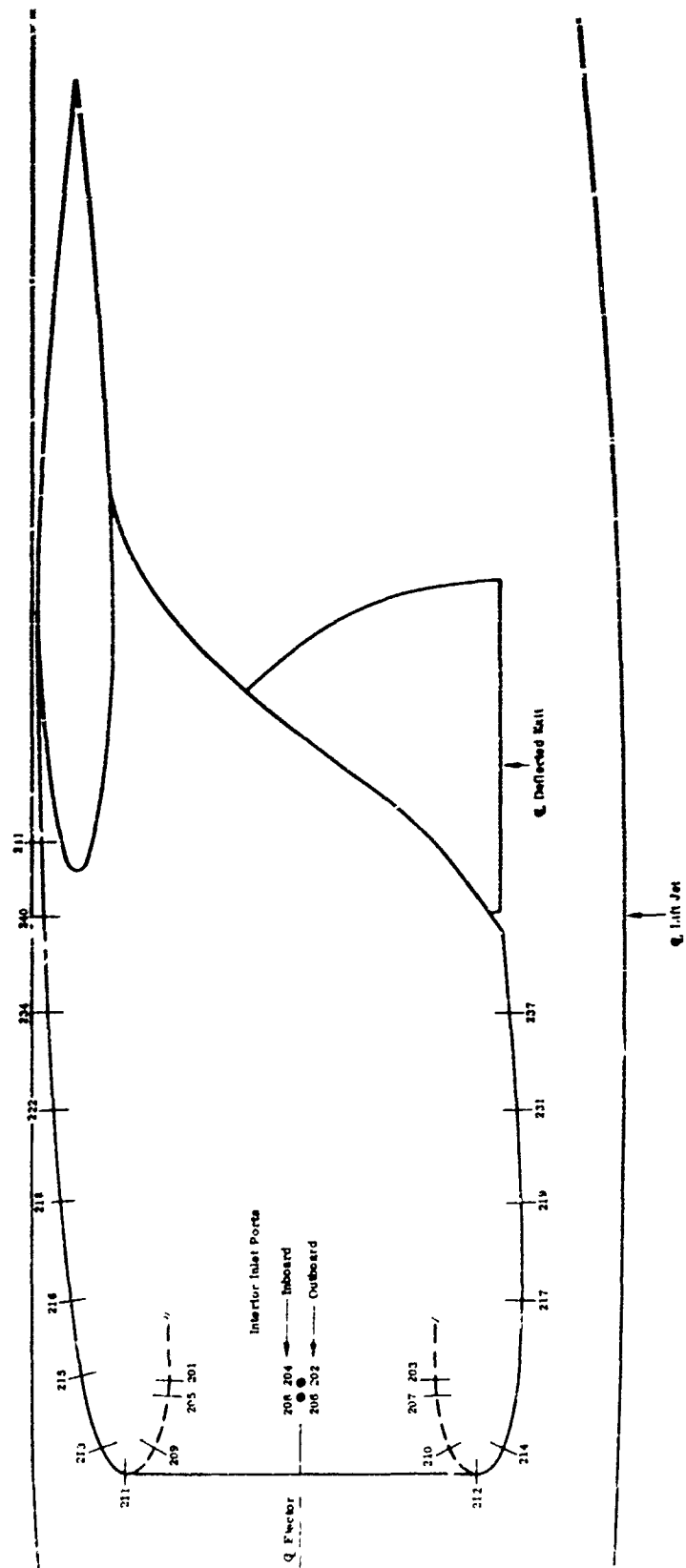


FIGURE I-8. NACELLE CENTERLINE PRESSURE PORTS

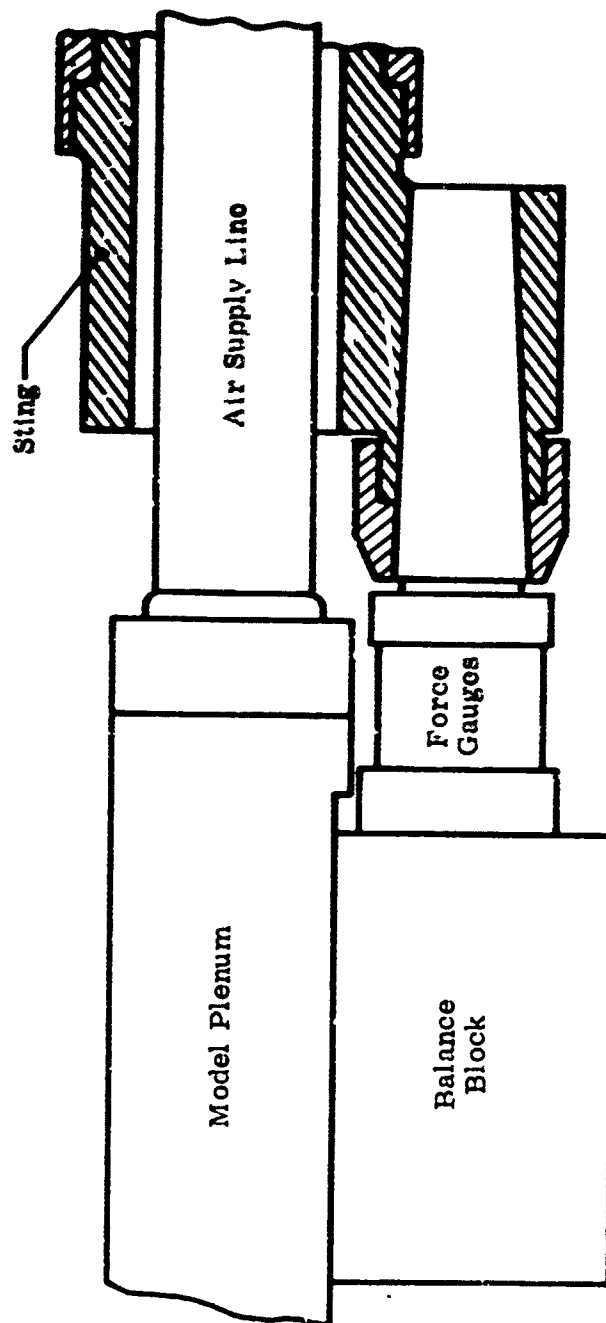


FIGURE I-9. AIR SUPPLY STING - BALANCE ASSEMBLY

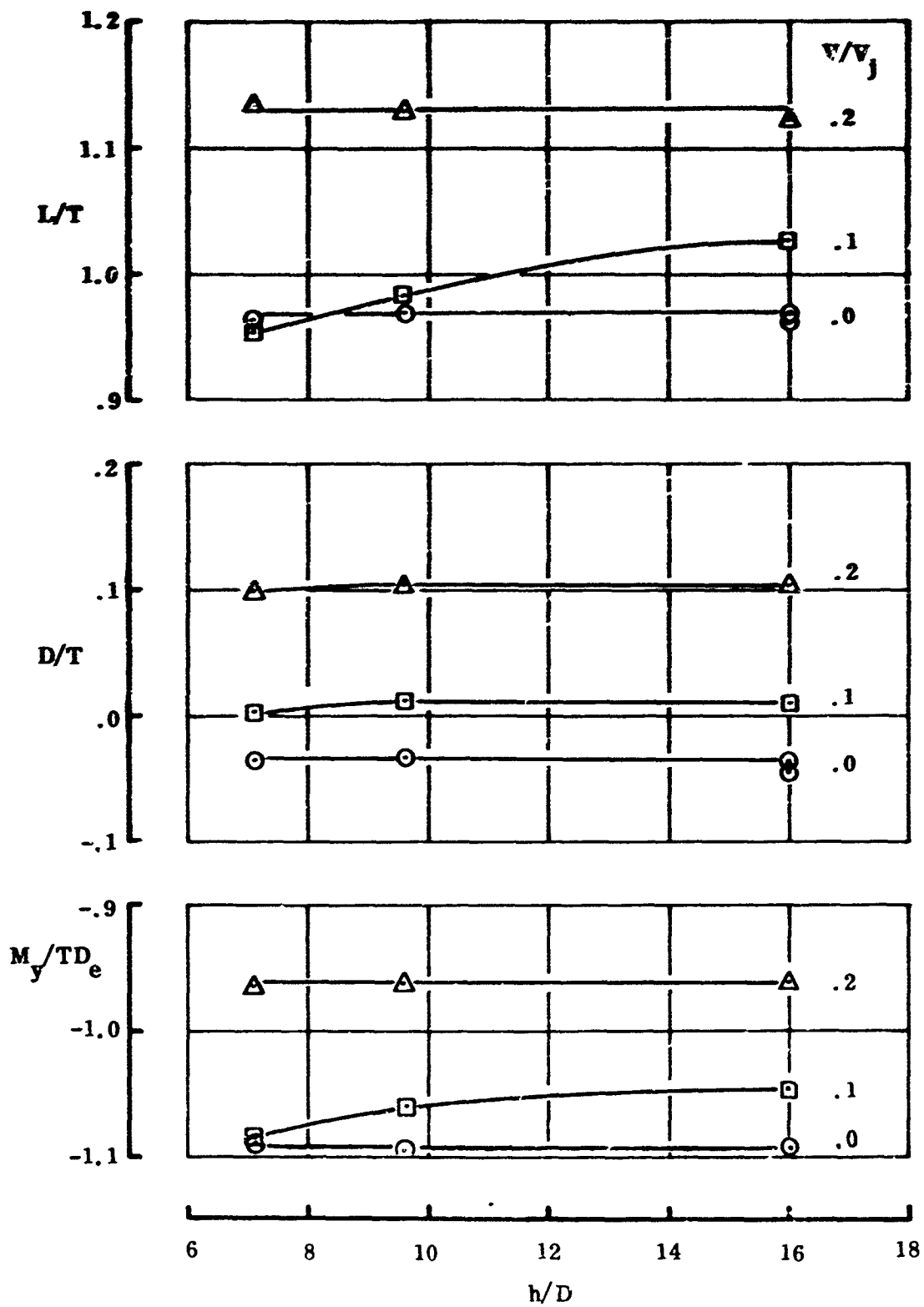


FIGURE I-10. EFFECT OF MODEL HEIGHT, $\alpha = 6^\circ$

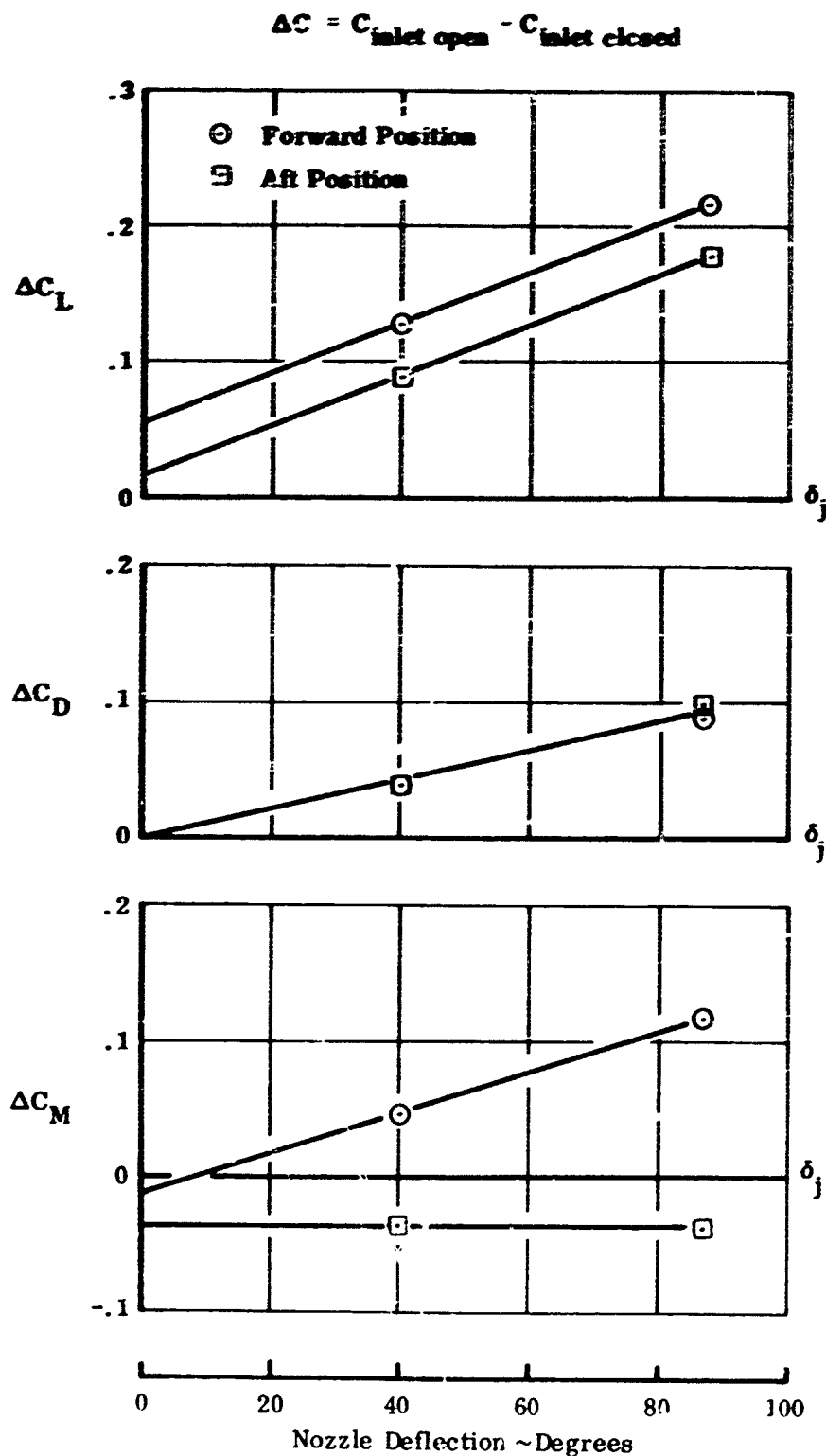


FIGURE I-11. EFFECT OF FREE FLOW THROUGH INLET ON
 MODEL AERODYNAMIC LOADS AT $\alpha = 0$ DEG.
 WING-BODY-NACELLE WITH SMALL NOZZLES

$Q = 59.5$ PSF

$P_{ep} = 0$ PSIG

$\alpha = 0$ Deg.

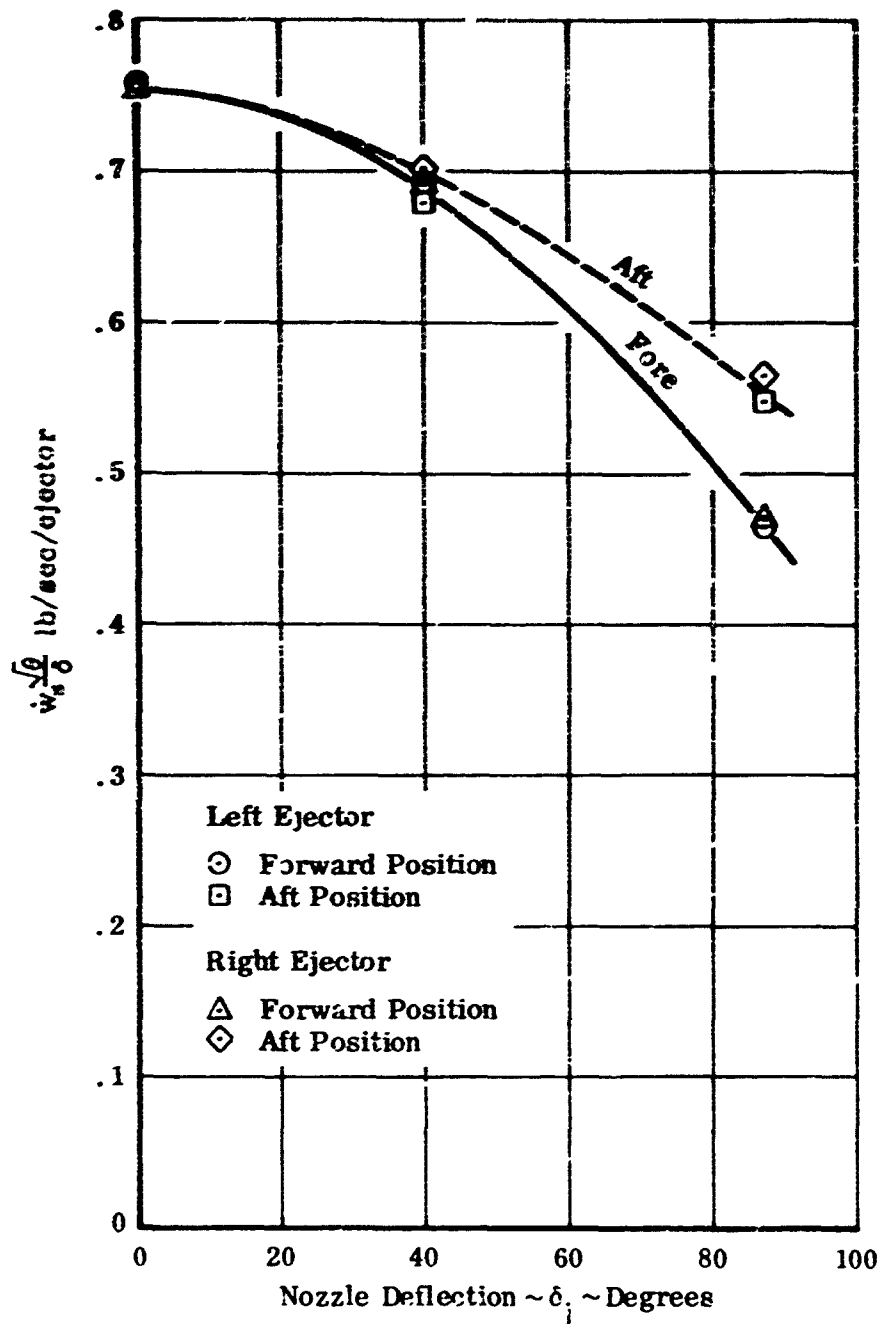
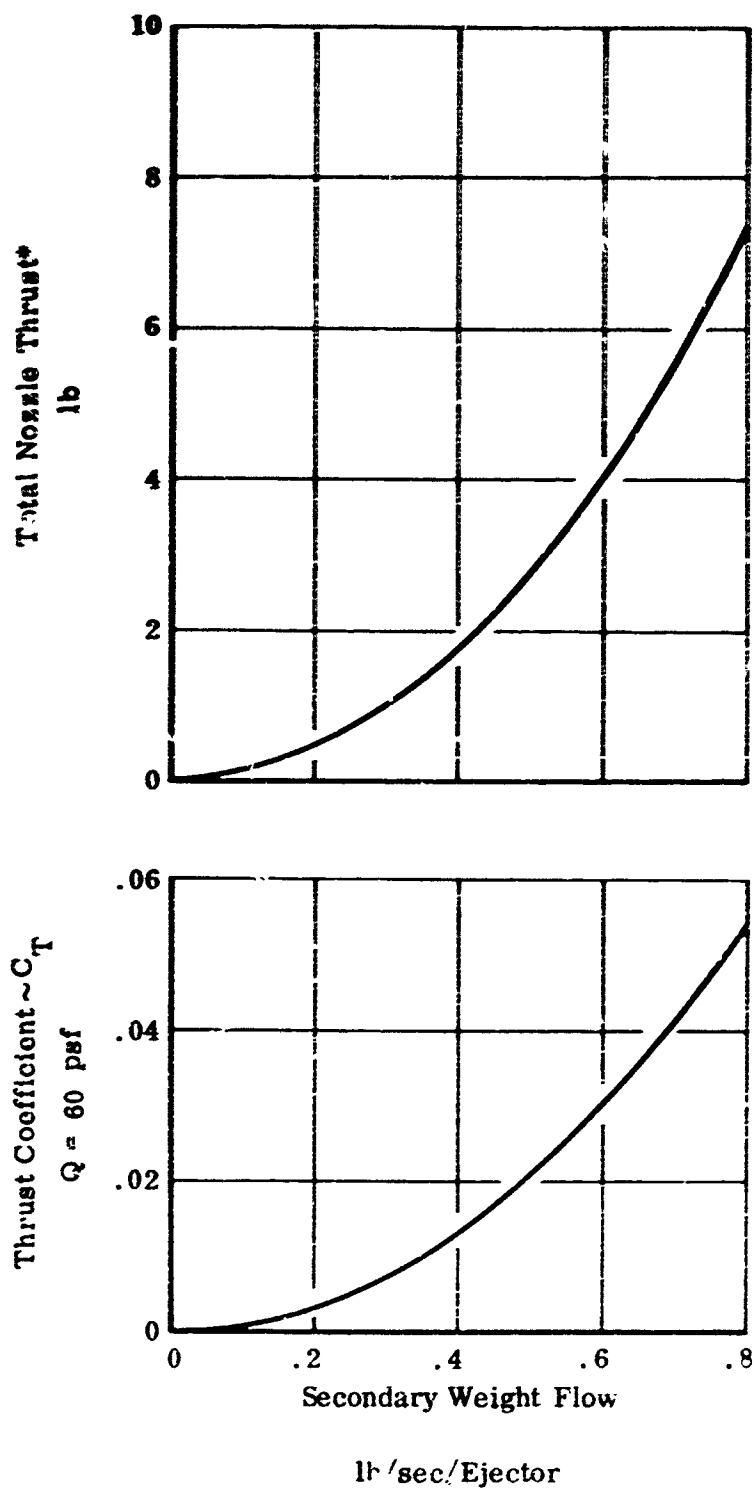


FIGURE I-12. INLET WEIGHT FLOW FOR UNPOWERED EJECTOR
SMALL NOZZLES



* Both ejectors -
Uniform exit flow is assumed

FIGURE I-13. THRUST DUE TO FREE FLOW INLET
SMALL NOZZLES

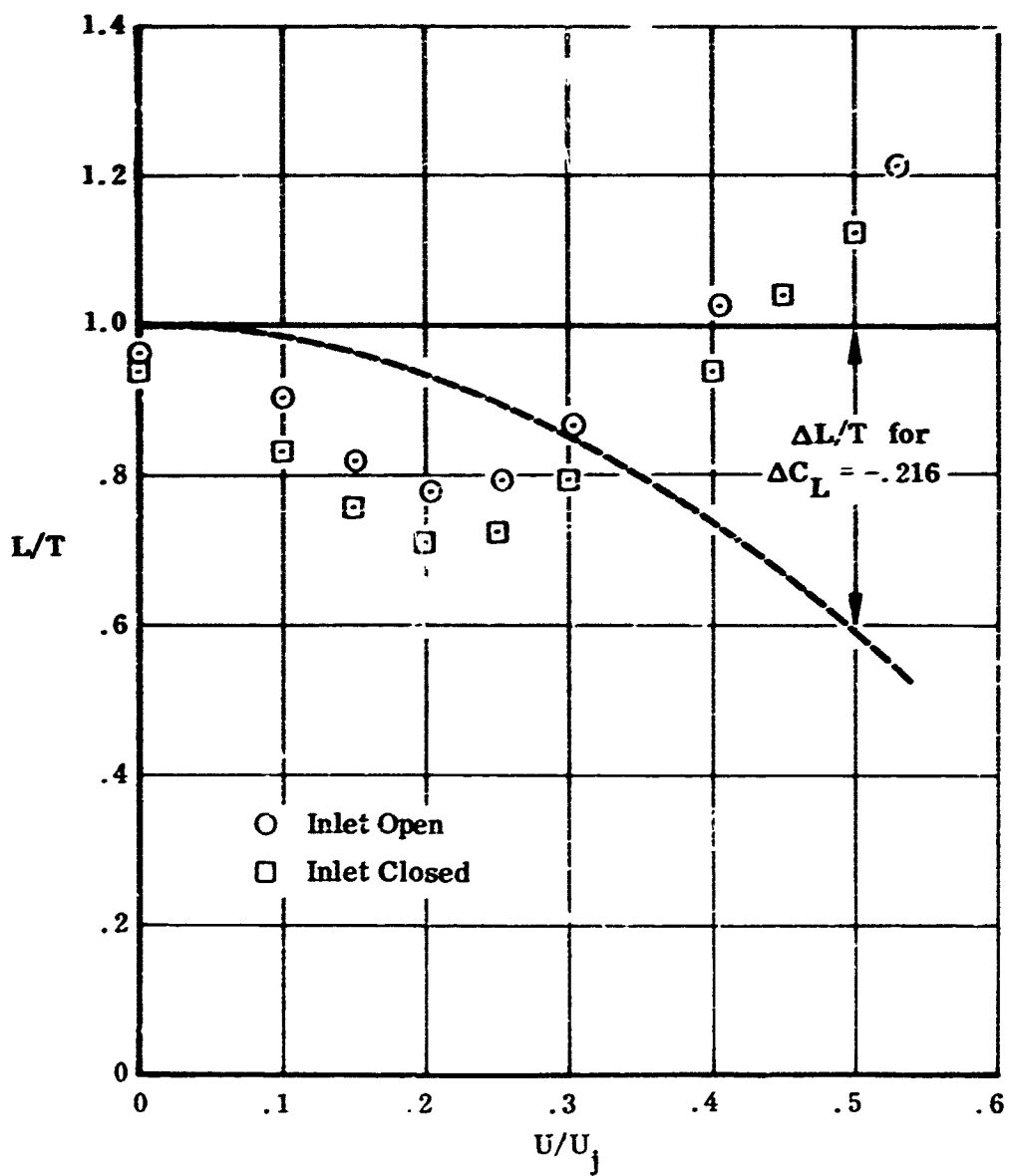


FIGURE I-14. EFFECT OF OPEN INLET ON POWER MODEL LOADS
WING-BODY-NACELLE, SMALL FORWARD NOZZLES
DEFLECTED 90 DEG.

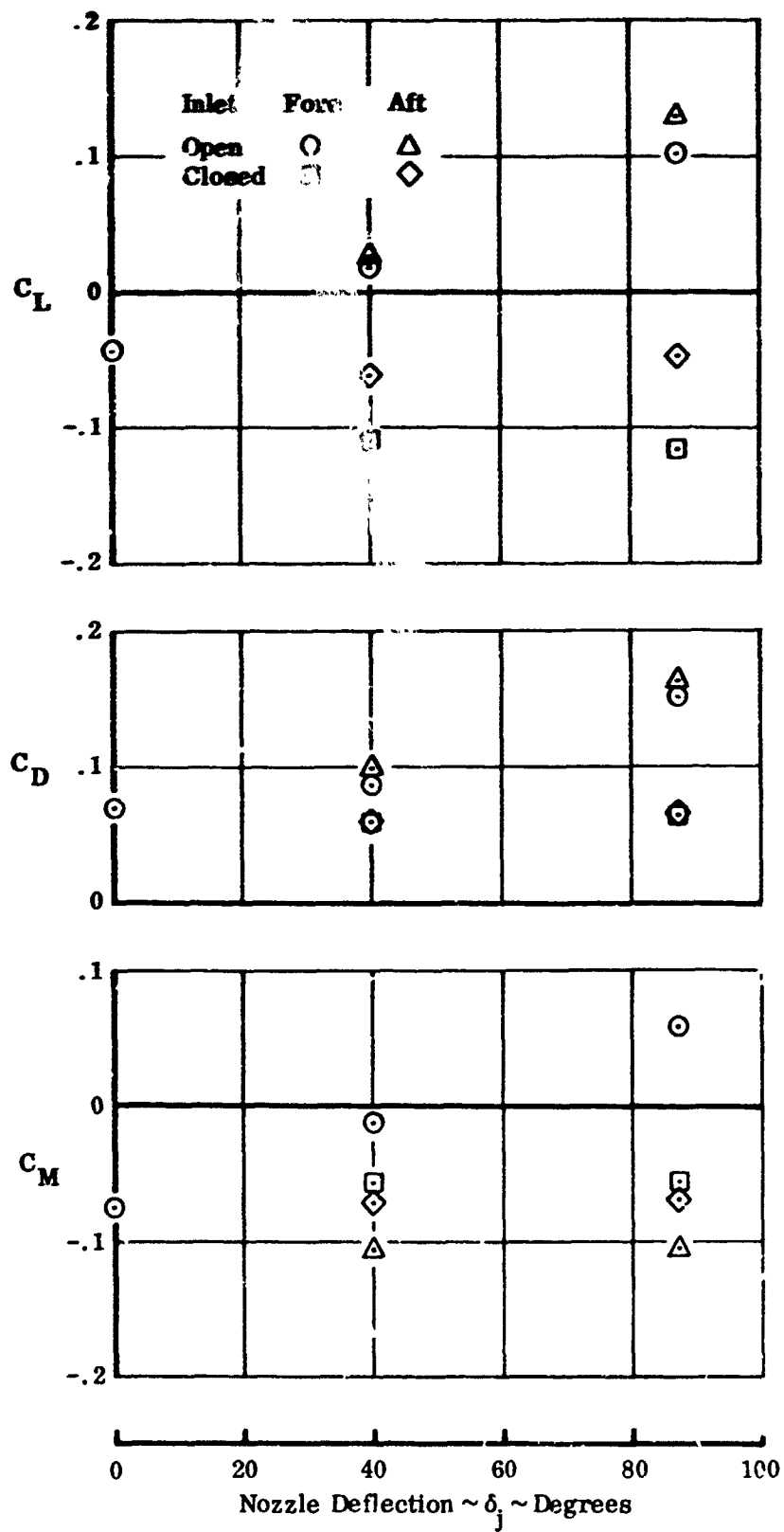


FIGURE I-15. UNPOWERED AERODYNAMIC COEFFICIENTS
WING-BODY-NACELLE, SMALL NOZZLES $\alpha = 0$

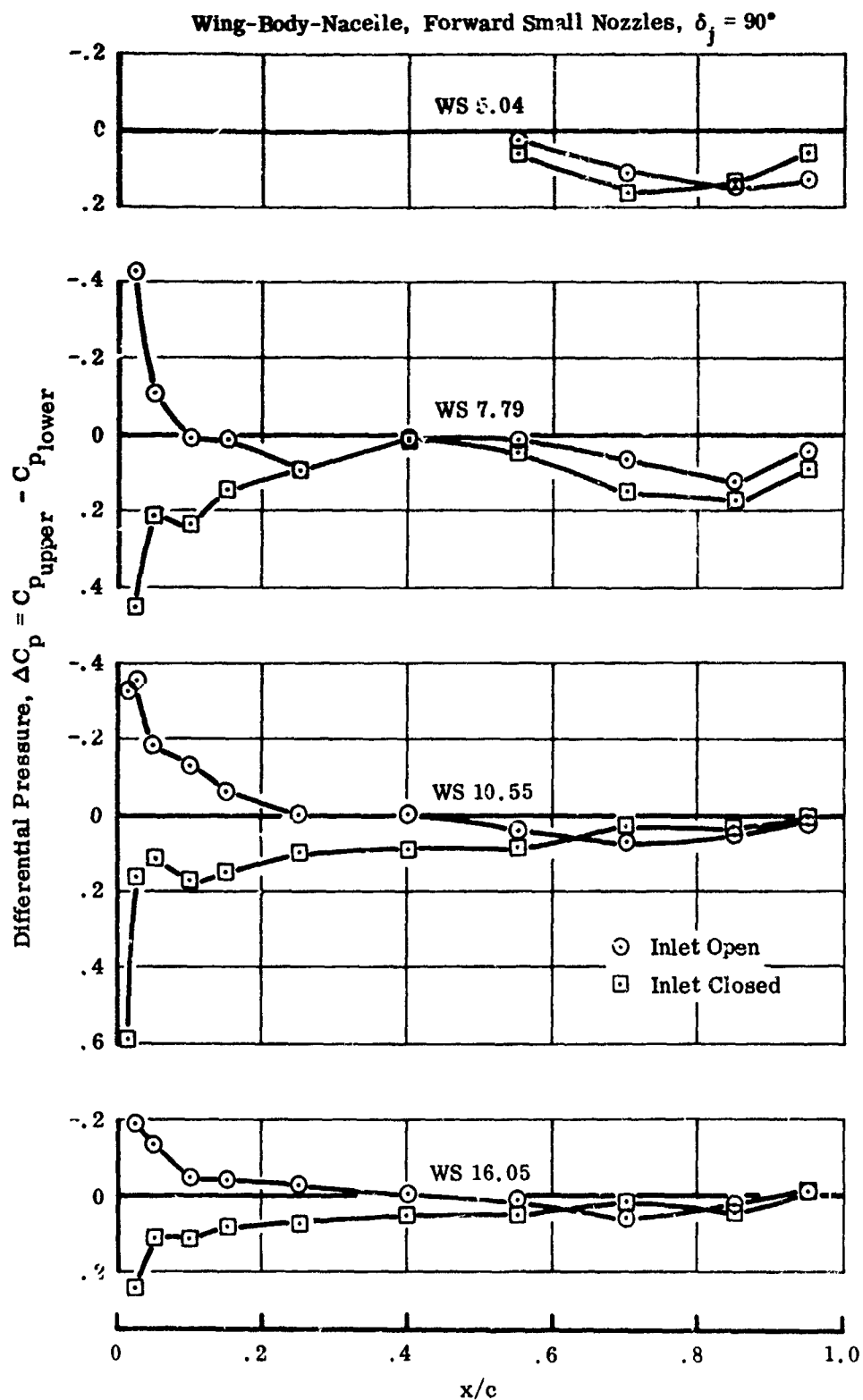


FIGURE I-16. EFFECT OF FREE FLOW THROUGH INLET ON WING PRESSURE LOADING

Wing-Body-Nacelle, Forward Small Nozzles, $\delta_j = 90^\circ$

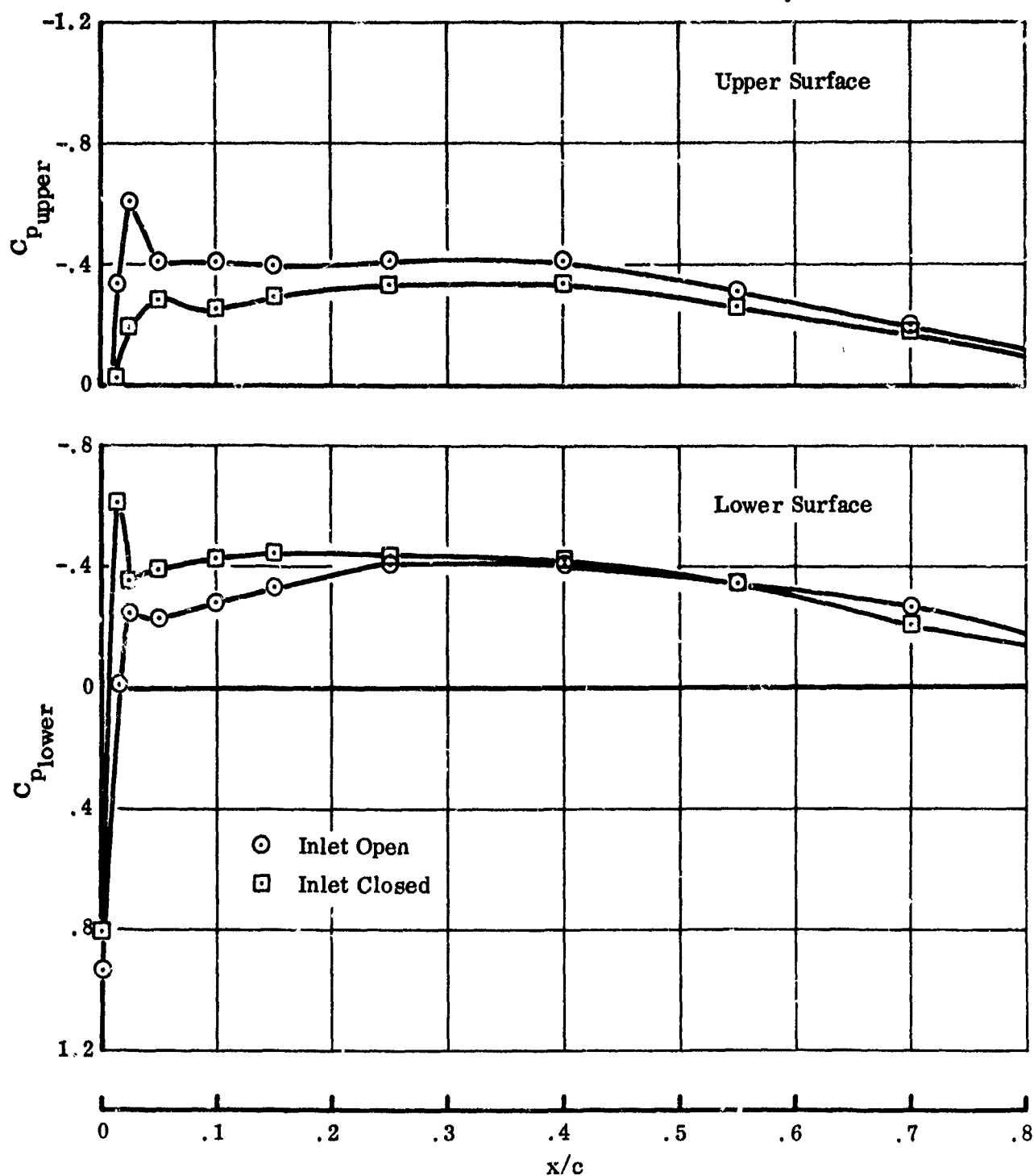


FIGURE I-17. EFFECT OF FREE FLOW THROUGH INLET ON SECTION PRESSURE LOADINGS

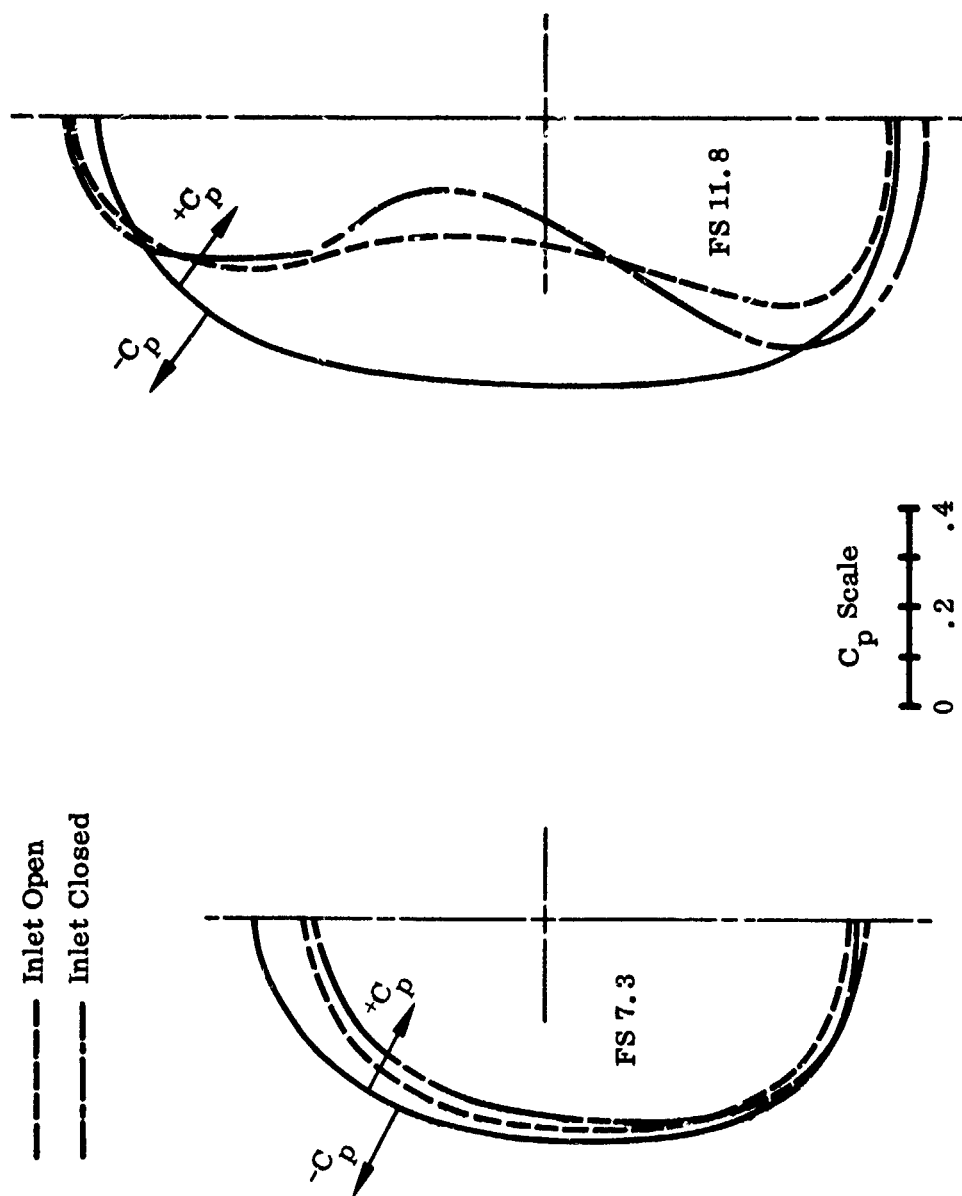


FIGURE I-18. EFFECT OF FREE FLOW THROUGH INLET ON FUSELAGE PRESSURES
WING-BODY-NACELLE, FORWARD SMALL NOZZLES, $\delta_j = 90^\circ$

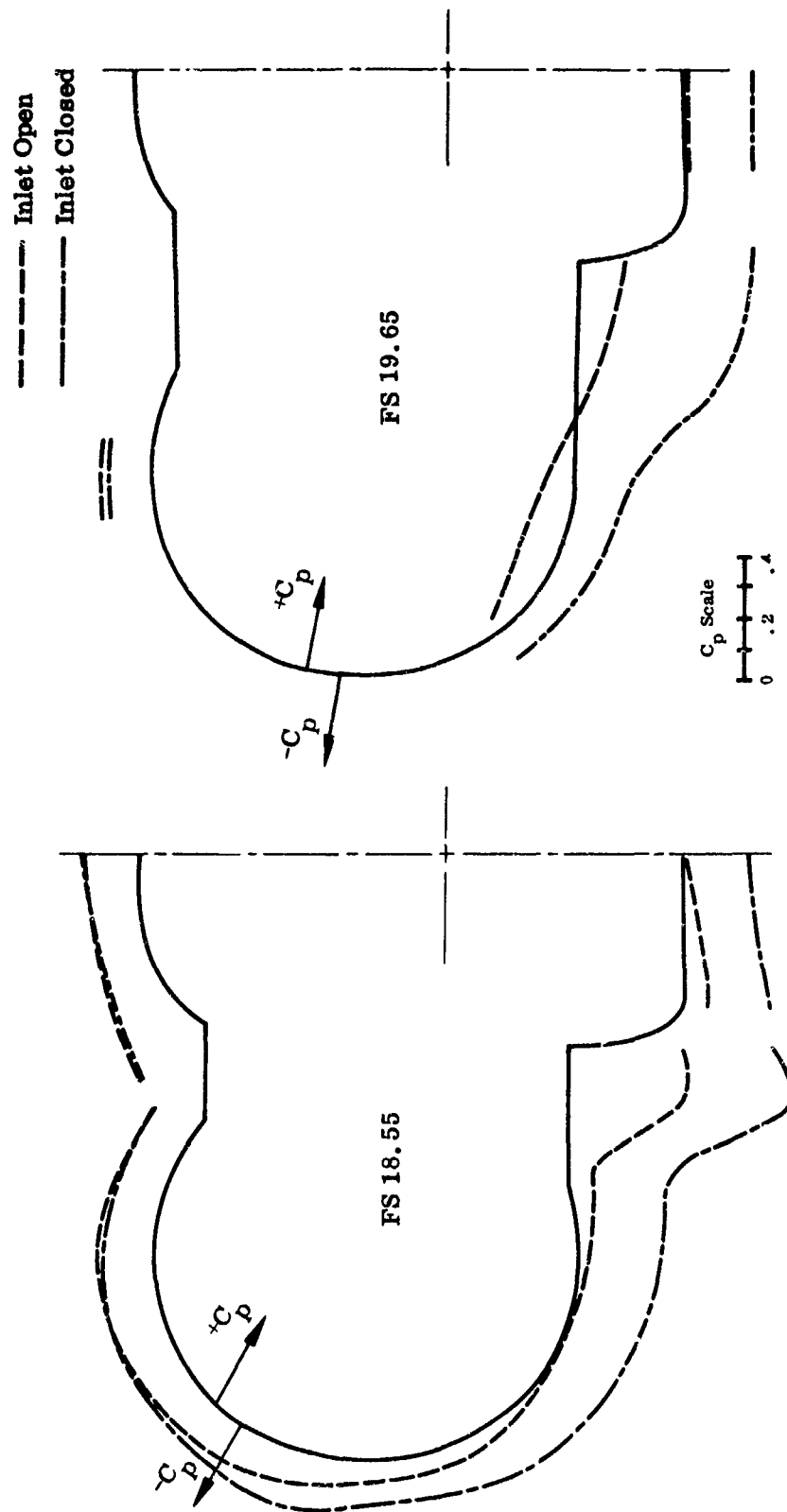


FIGURE I-18 (cont.)

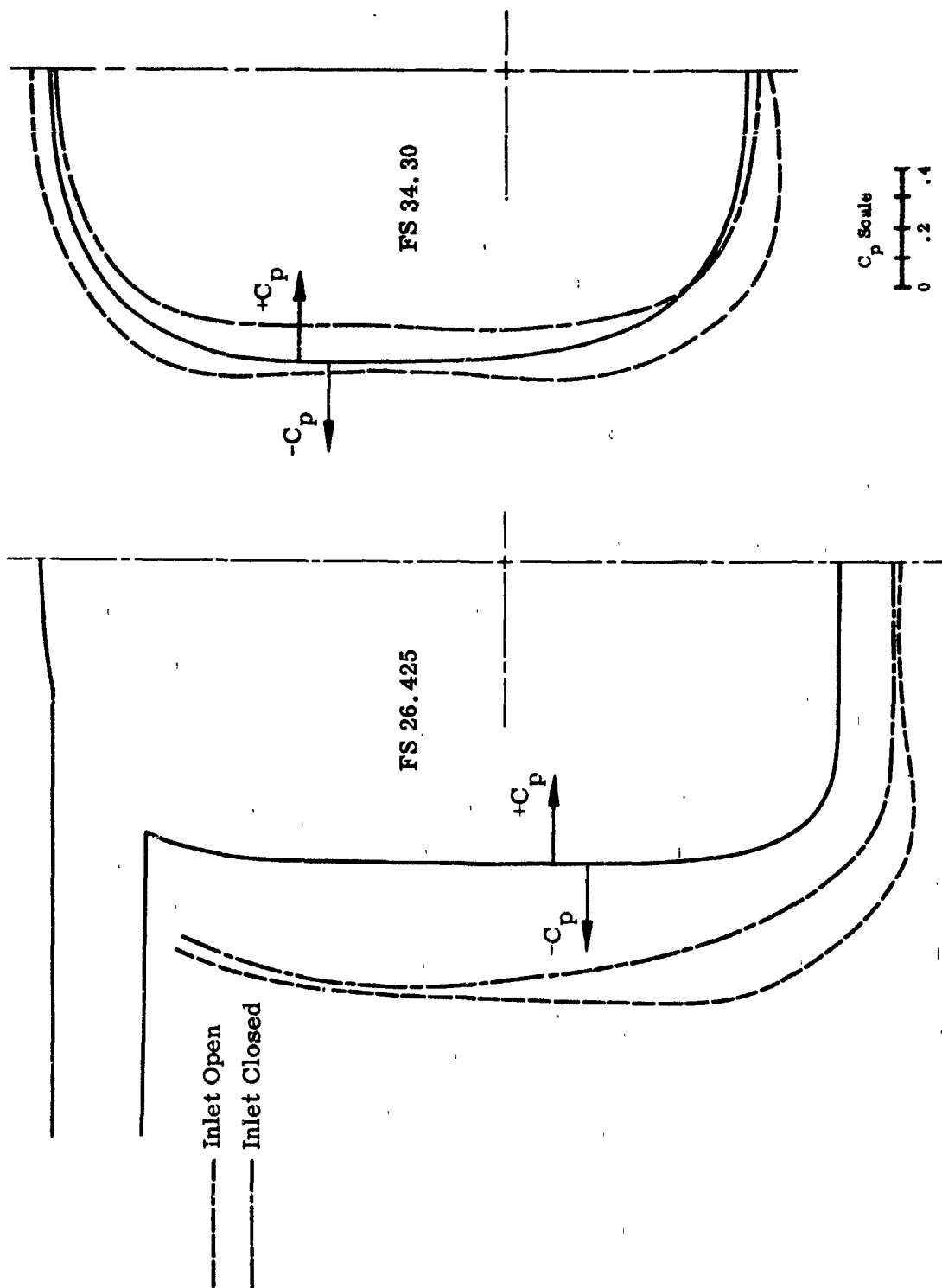


FIGURE I-18 (concluded)

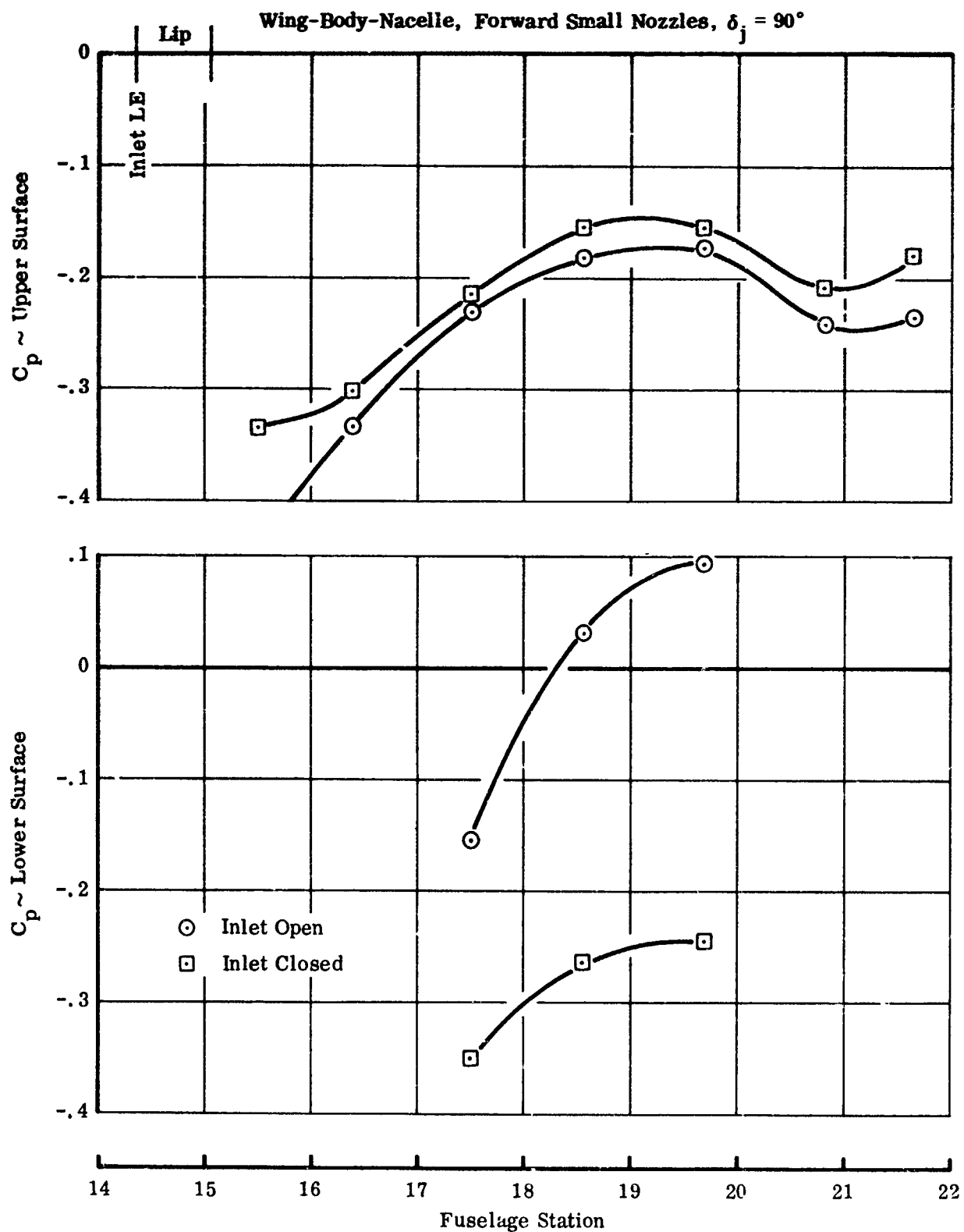


FIGURE I-19. EFFECT OF FREE FLOW THROUGH INLET ON NACELLE CENTERLINE PRESSURES

Wing Body Nacelle, Forward Small Nozzles, $\delta_j = 90^\circ$

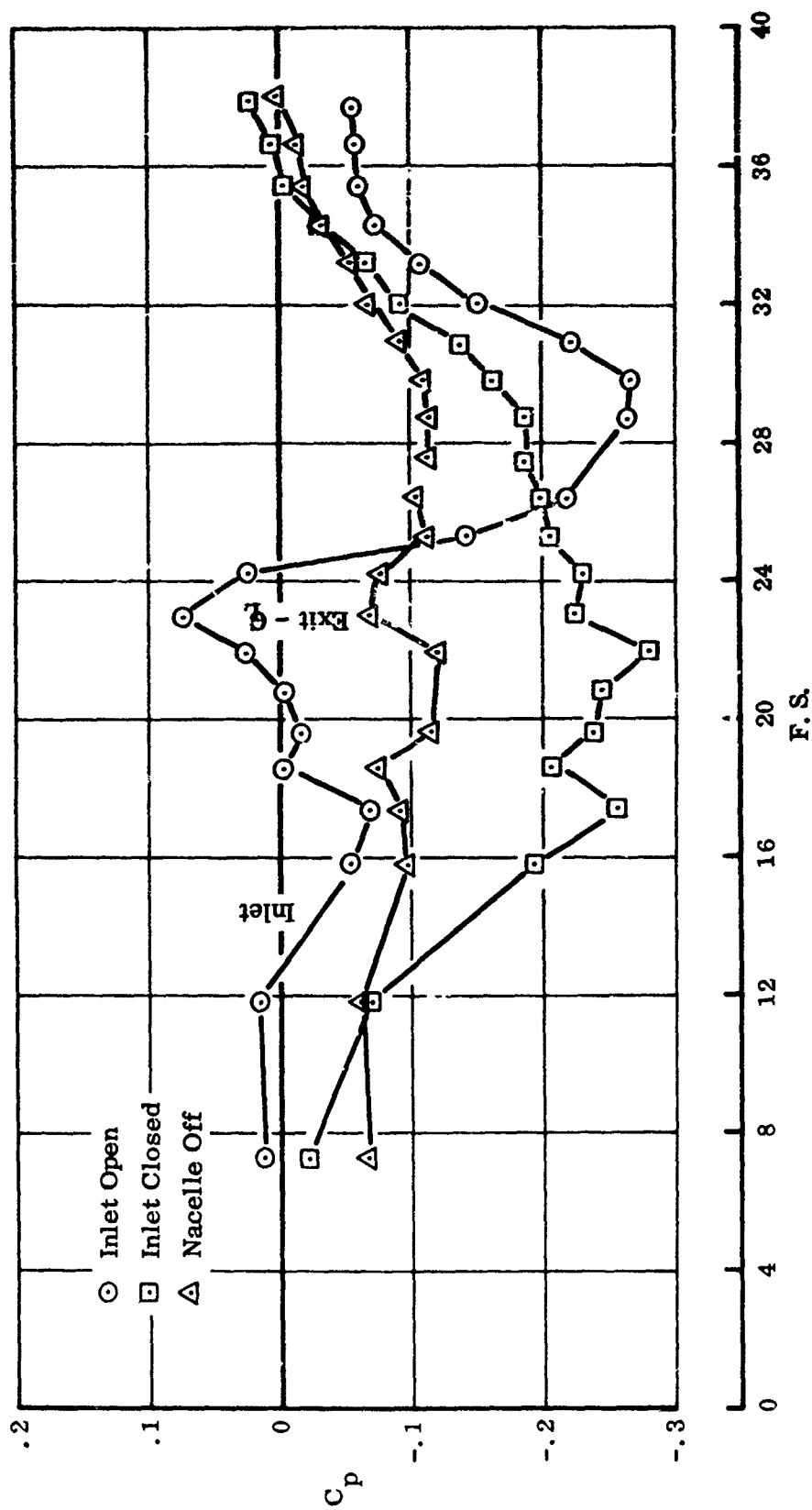


FIGURE I-20. FREE FLOW INLET EFFECT ON LOWER FUSELAGE CENTERLINE PRESSURES

Wing Body Nacelle, Forward Small Nozzles, $\delta_j = 90^\circ$

Unpowered



FIGURE I-21. EFFECT OF FREE FLOW THROUGH INLET ON DOWNWASH AT THE TAIL FLOW ANGULARITY RAKE

Wing Body Nacelle, Aft Large Nozzles, $\delta_j = 90$

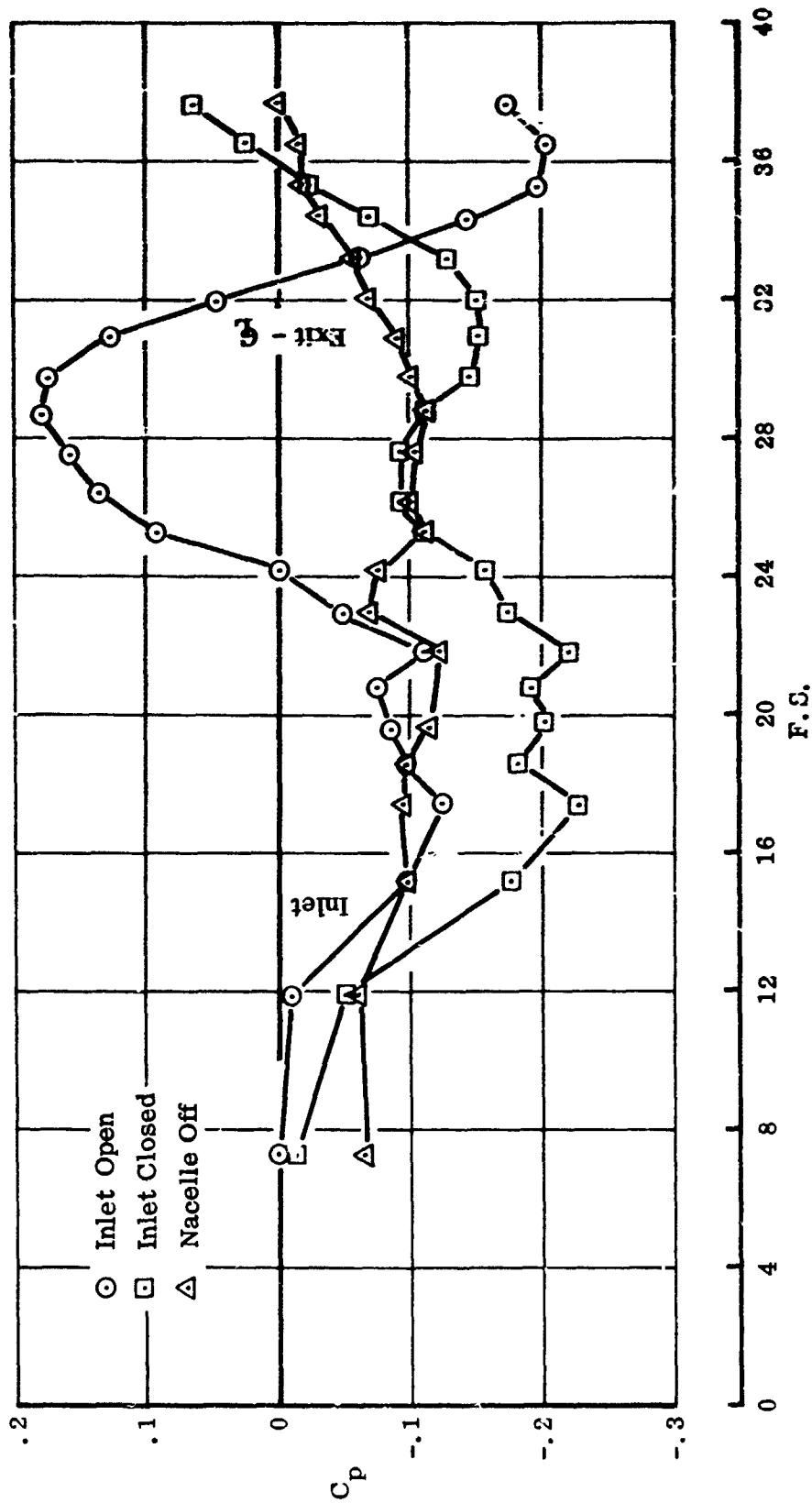


FIGURE I-22. FREE FLOW INLET EFFECT ON LOWER FUSELAGE CENTERLINE PRESSURES

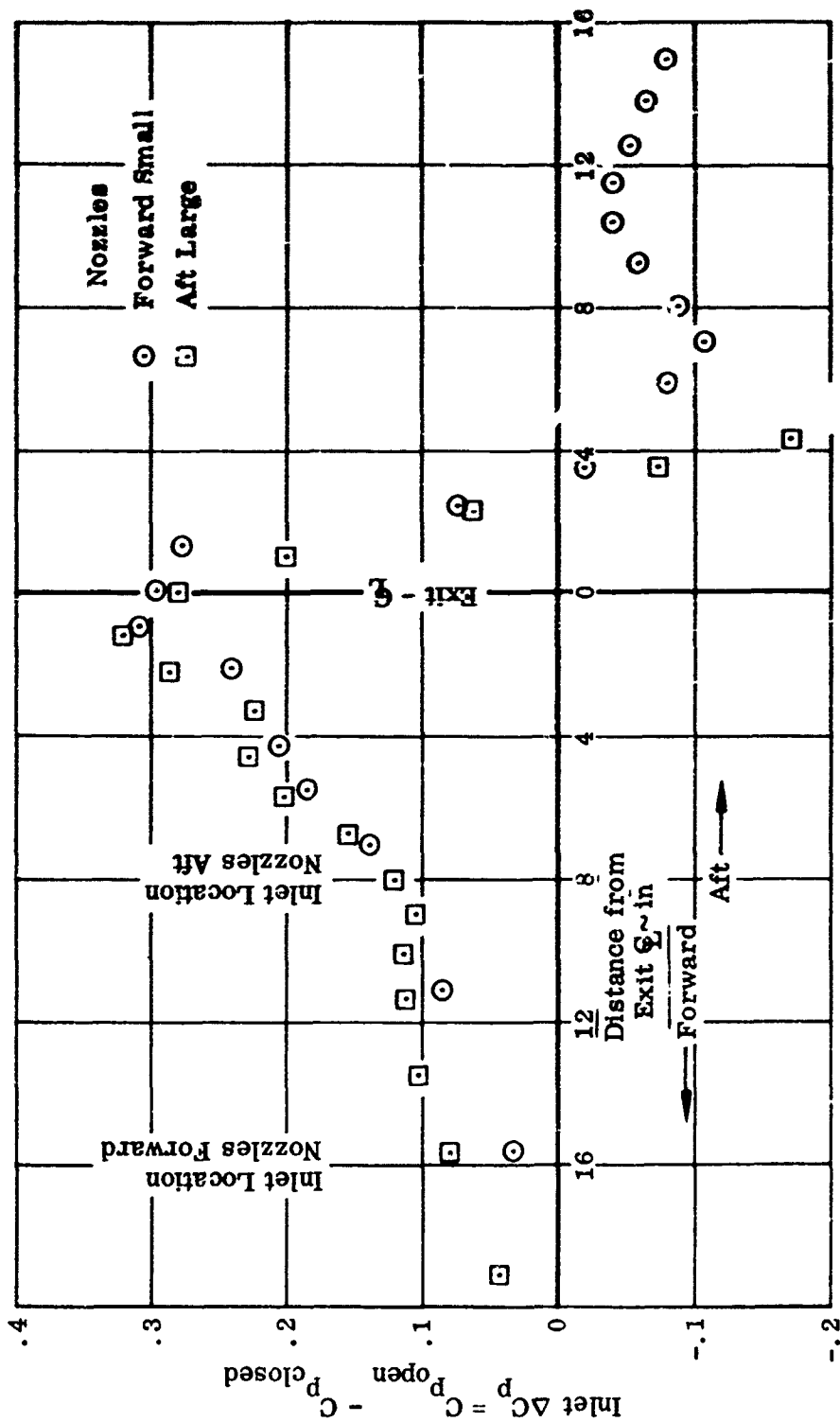


FIGURE I-23. EFFECT OF OPEN INLET ON LOWER FUSELAGE CENTERLINE PRESSURES WITH FORWARD AND AFT NOZZLES

APPENDIX II

BALANCE CORRECTIONS AND CALIBRATION

Calibration of the basic balance was performed by NASA Langley using well established procedures. The effects of the air supply line, which spanned the balance, were determined by loading of the balance both with and without the airline using the same series of loads. A matrix of correction coefficients was then derived which caused the corrected airline-on loads to match the measured airline-off or applied loads. The loads were applied through the use of a complex device utilizing a system of weight pans, fulcrums, and levers. The resulting correction factors are shown below. The 6 x 6 matrix indicated in Appendix I is shown here as two 3 x 3 matrices as longitudinal and lateral components were not found to interact.

$$\begin{Bmatrix} \text{Corrected} \\ \text{Loads} \end{Bmatrix} = \begin{Bmatrix} \text{Correction} \\ \text{Matrix} \end{Bmatrix} \begin{Bmatrix} \text{Measured Loads} \\ \text{Airline-On} \end{Bmatrix}$$

$$\begin{Bmatrix} N \\ A \\ M_y \end{Bmatrix}_{C_1} = \begin{bmatrix} 1.0 & 0 & -.0021 \\ -.0019 & 1.002 & -.0014 \\ .056 & -.0115 & 1.107 \end{bmatrix}_1 \begin{Bmatrix} N \\ A \\ M_y \end{Bmatrix}_{\text{Bal}}$$

$$\begin{Bmatrix} M_x \\ M_z \\ Y \end{Bmatrix}_C = \begin{bmatrix} 1.025 & -.0181 & 0 \\ -.0592 & 1.085 & 0 \\ .0008 & -.0014 & .9960 \end{bmatrix} \begin{Bmatrix} M_x \\ M_z \\ Y \end{Bmatrix}_{\text{Bal}}$$

Because of initial difficulties in obtaining the longitudinal corrections shown above, a second loading of normal force and pitching moment was made with the use of a bar and moving weight pan. This resulted in a different set of longitudinal corrections. Interactions due to axial force were taken from the previous loading.

$$\begin{Bmatrix} N \\ A \\ M_y \end{Bmatrix}_{C_2} = \begin{bmatrix} .9945 & 0 & -.00198 \\ .01167 & 1.002 & -.00316 \\ .27 & 0 & 1.109 \end{bmatrix}_2 \begin{Bmatrix} N \\ A \\ M_y \end{Bmatrix}_{\text{Bal}}$$

This matrix differs significantly from the original in the calibration of corrected axial force and pitching moment. The pitching moment difference would cause normal forces to appear approximately .2 inch farther forward if the second matrix is used in preference to the first. The use of the second matrix would also indicate increased drag with positive normal force and decreased drag with positive pitching moment when compared with data reduced by the first matrix.

The second matrix has been used to reduce the data presented in this report because more experience was available with the method of loading. In addition, the second matrix gave better results on the position of a small test weight and it indicated that the lift jet center of pressure, which was not constant, approached the geometric center of the exit at higher thrusts as opposed to moving away. However, the results of these checks were not conclusive. The matrix below indicates the final matrix of correction coefficients \tilde{K} .

$$\tilde{K} = \begin{vmatrix} .9945 & 0 & -.00198 & 0 & 0 & 0 \\ .01167 & 1.002 & -.00316 & 0 & 0 & 0 \\ .27 & 0 & 1.109 & 0 & 0 & 0 \\ 0 & 0 & 0 & 1.025 & -.0181 & 0 \\ 0 & 0 & 0 & -.0592 & 1.085 & 0 \\ 0 & 0 & 0 & .0008 & -.0014 & .9960 \end{vmatrix}$$

The matrix shown below will convert the longitudinal data presented in this report to the form it would have had if the original corrections were used.

$$\begin{vmatrix} N \\ A \\ M_y \end{vmatrix}_{C_1} = \begin{vmatrix} 1.0055 & 0 & -.0001 \\ -.0142 & 1.000 & .0016 \\ -.213 & -.0115 & .9975 \end{vmatrix} \begin{vmatrix} N \\ A \\ M_y \end{vmatrix}_{C_2}$$

Nominal accuracy of the basic balance is indicated below.

Component	N	A	Y	M _x	M _y	M _z
Accuracy — lb or in.-lb	±2.5	±1.0	±1.5	±5	±15	±10

APPENDIX III

EFFECT OF FORWARD SPEED ON EJECTOR JET ENGINE SIMULATORS

In order to investigate the effect of forward speed on the thrust of the ejector jet engine simulators, the bellmouth used during static calibration was attached to the ejector unit mounted in the test section. The inlet mass flow variation with forward speed was then determined. The effect of forward speed on inlet mass flow is shown in Figure III-1. The changes shown are small, less than six percent, and may reflect changes in the effective area of the bellmouth which was calibrated under static conditions.

If the thrust of the ejectors is assumed to vary with the square of the total mass flow, the change in thrust may be computed.

$$\frac{T}{T_o} = \frac{(\rho A_j U_j) U_j}{(\rho A_j U_{j_o}) U_{j_o}} = \frac{\dot{w}^2}{\dot{w}_o^2}$$

The computed change in thrust due to forward speed is shown below. The maximum thrust change occurs at the highest forward speed.

Nozzle	T_o , lb	$\frac{T}{T_o}$ Max	Q, psf
Small Forward $\delta_j = 90^\circ$	136	1.026	0 - 60
	105	1.026	0 - 60
	80	1.059	0 - 70
	60	1.061	0 - 60
Large Aft $\delta_j = 90^\circ$	178	1.001	0 - 60

A greater change occurs at lower thrust levels because of the larger ratio of secondary to primary flow.

The maximum thrust errors are of a magnitude less than twice the nominal accuracy of the normal force beam, and the maximum pitching moment errors are of the same relative magnitude. Correction for the errors would be significant only at the higher velocity ratios tested. At maximum dynamic pressures correction would result in a three percent reduction in velocity ratio and a six percent reduction in thrust nondimensionalized data. As the majority of data show a positive slope at high velocity ratios, the effect is minimized, because the corrected datum tends to move along the established curve.

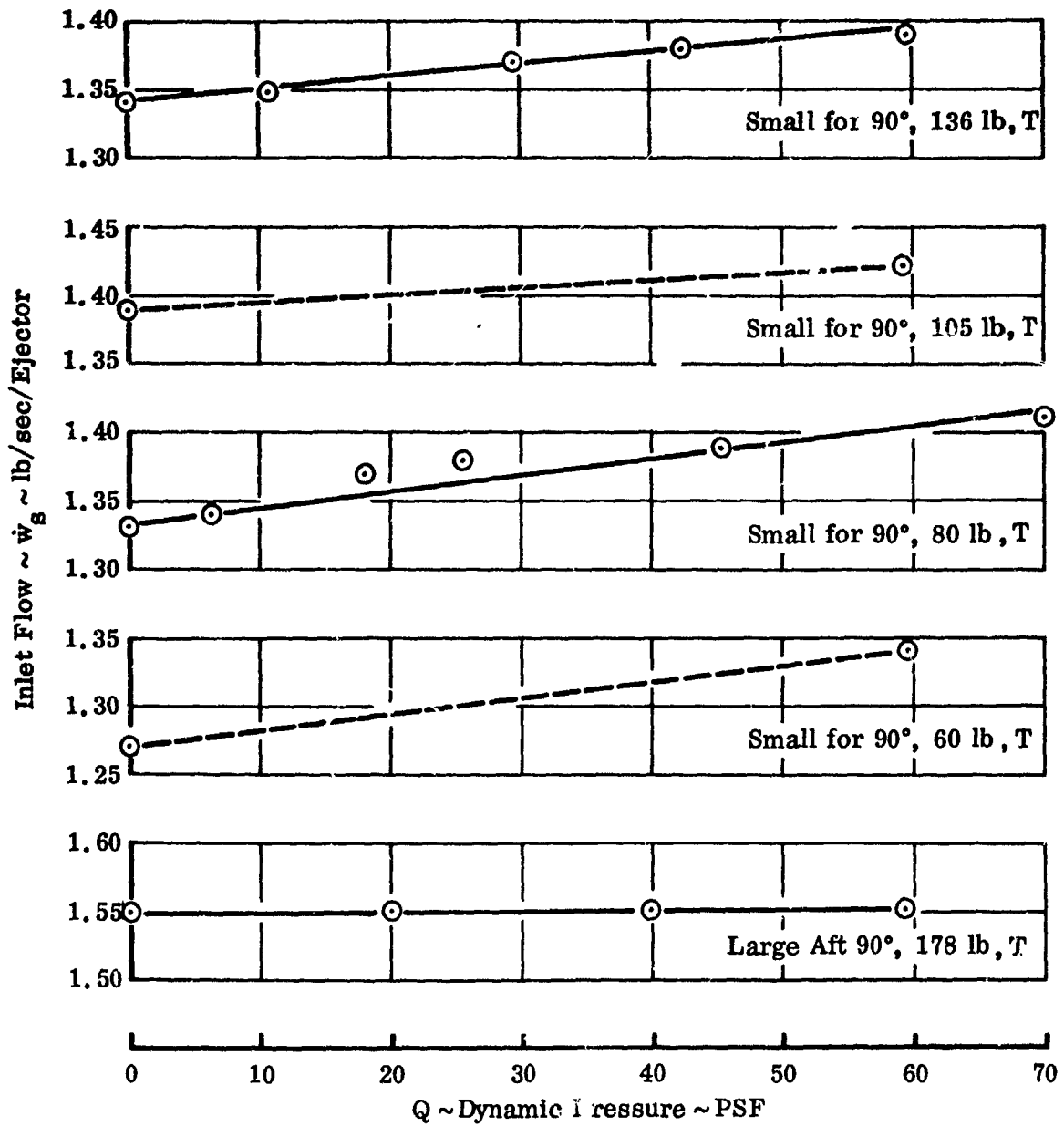


FIGURE III-1. EFFECT OF FORWARD SPEED ON INLET FLOW FROM BELLMOUTH MEASUREMENTS

APPENDIX IV

NORMAL FORCE AND PITCHING MOMENT IN THE LIFT JET WAKE

The jet model includes no mechanism which will account for the wake region behind the jet. Consequently, calculations utilizing the jet flow field program are not in good agreement with test data in this region. As indicated in Section III the wake region contributes the major part of the loads on the fuselage so that it is desirable to have some method for estimating the integrated force and pitching moment for this region.

To enable estimates of the fuselage loads in the wake behind the lift jet to be made, it has been assumed that the difference between test data and calculations in this region is the same as the difference between test data and calculations for the component model of Reference 99.

Thus, for example, if the fuselage is at zero degrees angle of attack and sideslip, the wake contribution to the interference lift, ΔL_i , is given by

$$\frac{\Delta L_i}{T} = \frac{2}{\pi} \left(\frac{U_\infty}{U_{j0}} \right)^2 \iint_{\text{WAKE}} \left((C_P)_{\text{test}} - (C_P)_{\text{calculation}} \right) \frac{\delta_{\text{WAKE}}}{d_o^2}$$

in which T is the jet thrust. This double integral has been evaluated for a range of position along the test fuselage and is shown in Figure IV-1.

The wake contributions to pitching moment may be determined in a similar manner. The results, for the three velocity ratios .125, .2, .3 are shown in Figure IV-2. The moment axis has been taken through the center of the jet.

In Section III adjustments to the calculations have been made to account for the jet wake effect. The jet wake contributions were obtained from Figure IV-1 for a wake length of 13.5 jet diameters.

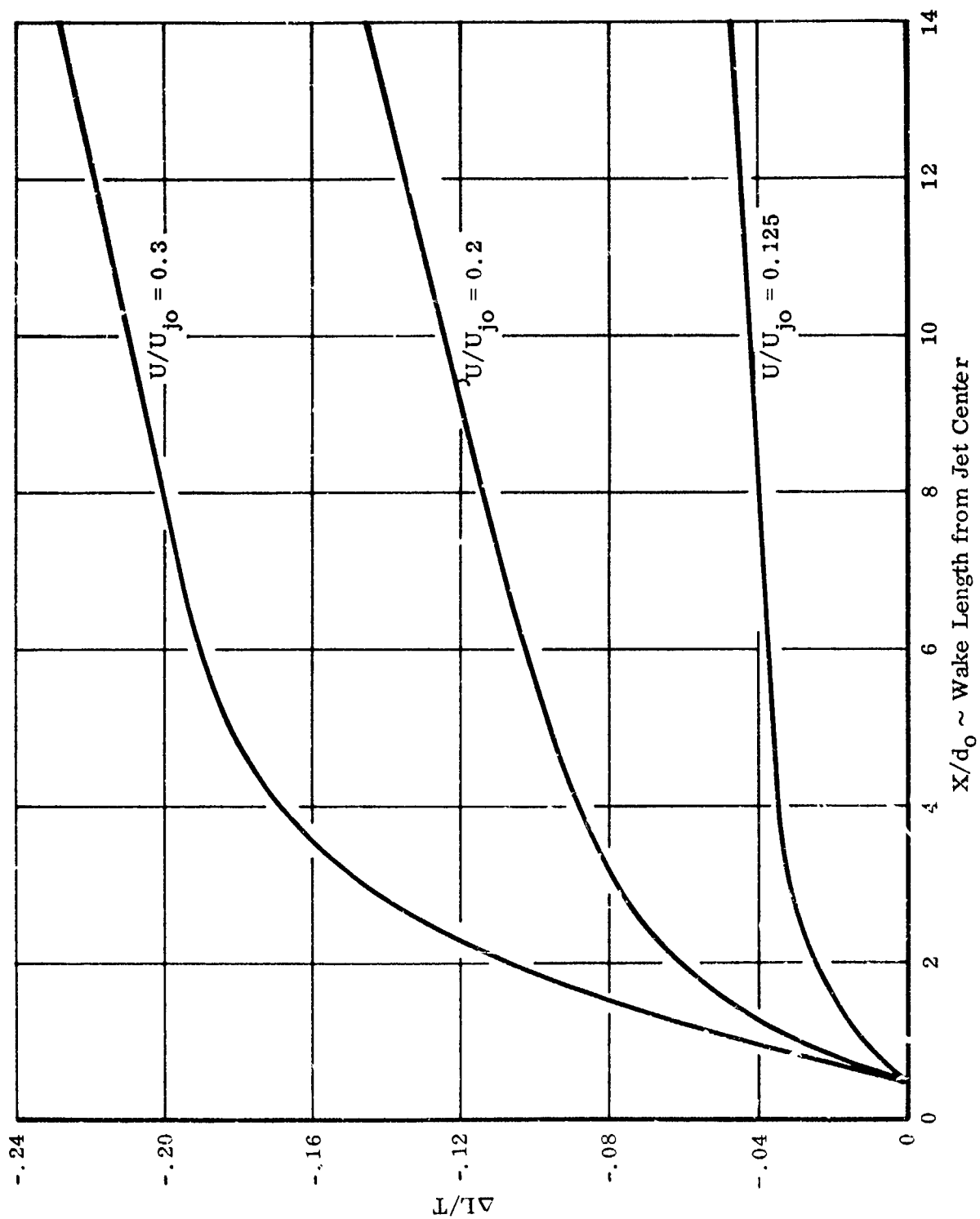


FIGURE IV-1. JET WAKE CONTRIBUTIONS TO FUSELAGE LIFT

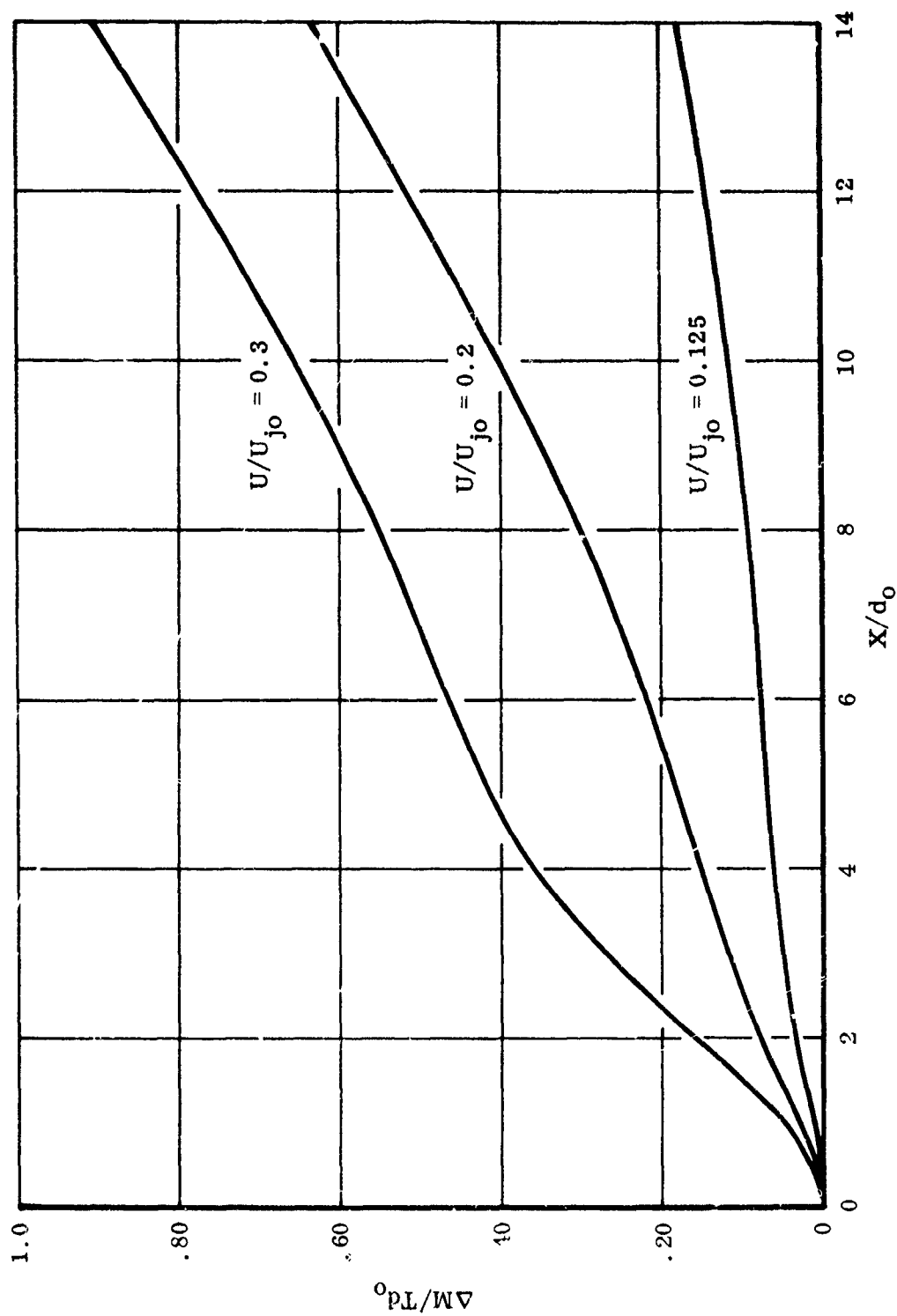


FIGURE IV-2. JET WAKE CONTRIBUTIONS TO FUSELAGE PITCHING MOMENT

REFERENCES

1. Dazek, G. L., "Body Jet Interference Lift Data," NRL-A-769, Northrop Memo No. 3744-67-33, Northrop Corporation, Norair Division, 1967.
2. Gregory, N., Raymer, W. G., Love, E. M., "The Effect of Forward Speed on the Inlet Flow Distribution and Performance of a Lifting Fan Installed in a Wing," Aeronautical Research Council, R&M 3388, June 1962.
3. Aoyagi, K., Hickey, D. H., Desavigny, R. A., "Aerodynamic Characteristics of a Large-Scale Model with a High Disk-Loading Lifting Fan Mounted in the Fuselage," NASA TN D-775, October 1961.
4. Hickey, P. H., Hall, L. P., "Aerodynamic Characteristics of a Large Scale Model with Two High Disk-Loading Fans Mounted in the Wing," NASA TN D-1650, February 1963.
5. Margason, R. J., Gentry, G. L., "Aerodynamic Characteristics of a Five-Jet VTOL Configuration in the Transition Speed Range," NASA TN D-4812, October 1968.
6. Trebble, W. J. G., Williams, J., "Exploratory Wind Tunnel Investigations On a Bluff Body Containing a Lifting Fan," Aeronautical Research Council CP 597, 1962.
7. Anon, "Wind Tunnel Test Report, Lift-Fan Powered Scale Model," G. E. Report No. 137, November 1963.
8. Sacks, A. H., "Aerodynamic Forces, Moments, and Stability Derivatives for Slender Bodies of General Cross Section," NACA TN 3283, November 1954.
9. Hoerner, S. F., Fluid Dynamic Drag, 1958.
10. Loftin, L. K., Jr., and Smith, H. A., "Aerodynamic Characteristics of 15 NACA Airfoil Sections at Seven Reynolds Numbers from 0.7×10^6 to 9.0×10^6 ," NACA TN 1945, October 1949.
11. Heyson, H. H., "Use of Superposition in Digital Computer to Obtain Wind Tunnel Interference Factors for Arbitrary Configurations, with Particular Reference to V/STOL Models," NASA-TR-R-302, February 1967.
12. Stevens, J. R., McDonald J. W., "Subsonic Lifting Surface Design and Analysis Procedure", Northrop Report NOR 64-196, April 1964.